Mechanical Properties of Fats in Relation to their Crystallization

Promotor:	dr. ir. P. Walstra emiritus-hoogleraar in de zuivelkunde
Co-promotor	dr. ir. T. van Vliet universitair hoofddocent levensmiddelennatuurkunde, werkzaam bij het departement Levensmiddelentechnologie en Voedingswetenschapen

NN08701,2436

W. Kloek

Mechanical Properties of Fats in Relation to their Crystallization

Proefschrift
ter verkrijging van de graad van doctor
op gezag van de rector magnificus
van de Landbouwuniversiteit Wageningen,
dr. C.M. Karssen,
in het openbaar te verdedigen
op dinsdag 22 september 1998
des namiddags te vier uur in de Aula.

ISN 9789

CIP-Data Koninklijke Bibliotheek, Den Haag

Kloek, W.

Mechanical properties of fats in relation to their crystallization / W. Kloek, - [S.I.: s.n.]
Thesis Wageningen. - With ref. - With summary in Dutch
ISBN 90-5485-947-4
Subject headings: fat / crystallization / rheology

Omslagillustratie: Jeanine Lanen

This research was co-financed by TNO Nutrition and Food Research Institute.

BIBLIOTHEEK
LANDBOUWUNIVERSITEIT
WAGENINGEN

NN08701, 2486

Stellingen

1. De langzame kristallisatie van zuivere triglyceriden wordt voornamelijk veroorzaakt door het grote entropieverlies tijdens inpassen van triglyceridemoleculen in het kristalrooster.
Dit proefschrift – hoofdstuk 3 en 4

2. De initiële ruimtelijke aggregaatstructuur in een snel kristalliserende vetdispersie is fractaal maar zal daarna, doordat aggregatie en kristallisatie dan gelijktijdig optreden, niet meer een eenduidige constante fractale dimensionaliteit hebben.
Dit proefschrift – hoofdstuk 5 en 6

3. Bij een snel kristalliserend vet is minder dan 1% vaste fase nodig om een continu netwerk te vormen. Om een sterk vetkristalnetwerk te krijgen met zo weinig mogelijk vast vet moet aggregatie in rust plaats vinden en gevolgd worden door een snelle polymorfe overgang.
Dit proefschrift – hoofdstuk 4 en 5

4. Een sterke mate van sintering van vetkristallen in vet-continue systemen veroorzaakt een geringe smeerbaarheid. Daarom moet in dat geval altijd mechanisch worden nabewerkt.
Dit proefschrift – hoofdstuk 6

5. Door hun sterke anisometrie kunnen triglyceridekristallen in een door van der Waalskrachten bijeengehouden netwerk tijdens vervorming buigen zonder het netwerk op te breken.
Dit proefschrift – hoofdstuk 6

6. De brede triglyceridesamenstelling van een vetblend heeft tot gevolg dat verschillen in mechanische eigenschappen door verschillen in procesvoering vaak te niet worden gedaan door de vorming van gesinterde kristalverbindingen als gevolg van herkristallisatie.
Dit proefschrift – hoofdstuk 7 en 8

7. De conclusie van Johansson en Bergenståhl dat de elastische moduli van dispersies van tristearaatkristallen in olie niet verklaard kunnen worden op basis van van der Waals attractie is niet juist, omdat de door hen gebruikte Hamaker-constante met een factor 10 – 100 is onderschat door de veronderstelling dat de brekingsindex van gekristalliseerd tristearaat kleiner is dan die van de olie.
D. Johansson and B. Bergenståhl (1992), *J. Am. Oil Chem. Soc.* **69**, 718-727

8. Instabiliteit van schuim en emulsies wordt vaak ten onrechte aan coalescentie toegeschreven terwijl Ostwald-vergroving minstens zo belangrijk kan zijn.
A.S.Kabalnov and E.D. Shchukin (1992), *Adv. In Colloid and Interface Sci.* **38**, 69-97

9. Het mechanisch gedrag van xanthaan-galactomannaan gelen bij kleine vervormingen wordt voornamelijk bepaald door de rigiditeit van de xanthaanketen.
W.Kloek, H.Luyten en T. van Vliet (1996), *Food Hydrocolloids* **10**, 123-129

10. Protocooperatie van endofytische *Acremonium*-soorten met grassen (*Lolium* spp.; *Festuca* spp.) leidt bij hoge temperaturen tot de vorming van de pyrrolizidinealkaloiden *N*-formyl-loline en *N*-acetyl-loline. Dit geeft voor de grassen bescherming tegen vraat door insecten.
H. Huizing, W. Kloek en T. den Nijs (1989), *Prophyta* **1**, 24-25

11. Het drogen van groenten en fruit met behulp van microgolven in combinatie met gelijktijdige droging met hete lucht is alleen zinvol in het eerste stadium van dit proces; in latere stadia leidt het tot achteruitgang van de sensorische kwaliteit.
AIR-3-CT94-2254: *A novel approach to preserve the intrinsic quality of fruits and vegetables in dry conservation processes*

12. Het zogenaamde lineaire gebied (evenredigheid van spanning en vervorming) van allerlei gelen wordt kleiner naarmate de reologische apparatuur nauwkeuriger wordt.

13. Light-producten zijn echte dikmakers.

14. Dat een zoekopdracht in literatuurzoeksystemen naar *rheological properties* vaak als resultaat *theological properties* oplevert kan mogelijk verklaard worden met het Deborah-getal dat genoemd is naar de gelijknamige profetes die zegt (Richteren 5: 5): "De bergen vloeiden weg voor den Heer...."

15. Promoveren hoeft niet Ir-rationeel te zijn, maar is wel ing-rijpend.

ing. William Kloek
Mechanical Properties of Fats in Relation to their Crystallization
Wageningen, 22 september 1998

Abstract

Kloek, W. (1998). Mechanical properties of fats in relation to their crystallization. Ph.D. thesis, Wageningen Agricultural University, Wageningen, The Netherlands. (pp. 241, English and Dutch summaries).

Keywords:
fat, triglycerides, crystallization, nucleation, fractal aggregation, rheology, sintering, particle networks, surface scraped heat exchanger.

Abstract:

Crystallization in bulk fats is always initiated by a heterogeneous nucleation process. Homogeneous nucleation conditions for fully hydrogenated palm oil (HP) in sunflower oil (SF) could be obtained by emulsifying the fat phase into very fine droplets and using sodium caseinate as an emulsifier. The crystallization kinetics of such a dispersion was determined by means of ultra sound velocity measurements and could be modeled by a classical nucleation model. The temperature dependency of the kinetics yielded a surface free energy for nucleus formation of about 4 $mJ \cdot m^{-2}$ and almost the whole triglyceride molecule should be in the right conformation for incorporation in a nucleus.

The isothermal crystallization kinetics of bulk solutions of HP in SF in the β' polymorph could be described well by combination of a classical nucleation function and an empirical crystal growth rate equation taking into account the decrease of supersaturation during crystallization. This yielded a surface free energy for heterogeneous nucleus formation of 3.8 $mJ \cdot m^{-2}$ and about 80 % of the triglyceride molecule to be in the right conformation for incorporation in a nucleus.

Fat crystals in oil exhibit Brownian motion and attract each other due to van der Waals attraction that results in dispersions with fat crystal aggregates. The structure of the fat crystal aggregates could be described well by a fractal approach as was shown by light scattering and modeling of the viscosity as function of shear rate. Low volume fraction HP/SF dispersion yielded fractal dimensionalities of about 1.7 - 1.8 which is indicative for rapid diffusion limited aggregation and increased with increasing shear rate. Volume fraction of solids of about 0.005 appeared to be sufficient to form a weak gel built from aggregates with a dimensionality of about 1.7 - 1.8.

Simultaneous crystallization and aggregation of high volume fraction HP/SF dispersion leads to compaction of aggregates after primary network formation. The elastic moduli of these dispersion can be described by higher apparent dimensionalities. Crystallization after gelation also makes the stress carrying strands less flexible and leads to sintering of the fat crystals. The latter occurred more easily for fats having a broad fatty acid distribution. Sintering of fat crystals was shown by comparison of elastic moduli and loss tangents before and the development of moduli after mechanical treatment. From model calculations, it was shown that for dispersions in which van der Waals forces are the only interaction forces, crystals can easily bend on deformation of the crystal network.

Application of shear during crystallization leads to more compact crystal aggregates as was shown by determination of elastic moduli in compression on dispersions that were crystallized in a surface scraping heat exchanger.

voor mijn ouders
voor Jeanine

Contents

1 INTRODUCTION **1**

1.1 FATS 2

1.1.1 Nutritional aspects *2*

1.1.2 Properties of fats *2*

1.2 CRYSTALLIZATION 6

1.2.1 Supersaturation *6*

1.2.2 Nucleation *8*

1.2.3 Crystal growth *10*

1.3 MECHANICAL PROPERTIES 11

1.3.1 Aggregation *11*

1.3.2 Rheological properties *12*

1.3.2.1 Small deformations 12

1.3.2.2 Large deformations 13

1.4 AIM AND APPROACH 14

1.5 REFERENCES 16

2 MATERIALS AND METHODS **19**

2.1 TRIGLYCERIDE COMPOSITION AND THERMAL PARAMETERS 20

2.2 OTHER PHYSICAL PROPERTIES 22

2.3 REFERENCES 22

3 CRYSTALLIZATION KINETICS OF EMULSIFIED TRIGLYCERIDE MIXTURES **23**

3.1 INTRODUCTION 24

3.1.1 Nucleation *24*

3.1.2 Nucleation kinetics *28*

3.1.3 Ultrasound velocity measurements *30*

3.2 MATERIALS AND METHODS 33

3.2.1 Materials *33*

3.2.2 Preparation of emulsions *33*

3.2.3 Pulsed NMR *34*

3.2.4 DSC *34*

3.2.5 Ultrasound velocity measurement *35*

3.3 RESULTS AND DISCUSSION 35

3.3.1 Pulsed NMR *35*

3.3.2 DSC *37*

3.3.3 Ultrasound velocity measurement *38*

3.3.3.1 Cooling heating cycles 38

3.3.3.2 Isothermal crystallization 41

3.3.4 Discussion of fit parameters and supercooling *48*

3.4 CONCLUSIONS 51
3.5 ACKNOWLEDGEMENTS 51
3.6 REFERENCES 52

4 CRYSTALLIZATION KINETICS OF FULLY HYDROGENATED PALM OIL IN SUNFLOWER OIL SOLUTIONS 53

4.1 INTRODUCTION 54
4.1.1 General *54*
4.1.2 Supersaturation *54*
4.1.3 Nucleation *55*
4.1.4 Crystal growth *57*
4.2 MATERIAL AND METHODS 60
4.2.1 Materials *60*
4.2.2 Methods *60*
4.3 RESULTS AND DISCUSSION 61
4.3.1 Thermal properties of fully hydrogenated palm oil *61*
4.3.2 Thermal properties of HP/SF mixtures *62*
4.3.3 Crystallization kinetics *66*
4.3.4 Aggregation times *73*
4.3.5 Crystal sizes after complete crystallization *75*
4.4 CONCLUSIONS 77
4.5 REFERENCES 77

5 STRUCTURE OF FAT CRYSTAL AGGREGATES IN LOW VOLUME FRACTION DISPERSIONS 79

5.1 INTRODUCTION 80
5.1.1 General *80*
5.1.2 Aggregation *80*
5.1.3 Viscometry *83*
5.1.4 Light scattering *86*
5.2 MATERIALS AND METHODS 87
5.2.1 Materials *87*
5.2.2 Methods *87*
5.3 RESULTS AND DISCUSSION 88
5.3.1 Viscometry *88*
5.3.2 Light scattering *96*
5.4 CONCLUSIONS 100
5.5 ACKNOWLEDGEMENTS 101
5.6 REFERENCES 101

6 STRUCTURE OF FAT CRYSTAL NETWORKS: MECHANICAL PROPERTIES AT SMALL DEFORMATIONS 103

Contents

6.1 INTRODUCTION 104
6.1.1 General *104*
6.1.2 Crystallization *104*
6.1.3 Aggregation *105*
6.1.4 Network models *108*
6.1.5 Particle interactions *113*
6.2 MATERIALS AND METHODS 117
6.2.1 Materials *117*
6.2.2 Methods *118*
6.2.2.1 Rheology 118
6.2.2.2 Permeability 119
6.3 RESULTS AND DISCUSSION 120
6.3.1 Elastic moduli during crystallization *120*
6.3.2 Elastic moduli as a function of volume fraction solids *124*
6.3.3 Permeability *131*
6.3.4 Interactions between fat crystals *132*
6.4 CONCLUSIONS 141
6.5 REFERENCES 142

7 LARGE DEFORMATION BEHAVIOUR OF FAT CRYSTAL NETWORKS 145

7.1 INTRODUCTION 146
7.1.1 General *146*
7.1.2 Fracture mechanics *146*
7.2 MATERIALS AND METHODS 149
7.2.1 Materials *149*
7.2.2 Methods *149*
7.3 RESULTS AND DISCUSSION 151
7.3.1 Compression *151*
7.3.1.1 Calculation of large deformation- and fracture parameters 151
7.3.1.2 Effect of fraction solids on parameters obtained from compression 154
7.3.2 Wire Cutting *159*
7.3.3 Comparison between compression and cutting experiments *162*
7.4 CONCLUSIONS 167
7.5 REFERENCES 168

8 MECHANICAL PROPERTIES OF FAT DISPERSIONS PREPARED IN A VOTATOR LINE 169

8.1 INTRODUCTION 170
8.1.1 General *170*
8.1.2 Mechanical Properties *171*
8.1.3 Votator Line *172*

8.2 MATERIALS AND METHODS 173
8.2.1 Materials *173*
8.2.2 Crystallization in votator *173*
8.2.3 Analysis *175*
8.2.3.1 Crystallinity 175
8.2.3.2 Mechanical properties 175
8.3 RESULTS 176
8.3.1 Crystallization *176*
8.3.2 Mechanical properties *179*
8.3.2.1 Penetration depths 179
8.3.2.2 Compression tests 182
8.3.3 General discussion *187*
8.4 CONCLUSIONS 190
8.5 REFERENCES 191

9 GENERAL DISCUSSION AND CONCLUSIONS **193**

9.1. GENERAL DISCUSSION 194
9.1.1 Introduction *194*
9.1.2 Crystallization of HP/SF dispersions *195*
9.1.2.1 Thermal behavior 195
9.1.2.2 Nucleation 196
9.1.2.3 Crystallization kinetics 199
9.1.3 Structure of fat crystal aggregates in HP/SF dispersions *202*
9.1.3.1 Aggregation of crystals in low volume fraction dispersions 202
9.1.3.2 Aggregation of crystals in high volume fraction dispersions 203
9.1.3.3 Interactions between fat crystals 206
9.1.3.4 Large deformation properties of fat crystal dispersions crystallized in shear 207
9.1.4 Comparison between butter, margarine and the model system *213*
9.1.5 Applicability to margarine production *215*
9.2. CONCLUSIONS 216
9.3. REFERENCES 217

LIST OF SYMBOLS AND ABBREVIATIONS **219**

SUMMARY **227**

SAMENVATTING **233**

DANKWOORD **239**

CURRICULUM VITAE **241**

Chapter 1

Introduction

1.1 Fats

1.1.1 Nutritional aspects

Fats are important suppliers of energy and essential fatty acids in the human diet. Besides direct supply of energy and essential fatty acids, fats are important as carriers of fat-soluble vitamins. For a daily energy intake of less than 12.5 MJ, it is recommended that this is supplied for at least 25 % by fats. For a daily energy intake of more than 12.5 MJ, this should be at least 30 %. The recommended intakes correspond to 56 - 140 g fat·day^{-1} (Harwood *et al.* (1986)). The energy value of fats is about 38 kJ·g^{-1}, which is much higher than the energy values for proteins (17 kJ·g^{-1}) or for polysaccharides (16 kJ·g^{-1}) (Gurr (1995)). Nowadays, in western countries fats provide up to 40 % of the daily energy intake. These high fat intakes can lead to obesity and coronary heart disease, the latter being an important cause of death in most industrialized countries.

Besides a decrease in fat consumption, it is often considered desirable to change the nature of the fat intake. There are guidelines that advise to lower the consumption of fats containing (long) saturated fatty acids (C12-C16) and *trans* unsaturated fatty acids (Lambertsen (1992)). It should be stressed that there is no clear evidence for a decrease in mortality if the intake of fats containing saturated fatty acids and *trans* unsaturated fatty acids is decreased without a decrease of the total fat intake (Harwood *et al.* (1986)) and possibly also for constant total fat intake.

The change in the fatty acid patterns of fats has important consequences for the melting properties of the fats, specially melting temperature and melting enthalpy. This has important consequences for those food products in which fats give the product desired, structural properties.

1.1.2 Properties of fats

Fats and oils belong to the class of compounds called lipids, to which also belong alkanes, soaps, fatty acids, sterols, carotenoids, methyl esters of fatty acids and various polar lipids, including phospholipids. An important property of lipids is that they are soluble in non-polar organic solvents and (almost) insoluble in aqueous solutions.

Fats in the liquid state are termed oils, while when in a partially solid state, they are called fats. We will use the word fat to indicate both the crystals and a mixture of crystals in oil. Whether we have a fat or an oil depends on the temperature.

From a chemical point of view, fats and oils consist of triesters of the triol glycerol, and they are called triacylglycerols or triglycerides (Figure 1-1). The carboxylic acids that are esterified are the fatty acids. Natural fats and oils contain almost exclusively consist of fatty acids with an even number of carbon atoms since they are biosynthesized by sequential addition of acetyl compounds.

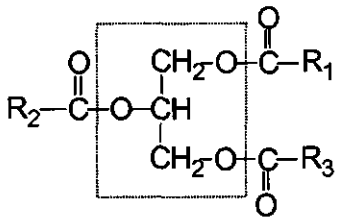

Figure 1-1. *Structure of a triacylglycerol. The dotted box indicates the glycerol residue while R_1, R_2 and R_3 are the fatty acid carbon chains.*

Chemical constitution and the position of fatty acids residues determine the thermal behaviour of a triglyceride. The fatty acids can differ in carbon chain length, number of unsaturated bonds and the type of unsaturated bonds (*cis/trans*).

Triglycerides can be identified on the basis of their fatty acid composition by using a 3-letter-code. The first letter identifies the fatty acid esterified at the 1-position and so on. We will use the fatty acid codes as given in the thesis of Wesdorp (1990) (Table 1-1). For example, the code PSP represents the triglyceride glycerol-1,3-dipalmitate-2-stearate.

Table 1-1. *Coding of fatty acids after Wesdorp (1990)*

Code	fatty acid	Code	fatty acid
C	Capric acid (decanoic acid)	O	Oleic acid (*cis*-9-octadecenoic acid)
L	Lauric acid (dodecanoic acid)	E	Elaidic acid (*trans*-9-octadecenoic acid)
M	Myristic acid (tetradecanoic acid)	l	Linoleic acid (*cis-cis*-9,12-octadecadienoic acid)
P	Palmitic acid (hexadecanoic acid)	A	Arachidic acid (eicosanoic acid)
S	Stearic acid (octadecanoic acid)	B	Behenic acid (docosanoic acid)

Cocoa butter contains high amounts of POP, POS and SOS while palm oil contains high amounts of POP, POO and PPP. Sunflower oil and soy oil contains high amounts of lll, llO, llS, lOO and lSS. Rapeseed oil contains high levels of the long fatty acid erucic acid (*cis*-13-docosanoic acid). Most natural fats consist of hundreds of different triglycerides. For use in foods and other products, vegetable oils are often (partially) hydrogenated to yield fats with a special melting behaviour. For example, hydrogenation of palm oil yields high amounts of PSP and PSS that have higher melting temperatures than POP and POO, which are present in palm oil. For margarine production, fat blends are used that consist of both hydrogenated fats and natural fats to obtain such a melting profile that at mouth temperature no solid fat is left.

Besides the important property of lipids that they are soluble in non-polar organic solvents, another important characteristic is that they can crystallize in various crystal modifications. For SSS this was first observed by Heintz (after Hagemann (1988)) who observed melting at 52 °C, and

subsequently on heating saw re-solidification and melting at 62 °C. Duffy showed the existence of 3 melting temperatures for SSS at 52, 64 and 70 °C (after Hagemann (1988)). Evidence for the existence of 3 basic crystal forms was given by X-ray diffraction spectra (Lutton (1950), Malkin (1954)) and became more clear by correlation of X-ray spectra and infrared spectroscopic observations (Chapman (1962)). Later, more fundamental structural studies on polymorphism of triglycerides were carried out after 1964 by Larsson (1986), Hernqvist (1984) and de Jong (1980).

Table 1-2. *Classification of polymorphic modification of monoacid triglycerides based on X-ray diffraction and infrared absorption (Hagemann (1988)). s = strong line, β_1' and β_2' are sub-modifications of the β' polymorph*

polymorphic modification	Unit cell	short spacings from X-ray diffraction lines (nm)	Infrared absorption wavenumbers (cm^{-1})
α	hexagonal	0.415 (s)	720
β'	orthorhombic	0.38 (s), 0.42 (s)	719 and 726 (β_1'), 719 (β_2')
β	triclinic	0.455 (s), 0.36-0.39	717

The three basic modifications are the α, β' and β polymorphs and are classified on bases of the short spacings in the X-ray diffraction spectra and absorptions in the infrared spectra (Table 1-2). Although there exist sub-modifications in the β' and β polymorphs, the use of only the 3 basic polymorphs is sufficient in this thesis.

The existence of polymorphs is the result of the possibility to pack the long hydrocarbon chains in various ways. Only one polymorph is the most stable one, generally the β polymorph, which implies monotropic polymorphism. The stability generally increases in the order of α to β' to β.

The α polymorph is very unstable and is normally only present during processing of fats, thus on a time scale of minutes or less. However, in milk fat the α polymorph can be present over very long times (over years) due to the wide triglyceride composition. The crystal packing of the α polymorph is fairly loose and the aliphatic chains have some rotational freedom. The β' polymorph is more densely packed and is often desired during storage of fatty food products. Depending on the triglyceride composition of the fat, this polymorph can be stable over a period of years. The β polymorph is the most densely packed and is normally not desired in food products or more specific in margarine since the slow formation of this polymorph is often accompanied by sandiness of the product. For fractionation of fats, the β polymorph is often desired due to formation of large spherulitic crystal structures which can easily be separated from the mother liquor and are well washable. It is not always clear whether polymorphic transitions occur via the liquid or the solid state. Figure 1-2 shows a schematic representation of the possible polymorphic transitions.

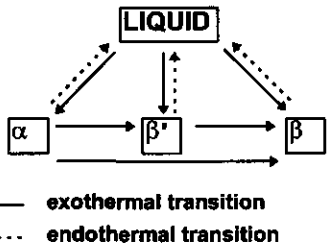

Figure 1-2. *Possible transitions between the liquid state and the various polymorphic modifications of triglycerides (common case).*

For pure triglycerides the melting temperature and the melting enthalpy increase in the order α to β' to β. The melting temperature of the α polymorph of monoacid saturated triglycerides increases smoothly with increasing fatty acid chain length. Also for the β' and the β polymorph the melting temperature increases with fatty acid chain length although there is a zigzag pattern for odd- and even fatty acid chain lengths with the latter having higher melting temperatures (Hagemann (1988)). Melting enthalpies of monoacid saturated triglycerides are described rather well by parabolic equations with a maximum at a fatty acid chain length of 22 carbon atoms for the α polymorph, about 24 carbon atoms for the β' polymorph and even higher for the β polymorph (Hagemann (1988)).

For unsaturated monoacid triglycerides both melting temperature and melting enthalpies are lower than for the saturated monoacid triglycerides of the same fatty acid chain lengths. The melting temperatures and melting enthalpies for *cis*-unsaturated monoacid triglycerides are lower than for the *trans*-equivalent.

The description of the polymorphic behaviour of fat blends is greatly hampered due to the great number of different triglycerides, which can lead to the formation of compound crystals. They can form solid solutions, in which the different triglycerides can be present in all proportions, or the composition can be restricted, dependent on the triglyceride composition of the fat blend. Compound crystal formation readily occurs in the α polymorph since the packing in this polymorph is not very dense so that different molecules can fit the same lattice. Compound crystal formation also occurs in the β' polymorph but since the crystal lattice is more dense, it is restricted to groups of similar triglycerides. In the β polymorph, compound crystal formation only occurs for very similar triglycerides in restricted compositional ranges.

Calculation of phase diagrams of binary systems from thermodynamic solution theory is possible for the β' and β polymorphs (Wesdorp (1990)), but for systems containing more than 2 compounds it is hardly possible to calculate the phase diagrams. In multi-component systems it is often possible to treat a group of similar triglycerides as an one component system.

Consequences of the occurrence of compound crystallization are (Walstra *et al.* (1995)):

- Narrowing of the melting range

- The predominant melting temperature of a fat depends on the crystallization temperature.
- Stepwise cooling or very slowly cooling of a liquid fat leads to less solid fat than rapid cooling to the same final temperature.
- Unstable polymorphs persist much longer. For instance in milk fat, the α polymorph can be present for years.

After and even during the primary crystallization of fats, recrystallization occurs since the crystallized dispersions are far from thermodynamic equilibrium. Various changes can occur (Walstra *et al.* (1995)):

- Change in the composition of compound crystals. This can lead to a change in the number of melting peaks and/or narrowing of these peaks, as determined by DSC (Differential Scanning Calorimetry).
- Polymorphic transitions of unstable polymorphs to more stable polymorphs.
- Occurrence of Ostwald ripening: regions of the crystals with small radii of curvature have such high solubilities that they dissolve and recrystallize to regions with higher radii.

Polymorphic transitions are accompanied by a change in composition of compound crystals and a decrease of the fraction solid fat.

1.2 Crystallization

1.2.1 Supersaturation

The primary crystallization process can be divided in nucleation and crystal growth. Both processes can only occur if the triglycerides or, a part of them, are supersaturated. A solution is supersaturated if the solubility of a component is smaller than the amount present. For ideal mixtures, the solubility x_x of compound x expressed as mole fraction at absolute temperature T is given by (Wesdorp (1990)):

$$\ln x_x = \frac{\Delta H_{f,i}}{R_g} \cdot \left(\frac{1}{T_{m,i}} - \frac{1}{T} \right) \qquad \textbf{(1-1)}$$

where R_g the gas constant, $\Delta H_{f,i}$ is the molar enthalpy of fusion of the crystallizing component of polymorph i and $T_{m,i}$ the absolute melting temperature of the crystallizing component of polymorph i. This equation can be used to calculate the solubility of a high melting triglyceride in oil, like SSS in OOO, but can also be used to calculate the solubility of a high melting composite fat, like a fully hydrogenated fat in composite oil.

The driving force for crystallization is the difference in chemical potential, $\Delta\mu$, between a supersaturated solution (fraction dissolved c_x) and a saturated solution (fraction dissolved x_x), and is for ideal solutions given by:

$$\Delta\mu = R_g T \cdot \ln\frac{c_x}{x_x} = R_g T \cdot \ln\beta \qquad \textbf{(1-2)}$$

where β is called the supersaturation ratio and $\ln\beta$ the supersaturation.

Figure 1-3 shows iso-$\ln\beta$ lines as function of temperature and the fraction dissolved component for the model system used in this thesis. The solid phase consisted of fully hydrogenated palm oil (HP) and the oil phase was sunflower oil (SF). The iso-$\ln\beta$ lines for the α- and β' polymorph are calculated from Equations 1-1 and 1-2.

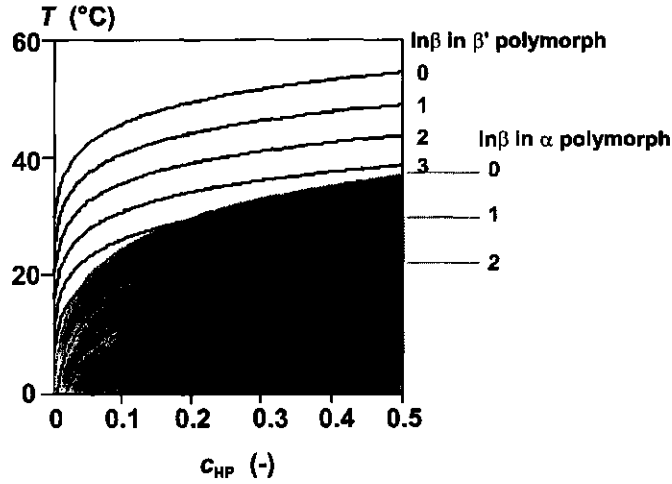

Figure 1-3. *Iso-$\ln\beta$ curves of HP/SF dispersions in the α- and the β' polymorph as function of temperature (T) and fraction HP (c_{HP}) calculated from Equations 1-1 and 1-2. Solid lines refer to the β' polymorph and dashed lines correspond to the α polymorph. The dashed region is supersaturated in both α- and β' polymorph.: $T_{m,\alpha}$ = 41.8 °C, $\Delta H_{f,\alpha}$ = 98 kJ·mol^{-1}, $T_{m,\beta'}$ = 57.3 °C, $\Delta H_{f,\beta'}$ =161 kJ·mol^{-1}.*

Figure 1-3 shows that the maximum initial $\ln\beta$ that can be obtained in the β' polymorph before the α polymorph becomes supersaturated, depends on the fraction material dissolved. A solution with c_{HP} = 0.20, that has crystallized isothermally at a temperature of 20 °C, is initially supersaturated in the α polymorph. As crystallization proceeds, the fraction dissolved decreases and at a certain moment the α polymorph is not supersaturated anymore and crystallization can only take place in the β' polymorph. Whether crystallization in the β' polymorph indeed occurs also

depends on the kinetics of the crystallization process; Figure 1-3 is based on equilibrium thermodynamics.

1.2.2 Nucleation

In this thesis, the classical nucleation theory will be used, although this theory nowadays is considered not to be right. Statistical models would be more appropriate, but are mathematically too complex to be used for ill-defined triglyceride mixtures.

Nucleation is the formation of ordered crystal regions on a molecular scale, with sizes that are large enough not to dissolve. For a given supersaturation, this critical size r^* of an assumed spherical crystal is given by the Kelvin equation:

$$r^* = \frac{2 \cdot \gamma \cdot \bar{V}}{\Delta \mu} \tag{1-3}$$

where γ is the surface free energy between nucleus and mother phase and $\bar{V}$ the molar volume of the material in the crystalline state. The critical size can be calculated by equating Equation 1-3 and 1-2. For a supersaturation of 3 in the β' polymorph at $T = 298$ K, $\gamma = 4$ mJ·m^{-2} and $\bar{V} = M/\rho \approx 0.86/1000 = 8.6 \cdot 10^{-4}$ m^3·mol^{-1} this would yield a critical radius r^* of about 0.9 nm. This would correspond to about 3 molecules in a nucleus of critical size. This order of magnitude calculation shows that the nuclei are very small, too small to apply any macroscopic theory on the formation of nuclei.

The activation free energy ΔG^*_{3D} for formation of a spherical nucleus with critical size is given by (Garside (1987)):

$$\Delta G^*_{3D} = \frac{16\pi \cdot v_c^{\,2} \cdot \gamma^3}{3 \cdot (k_b T \cdot \ln \beta)^2} \tag{1-4}$$

where v_c is the molecular volume in a crystal lattice and k_b the Boltzmann constant. Increase of supersaturation will lead to a smaller critical nucleus size and a smaller activation free energy for nucleus formation. The nucleation rate J, the number of nuclei formed per unit time and per unit volume, is according classical nucleation theory, written as an Arrhenius type of equation (Garside (1987))

$$J = J_{max} \cdot \exp\left(\frac{-\Delta G^*}{k_b T}\right) \tag{1-5}$$

where J_{max} is the maximum nucleation rate. J_{max} would depend on the maximum molecular collision frequency, which is often given by $k_b T/h$, with h the Planck constant. Furthermore, J_{max} would depend on the configuration of the nucleating molecules. For triglycerides, the long aliphatic chains

have to be in a suitable conformation that leads to an strong decrease of entropy. For a given system J_{max} will be constant. The nucleation rate will be strongly dependent on ΔG_{3D}^* and therefore strongly dependent on $\ln\beta$ and γ.

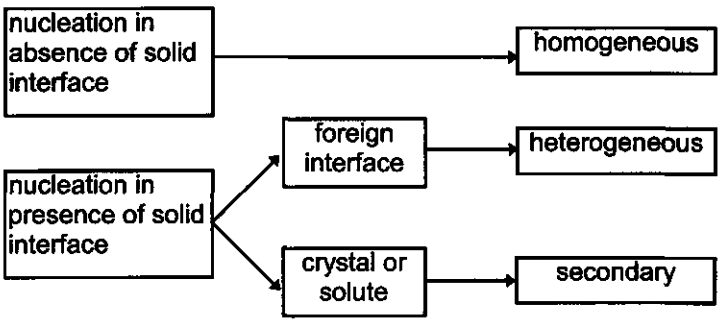

Figure 1-4. *The various types of nucleation (Garside (1987))*

Several types of nucleation can be distinguished (Figure 1-4). If not catalyzed by the presence of triglyceride crystals or foreign solid surfaces, nucleation is called homogeneous. In the case of homogeneous nucleation of triglycerides, supercooling up to 30 K can be applied before crystallization occurs. This type of nucleation only occurs if the fat is divided in such small volumes that on average no foreign particle (catalytic impurity) per droplet is present. Since the supercooling needed for homogeneous nucleation is so high, homogeneous nucleation of triglycerides always takes place in the α polymorph.

If catalyzed by foreign particles, nucleation is called heterogeneous. The activation free energy for heterogeneous nucleus formation is lowered due to chemical or physical affinity of the nucleus for the foreign particle. A consequence of this affinity is the lower supercooling needed to initiate crystallization. This can be quantitatively expressed by a contact angle between the nucleus and the foreign surface, which is determined by the interfacial free energies between the nucleus, foreign surface and the mother phase.

Supercooling of only 1 - 3 K is needed to initiate crystallization of triglycerides on time scales of seconds to minutes. Secondary nucleation is catalyzed by the presence of a crystal surface of the crystallizing component and can therefore only occur after primary homogeneous or heterogeneous nucleation and subsequent crystal growth. The occurrence of secondary nucleation in triglycerides has been shown by Walstra and van Beresteyn (1975) who demonstrated the presence of numerous crystals in an emulsified triglyceride droplet that had crystallized under such homogeneous nucleation conditions that only one or two crystals per droplet were expected. The mechanism of secondary nucleation in triglycerides is not clear. A possible explanation is the existence of very ordered layers near the crystal surface and less ordered layers somewhat further away from the

crystal surface. Due to such ordering, nucleation becomes easier. Both heterogeneous nucleation and secondary nucleation are believed to dominate in bulk fats.

1.2.3 Crystal growth

After nuclei are formed, they grow by the addition of molecules to the crystal face(s). Garside (1987) and Boistelle (1988) give general reviews about this subject. The state of the crystal surface is an essential parameter in describing the crystal growth rate G_c. The growth rate of rough crystal faces is about proportional to the (local) supersaturation. Growth units can easily attach to kinks on the surface and growth is continuous. This type of growth occurs at high supersaturations. The growth of flat surfaces occurs by a layer after layer mechanism. On the flat surface, first a surface nucleus with critical size has to be formed. To this nucleus, growth units can attach thereby forming a flat surface. In this growth model, G_c is proportional to the surface nucleation rate which depends on the activation free energy for formation of surface nucleus. Therefore, the G_c of a flat surface would be an exponential function of supersaturation. Layer growth mechanisms occur at low supersaturations. Crystal growth rates depend, besides on the state of the crystal surface, on factors like viscosity, conformation of molecules, surface defects, presence of impurities, shear rates and so on.

Theoretically, crystal growth rates are proportional to the supersaturation if it is high and proportional to supersaturation at a power higher than 1 if it is low. Skoda and Van den Tempel (1967) also found these proportionalities for the growth of pure triglycerides in oil. Apart from this study, hardly any growth rates for triglycerides have been reported in the literature. Therefore, it is difficult to model crystal growth rates for fats, especially for systems containing many different molecules, like in a fat blend. If both nucleation rate and crystal growth rate are known as a function of supersaturation, it is, in principle, possible to model the crystal size distribution as a function of time. From this distribution, the fraction of crystallized material can be obtained as function of time. In the case of spherical crystals, a constant crystal growth rate and a constant nucleation rate (so at a constant supersaturation), the volume fraction of solids ϕ as a function of time t is given by Avrami's equation (1939a,b)

$$\phi = \frac{1}{3}\pi \cdot G_c^{\,3} \cdot J \cdot t^4 \qquad \textbf{(1-6)}$$

where it is assumed that no impingement or aggregation of crystals occurs.

1.3 Mechanical properties

1.3.1 Aggregation

Fat crystals in oil attract each other by van der Waals-forces. The only repulsive interaction is hard-core repulsion, which acts only at very small separation distances. The fat crystals aggregate due to the attractional forces and form voluminous aggregates. These aggregates can grow so far that they form a continuous network or a gel. The time $t_{0.5}$ needed to half the initial number of particles c_0 due to collisions by Brownian movement is, for spherical particles given by:

$$t_{0.5} = \frac{\pi \cdot \eta_0}{4 \cdot k_b T \cdot c_0} \tag{1-7}$$

where η_0 is the viscosity of the continuous phase. The flocculation time $t_{0.5}$ is an indication for the time scale over which aggregation takes place. For a dispersion having a volume fraction particles ϕ_0 of 0.01, a particle radius of 0.1 μm and assuming η_0 = 60 mPa·s (viscosity of oil at room temperature, T = 298 K) yields a flocculation time of about 4.5 s. In reality, fat crystals have anisometric shapes, and Equation 1-7 will therefore only give a rough estimate of the time scale of aggregation.

A complicating factor in describing the aggregation of a crystallizing system is that both the mass fraction of particles and the particle size increase in time. Depending on the nucleation rate and the crystal growth rate, early in the crystallization process the time scale of aggregation already becomes shorter than the time scale of crystallization. A consequence of simultaneous crystallization and aggregation is that at a low fraction of crystallized fat already a continuous network is formed, while still a substantial amount of fat has to crystallize. This generally leads to sintering *i.e.* the formation of solid bridges between aggregated crystals and aggregates.

Random aggregation of monodispersed spherical particles leads to aggregates of a fractal nature (Meakin (1984)). The number of particles with radius a in an aggregate of radius R is then given by:

$$N_p = \left(\frac{R}{a}\right)^D \tag{1-8}$$

where D is the fractal dimensionality, a measure for the compactness of an aggregate. The compactness increases with increasing D. In the case of perikinetic aggregation (Brownian motion), it would result in a dimensionality of 1.8. Higher D values are obtained if repulsion between the particles is present or if the aggregates are grown under shear (Family and Landau (1984)).

Since the number of volume elements in a spherical aggregate scales with $(R/a)^3$, the volume fraction of particles in a fractal aggregate is given by:

$$\phi_{int} = \left(\frac{R}{a}\right)^{D-3} \quad (1\text{-}9)$$

This equation shows that the internal volume fraction of an aggregate decreases on aggregate growth. At the moment that ϕ_{int} equals the volume fraction of primary particles in the system, a gel is formed.

For SSS (0.5 %) crystal aggregates in olive oil, a D of 1.7 was determined by means of light scattering (Vreeker *et al.* (1992)). This dimensionality should be considered as an apparent dimensionality since crystallization and aggregation step during preparation of the aggregates occurred simultaneously.

1.3.2 Rheological properties

1.3.2.1 Small deformations

The rheological properties of fats are primary determined by the fraction of crystallized fat. Papenhuijzen (1971) observed a shear modulus G proportional to the power 4 of the volume fraction solid. Low fractions yield a soft, spreadable product while a high fraction can yield a hard, brittle product. A consumer normally desires a product that is spreadable at both room temperature and refrigerator temperature and that completely melts in the mouth. Therefore, a specific melting range of the fat is required.

Another important factor that determines the rheological properties is the interaction between the crystals. Initially, crystals are aggregated due to van der Waals attraction. Deformation of a network that consists of undeformable crystals aggregated by van der Waals attraction, leads to an enlargement of the separation distance between the crystals. However, if the crystals are sintered due to simultaneous crystallization and aggregation or due to recrystallization, the crystals have to bend on deformation of the network. In this case the elasticity modulus depends on the bending modulus of the crystals. Bending of crystals can also be important for non-sintered dispersions if the crystals are long and thin. When moving the aggregated crystals away from each other from the situation where the net van der Waals forces are zero, the van der Waals attractional force initially increases. This force can be sufficient to deform the crystals to large bending deformations, which are dependent on the size, shape and bending modulus of the crystals.

The geometric arrangement of the crystals and the aggregates is also an important factor in determining the elasticity moduli. The first presented network models assumed the crystals to be arranged in linear chains in 3 perpendicular directions in which every particle contributed to the elastic modulus (van den Tempel (1961), Nederveen (1963)). A later model of Papenhuijzen (1971) assumed that not every particle contributed to the modulus. He assumed the network to be built of compact crystal clusters connected by linear crystal chains. According to his calculations, for a 8 % SSS in olive oil dispersions only 4 % of the solid fat was elastically effective.

The effectiveness of the solid fat to form a network with a high elastic modulus can also be described by assuming that the network is built of fractal aggregates. The elastic modulus of a network of fractal aggregates is given by the general equation (Bremer *et al.* (1990), Bremer (1992)):

$$G = A \cdot \phi^{\frac{x}{3-D}} \qquad \textbf{(1-10)}$$

where A is a constant related to the interparticle interaction and x is a constant that is related to the geometry of the stress-carrying strands. Factor x may vary from 2 for linear stress-carrying strands to 4.3 for stress-carrying strands having a fractal geometry. So for $D = 1.7$ this equation can explain scaling exponents between elastic moduli and volume fraction solids varying from 1.5 for $x = 2$ to 3.3 for $x = 4.3$.

From the concentration dependency ($G \propto \phi^{4.1}$) of the elastic moduli of SSS in paraffin oil dispersions observed by Papenhuijzen (1971), Vreeker *et al.* (1992) calculated a dimensionality of 1.95 assuming $x = 4.3$. These dispersions had first crystallized and were afterwards diluted with paraffin oil to the desired volume fraction. This separates the crystallization step from the aggregation step.

From unpublished data of Hoekstra and van den Tempel (1964), it was shown that the yield stress σ_y scaled with ϕ to a power of 3.6. This exponent can be explained by the stretching of the stress-carrying strands on deformation up to the yield deformation. The stretching results in a lower x value. Assuming the dimensionality of the aggregates to be 1.95, as calculated by Vreeker *et al.* (1992) for $x = 4.3$, an exponent of 3.6 corresponds to $x = 3.8$ which is lower than 4.3.

Applying fractal aggregate theories to explain relations between G and ϕ of dispersions that already aggregate during crystallization is far from straightforward, since a substantial fraction fat may still crystallize after a gel is formed. This may lead to compaction of the aggregates. On the other hand, fractal aggregate theories may provide important information about the structure of fat crystal networks.

1.3.2.2 Large deformations

Small deformation experiments yield information about the structure of the network and about interaction forces between the structural elements. For fat dispersions these properties have to be determined at very small deformations; otherwise, the structure is irreversibly affected. The linear region of deformation of fat crystal networks is smaller than 0.001, and the network structure can be affected at higher deformations.

Large deformation experiments yield information about important quality characteristics, which are relevant to processing, handling and eating. An important property for margarines is spreadability. During spreading, the crystallized network is subjected to large deformations and high

velocity gradients. This causes the fracture of sintered crystal bonds at certain length scales and rearrangement of the network structure. If fats are mechanically worked, the modulus of elasticity as measured within the linear region, decreases. The percentual decrease of this modulus is often called the work softening.

The theory of fracture mechanics is a powerful tool to understand the fracture behavior of various types of materials. It can give information about the type of the bonds and the structural elements involved in the fracture process. The theory of fracture mechanics assumes that all materials are inhomogeneous and/or have defects. These inhomogeneities or defects are the starting point for fracture because on deformation of the material stress is concentrated at these points. If the local stress at these points is higher than the bond strength, fracture can start. If the differential deformation energy that is released due to ongoing fracture is equal to or higher than the differential energy that is needed to create the new surfaces, fracture can propagate (Gordon (1978)).

The simplest form of fracture mechanics is linear elastic fracture mechanics (LEFM) which assumes that the amount of energy that is dissipated due to flow can be neglected. So LEFM assumes that all the stored deformation energy is available for creation of new surfaces. However, many food products are visco-elastic so that the amount of energy that is dissipated has to be taken into account. If the flow is limited to the region were fracture occurs, fracture parameters can be determined using elastic plastic fracture mechanics (EPFM). Fracture mechanics theory has been successfully applied to explain the fracture properties of cheese (Luyten (1988)) although it is more complicated for such a truly visco-elastic material.

It is likely that these theories are also useful in describing the fracture or yielding properties of fat crystal networks. If a sintered fat crystal network is deformed, most of the deformation energy will be stored in the crystal chains. Some flow of oil through the pores of the network may occur but this dissipation will be neglectable compared to the amount of energy stored. However, if fracture occurs between aggregates, energy may also be dissipated due to friction between aggregates.

The importance of energy dissipation on fracture of fat crystal networks is also shown when, for instance, a fully hardened fat that hardly contains any oil, is fractured. The fracturing is accompanied by a loud popping noise. This sound is the result of a shock wave caused by very fast crack growth due to the release of stored deformation energy, without energy being dissipated in viscous flow or friction. If a margarine, which contains about 20 % solid fat, is spread, no sound is heard, indicating that much of the energy is dissipated by oil flow or friction between aggregates.

1.4 Aim and approach

The purpose of this work is to study the small and large deformation behavior of crystallized fat dispersions and to relate the resulting mechanical properties to the crystallization conditions of

the fat. The fat system studied is a mixture of fully hydrogenated palm oil (HP) in sunflower oil (SF). This system can be considered as a model system for fat blends that are used for margarine manufacturing.

chapter 3: The nucleation kinetics of the system are studied by determining the crystallization kinetics of emulsified model systems. From the conditions at which homogeneous nucleation occurs it is possible to estimate the surface free energy of a nucleus and the part of a triglyceride molecule that should be in the right conformation for incorporation in a nucleus. From the kinetics of heterogeneous nucleation it is possible to calculate the concentration of catalytic impurities.

chapter 4: The crystallization kinetics of the bulk model system at various initial supersaturations and various fractions of crystallizable solid fat yields information about the amount of solid fat and the average crystal size in time. The surface free energy for nucleus formation and the part of a triglyceride molecule that should be in the right conformation for incorporation in a nucleus as obtained from nucleation kinetics can be used to estimate nucleation rates. Together with determined crystallization curves, it is possible to model crystal growth rate as function of time and thus as function of supersaturation.

chapter 5: The structure of fat crystal aggregates can be studied well at low volume fractions of solid fat ($\phi < 0.01$) since at these volume fractions it is possible to separate the crystallization and aggregation processes. Suitable techniques for studying the aggregate structure are viscometry (determination of volume fraction of aggregates as function of shear rate) and light scattering (determination of D by measuring the scattered intensity as function of scattering angle). From the viscosities, the interaction force between primary particles can be estimated.

chapter 6: By measuring the elastic moduli at small deformations as a function of the volume fraction of solid fat ($0.06 < \phi < 0.14$) of dispersions that had crystallized in the rheometer, it is possible to determine the aggregate structure of a dispersion in which crystallization and aggregation proceeded simultaneously. This structure can be related to the structure obtained for dispersions in which the aggregation and crystallization processes are separated.

Frequency spectra of fat dispersions containing a solid phase that is expected to sinter (HP) or a solid phase that is expected to show hardly any sintering (PPP) can give information about the type of interaction between the structural elements and the extent of relaxation occurring at various time scales.

chapter 7: Compression and wire cutting experiments give information about large deformation properties of fat dispersions such as spreadability. These properties are important for the consumer perception of a product. By combination of the results of both type of experiments, it is possible to calculate the defect size. Defects are those inhomogeneities (tiny cracks) in the structure where yield or fracture starts.

chapter 8: Since fats are generally crystallized in a votator line under high shear conditions in practice, the model system was processed in a votator. The properties of the crystallized products were determined by compression tests and penetrometer tests.

chapter 9: The results presented and discussed in the previous chapters are compared, interrelated and discussed and an overview of the variables that determine the mechanical properties of a plastic fat is given.

1.5 References

Avrami, M. (1939a), Kinetics of Phase Change. I- General Theory, *J. Chemical Physics* **7**, 1103

Avrami, M. (1939b), Kinetics of Phase Change. II- Transformations - time relations for random distribution of nuclei, *J. Chemical Physics* **8**, 212

Boistelle, R. (1988) Fundamentals of nucleation and crystal growth, In *crystallization and polymorphism of fats and fatty acids*, Eds: N. Garti, K. Sato, Marcel Dekker, New York

Bremer, L.G.B. (1992) *Fractal aggregation in relation to formation and properties of particle gels*, Ph.D. Thesis, Agricultural University Wageningen, the Netherlands

Bremer, L.G.B., Bijsterbosch, B.H., Schrijvers, R., Vliet, van T and Walstra, P. (1990) On the fractal nature of the structure of acid casein gels, *Colloids and Surfaces* **15**, 159

Chapman, D. (1962) The polymorphism of glycerides , *Chem. Rev.***62**, 433

Family, F. and Landau, D.P. (Eds.) In *"Kinetics of aggregation and gelation"*, Elsevier, Amsterdam/New York

Garside, J. (1987) General principles of crystallization, In *Food structure and behaviour*, Eds: J.M.V. Blanshard, P. Lillford, Academic press, London, pg. 51

Gordon, J.E. (1978) *Structures, or why things don't fall down*, Penguin

Gurr, M.I. (1995) Nutritional significance of fats, In *Advanced dairy chemistry volume 2 Lipids 2nd ed.* Ed P.F. Fox, Chapman and Hall, London, pg. 349-402

Hagemann, J.W. (1988) Thermal behavior and polymorphism of acylglycerides, In *Crystallization and polymorphism of fats and fatty acids*, Eds. N. Garti, K. Sato, Marcel Dekker, New York, pg. 9-96

Harwood, J.L., Cryer, A. and Gurr, M.I. (1986) Medical and agricultural aspects of lipids, In *The lipid handbook*, Eds F.D. Gunstone, J.L. Harwood and F.D. Padley, Chapman and Hall, London, pg.527

Hernqvist, L (1984) *Polymorphism of fats*, PhD Thesis, University of Lund, Sweden

Hoekstra, L.L. and Tempel, van den M. (1964), unpublished results

Jong, de S. (1980) *Triacylglycerol crystal structures and fatty acid conformation*, Ph.D. Thesis, State University of Utrecht, The Netherlands

Lambertsen, G. (1992) Trans fatty acids topic for lipid forum, *Inform* **3**, 196

Larsson, K. (1986) Physical properties - structural and physical characteristics -, In *The lipid handbook*, Eds F.D. Gunstone, J.L. Harwood, F.D. Padley, Chapman and Hall, London, pg.321-384

Lutton, E.S. (1950) , *J.Am.Oil Chem.Soc.* **27**, 276

Luyten, H. (1988) *The rheological and fracture properties of Gouda cheese*, Ph.D. thesis Wageningen Agricultural University, the Netherlands

Malkin, T. (1954) The polymorphism of glycerides , *Prog. Chem Fats other Lipids* **2**, 1-50

Meakin, P. (1984) Diffusion-controlled aggregation on 2-dimensional square lattices, *Phys. Rev. B*, **29**, 2930

Nederveen, C.J. (1963) Dynamical mechanical behaviour of of suspensions of fat particles in oil, *J. Colloid Sci.* **18**, 276

Papenhuizen, J.M.P. (1971) Superimposed steady and oscillatory shear in dispersed systems, *Rheol. Acta* **10**, 493

Skoda, W. and Tempel, M. van den (1967) Growth kinetics of triglyceride crystals, *J. Crystal Growth* **1**, 207

Tempel, van den M. (1961) Mechanical properties of plastic-disperse systems at very small deformations, *J. Colloid. Sci* **16**, 284

Vreeker, R., Hoekstra, L.L., Boer, den D.C. and Agterof, W.G.M. (1992) The fractal nature of fat crystal networks, *Colloids Surf.* **65**, 185.

Walstra, P. and Beresteyn, E.C.H. van (1975) Crystallization of milk fat in the emulsified state, *Neth. Milk Dairy J.* **29**, 35

Walstra, P., Vliet, van T. and Kloek, W., Crystallization and rheological properties of milk fat, In *Advanced Dairy Chemistry Vol. 2; Lipids* 2nd *ed.*, Ed. P.F. Fox, Chapman & Hal, London,1995, pg.179

Wesdorp, L.H. (1990) *Liquid - multiple solid phase equilibria in fats - theory and experiments-*, Ph.D. Thesis, Technical University Delft, The Netherlands

Chapter 2

Materials

2.1 Triglyceride composition and thermal parameters

This chapter briefly explains some properties of the model fat system that is used in this study. It consists of mixtures of fully hydrogenated palm oil (HP) and sunflower oil (SF), the HP being the solid phase and the SF being the liquid phase. None of the fats were purified. The fatty acid composition of the HP and SF is given in Table 2-1.

Table 2-1. *Fatty acid composition (w/w) of sunflower oil (SF) and fully hydrogenated palm oil (HP). Fatty acid codes Cx:y ; x = number C-atoms; y = number of unsaturated bonds.*

fatty acid	code	percentage in HP (-)	percentage in SF (-)
C12:0	L	0.3	
C14:0	M	1.0	0.1
C16:0	P	41.3	6.1
C18:0	S	55.9	2.2
C18:1	O	0.1	27.3
C18:2	I		64.2
C20:0	A	1.0	
C22:0	B	0.3	

This table shows that the HP is made up of glycerides containing saturated fatty acids, specially palmitic acid and stearic acid. The SF contains a high fraction of unsaturated fatty acids and only a small fraction of palmitic acid and stearic acid.

The HP contains less than 1 % monoglycerides, about 6 % diglycerides and about 94 % triglycerides. The triglycerides in HP mainly contain stearic acid and palmitic acid. The triglyceride composition is calculated from the total fatty acid composition and the composition of the fatty acids esterified at the 2-position of glycerol, assuming random distribution of the fatty acids over the 1- and 3-positions. Only the combinations containing stearic acid and palmitic acid were considered. Table 2-2 shows that the HP would be rich in the triglycerides PSS, PSP and SSS. Besides the triglyceride composition, also the melting temperatures $T_{m,i}$ and the enthalpies of fusion $\Delta H_{f,i}$ of the various polymorphs are compiled. The T_m for all the triglycerides are all far above room temperature so that at these conditions HP is a hard fat. The SF started to crystallize at a temperature of about -5 °C. Since experiments were only carried out at temperatures above 0 °C, no data about the triglyceride composition of SF and their thermal behaviour are given.

Thermodynamic parameters of the model system were determined by measuring the crystallization temperature T of the α polymorph (rapid cooling) and the melting temperature T of the β' polymorph (after isothermal crystallization above the α melting temperature) as a function of the mole fraction HP, c_{HP}, by Differential Scanning Calorimetry (DSC). The temperatures T were

the peak temperatures in the thermograms. From the obtained temperatures as function of the mole fraction HP, $\Delta H_{f,i}$ and $T_{m,i}$ of the pure HP in polymorph i were calculated assuming ideal mixing using the following equation:

$$\ln c_{HP} = \frac{\Delta H_{f,i}}{R_g} \cdot \left(\frac{1}{T} - \frac{1}{T_{m,i}} \right) \qquad \textbf{(2-1)}$$

An advantage of determining $\Delta H_{f,i}$ and $T_{m,i}$ using this method instead of using $\Delta H_{f,i}$ and $T_{m,i}$ as determined from pure HP, is that correction is made for non-ideal solubility behaviour of HP in SF. These results, which could only be obtained for the α polymorph and the β' polymorph, are compiled in Table 2-3. Also the calculated average molar mass, based on the triglyceride composition, is given.

Table 2-2. *Triglyceride composition of fully hydrogenated palm oil calculated from the total fatty acid composition and the composition of the fatty acids esterified at the 2-position of glycerol, assuming random distribution of the fatty acids over the 1- and 3-positions. Only triglycerides containing palmitic acid (P) and stearic acid (S) are taken into account. Also melting temperatures ($T_{m,i}$) and enthalpies of fusion ($\Delta H_{f,i}$) of the pure triglycerides in polymorph i are compiled (from Wesdorp (1992))*

triglyceride	percentage (%)	$T_{m,\alpha}$ (°C)	$\Delta H_{f,\alpha}$ kJ·mol^{-1}	$T_{m,\beta'}$ (°C)	$\Delta H_{f,\beta'}$ kJ·mol^{-1}	$T_{m,\beta}$ (°C)	$\Delta H_{f,\beta}$ kJ·mol^{-1}
PPP	4.0	44.7	95.8	55.7	126.5	65.9	171.3
PSP	26.1	47.2	112.2	67.7	165.5	65.3	173.6
PSS	39.0	50.1	106.0	61.8	-	64.4	172.9
SSS	14.5	54.7	108.5	64.3	156.5	72.5	194.2
PPS	6.0	46.4	100.0	58.7	124.0	62.6	166.3
SPS	2.2	50.7	103.0	-	-	68.0	170.3

Table 2-3. *Some properties of the model system used.*

component	molar mass (g.mol^{-1})	$T_{m,\alpha}$ (°C)	$\Delta H_{f,\alpha}$ (J.mol^{-1})	$T_{m,\beta'}$ (°C)	$\Delta H_{f,\beta'}$ (J.mol^{-1})
HP	854	41.8	$9.8 \cdot 10^4$	57.3	$1.61 \cdot 10^5$
SF	877	-	-	-	-

2.2 other physical properties

The density of SF, as function of temperature T in °C, is given by 920-0.673·T in kg·m^{-3}. The density of HP in the liquid state is given by 929.4-0.680·T in kg·m^{-3}. The density difference between the liquid and the solid phase of HP is about 84, 89, 94, 99 and 105 kg·m^{-3} at temperatures of 0, 20, 40, 60 and 80 °C, respectively (Meeussen (1995)).

We determined the viscosity of SF as function of shear rate and temperature using a Bohlin VOR equipped with a 5° cone-plate geometry. SF behaved Newtonian. The temperature dependency of the viscosity of SF is shown in Figure 2-1. When decreasing the temperature from 60 °C to 5 °C, the viscosity increased by a factor 5. The viscosity is given by $\eta = \exp(-14.28+3.37\cdot10^3/T)$ where T is the absolute temperature.

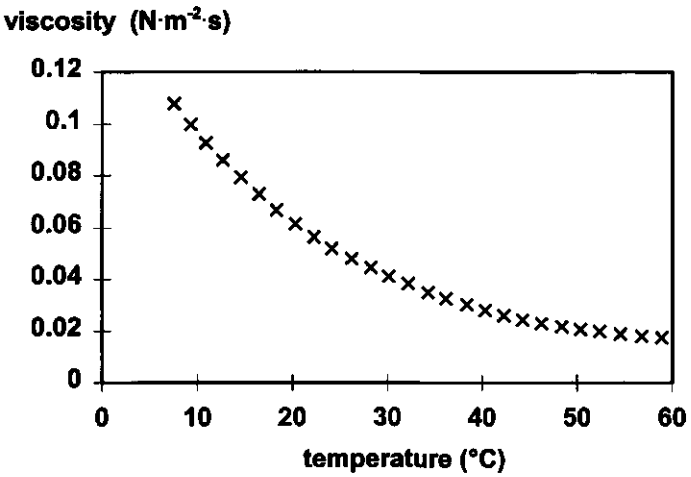

Figure 2-1. *Viscosity of sunflower oil as function of temperature.*

2.3 References

Meeussen, W. (1995) *Personal communication*

Wesdorp, L.H. (1990) *Liquid - multiple solid phase equilibria in fat - theory and experiments-*, Ph.D. Thesis Technical University Delft, the Netherlands

Chapter 3

Crystallization Kinetics of Emulsified Triglyceride Mixtures

3.1 Introduction

3.1.1 Nucleation

Nucleation is one of the most important steps in crystallization but also the one that is least accessible to experiments. Nucleation is the formation of ordered domains by bimolecular reactions. When these ordered domains or embryos exceed a certain critical size, their Gibbs energy will decrease on further addition of monomers and a nucleus is formed. A nucleus can grow further and form a crystal. We will use the classical nucleation theory (Volmer (1939)), although it is known that it contains several errors (Lyklema (1991)). The main error is that by using the classical theory, a macroscopic model is applied to ordered domains that are very small. Furthermore, the classical theory uses Gibbs energy changes from equilibrium thermodynamics as a measure for the activation Gibbs energy which is a kinetic parameter. It would be better to use mechanico-statistical models but in our case we are mainly interested in obtaining some characteristic parameters that can be used to estimate nucleation rates in order to model crystallization kinetics. Therefore, the more simple classical nucleation theory may be sufficient.

The Gibbs energy change ΔG_{3D} for formation of an embryo is determined by a positive surface term ΔG_S due to surface tension and a negative volume term ΔG_V due to enthalpy of fusion.

$$\Delta G_{3D} = \Delta G_S + \Delta G_V = \sum_i a_i \cdot \gamma_i + V \cdot \Delta G_v \tag{3-1}$$

where a_i is the area of face i, γ_i the surface Gibbs energy of face i, V the volume of the embryo and ΔG_v the change in Gibbs energy due to phase transition per unit volume. The critical size of an embryo for formation of a nucleus can be calculated by differentiating Equation 3-1 with respect to the dimension(s) of the nucleus and finding the maximum ΔG^*_{3D}. For a spherical nucleus, Equation 3-1 can be written as:

$$\Delta G_{3D} = 4\pi \cdot r^2 \cdot \gamma + \tfrac{4}{3}\pi \cdot r^3 \cdot \Delta G_v \tag{3-2}$$

Differentiating with respect to r and equating to 0 yields a critical size r^* for a spherical and a cubic nucleus shape respectively, of:

$$r^*_{\text{sphere}} = \frac{-2\gamma}{\Delta G_v} \; ; \; r^*_{\text{cubic}} = \frac{-4\bar{\gamma}}{\Delta G_v} \tag{3-3}$$

In case of a cubic nucleus shape with axes a, b and c on a orthogonal co-ordinate system, $\bar{\gamma}$ is an average surface Gibbs energy given by $(\gamma_{ab} \cdot \gamma_{ac} \cdot \gamma_{bc})^{1/3}$ were ab, ac and bc refer to the different nucleus faces

Substituting r^* and $\Delta G_v = \Delta\mu / \bar{V}$ where $\bar{V}$ is the molar volume in a crystal lattice and $\Delta\mu$ the chemical potential difference between the supersaturated and the saturated solution or melt, yields

the activation Gibbs energy ΔG^*_{3D} for the formation of a spherical nucleus as function of the supersaturation:

$$\Delta G^*_{3D,hom} = \frac{16\pi \cdot v_c^{\,2} \cdot \gamma^3 \cdot N_{av}^2}{3 \cdot \Delta\mu^2} \qquad \textbf{(3-4)}$$

$$\Delta\mu_{solution} = R_g T \cdot \ln\beta \qquad \Delta\mu_{melt} \approx \Delta H_{f,i} \cdot \frac{T_{m,i} - T}{T_{m,i}}$$

where β is the supersaturation ratio which gives the ratio between the solubilities of the crystallizing component at saturated and supersaturated conditions, R_g the gas constant, T the crystallization temperature, v_c the molecular volume of a crystal, N_{av} Avagadro's number, $\Delta H_{f,i}$ the enthalpy of fusion of polymorph i and $T_{m,i}$ the melting temperature of polymorph i. The natural logarithm of β is called the supersaturation. The numerical factor $16\pi/3$ is the shape factor for a spherical nucleus. Assuming a cubic nucleus shape yields a shape factor 32 and a surface Gibbs energy which is an average of the surface Gibbs energy of the three different faces. Figure 3-1 gives a plot of the Gibbs energy change as function of the radius of a spherical nucleus.

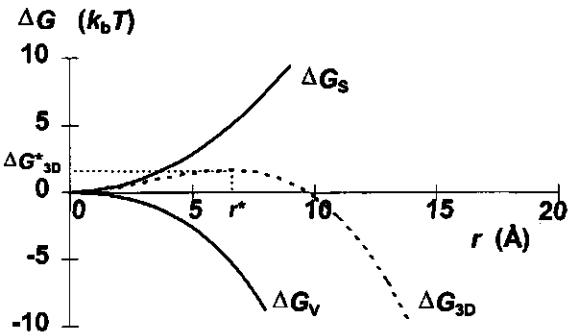

Figure 3-1. *Gibbs energy change of the surface term ΔG_S and the volume term ΔG_V on "growth" of a spherical ordered structure assuming some realistic values for triglycerides.* $\ln\beta = 4$, $v_c = 1.4 \cdot 10^{-27}$ m^3, $T = 298$ K *and* $\gamma = 3.8$ mJ·m^{-2}.

The activation Gibbs energy and the critical nucleus size both decrease on increase of supersaturation or decrease with temperature. The number of molecules i^* in a nucleus of critical size for a spherical and cubic geometry is given by:

$$i^* = \frac{V}{v_c} \quad \text{respectively;} \qquad \text{(a)}$$

$$i^*_{\text{sphere}} = \frac{32\pi \cdot \gamma^3 v_c^{\,2}}{3 \cdot (k_b T \cdot \ln\beta)^3} \qquad \text{(b)} \qquad \textbf{(3-5)}$$

$$i^*_{\text{cubic}} = \frac{64 \cdot \bar{\gamma}^3 v_b^{\,2}}{(k_b T \cdot \ln\beta)^3} \qquad \text{(c)}$$

where k_b is Boltzmann's constant.

The number of nuclei that are formed per unit volume and unit time is called the nucleation rate J and is mostly expressed as an Arrhenius-type of equation using ΔG^*_{3D} as the activation Gibbs energy. Besides the barrier for nucleation there is also a "barrier" for transport of the molecule over the liquid-solid interface. This barrier is often related to the delay that the viscosity causes on the diffusion of a crystallizing molecule over the liquid-solid interface. For glass-forming systems, this "barrier" can slow down the nucleation process dramatically due to very high viscosities. Triglycerides do not show glass formation but there can be another "barrier" for nucleation: the triglyceride has to be in the right conformation before it can be incorporated in a nucleus. This term can become important in the case of long-chain molecules. The loss of entropy ΔS on incorporation in a nucleus is given by $\Delta H_{f,i} / T_{m,i}$. The probability that a fraction α of the molecule is in the right conformation is given by $\exp(-\alpha \cdot \Delta S / R_g)$. The above-discussed "barriers" should not be regarded as separate "barriers" but as factors that delay the occurrence of a nucleation event.

The collisions frequency in a system containing N molecules that can crystallize is given by $N \cdot (k_b T/h)$ with h the Planck-constant, so that nucleation rate for homogeneous nucleation is given by:

$$J = N \cdot \frac{k_b T}{h} \cdot \exp\left(\frac{-\alpha \cdot \Delta S}{R_g}\right) \cdot \exp\left(\frac{-\Delta G^*_{3D}}{k_b T}\right) \qquad \textbf{(3-6)}$$

Factor α does not only give the fraction of the molecule that should be in the right conformation for incorporation in a nucleus, but will also take into account a factor like viscosity.

Homogeneous nucleation is the type of nucleation in which no surface acts as catalyst: the crystallizing molecules spontaneously form nuclei. Homogeneous nucleation conditions are normally only reached when the solution or melt is dispersed into a number of droplets that exceeds the number of catalytic impurities present in the system. For crystallization of dispersed tristearate and tripalmitate, supercooling in the α polymorph up to 26 K was measured (Phipps (1964); Skoda and van den Tempel (1963)). For emulsified milk fat, supercooling up to 20 K was obtained

(Walstra and van Beresteyn (1975)); the extent of supercooling needed depended on the spread in droplet composition.

In bulk fats, supercooling of only a few K is needed to induce crystallization. This is explained by the presence of (solid) impurities of a size larger than the dimensions of a nucleus. These impurities can act as a catalyst for nucleation by lowering the activation Gibbs energy for formation of a nucleus. Depending on the wetting of the solid surface by the nucleus, a smaller liquid-crystal interface needs to be created. Figure 3-2 shows a geometrical consideration of the heterogeneous nucleation process.

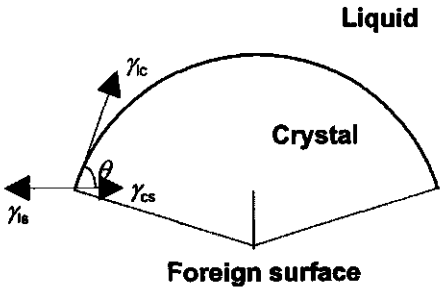

Figure 3-2. *Geometrical principle of heterogeneous nucleation. Vectors indicate the surface free energies: l = liquid; s = solid (foreign); c = crystal nucleus*

The volume and surface area of the nucleus depend on the liquid solid contact angle θ. For θ = 180°, no "wetting" of the foreign surface by the "crystal" occurs and the type of nucleation is homogeneous. For θ = 0° there is no barrier for nucleation and instantaneous phase separation occurs. For intermediate values of θ, nucleation is heterogeneous and the free activation energy for nucleation is given by (Zettlemoyer (1969)):

$$\Delta G_{3D} = f(\theta) \cdot \Delta G_{3D,\text{hom}} \quad \text{with} \quad f(\theta) = \tfrac{1}{4}(2+\cos\theta)\cdot(1-\cos\theta)^2 \qquad \textbf{(3-7)}$$

Nucleation in bulk fats is often believed to be of an heterogeneous nature (Walstra *et al.* (1995)). Particles that can act as a catalyst are probably micelles of monoglycerides, ordered emulsifiers and walls of crystallization vessels.

Another type of nucleation is secondary nucleation. This is nucleation occurring due to the presence of crystals of the crystallizing compound. Different types of secondary nucleation are known: apparent, true and contact (Garside (1987)). On apparent secondary nucleation, small fragments of crystals are washed of by flow of solute along the crystals and act as new nuclei. On true secondary nucleation, embryos of sizes smaller than the critical nucleus size are introduced by

the presence of crystals. These embryos disturb the steady state distribution of ordered domains and can enhance nucleation. Contact secondary nucleation originates from collisions of crystals with other crystals, walls of vessels, impellers and so on. The importance of the role of secondary nucleation in fat crystallization has been stressed by Walstra (1975,1987,1995). Emulsified triglyceride droplets, crystallized at conditions for homogeneous nucleation, showed hundreds of crystals per droplet while only one or two crystals were expected (Walstra and van Beresteyn (1975)). If emulsion droplets of mixed paraffins had crystallized, only one or two big crystals were observed (van Boekel (1980)). The strong secondary nucleation can probably be explained by the existence of ordered transition layers between the crystal surface and the solution and should depend on the type of molecule (paraffins vs. triglycerides). Walstra (1998) gave a hypothetical explanation for secondary nucleation in fats which implies that clusters of partially oriented triglyceride molecules diffuse away from a crystal face that grows via kinetic roughening. These clusters may give rise to separate nuclei if the crystal growth rate is small enough to enable considerable diffusion of the clusters.

3.1.2 Nucleation kinetics

The concentration of catalytic impurities is important for modeling the crystallization kinetics of bulk fats. To determine the effect of impurities on the crystallization kinetics, the crystallizing phase has to be divided in such volumes that at most one catalytic impurity per droplet is present. This can be achieved by emulsifying the fat phase. If the fat is divided over a number of droplets that is very large compared to the number of catalytic impurities per volume, homogeneous nucleation will predominate.

Nucleation rates in emulsified fats can be determined by measuring the volume fraction of solid fat (ϕ) as function of time (t). Thereto, one has to assume that the average time needed for a nucleation event is much longer than the time needed for the droplet to achieve complete crystallization. In that case, the volume crystallization rate is determined by the nucleation rate. The crystallization rate will be proportional to the volume fraction of droplets that contains no crystals ($1-\phi$) (Turnbull (1952), Turnbull and Fischer (1949), Turnbull and Cormia (1960)) and will therefore decrease with time.

$$\frac{d\phi}{dt} = k \cdot (1-\phi) \tag{3-8}$$

The reaction rate constant k can be written as a function of the nucleation rate J. For homogeneous volume nucleation, the rate constant k_v is proportional to the droplet volume v_d and is given by:

$$k_v = J \cdot v_d \tag{3-9}$$

If nucleation is catalyzed by impurities at the droplet surface, the rate constant k_s is proportional to the droplet surface a_d.

$$k_s = J \cdot a_d \tag{3-10}$$

Solving the differential equation leads to the following expression that gives the volume fraction solidified droplets as function of time:

$$\phi = 1 - \exp(-k \cdot t) \tag{3-11}$$

Taking into account the droplet size distribution, this expression has to be summed over all droplet sizes:

$$\phi = 1 - \int_0^\infty \phi_d^0 \cdot \exp(-k \cdot t)\mathrm{d}d \tag{3-12}$$

where ϕ^0_d is the differential volume fraction of droplets with sizes between d and d+dd. In the case of homogeneous volume nucleation or nucleation catalyzed by the homogeneous droplet boundary, the isothermal crystallization rate can be modeled by only one nucleation rate independent of d. It is assumed that the droplet composition and the composition of the droplet surface are invariant.

In case of heterogeneous nucleation, the crystallization volume contains impurities that catalyze the nucleation process. This nucleation process can not be modeled by a single nucleation rate because the number of impurities per droplet varies with diameter. Furthermore, there is a distribution of the catalytic activity of the impurities. The nucleation rate decreases with time. At the start of the heterogeneous nucleation process, the droplets containing the highest number of catalytic impurities will crystallize. This maximum nucleation rate can probably be related to the nucleation rates of bulk fats. As the crystallization process proceeds, smaller droplets will crystallize because they contain fewer impurities. At the end of the crystallization process, the volume fraction of solidified droplets will reach a plateau value ϕ_m because some droplets are void of impurities and therefore will not nucleate heterogeneously. If it is assumed that the catalytic impurities are distributed at random over the volume, the maximum achievable volume fraction of solid droplets can be related to the number of impurities per volume by:

$$\phi_m = 1 - \exp(-v_d \cdot N_{imp}) \tag{3-13}$$

where N_{imp} is the number density of catalytic impurities which is strongly dependent on temperature.

Walstra and van Beresteyn (1975) showed that the nucleation rate can approximately be written as function of the initial, *i.e.* maximum nucleation rate J_0 and the volume fraction of solid droplets by a linear relation:

$$J = J_0 \cdot \left(1 - \frac{\phi}{\phi_m}\right) \tag{3-14}$$

Combining Equations 3-8, 3-9, 3-13 and 3-14 and solving the differential equation yields the volume fraction of droplets containing crystals in the case of heterogeneous nucleation as a function of time:

$$\phi = \frac{1 - \exp\left(-J_0 \cdot v_d \cdot t \cdot \frac{\phi_m - 1}{\phi_m}\right)}{1 - \frac{1}{\phi_m} \cdot \exp\left(-J_0 \cdot v_d \cdot t \cdot \frac{\phi_m - 1}{\phi_m}\right)} \tag{3-15}$$

which is approximated by:

$$\phi = \phi_m \cdot \frac{J_0 \cdot v_d \cdot t}{1 + J_0 \cdot v_d \cdot t} \tag{3-16}$$

Fitting crystallization curves of emulsified triglycerides to a heterogeneous nucleation model requires the fit parameters J_0 and N_{imp} while using a homogeneous nucleation model requires only one nucleation rate as a fit parameter.

3.1.3 Ultrasound velocity measurements

Several techniques like dilatometry, differential scanning calorimetry (DSC), pulsed wide-line nuclear magnetic resonance spectrometry (p-NMR) and recently ultrasound velocity measurements are available to determine the crystallization kinetics of fats. All the techniques use the change of one or more physical properties on crystallization. Dilatometry was used with success in the past. It uses the difference in specific volume of the liquid and the crystalline phase. DSC detects the change in enthalpy on crystallization which is measured as a heat flux. For slow thermal processes the heat flux is often too low to be determined very accurately.

Nowadays, p-NMR is the most widely used technique to determine the amount of solid fat. This technique is based on the large difference in relaxation time between protons in a solid and a liquid environment. By measuring the signal directly after the pulse, which is proportional to the total amount of protons, and after such a time that only the solid protons have relaxed, it is possible to calculate the amount of solid fat (van Boekel (1980); van Putte and van den Enden (1974)). The amount of solid fat in emulsified fats can be determined by measuring only the signal after

relaxation of the solid protons, and calculating the amount of liquid oil from the specific signals of the continuous water phase and the liquid oil phase (van Boekel (1980)). The advantage of using only the liquid signal, is that the results do not depend on the polymorphic modification of the solid phase.

Ultrasound velocity measurement is a promising technique that is recently introduced for the determination of solid fat contents (Povey (1995)). The technique is rather simple: a low intensity, high frequency sound wave pulse is emitted through a sample and the time is measured that is needed for the pulse to travel twice the distance through the sample from which the velocity of the ultrasound in the sample, v, is calculated. The sound wave is a longitudinal wave: the propagation direction is the same as the vibration direction. The sound wave causes local compression and extension in the material.

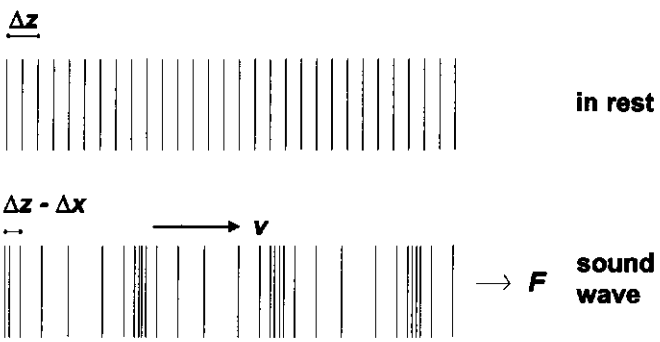

Figure 3-3. *Local compression and elongation due to a compressional sound wave*

Suppose that a material segment of length Δz, cross-sectional area a and compression modulus K is compressed by a force F to a length Δz-Δx. The strain in this segment is then given by $\Delta x/\Delta z$ (Figure 3-3). The stress is given by:

$$\frac{F}{a} = K \cdot \frac{\Delta x}{\Delta z} \tag{3-17}$$

The excess force ΔF that causes an infinitely thin segment of material to accelerate is given by:

$$\Delta F = a \cdot K \cdot \left(\frac{\mathrm{d}^2 x}{\mathrm{d}z^2} \right) \cdot \Delta z \tag{3-18}$$

This force is given by the product of mass ($\rho \cdot a \cdot \Delta z$) and acceleration ($\mathrm{d}^2x/\mathrm{d}t^2$) so that the acceleration can be written as:

$$\frac{d^2x}{dt^2} = \frac{K}{\rho} \cdot \left(\frac{d^2x}{dz^2} \right) \tag{3-19}$$

where ρ is the density of the material. The velocity of sound v is then given by:

$$v = \frac{dz}{dt} = \sqrt{\frac{K}{\rho}} = \frac{1}{\sqrt{\kappa \cdot \rho}} \tag{3-20}$$

where κ is the adiabatic compressibility which equals the reciprocal of the compression modulus. These equations are valid for systems in which no loss of intensity of the primary sound wave occurs. In a mixture of i components (phases), the ultrasound velocity is a function of the volume average of the density and the compressibility:

$$v = \frac{1}{\sqrt{\sum_i (\phi_i \cdot \kappa_i) \cdot \sum_i (\phi_i \cdot \rho_i)}} \tag{3-21}$$

where ϕ_i is the volume fraction of phase/component i. It is not necessary to determine κ and ρ at the experimental conditions to calculate the volume fractions from the ultrasound velocity. The volume fraction can be calculated from the velocities of the individual components. In the case of emulsified fats, the volume fraction solidified droplets can be calculated if the ultrasound velocity in an emulsion with completely liquid droplets (v_l) and completely solid droplets (v_s) is known at comparable temperature. The volume fraction solids ϕ can be calculated by the Urick-equation (Povey (1995)):

$$\phi = \frac{\frac{1}{v^2} - \frac{1}{v_l^2}}{\frac{1}{v_s^2} - \frac{1}{v_l^2}} \cdot \phi_d \tag{3-22}$$

where ϕ_d is the volume fraction of crystallizing component in the dispersed phase.

An advantage of using the solid and liquid velocities of the dispersed system is that no correction has to be made for scattering by the dispersed particles. Multiple scattering increases the travelling length of the sound wave pulse and therefore causes an underestimation of the actual ultrasound velocity. Due to multiple scattering broadening of the primary pulse occurs also.

Application of the ultrasound velocity measurement to determine the crystallization kinetics of (emulsified) fats is only useful for fats with narrow melting ranges and very simple polymorphic behaviour. Polymorphic transitions and recrystallization will lead to more densely packed crystals and therefore smaller compressibilities, resulting in a higher ultrasound velocity.

3.2 Materials and methods

3.2.1 Materials

A description of the physical properties and the triglyceride composition of the model system is given in chapter 2 of this thesis.

3.2.2 Preparation of emulsions

The aqueous phase of the emulsions consisted of 2 % (w/w) freeze-dried sodium caseinate in 0.005 M sodium chloride (pH = 6.9), or 1 % Tween20. Sodium caseinate was chosen as an emulsifier because it gives a thick layer around the droplet to achieve maximum protection against partial coalescence. The SF was added to the aqueous phase at room temperature. The HP was first melted at 80 °C and then added to the unheated aqueous phase. Every emulsion contained 20 % (w/w) dispersed phase. The percentage HP in the dispersed phase was varied.

Prior to (pre)emulsification, the mixture was heated to 75 °C to be sure that all HP had melted. A pre-emulsion was made by mixing in a Waring Blendor or an Ultra Turrax for 15 seconds. This pre-emulsion was emulsified with a high-pressure homogenizer (Foss Electric, Shields or Ranny). Prior to homogenization, the homogenizer was rinsed with water of 75 °C for 15 minutes to thermostat the homogenizer. This avoided crystallization of HP in the homogenizer. Before using the emulsion, it was heated to 75 °C for 15 minutes to melt the HP and to destroy any crystal memory.

The particle size distribution of the emulsions was determined using a Coulter Counter or a Malvern Master Sizer. From this distribution some characteristic droplet size (d_{ab}) and the relative standard deviation of the droplet size distribution (C_x) were calculated using the following equations in which n_i is the number of droplets with diameter d_i.

$$d_{ab} = \left(\frac{S_a}{S_b}\right)^{\frac{1}{a-b}} \quad \text{with} \quad S_x = \sum_i n_i \cdot d_i^x \qquad \text{(3-23)}$$

$$C_x = \sqrt{\frac{S_x \cdot S_{x+2}}{S_{x+1}^2} - 1}$$

The results are compiled in Table 3-1.

Table 3-1. *Characteristic parameters calculated from the droplet size distribution of emulsified HP/SF mixtures with a fat content of 20 % (w/w)*

HP/SF (%)	continuous phase	homogenizer and number of passes	d_{32} (μm)	C_2 (μm)
100	caseinate	Shields; 1	0.54	0.68
100	caseinate	Foss; 8	1.13	-
25	caseinate	Ranny 5 bar; 6	2.93	0.40
25	caseinate	Ranny 10 bar; 6	1.96	0.44
25	caseinate	Ranny 20 bar; 6	1.13	0.45
10	caseinate	Shields; 2	0.41	0.56
10	caseinate	Shields; 6	0.39	0.51
10	Tween 20	Shields; 6	0.38	0.50
0	caseinate	Shields; 2	0.47	0.53

3.2.3 Pulsed NMR

The p-NMR used was a Bruker-minispec P20i which operates at a frequency of 20 MHz. NMR tubes were filled with a known weight of emulsion (about 0.8 g.). For determination of the amount of solid fat, only the liquid signals were measured. The solid fat content of a crystallizing emulsion can be determined by measuring the liquid signal of the emulsion (S_{em}), the liquid signal of a completely solidified emulsion (S_{sol}) and the liquid signal of a non-solidified emulsion (S_{liq}) by using the next equation:

$$\phi = \frac{S_{em} - S_{liq}}{S_{sol} - S_{liq}} \tag{3-24}$$

Prior to isothermal crystallization experiments, a cooling-heating scan was performed to determine the temperature at which crystallization started.

3.2.4 DSC

Experiments were carried out using a Perkin Elmer DSC-7. Emulsions had crystallized by cooling the emulsion from 80 °C to 5 °C at a rate of 2 K·min^{-1}. After keeping a sample for 2 minutes at 5 °C, it was heated at a rate 2 K·min^{-1} to determine the melting endotherm.

3.2.5 Ultrasound velocity measurement

The ultrasound cell was filled with 75 ml emulsion and placed in a waterbath for temperature control. The time for the sound pulse to travel twice the diameter of the cell was measured by the ultrasonic velocity meter (UVM1, Cygnus Instruments). Temperature, velocity and time were on-line transmitted to a spreadsheet. Every minute, average readings of the velocity and of the temperature were made. The timing accuracy was 0.01 μs in the range of 10-200 μs. The velocity could be measured with an accuracy of 0.1 $m \cdot s^{-1}$. The temperature precision was 0.01 K and the temperature accuracy inside the cell was 0.05 K.

The ultrasonic transmitter and receiver consisted of lead zirconium titanate ceramic crystals and operated at a frequency of 2.25 MHz. At a typical velocity of 1500 $m \cdot s^{-1}$ the wavelength of sound is about 0.7 mm so that the wavelength is much larger than the emulsion droplet diameter. Figure 3-4 gives a schematic representation of the UVM1 and the auxiliary equipment.

The emulsion inside the cell was continuously stirred using a magnetic stirrer (300 rpm). Temperature cycling was programmed using a Grant PZ1 temperature programmer. Prior to isothermal crystallization experiments, a cooling-heating scan was made to determine at what temperature the emulsion started to crystallize. This temperature scan was also used to determine the dependency of the solid and liquid velocities of the emulsions on temperature.

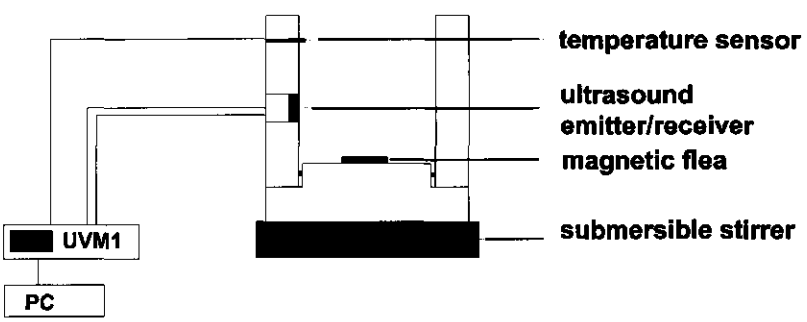

Figure 3-4. *Schematic representation of the ultrasound velocity measurement set-up.*

3.3 Results and discussion

3.3.1 Pulsed NMR

Figure 3-5 shows the cooling-heating curves of emulsions with various fractions of HP in SF homogenized with the Foss-Electric homogenizer (d_{32} = 1.1 μm) by measuring the liquid NMR signal.

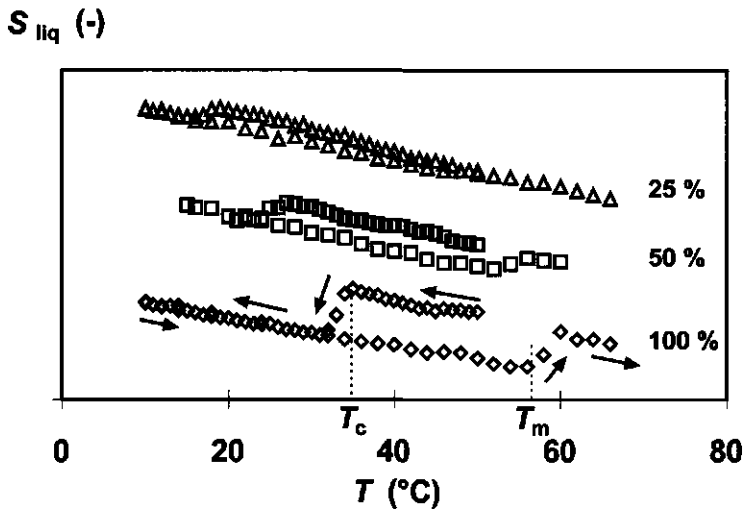

Figure 3-5. *Liquid signals as determined by p-NMR on cooling and heating of emulsified HP/SF. The arrows indicate the direction of temperature change. The percentages near the graphs indicate the amount of HP in the dispersed phase. T_c and T_m indicate the temperatures at which crystallization and melting occurs for emulsified 100 % HP.*

The liquid signals for the various fractions HP are shifted along the Y-axis to make the graph more clear. The graph is explained by means of the measurement on the 100 % HP emulsion. On cooling from 50 °C the liquid signal increased due to the influence of temperature on the liquid signals of the water phase and the liquid HP. At a temperature of about 35 °C the liquid signal suddenly decreased due to the crystallization of HP. At a temperature of 32 °C, crystallization was completed and the liquid signal increased on further cooling. Heating the crystallized emulsion showed that the melting process started at about 56-57 °C and was completed around 60 °C.

The decrease of the liquid signal on complete crystallization of emulsified HP at a volume fraction of the dispersed phase of 0.20 was by about 6.5 units. The accuracy at which the signal could be determined was 0.1, which would result in an error in the fraction of solidified droplets of 1.5 %. Increasing the volume fraction of the dispersed phase could reduce the error but this could lead to destabilisation of the emulsion. If the dispersed phase consisted of 10 % HP/SF, the error in the percentage solidified droplets was about 15 %. This is far too much to use this method for a quantitative description of the crystallization process.

The supercooling needed to initiate crystallization in the various dispersions will be discussed later.

3.3.2 DSC

The emulsions were prepared at various homogenisation pressures to vary the droplet size distribution. Table 3-1 shows that the average droplet size decreased with increasing homogenisation pressure. Figure 3-6 shows the cooling curves of emulsified 25 % HP/SF as measured with DSC. The cooling curve of the emulsion homogenised at 20 bar is not shown but yielded the same peak temperature as the emulsion homogenised at 10 bar.

The clear point of a 25 % HP/SF dispersion as calculated from the melting temperature and enthalpy of fusion of the HP (Table 2-3) assuming ideal solution behaviour, was about 50 °C for the β' polymorph and about 31 °C for the α polymorph. The emulsions that were prepared at pressures of 10 and 20 bar could be supercooled by about 14 K in the α polymorph, independent of droplet size (results 20 bar not shown in Figure 3-6). This independence suggests that crystallization in these droplets was induced by homogeneous nucleation, although the supercooling relative to the bulk melting temperature was not very high. The emulsion that was homogenised at a pressure of 5 bar showed crystallization over a broad temperature range but it was most extensive at 31 °C, roughly the α clear point, and less extensive at about 15 °C. The major crystallization at 31 °C is at a temperature at which the bulk fat with the same composition starts to crystallize in the α polymorph. It is not likely that an increase of the average droplet size from 1.9 μm (10 bar) to 2.9 μm (5 bar) results in an increase of the onset crystallization temperature from 16 °C to 31 °C due to a higher number of impurities per droplet. It is more likely that the emulsion, homogenized at a pressure of 5 bar, was partially destabilized and therefore behaves more or less like bulk fat since the emulsions were stored at refrigerator temperature.

It was not possible to do very accurate isothermal crystallization experiments using DSC due to the differential nature of the method: for slow crystallization rates, the heat flux was too low to

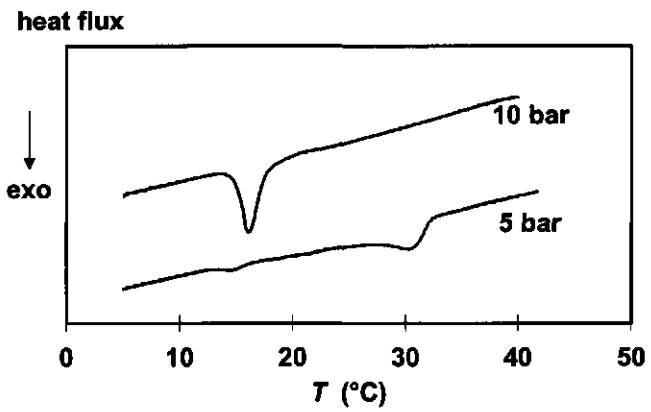

Figure 3-6. *Cooling DSC-scans of emulsified 25 % HP/SF (volume fraction = 0.20). The emulsions were homogenised with a Ranny homogeniser at different pressures (indicated in bar) to create emulsions with different droplet size distributions*

allow accurate determinations. Moreover the time needed for stabilisation of the base line after bringing the sample to the isothermal temperature was too long.

3.3.3 Ultrasound velocity measurement

3.3.3.1 Cooling heating cycles

Figure 3-7a shows that the ultrasound velocity of the continuous phase increased with increasing temperature but the rate of increase decreased with increasing temperature. The ultrasound velocity of sunflower oil decreased almost linearly with increasing temperature. Figure 3-7b shows that the ultrasound velocity of emulsified sunflower oil as a function of temperature showed an maximum value. The temperature at which the maximum velocity occurred, increased with decreasing volume fraction of the dispersed phase. The curve fitted a third degree polynomial.

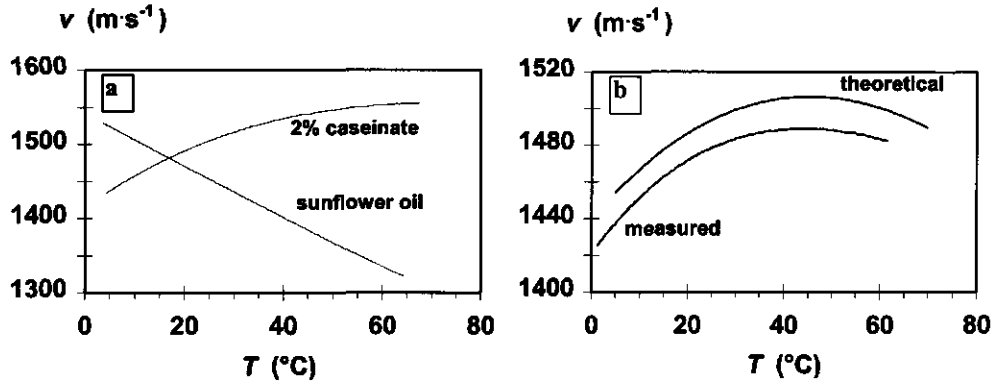

Figure 3-7. *Ultrasound velocities as function of temperature for (a) pure sunflower oil and 2% sodium caseinate in water and (b) the measured and velocities calculated according to equation 3-21 for a sunflower oil emulsion ($\phi_{sf} = 0.20$)*

The theoretical ultrasound velocity-temperature curve was calculated by using the velocities of the water phase and the oil phase in the non-emulsified state and substituting the velocities in Equation 3-21. The theoretical velocity is higher than the measured velocity in the whole temperature range. The difference is about constant and the maximum occurs at the same temperature. This suggests that the difference is caused only by scattering of the sound waves by the dispersed particles. Scattering results in a longer travelling length of the sound wave and therefore an underestimation of the velocity. Due to scattering also the shape of the reflected pulse was changed.

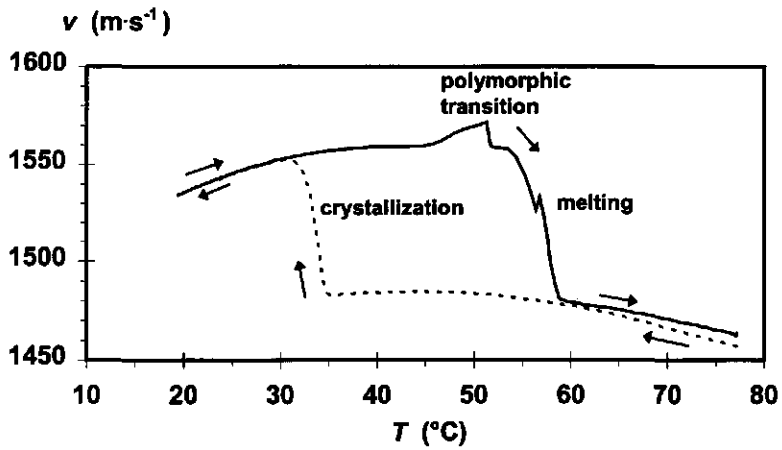

Figure 3-8. *Ultrasound velocity of emulsified HP as function of temperature on subsequent cooling (dotted line) and heating (solid line).*

Figure 3-8 shows the cooling (from 80 °C to 20 °C) and heating curve (from 20 °C to 80 °C) of an emulsified HP dispersion as measured with ultrasound velocity measurements. On cooling, the ultrasound velocity initially followed a third degree polynomial like in case of the sunflower oil emulsion. At 35 °C the ultrasound velocity started to increase steeply with decreasing temperature from 1480 $m \cdot s^{-1}$ to about 1550 $m \cdot s^{-1}$ at 30.5 °C due to crystallization of the HP. Crystallization of the HP would result in an increase in density and a decrease in compressibility. The increase of the velocity on crystallization shows that the relative change in compressibility is stronger than the relative change in density. On further cooling after crystallization, the velocity decreased again with decreasing temperature. On heating after cooling the velocity initially followed the cooling line indicating that the emulsion was not destabilized at this stage. At temperatures above the crystallization temperature, the velocity also followed a cubic curve like the sunflower in water emulsion indicating that no melting process occurred. Around 48 °C the velocity increased over a temperature interval of about 7 °C. At 52 °C the velocity suddenly dropped as the melting process started. The increase of the velocity could have been caused by a polymorphic transition from α to a mixture of mainly β and some β' because a more stable polymorph will have a lower compressibility. For a polymorphic transition, one would expect the velocity to stay high on further heating and not to decrease suddenly since the compressibility decreases due to denser crystal packing. Between 55 and 59 °C the velocity decreased strongly, due to melting of the crystals. This melting temperature agrees well with the melting temperatures of the β' polymorph or the β polymorph of HP. After the HP had completely melted (T > 59 °C), the heating curve initially followed the cooling curve but soon deviated from the cooling curve. This deviation was caused by coalescence of the emulsion droplets, resulting in creaming of oil droplets; The emulsion was not homogeneous anymore and the measured velocity does not correspond with the initial emulsion. Since destabilisation of the emulsion only occurred after melting of the crystallized emulsion during

high shear and not during cooling, it is unlikely that destabilisation would occur during isothermal crystallization.

The crystallization and melting temperatures agreed well with the temperatures determined by p-NMR measurements (Figure 3-5). The figure also seems to show a stronger decrease of the liquid signal at a temperature of about 48 °C, which could be indicative for a transition to a more stable polymorph.

The increase of the sound velocity on crystallization of a 20 % emulsion was about 70 $m \cdot s^{-1}$. When the accuracy of the velocity is 0.1 $m \cdot s^{-1}$, this means that the amount of solid fat can be determined with an accuracy of 0.3 %. This is much better than the accuracy of 1.5 % that was reached by the p-NMR method

Figure 3-9 shows a cooling-heating cycle of a 20 % emulsion of which the dispersed phase consisted of 10 % HP/SF. The general form of the curve is comparable to that of the 100 % HP emulsion. Crystallization occurred at a much lower temperature. Instead of showing an increase in velocity on crystallization, only a somewhat smaller decrease in velocity on cooling was seen. This can be explained by the higher negative value of the temperature coefficient of the velocity due to the presence of sunflower oil.

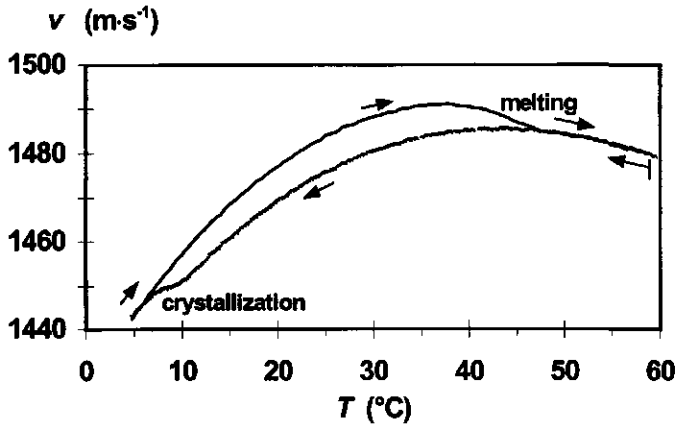

Figure 3-9. *Ultrasound velocity of emulsified 10 % HP/SF using sodium caseinate as emulsifier as a function of temperature on subsequent cooling and heating.*

The heating curve initially followed the cooling curve, indicating that all the HP had crystallized over a narrow temperature range. The melting process started around a temperature of 35 °C. After melting was complete, the velocity was the same as for the cooling curve. This shows that no significant coalescence had occurred. After the first cooling-heating cycle, a second one was performed. This curve perfectly matched the first cooling-heating curve. The heating curve showed no indication for a polymorphic transition from α to β or β'. We showed that the time scales of this transition in 10 % HP/SF dispersions were 30 minutes and 3 minutes at temperatures of 5 °C

and 15 °C, respectively (Kloek (1998), chapter 4). Taking into account these time scales, the polymorphic transition was expected to occur at a temperature of about 14 °C. The increase in velocity due to a polymorphic transition was possibly too small to be noticed.

The supercooling needed for crystallization of emulsified 10 % HP/SF was 13 °C for the α polymorph and 34 °C for the β' polymorph. These supercoolings were higher than the supercooling for emulsified 100 % HP which were 7 °C and 22 °C for the α and β' polymorph, respectively. If nucleation is heterogeneous, this would mean that the HP contained most of the impurities.

Emulsified 10 % HP/SF with Tween 20 as the emulsifier gave a velocity-temperature curve of the same shape (Figure 3-10). Crystallization started at 13 °C, which is 3 °C higher than for sodium caseinate as the emulsifier. The hydrophobic lauryl chain of Tween 20 possibly induces structuring of the triglycerides molecules near the droplet boundary so that a smaller activation Gibbs energy would be needed for nucleation and therefore crystallization temperature will be higher. The melting process started at the same temperature as for the sodium caseinate stabilised 10 % HP/SF emulsion. The emulsion also appeared to be stable against (partial) coalescence, despite a less protective emulsifier. Repeated temperature cycles with the same emulsion gave velocity-temperature curves that perfectly matched the curve obtained at the first cycle.

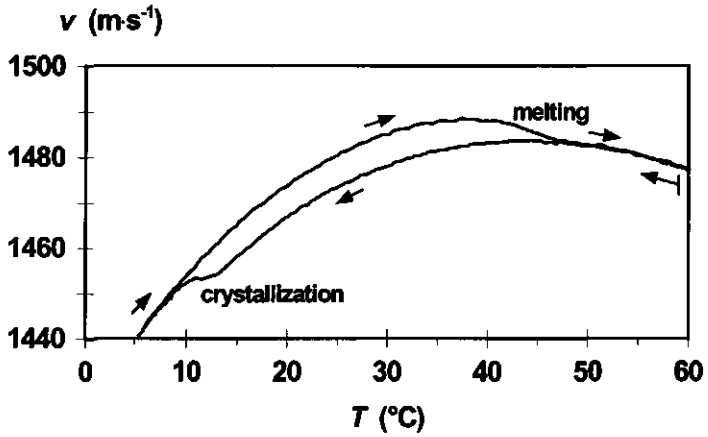

Figure 3-10. *Ultrasound velocity of emulsified 10 % HP/SF using Tween 20 as the emulsifier as function of temperature on subsequent cooling and heating.*

3.3.3.2 Isothermal crystallization

Isothermal crystallization experiments were carried out on HP emulsions at temperatures that were selected on basis of the cooling-heating cycles. The sound velocities in dispersions containing completely solid or completely liquid droplets as a function of temperature were described by curvi-linear regression. The volume fraction of solidified droplets was calculated by the Urick-equation (Equation 3-22).

After introduction of the emulsion in the ultrasound cell, it took about 4-5 minutes for the temperature to reach its final value. During this time crystallization should not occur. At high supercoolings, a little crystallization sometimes occurred before the final temperature was reached. This will have some effect on the results at the beginning of the crystallization process but it will not affect the crystallization curve after, say, 10 minutes. In calculating the fraction of solidified droplets from the liquid- and solid velocities, the actual temperatures were used.

Figure 3-11 shows that the (initial) crystallization rate of emulsified HP increases with decreasing temperature. After 90 minutes the fraction of solidified droplets was almost constant. The fraction solidified droplets increased with decreasing crystallization temperature. This can be explained by heterogeneous nucleation: at lower temperatures the fraction of droplets void of catalytic impurities was smaller so the fraction of droplets that had not crystallized would also be smaller. If nucleation would be homogeneous, crystallization would proceed until all droplets had crystallized.

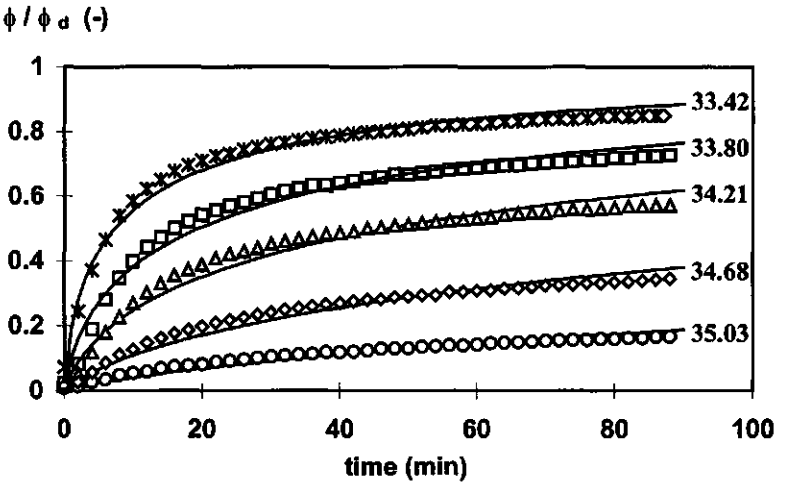

Figure 3-11. *The volume fraction of solidified droplets on isothermal crystallization of emulsified HP with sodium caseinate as emulsifier. Temperatures are indicated (°C).*

The crystallization curves were fitted to homogeneous and heterogeneous nucleation models taking into account the droplet size distribution (Figure 3-12). The experimental crystallization curves were fitted best by a heterogeneous nucleation model although it should be remembered that the heterogeneous model contains two fit parameters (the maximum nucleation rate J_0 and the number density of impurities N_{imp}) while the homogeneous nucleation model has only one fit parameter (the nucleation rate). The initial crystallization rate is somewhat overestimated what can be explained by that the temperature had not reached its final value in the first few minutes.

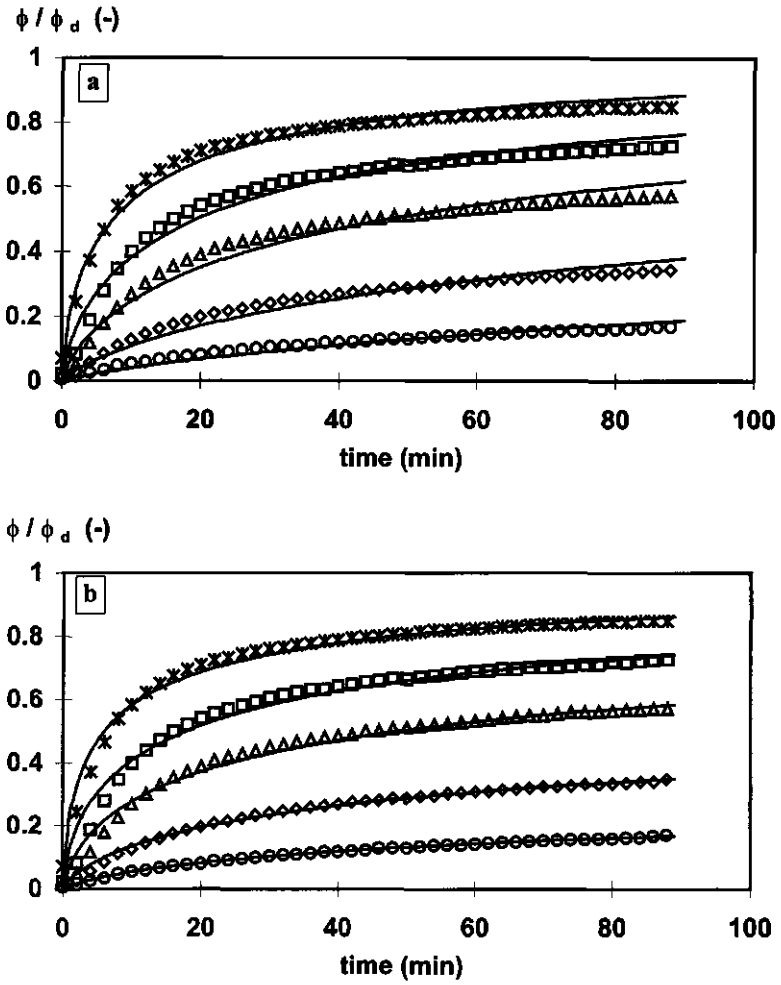

Figure 3-12. *Fitted isothermal crystallization curves (solid lines) of emulsified HP using (a) a homogeneous volume nucleation model and (b) a heterogeneous nucleation model. The markers correspond to the markers in Figure 3-11.*

According to equations 3-4, 3-6 and 3-7, it is possible to extract the surface Gibbs energy γ for (heterogeneous) nucleation from the slope of a plot of $\ln J_0$ against a supercooling term. Figure 3-13a shows an excellent linear relation between $\ln J_0$ and the supercooling term. The obtained slope corresponds to a value for the surface Gibbs energy for a nucleus of 2.6 $mJ \cdot m^{-2}$. However, as the type of nucleation is heterogeneous, the liquid solid contact angle factor $f(\theta)$ is smaller than 1 and therefore the surface Gibbs energy for nucleation would be higher than 2.6 $mJ \cdot m^{-2}$.

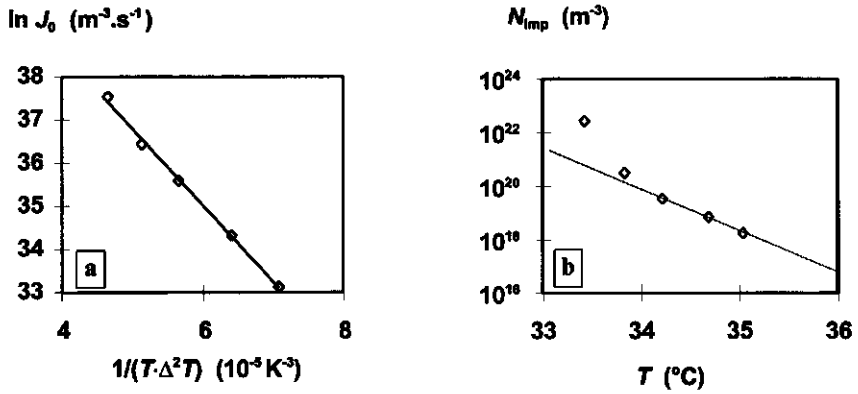

Figure 3-13. *Fitted maximum nucleation rate J_0 as function of an supercooling term (a) and the number density of catalytic impurities N_{imp} versus temperature (b) obtained from crystallization kinetics of emulsified HP using sodium caseinate as the emulsifier. Nucleation is assumed to occur in the α polymorph.*

According to Walstra and van Beresteyn (1975), the number density of catalytic impurities increases with decreasing temperature, often following the empirical relation $\log N_{imp} = A\text{-}B\cdot T$. Figure 3-13b shows a negative correlation between the number of impurities and temperature. Coefficient B expresses the temperature sensitivity of the number density of catalytic impurities and is about 1 in the temperature range of 34 - 35 °C: this means an increase of N_{imp} by a factor 10 for a decrease in temperature by 1 K. This value is very high. Walstra and van Beresteyn determined B to be 0.16 for emulsified milk fat. At lower temperatures the logarithm of N_{imp} increases more than linear with decreasing temperature. This can be due to the high values of N_{imp} , so that the term $1\text{-}\exp(-v_d\cdot N_{imp})$ (Equation 3-13) becomes insensitive to N_{imp}.

In order to determine under which conditions homogeneous nucleation occurs, it is necessary to decrease the number of impurities per droplet. This can be achieved by dispersing the fat phase into smaller droplets or by diluting the hardened palm oil with sunflower oil. Since it was not possible to homogenize at various pressures, the HP was diluted 10 times with sunflower oil. An additional advantage is that the composition of the fat phase is close to that of the dispersions used for the rheological and bulk crystallization studies. A disadvantage is that a whole new range of triglycerides containing unsaturated fatty acids is introduced and that the temperature at which crystallization starts will be much lower.

Figure 3-14 shows the isothermal crystallization curves of emulsified 10 % HP/SF stabilized with sodium caseinate. They are described well by assuming homogeneous nucleation. It was not possible to distinguish between volume or surface nucleation. Fitting the crystallization curves by a heterogeneous model showed significant poorer fits for all temperatures.

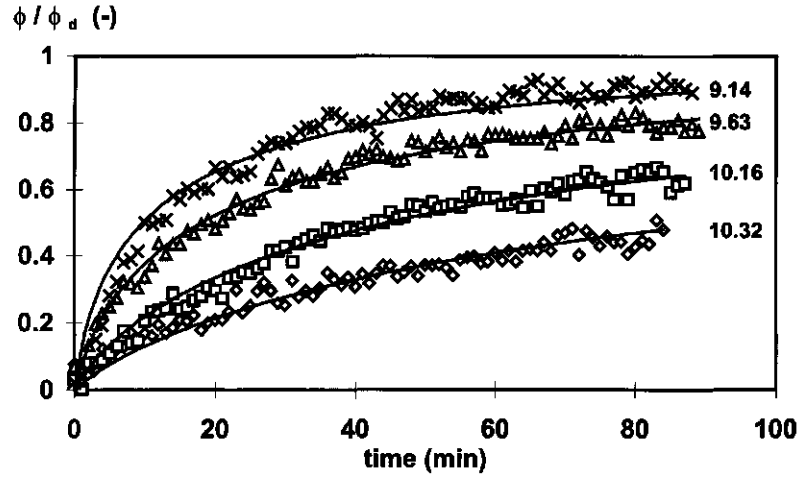

Figure 3-14. *The volume fraction of droplets containing solid fat during isothermal crystallization of emulsified 10 % HP/SF using sodium caseinate as emulsifier at various temperatures (indicated in °C). The solid lines are fits assuming homogeneous nucleation.*

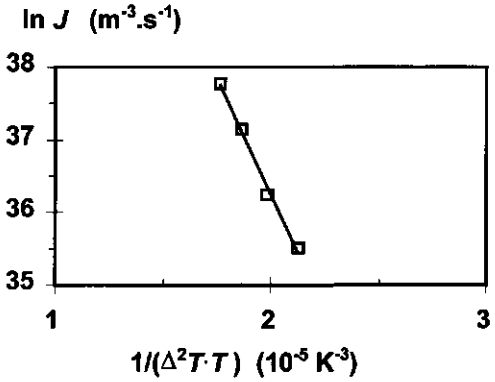

Figure 3-15. *Fitted nucleation rates assuming homogeneous nucleation of emulsified 10 % HP/SF stabilised with sodium caseinate as function of a supercooling term.*

A plot of ln$J$ against a supercooling term again yields a straight line (Figure 3-15). The slope corresponds to a surface Gibbs energy for a nucleus of 4.1 mJ.m^{-2} and the intercept yields a pre-exponential term of $1.9 \cdot 10^{21}$ m^{-3}.s^{-1}. The surface Gibbs energy is significantly higher than the value obtained from the maximum heterogeneous nucleation rates for emulsified HP.

On diluting the solid phase 10 times with sunflower oil, the nucleation type apparently changes from heterogeneous to homogeneous if it is assumed that the nucleation of emulsified HP

is of a heterogeneous nature. There are two possible explanations for the change. First, the HP is diluted so that the concentration of the catalytic impurities is decreased by a factor 10. The decrease of this number can even be much higher if micelles of monoglycerides are the catalytic impurities, since it is possible that the critical micel concentration is not reached. Second, the solubility of the HP and the impurities in the sunflower oil is influenced by the addition of triglycerides containing many unsaturated fatty acids.

It was shown earlier that the presence of Tween 20, a molecule containing a lauryl chain, increased the onset crystallization temperature of emulsified 10 % HP/SF by about 3 K. This was explained by structuring of the triglycerides near the droplet boundary, although one should keep in mind that Tween 20 contains a rather bulky hydrophilic group that hinders a close packing of lauryl chains in the fat phase. Another reason for the higher onset crystallization temperature can be the lower activity coefficient of triglycerides close to the droplet boundary due to the presence of the lauryl chains. The lower activity coefficient reduces the solubility near the droplet boundary. If the adsorption layer consist of pure Tween 20, it is expected that the whole droplet boundary acts as a catalytic impurity and therefore the nucleation kinetics should be modeled by a homogeneous model with a low effective surface energy.

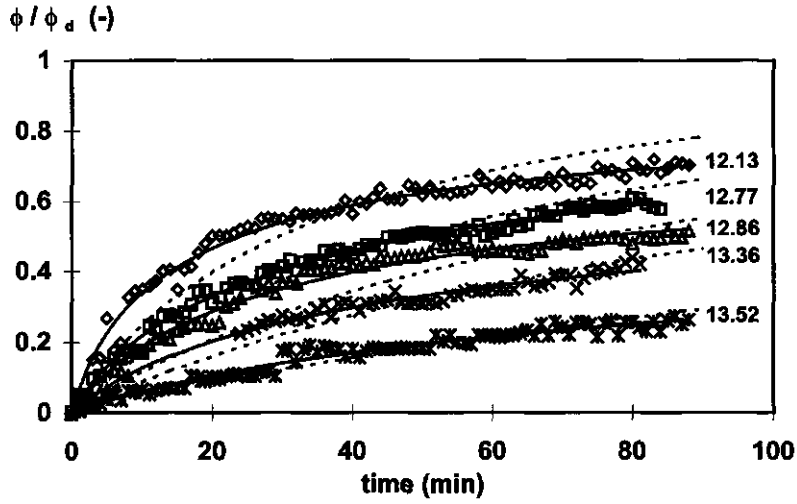

Figure 3-16. *The volume fraction of droplets containing solid fat on isothermal crystallization of emulsified 10 % HP/SF using Tween 20 as the emulsifier at various temperatures (indicated in °C). The solid lines are fits assuming heterogeneous nucleation and the dotted lines are fits assuming homogeneous nucleation.*

Figure 3-16 shows that the nucleation kinetics of Tween 20 stabilized dispersed 10 % HP/SF are best described by a heterogeneous nucleation model. The surface fit is slightly better than the volume fit (results not shown). A possible explanation is that not the whole droplet boundary is

catalytic, but only some areas at the droplet boundary to which impurities from Tween 20 are adsorbed. Figure 3-17a shows that there is a roughly linear relation between $\ln J_0$ and the supercooling term. The number of impurities per unit surface area would be about 10^{12} per m^{-2} and decreases slightly with increasing temperature as can be seen from Figure 3-17b. Assuming an average particle diameter of 0.38 μm yields about 0.5 catalytic impurity per droplet for $N_{imp} = 10^{12}$ m^{-2}.

Figure 3-17 shows that the fits are poorer compared to the fit of $\ln J$ versus the supercooling term of 10 % HP/SF dispersions stabilised with sodium caseinate (Figures 3-14 and 3-15). Especially the fit parameters obtained at a temperature of 12.77 (*i.e.* a supercooling term of $3.01 \cdot 10^{-5}$ K^{-3}) seem to deviate from the fit parameters obtained at other temperatures.

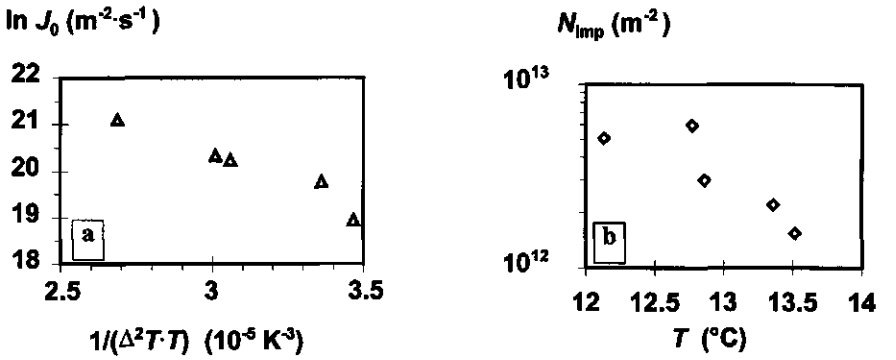

Figure 3-17. *Fitted maximum surface nucleation rate J_0 (a) and number density of catalytic impurities N_{imp} (b) as function of a supercooling term and temperature, as obtained from crystallization kinetics of emulsified 10 % HP/SF using Tween 20 as emulsifier. The supercooling term is calculated by assuming that nucleation occurred in the α polymorph.*

3.3.4 Discussion of fit parameters and supercooling

Table 3-2 gives a compilation of the supercooling needed to initiate crystallization in emulsified HP/SF mixtures and the type of nucleation that was derived from the crystallization kinetics for the experiments described in this chapter.

Table 3-2. *Onset crystallization temperature $T_{c\text{-onset}}$ and supercooling ΔT in the α polymorph of emulsified HP/SF dispersions with various average particle sizes determined with different techniques and the type of nucleation derived from the crystallization kinetics*

% HP	technique	emulsifier	d_{32} (μm)	$T_{c\text{-onset}}$ (°C)	ΔT_α (K)	nucleation type from kinetics
100	NMR	caseinate	1.13	35	7	-
50	NMR	caseinate	1.12	27	9	-
25	NMR	caseinate	1.13	19	12	-
25	DSC	caseinate	1.13	19	12	-
100	Ultrasound	caseinate	0.54	35	7	heterogeneous
10	Ultrasound	caseinate	0.39	10	14	homogeneous
10	Ultrasound	Tween 20	0.38	13	11	heterogeneous

The supercooling in the α polymorph needed to initiate crystallization of emulsified HP is about 7 K. This low supercooling suggests that crystallization is initiated by heterogeneous nucleation as for homogeneous nucleation of purified fats supercooling up to 26 K is reported. The type of nucleation that was derived from the crystallization kinetics of emulsified HP was also of a heterogeneous nature. However, the supercooling of emulsified HP is independent of the average droplet size as follows from the crystallization temperatures from NMR and Ultrasound experiments. This suggests that the nucleation of emulsified HP is not catalyzed by impurities and thus is homogeneous because the reduction of the number density of impurities per droplet by a factor $(1.13/0.54)^3 = 9.2$ did not lead to a lower onset crystallization temperature.

If the HP is diluted with sunflower oil the maximum supercooling increases from 7 K for 100 % HP to 14 K for 10 % HP/SF. A more relevant term to indicate the supercooling is the supersaturation since this is the driving force for crystallization. The supersaturation needed to initiate crystallization can be calculated from Equation 3-4 and yields values ranging from 0.83 for 100 % HP to 1.90 for 10 % HP/SF. The crystallization kinetics of emulsified 10 % HP/SF could be described by only one nucleation rate for all droplet sizes and therefore nucleation seems to be homogeneous. On the other hand, the supercooling needed relative to the bulk melting temperature of the α polymorph is only 14 K and suggests heterogeneous nucleation.

A possible explanation for this confusing result can be the triglyceride composition of the HP. It consists of a fairly wide range of triglycerides each having their own melting enthalpy and melting temperature. Triglycerides containing short fatty acids will have a lower melting enthalpy and melting temperature then those containing long fatty acids. The solubility of triglycerides in oil depends on the melting enthalpy and melting temperature and decreases with decreasing temperature. Whether a triglyceride or a group of triglycerides is supersaturated depends on both solubility and the amount of those triglycerides present. Triglycerides that contain long chain fatty

acids (C20, C22) are only present at very small fractions and would not be supersaturated at conditions at which bulk crystallization occurs: bulk crystallization will be initiated by heterogeneous nucleation of triglycerides containing shorter fatty acids (C16, C18). In case of emulsified 10 % HP/SF, crystallization occurs at much lower temperatures, at which (groups of) triglycerides containing long chain fatty acids, present at small amounts, would be supersaturated. About 3 % of the triglycerides in HP consist of fatty acid residues with lengths of 18 and 20 C-atoms. Suppose this group has a melting enthalpy and melting temperature in the α polymorph of 125 $kJ \cdot mol^{-1}$ and 62.9 °C respectively. These values are the average of the values for tristearate (C18) and trieiconate (C20). The mole fraction soluble HP in SF (x_{HP}) as function of temperature can be calculated using the Hildebrand equation which assumes ideal mixing behaviour (Hannewijk (1964), Wesdorp (1990)):

$$\ln(x_{HP}) = \frac{\Delta H_{f,i}}{R_g} \cdot \left(\frac{1}{T_{m,i}} - \frac{1}{T} \right) \qquad \textbf{(3-25)}$$

where T_m is the melting temperature of the HP. Dispersed 10 % HP/SF with sodium caseinate as emulsifier started to crystallize at a temperature of about 10 °C. At this temperature the solubility of triglycerides containing C18 and C20 fatty acids is about 0.02 % in the α polymorph. A 10 % HP/SF mixture contains 10 % · 3 % = 0.3 % of these triglycerides so that they are supersaturated considerably. The supersaturation ($\ln\beta$) of the triglycerides containing long chain fatty acids is about 2.7, while the supersaturation calculated from the bulk properties is about 1.9. Whether using the bulk properties or using the properties of triglycerides containing long chain fatty acids, a supercooling of 14 K is calculated, although there is a considerable difference in supersaturation. This implies that the degree of supercooling would not be a good criterion to decide whether nucleation is homogeneous or heterogeneous. A better criterion would be the supersaturation, but this parameter is difficult to define in mixtures that contain a wide distribution of triglycerides.

Can we now explain why the crystallization kinetics of emulsified HP fits a heterogeneous nucleation model, whereas the supercooling or supersaturation needed to achieve crystallization is independent of average particle size? When fitting the crystallization curves of emulsified HP with a heterogeneous nucleation model, it is assumed that the nucleation rate decreases in time because the size of the droplets that crystallize, decreases in time and therefore the number of impurities per droplet also decrease in time. However, if the catalytic impurities are formed by a group of triglycerides that is present at small amounts but are supersaturated most, the number of triglyceride molecules per droplet and their molecular collision frequency can be the limiting factor for nucleation to occur. In that case nucleation would be catalyzed by groups of triglyceride molecules that are present in such small amounts that the kinetics are modeled best by a heterogeneous nucleation mechanism while in reality the nucleation type is homogeneous in being catalyzed by the triglycerides themselves. The reason that the crystallization temperature does not strongly decrease with decreasing particle size can be due to the narrow triglyceride composition. If the number of

molecules of a certain group of triglycerides per droplet becomes too small for the occurrence of nucleation in smaller droplets, only little further cooling is needed to increase the nucleation rate by the same factor as by which the droplet volume is reduced since the activation Gibbs energy for nucleation formation is strongly temperature dependent. Furthermore the number of molecules (N in Equation 3-6) that can participate in forming a catalytic unit will increase with a small decrease in temperature.

Performing calculations on the extent of supersaturation of certain groups of triglycerides at relevant temperatures would be very difficult, since accurate thermodynamic data are not available. Moreover, the formation of compound crystals will greatly complicate the theory.

From Figures 3-13 and 3-15, it is clear that in agreement with classical nucleation theory, there is a linear relation between $\ln J$ and the supersaturation term $1/(T \cdot \Delta^2 T)$ for the sodium caseinate stabilised emulsions. From the slope and the intercept, an (apparent) surface Gibbs energy of a nucleus and the pre-exponential frequency term may be calculated (Table 3-3).

Table 3-3. *Apparent surface Gibbs energy (γ) of a nucleus and the frequency term obtained from isothermal crystallization of emulsified HP/SF mixtures nucleating in the α polymorph. r^2 is the correlation coefficient.*

HP/SF (%)	emulsifier	nucleation type from fit	γ ($mJ \cdot m^{-2}$)	pre-exponential factor ($m^{-3} \cdot s^{-1}$)	r^2
100	caseinate	heterogeneous	2.6	$4.7 \cdot 10^{19}$	0.9995
10	caseinate	homogeneous	4.1	$1.9 \cdot 10^{21}$	0.9927
10	tween 20	heterogeneous	3.3	$8.6 \cdot 10^{19}$	0.9400

From the homogeneous nucleation rates of dispersions containing 10 % HP/SF stabilised with sodium caseinate, a surface Gibbs energy of 4.1 $mJ \cdot m^{-2}$ was calculated. If the same dispersed phase was stabilised with Tween 20, a surface Gibbs energy of 3.3 $mJ \cdot m^{-2}$ was obtained. The difference would be caused by the heterogeneous nucleation mechanism in stead of homogeneous nucleation. From the ratio of the calculated surface free energies, the heterogeneous nucleation factor $f(\theta)$ is calculated to be 0.52, yielding a liquid - solid contact angle $\theta \approx 90°$. There was no big difference in the calculated γ if for the same sodium caseinate stabilised 10 % HP/SF emulsion in stead of homogeneous nucleation, heterogeneous nucleation was assumed to occur (by about 5 %).

The calculated surface Gibbs energies are much smaller than the values determined by Phipps (1964), and Skoda and van den Tempel (1963) for emulsified tristearate and tripalmitate. They found values of about 10 $mJ \cdot m^{-2}$. This may be due to purity of the crystallizing phase and therefore the availability of more accurate thermal data.

Pre-exponential frequency terms were about 10^{21} $m^{-3} \cdot s^{-1}$ for homogeneous nucleation. If it is assumed that nucleation is homogeneous and we take the bulk properties of 10 % HP/SF (N = $7 \cdot 10^{25}$ molecules$\cdot m^{-3}$, T = 288 K and $\Delta S = \Delta H_{f,\alpha} / T_{m,\alpha}$ = 311 $J \cdot mol^{-1} \cdot K^{-1}$), the fraction α of the

molecule that should be in the right conformation for incorporation in a nucleus according to Equation 3-6 is 1.08. If it is assumed that only triglycerides having C18 and C20 fatty acids (2 % of the HP) can form nuclei, values for $\Delta H_{f,\alpha} = 125$ kJ·mol^{-1} and $T_{m,\alpha} = 336$ K, lead to $\alpha \approx 0.98$. These values indicate that virtually the whole triglyceride molecule should be in the right conformation for incorporation in a nucleus. This seems very unlikely. It is expected that a much smaller proportion of the triglyceride molecule should be in the right conformation: the rest of the triglyceride molecule can be incorporated relatively easy in a nucleus. The high value of α suggest that besides a certain part of the triglyceride should be in the right conformation, there are other factors that delay the formation of a nucleus.

3.4 Conclusions

Ultrasound velocity measurement is a sensitive technique to monitor crystallization kinetics of fat dispersions containing triglycerides with a simple phase behaviour.

Crystallization of emulsified fully hydrogenated palm oil (HP) started at a supercooling of about 7 K relative to the α clear point. The supercooling was independent of the average droplet size. The isothermal crystallization of emulsified HP was best fitted by assuming heterogeneous nucleation.

Crystallization of emulsified 10 % HP in sunflower oil (SF), stabilised with sodium caseinate, started at supercoolings of about 14 K below the α clear point. Isothermal crystallization of these dispersions was best described by assuming homogeneous nucleation.

If Tween 20 was used as stabilizer for the 10 % HP/SF emulsions, the crystallization temperature increased by 3 K. The isothermal crystallization curves were best fitted assuming heterogeneous nucleation. The nucleation is probably catalyzed by ordered lauryl chains of Tween 20 in the droplet boundary in combination with impurities in the Tween 20. It is also possible that the lauryl chains decrease the local solubility of the HP in the SF.

The surface Gibbs energy of a nucleus obtained from the temperature dependency of the nucleation rate of caseinate stabilised 10 % HP/SF emulsions is about 4 mJ·m^{-2}. Using this value yields a wetting angle of 90° between the nucleus and the catalytic surface for Tween 20 stabilised emulsions of 10 % HP/SF.

Nucleation in HP/SF mixtures is probably initiated by groups of triglycerides containing long chain fatty acids, which are present at low amounts.

Pre-exponential nucleation frequencies indicate that a large proportion of the triglyceride molecule should be in the right conformation to be incorporated in a nucleus.

3.5 Acknowledgements

I would like to thank Dr. M.J.W. Povey from the Procter Department of Food Science of Leeds University for his hospitality and help with ultrasound velocity measurements.

3.6 References

Boekel, M.A.J.S. van (1980) *Influence of fat crystals in the oil phase on stability of oil-in-water emulsions*, PhD thesis Wageningen Agricultural University, Wageningen, the Netherlands

Boistelle, R. (1988) Fundamentals of nucleation and crystal growth, in *Crystallization and polymorphism of fats and fatty acids*, Eds: N. Garti and K. Sato, Marcel Dekker, New York

Garside, J.. (1987) General principles of crystallization, In *Food structure and behaviour*, Eds: J.M.V. Blanshard and P. Lillford, Academic Press, London, pp. 35-49

Hannewijk, J. (1964) Kristallisatie van vetten I, *Chemisch Weekblad*, **60**, 309 (in dutch)

Kloek, W. (1998) *Mechanical properties of fats in relation to their crystallization*, PhD thesis, Wageningen Agricultural University, the Netherlands

Lyklema, J. (1991) *Fundamentals of interface and colloid science, vol.I, fundamentals*, Academic Press, London

Meeusen, W. (1995) personal communication

Phipps, L.W. (1964) Heterogenous and homogeneous nucleation in supercooled triglycerides and n-paraffins, *Trans. Faraday Soc.* **60**, 1873

Povey, M.J.W. (1995) Ultrasound studies of shelf-life and crystallization, In *New physico-chemical techniques for the characterization of complex food systems*, Ed. E. Dickinson, Chapman & Hall, London, pp. 196-212

Putte, K. van and Enden, J.C. van den (1974) Fully automated determination of the solid fat content by pulsed NMR, *J. Am. Oil Chem. Soc.* **51**, 316

Skoda, W. and Tempel, M. van den (1963) Crystallization of emulsified triglycerides, *J. Colloid Sci.* **18**, 568

Turnbull, D. (1952) Kinetics of solidification of supercooled liquid mercury droplets, *J. Chem. Physics* **20**, 411

Turnbull, D. and Cormia R.L. (1960) Kinetics of crystal nucleation in some normal alkane liquids, *J. Chem. Physics* **34**, 820

Turnbull, D. and Fisher, J.C. (1949) Rate of nucleation in condensed systems, *J. Chem. Physics* **17**, 71

Volmer, M. (1939) *Kinetik der phasenbildung*, Steinkoppf, Leipzig

Walstra, P. (1987) Fat crystallization, In *Food structure and behaviour*, Eds: J.M.V. Blanshard and P. Lillford, Academic Press, London, pp. 67

Walstra, P. (1998) Secondary nucleation in triglyceride crystallization, *Progr. Colloid Polym Sci* **108**, 4

Walstra, P. and Beresteyn, E.C.H. van (1975) Crystallization of milk fat in the emulsified state, *Neth. Milk Dairy J.* **29**, 35

Walstra, P., Vliet, van T. and Kloek, W. (1995) Crystallization and rheological properties of milk fat, In *Advanced Dairy Chemistry Vol. 2; Lipids 2nd ed.*, Ed. P.F. Fox, Chapman & Hal, London, pg.179

Wesdorp, L.H. (1990) *Liquid - multiple solid phase equilibria in fat - theory and experiments-*, PhD Thesis Technical University Delft, the Netherlands

Zettlemoyer, A.C. (1969) *Nucleation*, Marcel Dekker, New York

Chapter 4

Crystallization Kinetics of Fully Hydrogenated Palm Oil in Sunflower Oil Solutions.

4.1 Introduction

4.1.1 General

Fats are crystallized for several reasons, such as fractionation into certain groups of triglycerides or to give food products a certain structure. For fractionation of groups of triglycerides it is desirable that the remaining oil can be readily removed from the crystals by washing procedures. Therefore, a low total crystal surface or large crystal size is desired. If fats are crystallized to give food products textural properties like spreadability, very small crystals are desired. These small crystals aggregate due to van der Waals forces resulting in large aggregates or a continuous crystal network that gives the dispersions its consistency (van den Tempel (1961), Walstra *et al.* (1995)). A key parameter for describing the mechanical properties of a fat dispersion is the amount of crystallized fat. Low amounts of solid fat can give a spreadable product, but may also lead to undesired oiling-off; while high amounts of solid fat can give a hard, brittle product (Walstra and Jennes (1984)). Besides by the amount of solid fat, the textural properties will be influenced by the crystallization temperature. For example, if a solution of 10 % hardened palm oil in sunflower oil has crystallized at 25 °C, a spreadable, solid-like dispersion with small crystals is obtained while crystallization at about 38 °C yields a pourable dispersion with large spherulitic crystal agglomerates. The variations in structural properties initially arise from the variations in crystal size distribution and in the arrangement of the crystals in space. Both crystal size and the aggregation of crystals depend on the crystallization kinetics.

4.1.2 Supersaturation

A requirement for crystallization to occur is the existence of a supersaturation. A solution is supersaturated if the activity of a dissolved component x is higher than the activity of a just saturated solution. So in a supersaturated solution, there is a chemical potential difference $\Delta\mu$ between the supersaturated and the saturated solution. The chemical potential difference of an ideal solution is given by:

$$\Delta\mu = R_g T \ln \frac{c_x}{x_x} \qquad \text{(4-1)}$$

where R_g is the gas constant, T the absolute temperature, c_x the fraction soluble at supersaturated conditions and x_x the fraction soluble at saturated conditions of component x. The ratio c_x/x_x is called the supersaturation ratio β and $\ln\beta$ is the supersaturation. At low supersaturations, the supersaturation is often approximated by expanding the ln-term by a Taylor series and using only the first term. This results in:

$$\ln\beta \approx \frac{c_x - x_x}{x_x} = \beta - 1 \qquad \textbf{(4-2)}$$

This approximation gives a deviation of 10 % at a $\ln\beta$ of 0.20.

The fraction soluble for ideal solutions is given by the Hildebrand-equation (Hannewijk (1964), Wesdorp (1990)):

$$\ln x_x = \frac{\Delta H_{f,i}}{R_g} \cdot \left(\frac{1}{T_{m,i}} - \frac{1}{T} \right) \qquad \textbf{(4-3)}$$

where $\Delta H_{f,i}$ is the enthalpy of fusion and $T_{m,i}$ the melting temperature of polymorph i. The most common way to supersaturate a solution or supercool a melt, is by decreasing the temperature so that the fraction soluble becomes smaller than the fraction present. Other ways to apply supersaturation are solvent evaporation or increasing the pressure. In the latter case this is only possible if the crystal has the highest density.

4.1.3 Nucleation

I will briefly discuss the classical nucleation theory in this paragraph since the crystallization kinetics are determined by both nucleation and crystal growth. For a more complete description, I refer to chapter 3.1.1 (Kloek (1998)).

A small crystal is only stable if its size exceeds a certain critical size r^*. This critical size is directly related to the applied supersaturation by the Gibbs-Thomson equation. For a spherical nucleus the Gibbs-Thomson equation is given by:

$$r^* = \frac{2 \cdot \gamma \cdot v_c \cdot N_{av}}{\Delta\mu} \qquad \textbf{(4-4)}$$

where γ is the surface free energy of the nucleus with respect to the mother phase, v_c the molecular volume in a crystal lattice and N_{av} Avagadro's number. The product $v_c \cdot N_{av}$ equals the molar volume in a crystal lattice.

The activation free energy for formation of a spherical nucleus is given by:

$$\Delta G^*_{3D,hom} = \frac{16\pi \cdot v_c^{\,2} \cdot \gamma^3 \cdot N_{av}^2}{3 \cdot \Delta\mu^2} = \frac{16\pi \cdot v_c^{\,2} \cdot \gamma^3}{3 \cdot (k_b T)^2 \cdot (\ln\beta)^2} \qquad \textbf{(4-5)}$$

where k_b is Boltzmann's constant. To be more precisely, the activation free energy is the activation Gibbs energy since the pressure is assumed to be constant. The term free energy will be used in this chapter.

From isothermal crystallization experiments of emulsified hydrogenated palm oil/ sunflower oil mixtures, we were able to reach conditions of homogeneous nucleation and we determined $\gamma \approx$ 4.1 mJ·m^{-2} (Kloek (1998), chapter 3). Homogeneous nucleation occurs if the formation of a nucleus is not catalyzed by foreign surfaces from impurities, crystallizer walls, stirrer blades and so on. Homogeneous nucleation conditions for fats can only be reached by dispersing the fat in such small droplets, that in most droplets no catalytic impurities are present (Skoda and Tempel (1963), Phipps (1964), Walstra and van Beresteyn (1975)).

If nucleation is catalyzed by impurities that are larger than the nucleus, the nucleation is of a heterogeneous type. The activation free energy for heterogeneous nucleation is smaller than the activation free energy for homogeneous nucleation. The activation free energy for heterogeneous nucleation can be written as function of the contact angle θ between the nucleus, foreign surface and the mother phase. The activation free energy for heterogeneous nucleation in the case of a flat catalytic surface and assuming the nucleus is a segment of a sphere is given by (Zettlemoyer (1969)):

$$\Delta G^*_{3D} = f(\theta) \cdot \Delta G^*_{3D,hom} \qquad \text{with} \quad f(\theta) = \tfrac{1}{4} \cdot (2 + \cos\theta) \cdot (1 - \cos\theta)^2 \tag{4-6}$$

where $0 \leq f(\theta) \leq 1$. In reality, heterogeneous nucleation will occur in cavities which makes a quantitative description of the nucleation process much more difficult. Using Equation 4-6, we calculated a contact angle of about 90° from nucleation rates of emulsified fully hydrogenated palm oil/ sunflower oil mixtures that were stabilized with Tween 20, an emulsifier that contains a hydrophobic lauryl chain (Kloek (1998)). This hydrophobic part of the molecule may act as a template for the nucleating triglyceride molecules. Nucleation in bulk fats will always be of a heterogeneous nature.

The number of nuclei that are formed per unit volume and unit time is called the nucleation rate J and is mostly expressed as an Arrhenius-type of equation using ΔG^*_{3D} as the activation free energy for nucleus formation.

$$J = N \cdot \frac{k_b T}{h} \cdot \exp\left(\frac{-\alpha \cdot \Delta S}{R_g}\right) \cdot \exp\left(\frac{-\Delta G^*_{3D}}{k_b T}\right) \tag{4-7}$$

In this equation N is the number of crystallizing molecules per unit volume, $k_b T/h$ the maximum collision frequency where h is the Planck-constant, α the fraction of the molecule that should be in the right conformation for incorporation in a nucleus and $\Delta S = \Delta H_{f,i} / T_{m,i}$ the decrease of entropy on crystallization of one mole of triglyceride. The term $\exp(-\alpha \cdot \Delta S/R_g)$ is proportional to the probability that a triglyceride molecule is in the right conformation for incorporation in a nucleus. From homogeneous nucleation rates in the α polymorph in emulsified hydrogenated palm oil / sunflower oil mixtures, we estimated that almost the whole molecule should be in the right conformation for incorporation in an embryo/nucleus (Kloek (1998)). As already was indicated in chapter 3, one may

question the use of the term $\exp(-\alpha \cdot \Delta S/R_g)$ in Equation 4-7; it may also include other effects like diffusion from the bulk to the nucleus and anisometry of the triglyceride molecules.

Another type of nucleation is secondary nucleation. This is nucleation occurring due to the presence of crystals of the crystallizing compound. This is an additional nucleation which results in an extra production of potential crystals. Walstra (1987, 1995) stressed the importance of the role of secondary nucleation in triglycerides. Emulsified triglyceride droplets, crystallized at conditions for heterogeneous nucleation, showed hundreds of crystals per droplet while only one or two crystals are expected on basis of homogeneous nucleation (Walstra and van Beresteyn (1975)). When emulsion droplets of mixed paraffins had crystallized, only one or two big crystals were observed (van Boekel (1980)).

4.1.4 Crystal growth

The growth kinetics describes the crystal growth rate of a crystal face as function of the supersaturation or supercooling. For detailed discussions on crystal growth, I refer to some review papers (Garside (1985), Garside (1987), Boistelle (1988)). The growth rate of a crystal face depends on the state of the crystal surface, or more precisely, on the strength of the bonds between liquid molecules, solid molecules and liquid- and solid molecules. The state of a surface is defined by the surface entropy factor α_s which is given by (Jackson (1958)):

$$\alpha_s = \frac{4\varepsilon}{k_b T} = \frac{4}{k_b T} \cdot \left(\phi^{sf} - \tfrac{1}{2}(\phi^{ss} + \phi^{ff}) \right) \qquad \textbf{(4-8)}$$

where ε is the energy gain for formation of a solid (s)- liquid (f) bond. When starting with a pure solid and and a pure liquid, a solid and a liquid square cell are exchanged, 8 sf -bonds are formed and 4 ss-bonds and 4 ff bonds are broken. So for the formation of one sf-bond, a half ss-bond and a half ff-bond have to be broken. For low values of α_s ($\alpha_s < 3$), the crystal surface is rough and continuous crystal growth can occur. For this case, the growth rate G_c would be proportional to the supersaturation:

$$G_c = A_1 \cdot \ln \beta \qquad \textbf{(4-9)}$$

where A_1 is a constant. For higher values of α_s ($3 < \alpha_s < 4$) for which the crystal surface is smooth, two dimensional nucleation on a flat surface would be necessary for growth of a new crystal layer. This surface nucleation step then is rate-limiting. Once a surface nucleus is formed, the new crystal layer can be filled by attachment of molecules near the kink or by repeated surface nucleation and subsequent surface diffusion to existing surface nuclei. For attachment of molecules near a kink, less new surface needs to be created. The activation free energy for surface nucleation can be

calculated, analogue to 3 dimensional nucleation, and is proportional to exp(-1/lnβ). If a crystal growths by a surface nucleation process, the growth rate would be given by:

$$G_c = A_1 \cdot (\ln \beta)^p \cdot \exp\left(\frac{A_2}{\ln \beta}\right) \quad \text{with} \quad \tfrac{-3}{2} \le p \le \tfrac{5}{6} \tag{4-10}$$

Constant A_2 contains the activation free energy for formation of a surface nucleus with critical size.

For values of $\alpha_s > 4$ or very low supersaturations, the activation free energy for surface nucleation can become so high, that the crystal surface should contain defects to which growth units can attach. Such a defect can be a screw dislocation which can be seen as a step, from which a growth spiral can develop that can continuously grow. For this type of growth, Burton, Cabrera and Frank developed the BCF-relation that describes the growth rate as a function of the supersaturation.

$$G_c = A_1 \cdot \frac{(\ln \beta)^2}{\ln \beta_c} \cdot \tanh \frac{\ln \beta_c}{\ln \beta} \tag{4-11}$$

in which $\ln\beta_c$ is a constant specific to the system. For $\ln\beta \ll \ln\beta_c$ the BCF relation is equivalent to $G_c \propto (\ln\beta)^2$ and for $\ln\beta \gg \ln\beta_c$ this relation is equivalent to $G_c \propto \ln\beta$.

When starting from conditions which gives a flat crystal surface, the supersaturation is increased, a transition from a flat to a rough surface is observed. This transition is called the kinetic roughening transition and is physically explained by the vanishing of the nucleation barrier (Bennema (1992)).

Also a smooth-rough transition is observed when the temperature is increased at equilibrium or slightly supersaturated conditions. This transition is called thermal roughening and is due to statistical fluctuations only. Both thermal roughening transitions and kinetic roughening transitions have been shown for paraffins at critical supersaturation ratios of 0.0044 and 0.015 respectively and appeared to be reversible (Liu *et al.* (1992)).

Only few accurate crystal growth rate measurements on triglycerides are to be found in the literature. Skoda and van den Tempel (1967) determined growth rates of the lateral faces of single tristearate crystals in tristearate/trioleate mixtures at low supersaturations. Figure 4-1 shows their measured growth rates as function of supersaturation. The supersaturations are recalculated with Equations 4-1 and 4-3 using $T_{m\beta}$ = 343.7 K and $\Delta H_{f\beta}$ = 206 kJ·mol^{-1} rather than using the approximation that was used by Skoda and van den Tempel (1967) given by Equation 4-2.

For $\ln\beta < 0.47$, the crystals were regularly shaped and the growth rate increased non-linear with $\ln\beta$. According to the authors, growth by a surface nucleation mechanism could be ruled out because of the non-linearity of a plot of the logarithm of the growth rate against the reciprocal supersaturation. However, this is not very clear if we plot the data using the supersaturation calculated by Equations 4-1 and 4-3.

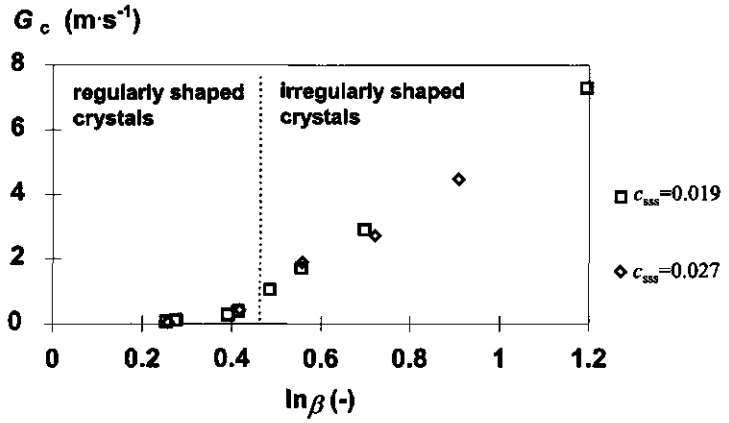

Figure 4-1. *Growth rate of the lateral faces of tristearate in trioleate as function of recalculated supersaturations. Data after Skoda and van den Tempel (1967).*

For $\ln\beta > 0.47$ the crystals were irregularly shaped and the growth rate increased about linearly with $\ln\beta$. Skoda and van den Tempel (1967) stated that due to the presence of permanent steps of 4Å, the short spacing length of triglycerides, no surface nucleation is necessary for growth. Steps with a height of about 4.5 Å were shown in electronmicrographs of triacylglycerol crystals (Heertje and Pâques (1995)). The presence of permanent steps would lead to continuous growth and Skoda and van den Tempel (1967) suggested that the growth rate is mainly determined by the probability that the triglycerides have a suitable orientation for incorporation in the surface. Other triglycerides like PPP and PSP showed similar growth behaviour.

Another important observation was that the growth rate at a certain $\ln\beta$ was history dependent. If a crystal was first grown at a certain supersaturation and subsequently grown at a lower supersaturation, the growth rate at this low supersaturation was slower than if this lower supersaturation was directly applied. This suggests that the state of the crystal surface and thereby crystal growth, can be influenced by the growth history.

This conclusion is important for the description of the crystal growth rate of natural fats, since they contain hundreds of different triglycerides. The different triglycerides can cause the formation of crystal defects and retard the crystal growth.

The aim of the work described in this chapter is to describe the crystallization kinetics of the model fat dispersion in terms of nucleation rates and crystal growth rates. To this end, also the polymorphic behaviour of this model system is studied The results of description of the crystallization kinetics will be compared to aggregation and gelling times of the dispersions in a following chapter.

4.2 Material and Methods

4.2.1 Materials

A description of the physical properties and the triglyceride composition of the model system is given in chapter 2 of this thesis.

4.2.2 Methods

Mixtures of HP in SF were made by melting the HP at 80 °C and bringing an amount of liquid HP in a vessel. Care was taken that the HP remained liquid while transferring it to the vessel to avoid fractionation due to crystallization. An appropriate amount of SF was added to give the final mixture. Mixtures were stored in such small volumes that they had to be heated not more than 3 times for use for experiments. Prior to any experiment, the mixtures were kept at 80 °C for 10 minutes to destroy any crystal memory.

The melting and crystallization behaviour of HP/SF mixtures was studied by means of Differential Scanning Calorimetric (DSC) studies using a Mettler DSC-30 equipped with a TC-10A processor or a TA-Instruments DSC type 2910.

Time resolved X-ray diffraction was used to determine the short spacings from which the crystal polymorph can be extracted. The radiation source (Cu-$K_{\alpha 1}$) used, operated at a wave length of 1.5405 Å. Radiation was detected by using an 1025 channel diode array positional detector. The position of the detector was calibrated with potassium iodide (4.08 and 3.53 Å). The sample holder could be heated and cooled at rates of about 1 $K \cdot s^{-1}$.

Isothermal crystallization of HP/SF dispersion was monitored by pulsed Nuclear Magnetic Resonance (p-NMR) measurements using a Bruker minispec P20i (20 MHz). The amount of solid fat was determined by measuring the relaxed signal at two times after applying a 90° pulse. The signal could not be measured during the first 10 μs after the pulse was applied due to electronic recovery from the electromagnetic pulse. Within this time already a part of the signal from protons in the crystal lattice decayed. After 40 μs the signal from the solid protons has decayed and the signal was only due to the signal of the liquid protons. The measured signal was proportional to the amount of protons. From the measured signal at 10 μs and 90 μs after applying a 90° pulse, and after applying a correction for the signal decay between 0 en 10 μs after the pulse by means of an *f*-factor, the fraction solid can be calculated. The *f*-factors were determined using the measured NMR signals and the expected fractions solids from Equation 4-3 using values of $\Delta H_{f,i}$ and $T_{m,i}$ that were determined by DSC. The *f*-factors for HP/SF dispersions crystallized in the α- and the β' polymorph were 1.14 and 1.44, respectively. The fraction solid fat was determined by averaging the signals from 3 pulses at repetition times of 5 s. This repetition time was sufficient to avoid saturation of the signal due to incomplete relaxation. The inaccuracy of this determination was about 0.3-0.4 % solid fat.

4.3 Results and discussion

4.3.1 Thermal properties of fully hydrogenated palm oil

Figure 4-2 shows the thermal effects during heating of HP that had crystallized at various conditions. The samples were first quenched to -80 °C to crystallize the HP. During heating of the sample (tracé 1) at a rate of 2 K·min^{-1}, first an endothermic heat flow was observed, followed by an exothermic heat flow and finally an endothermic heat flow. As the HP was cooled very rapidly to -80 °C, it is likely that HP had crystallized in the most instable α polymorph. The first endotherm on heating (T = 48 °C) would correspond with the melting of the α polymorph. The exotherm at 50 °C then corresponds with the recrystallization of the α polymorph to a more stable polymorph (β' and/or β) and the final endotherm at 59 °C corresponds with the melting of the more stable polymorph. Simultaneous with the endothermal melting of the α polymorph, also exothermal recrystallization to a more stable polymorph may occur which explains the small melting endotherm of the α polymorph compared to the large melting endotherm of the more stable polymorph. The final endotherm seems to be formed by more than one peak, which suggests the simultaneous occurrence of different polymorphs or the existence of compound crystals, or both.

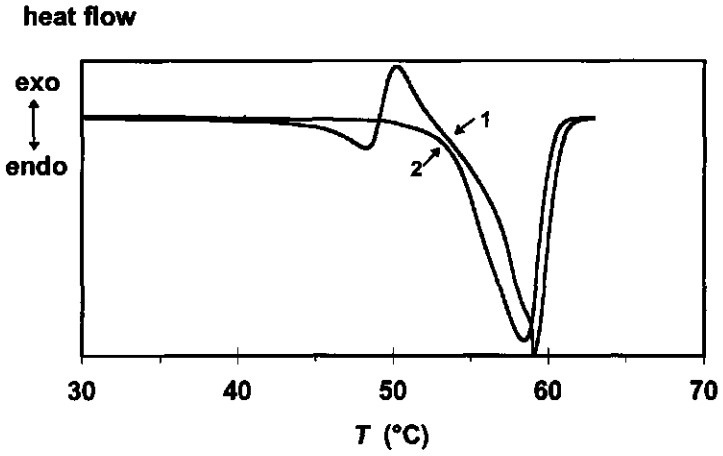

Figure 4-2. *DSC heating curves of HP, crystallized by rapid cooling from 80 °C to -80 °C. (trace 1) heating from -80 °C to 80 °C at 2* K·min^{-1}*; (trace 2) heating from 50 to 80 °C at 2* K·min^{-1} *after isothermal crystallization for 30* min *at 50 °C and cooling to 30 °C.*

When the melting scan was stopped at 50 °C for 30 minutes to allow the HP to (re)crystallize isothermally followed by cooling to 30 °C and next determining a melting scan (trace 2), only an endothermic melting effect was observed. The peak temperature was observed at a lower temperature than in a continuous scan and the melting peak seemed to be continuous. This indicates that after isothermal crystallization at a temperature slightly above the α clear point, the HP crystallizes in a less stable polymorph, probably the β' polymorph.

The polymorphs were checked by determining the X-ray diffraction spectra for HP, crystallized at 5 °C and at 45 °C for 30 minutes (Figure 4-3). It is clear that isothermal crystallization at 5 °C predominantly yielded the α polymorph while crystallization at 45 °C almost exclusively yielded the β' polymorph. It is not clear whether continuous heating of HP, crystallized in the α polymorph, yielded the β' polymorph, the β polymorph or a mixture of both polymorphs. The latter seems most likely to occur. If only the β' polymorph was formed, crystallization conditions may have had a considerable effect on the presence of crystal defects and on the composition of the resulting compound crystals regarding the differences in the DSC melting peaks after isothermal crystallization at 50 °C and recrystallization from the α polymorph. In the absence of oil, the α polymorph was observed to be stable for at least 30 minutes.

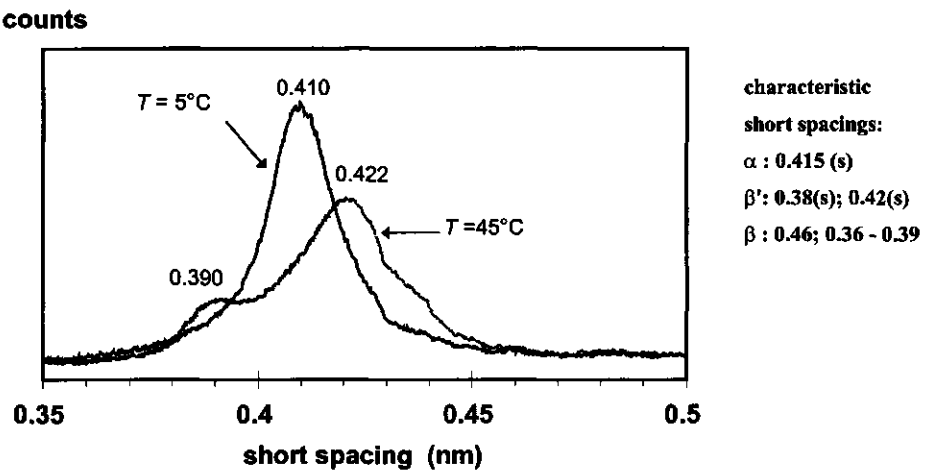

Figure 4-3. *X-ray diffraction spectra of HP crystallized at T = 5 °C and T = 45 °C. The indicated numbers are the short spacings in* nm. *Also the theoretical short spacings are given; s=strong.*

4.3.2 Thermal properties of HP/SF mixtures

The DSC melting curve of HP in the β' polymorph only shows one broad melting peak. Although extensive compound crystal formation will occur due to the variety of triglycerides present, we will treat the HP as an one component system with one melting point and one melting enthalpy for each polymorph. This is more or less allowed since, the triglycerides in HP are all similar: they all contain completely saturated fatty acid residues and most of these are palmitic and stearic acid. We will also treat the sunflower oil (SF) as a one component system. Under the experimental conditions, SF will always be a liquid. As the melting points of HP and SF differ by

more than 45 K, the solubility of HP in SF can be approximated by the Hildebrand-equation (Equation 4-3) (Hannewijk, 1964; Wesdorp, 1990)). This equation assumes ideal mixing behaviour, which will certainly be not be quite true for the β' polymorph of our model system. By fitting the melting temperatures of a certain polymorph of dispersions containing various amounts of HP to the Hildebrand-equation, effects due to non-ideal mixing will be incorporated in the calculated melting enthalpy and melting temperature. However, the combination of melting enthalpy and melting temperature will describe the solubility of HP in SF.

The α polymorph can be obtained by cooling a solution so rapidly that nucleation in the β' or β polymorph does not occur. Since the α polymorph in bulk fats cannot be supercooled deeply, the onset-temperature or the peak temperature measured by DSC would only be a little below the α-clear point. After crystallization in the α polymorph, the dispersions were heated at a rate of 2 $K \cdot min^{-1}$. None of the HP/SF dispersions showed an α-melting peak, nevertheless an exothermal crystallization peak was present. The endothermal effect of melting of the α polymorph may be compensated by the simultaneous exothermal effect of recrystallization of the more stable polymorph. Melting of the recrystallization product showed a large endothermic melting peak (β' or β polymorph). This peak did not show a discontinuity, as was seen for a 100 % HP sample. To obtain the β' polymorph, solutions were crystallized for 30 minutes at a temperature of 4 K above the clear point of α-crystals. After cooling back to -5 °C, the DSC melting profile was measured.

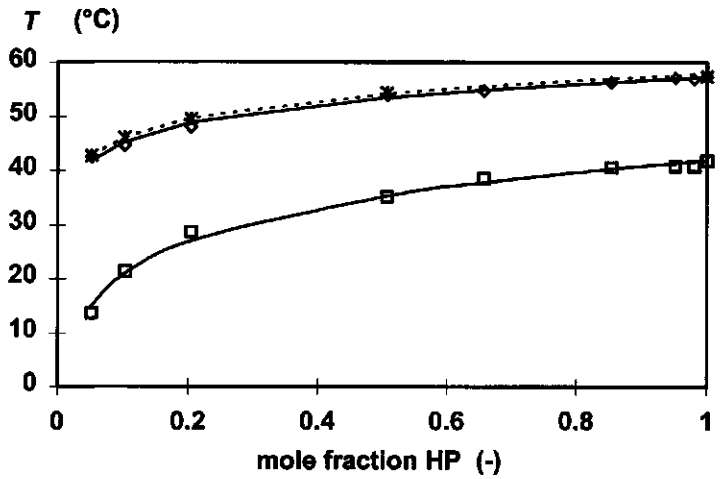

Figure 4-4. *Peak temperatures of the crystallization and melting processes measured by DSC as function of the fraction HP in HP/SF dispersions.* □ *crystallized in α polymorph;* ◊ *melting after crystallization in the α polymorph;* * *melting after isothermal crystallization at 4 K above the α clear point. The lines were fitted to the Hildebrand equation.*

Figure 4-4 shows that the measured peak temperatures can be fitted well using the Hildebrand equation. There is only a very slight difference between melting of the polymorph obtained after melting of the α polymorph and the polymorph obtained after isothermal crystallization at 4 K above the α clear point. The melting enthalpies and melting temperatures obtained from the fit, together with the data for 100 % HP are given in Table 4-1.

Table 4-1. *Melting enthalpies and melting temperatures of HP, with 95 % confidential limits, obtained by fitting peak transition temperatures of HP/SF dispersions to the mole fraction of HP, using the Hildebrand equation.*

experiment	From dispersions		From pure HP	
	$\Delta H_{f,i}$ ($J \cdot mol^{-1}$)	$T_{m,i}$ (°C)	$\Delta H_{f,i}$ ($J \cdot mol^{-1}$)	$T_{m,i}$ (°C)
α-crystallization exotherm	$(8.4 \pm 0.8) \cdot 10^4$	41.9 ± 1	$9.8 \cdot 10^4$	41.8
melting after α-crystallization endotherm	$(1.7 \pm 0.1) \cdot 10^5$	57.2 ± 0.5	$1.12 \cdot 10^5$	57.4
melting after β'-crystallization endotherm	$(1.7 \pm 0.1) \cdot 10^5$	57.9 ± 0.7	$1.35 \cdot 10^5$	57.6

The fitted melting temperature corresponds well with the temperatures measured for pure HP. There is only a slight difference in the enthalpy of fusion for the α polymorph, which suggests that the Hildebrand-equation well describes the solubility of the α polymorph of HP in SF. Wesdorp (1990) concluded from an extensive study that the formation of compound crystals in the α polymorph hardly disturbed crystal packing due to freedom of the fatty acids chain for oscillations. Therefore the mixing of the solid phase in the α polymorph is about ideal.

There was a big difference between the melting enthalpy for HP obtained from the fit of the peak temperatures and obtained from the pure HP sample when crystallization occurred in a more stable polymorph. This is probably due to the highly non-ideal mixing behaviour in the β'- and β polymorph (Wesdorp, 1990) and the application of the Hildebrand-equation. Another possibility for the lower molar enthalpy of "pure" HP, is that liquid impurities in the HP are dissolved in the oil phase in case of HP/SF dispersions and therefore do not cause crystal defects in HP. There is no significant difference between the melting temperature, when the more stable polymorph is prepared by recrystallization from the α polymorph or by direct crystallization at a temperature above the α clear point.

Although melting temperatures and melting enthalpies obtained from DSC melting scans can give some indication about the polymorph(s) that is/are present, the only reliable way to determine this is by means of X-ray diffraction. Therefore we determined X-ray spectra of 10 % HP/SF dispersions that had isothermally crystallized at 5 °C and 15 °C.

Figure 4-5 clearly shows that at a temperature of 5 °C, crystallization takes place in the α polymorph (0.415 nm). The intensity of the α-peak at 0.415 nm decreases in time and peaks at 0.37 and 0.39 nm and a strong double peak at 0.45 - 0.46 nm appear or increase in intensity. These peaks correspond to the β polymorph. There is also a increase in intensity of a peak at 0.42 nm which corresponds to the β' polymorph. So crystallization in the α polymorph of HP/SF mixtures leads to a fast transformation to a mixture of the some β'-crystals and predominantly β-crystals.

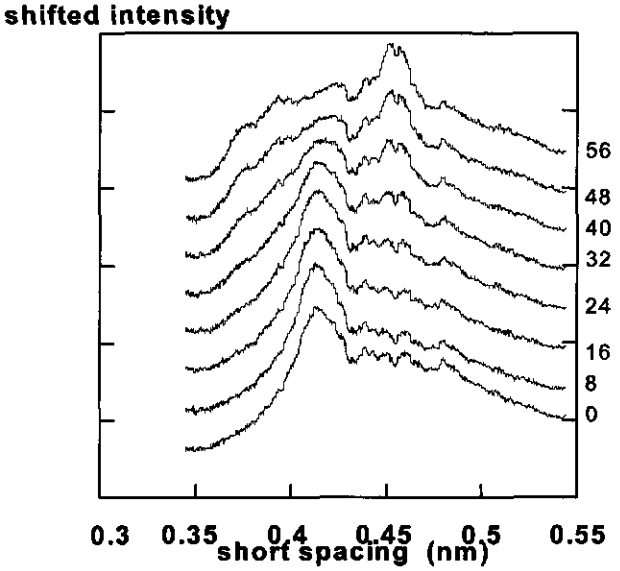

Figure 4-5. *X-ray diffraction spectra of a 10 % HP/SF dispersion crystallized at T = 5 °C as function of holding time (indicated in minutes near right-hand Y-axis).*

At a temperature of 5 °C the polymorphic transformation from α to β'/β in a 10 % HP/SF dispersion takes place in about 30 minutes. Isothermal crystallization experiments at a temperature of 15 °C gave transformation on a time scale of about 3 minutes. Pure HP crystallized at a temperature of 5 °C did not show any transformation at this temperature in 30 minutes. This shows that both the presence of liquid phase and a higher temperature increases the transformation rate from the α polymorph to a more stable polymorph.

The activation energy for the polymorphic transition can be estimated from the time scales of the transition at the two temperatures. The time scales of the transition are inverse proportional to the reaction rate of the transitions. The reaction rate is, in turn, proportional to $\exp[-\Delta E^*_a/(R_g T)]$, where ΔE^*_a is the activation energy of the rate limiting step of the polymorphic transition. The ratio between the time scales of the transition at temperatures T_1 and T_2 is given by $\exp(-\Delta E^*_a/R_g \cdot (T_1^{-1}-T_2^{-1}))$ from which ΔE^*_a can be calculated. Substituting time scales of 1800 and 180 s at temperatures of 278 and 288 K respectively gives an activation energy of 153 kJ·mol^{-1}. This value is close to the

melting enthalpy of HP in the β'/β polymorph as determined from the melting curves of HP/SF dispersions. Therefore it is likely that the crystallization of the β'/β polymorph is the rate limiting step in the polymorphic transition of the α polymorph. Probably the transition occurs by a dissolution- crystallization process since it is associated with a change in the extent of compound crystal formation. Initiation of the more stable polymorph can occur by nucleation in this polymorph as there is only a limited solubility of the α polymorph in the SF, so that the soluble material can become supersaturated for the more stable polymorph. The solubilities of the α polymorph at temperatures of 5 and 15 °C are, according to the Hildebrand equation, 0.7 % and 3 %, respectively. At these conditions the supersaturation of the soluble triglycerides in the β' polymorph, assuming their thermodynamic properties to be the same as for HP, would equal 6.0 and 5.0, respectively.

If the dispersions had crystallized at a temperature above the onset of the α-clear point, X-ray diffraction spectra only showed the β' polymorph, even after several days of storage.

This leaves the question why the transformation α → (β',β) does occur, even with some preference for the β polymorph, while after crystallizing in the β' polymorph no transition to the β polymorph occurs. This may probably be due to the formation of compound crystals. Extensive compound crystal formation in the α polymorph leads to a large difference in chemical potential difference between the α polymorph and the most stable β polymorph and therefore to a driving force for recrystallization. Formation of compound crystals in the β' polymorph is less extensive and therefore the driving force for recrystallization is smaller. Furthermore the Gibbs-activation energy for dissolution will be higher for the β' polymorph compared to the α polymorph

4.3.3 Crystallization kinetics

The crystallization kinetics of dispersions, containing 6, 8, 10, 12 or 14 % HP/SF at initial supersaturations ranging from 2.25 to 4.00 in steps of 0.25, were determined by p-NMR. Figure 4-6 shows the determined crystallization curves of 12 % HP/SF dispersions at various initial $\ln\beta$. It is clear that the induction time for crystallization increased with decreasing initial supersaturation. This can be explained by the strong dependence of the nucleation rate on supersaturation according to Equations 4-5 and 4-7. The final fraction of solid fat increased with increasing initial supersaturation due to the decrease of solubility as expected from Equations 4-2 and 4-3.

To model crystallization kinetics, one has to know the relation between crystal growth rate and supersaturation. To obtain the supersaturation as function of time we fitted the crystallization curves to a modified Gompertz equation. This fit yields an analytical expression that gives the supersaturation as a function of time.

The Gompertz equation is often used to described microbial growth but it can also be used to describe the crystallization process as there are several analogues with bacterial growth: production of bacteria - nucleation and growth of crystals; consumption of nutrients - decrease of supersaturation. The reparameterized Gompertz equation is given by (Zwietering *et al.* (1990)):

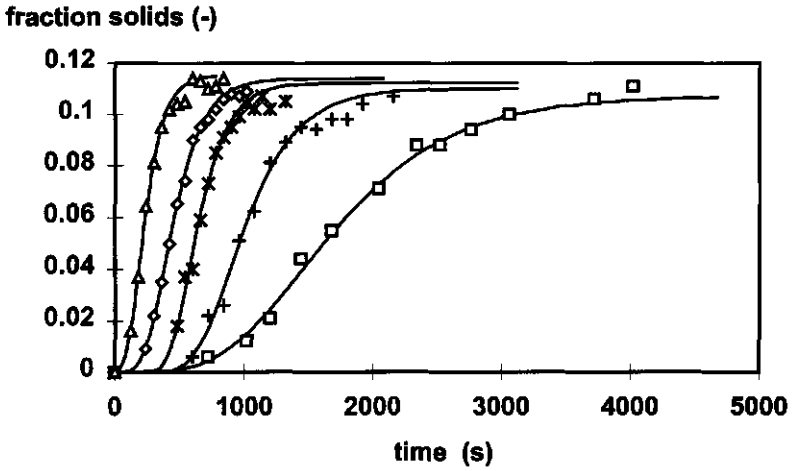

Figure 4-6. *Isothermal crystallization curves of 12 % HP/SF dispersions at various initial supersaturations. Solid lines are fitted using the Gompertz equation. Supersaturation:* □ *2.25,* + *2.50,* * *2.75,* ◊ *3.00,* Δ *3.25.*

$$s(t) = s_{max} \cdot \exp\left\{-\exp\left[\frac{\mu \cdot e}{s_{max}} \cdot (\lambda - t) + 1\right]\right\} \qquad \textbf{(4-12)}$$

where $s(t)$ is the fraction solid fat at time t, s_{max} the maximum fraction of solid fat, μ the maximum increase rate in fraction solid fat (or tangent in the inflection point of the crystallization curve), λ a measure for the induction time defined as the intercept of the tangent at the inflection point with the time-axis and e equals exp(1). The maximum fraction solid fat s_{max} can be written as:

$$s_{max} = c_{0,HP} - x_{HP} = c_{0,HP} \cdot \left(1 - \frac{1}{\beta_0}\right) \qquad \textbf{(4-13)}$$

where $c_{0,HP}$ is the fraction HP present and β_0 the supersaturation ratio at the start of the crystallization which are both constant. So only parameters μ and λ are left to fit the crystallization curve. Figure 4-6 shows that the reparameterized Gompertz equation described the crystallization curves very well.

The obtained induction time λ can be used to estimate the surface free energy for formation of a nucleus of critical size. If it is assumed that λ can be used as a measure for the nucleation rate in which $\lambda \propto J^{-1}$, the next proportionality would be valid for a cubic nucleus:

$$\ln\lambda \propto \frac{v_c^{\,2}\cdot\bar{\gamma}^{3}}{(k_b T)^3}\cdot\frac{1}{(\ln\beta_0)^2} \qquad \textbf{(4-14)}$$

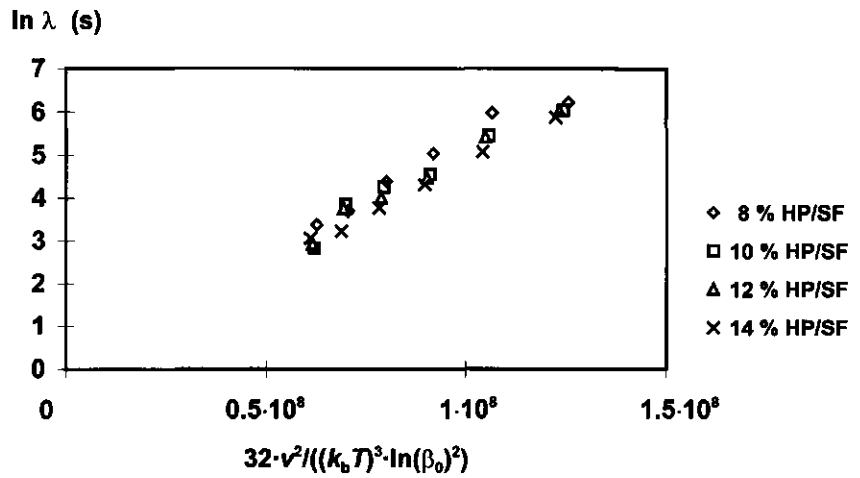

Figure 4-7. *Induction time λ as function of a supersaturation term to allow determination of the surface free energy for nucleus formation*

From the slope of a plot of $\ln\lambda$ against $(\ln\beta_0)^{-2}$, γ can be calculated. For the systems studied, this plot is shown in Figure 4-7 and the fit results are given in Table 4-2. The data in Figure 4-7 show that there is a linear relation with good correlation coefficients (Table 4-2). The slopes yield an average surface free energy for formation of an nucleus of about 3.4 - 3.9 $mJ\cdot m^{-2}$, independent on the fraction HP. This value can be used to calculate the nucleation rate for modelling the crystallization kinetics. The real value of the surface free energy of a nucleus will be higher since nucleation type in bulk fats is heterogeneous and Equation 4-14 is valid for homogeneous nucleation. From homogeneous nucleation rates in the α polymorph of emulsified 10 % HP/SF, we determined a surface free energy of 4.1 $mJ\cdot m^{-2}$ (Kloek (1998)).

Table 4-2. *Determination of the surface free energy for nucleation of HP/SF dispersions with various HP contents from the induction time for crystallization as function for initial supersaturation. The induction time is supposed to be equal to λ (Equation 4-12).*

HP/SF (%)	γ ($mJ.m^{-2}$)	r^2 (-)
8	3.7 ± 0.2	0.978
10	3.6 ± 0.3	0.976
12	3.6 ± 0.2	0.988
14	3.6 ± 0.1	0.998

The only unknown parameter for calculating the nucleating rate as a function of time or supersaturation is α, the fraction of the triglyceride molecule that should be in a suitable conformation to be incorporated in the nucleus. From modelling nucleation kinetics in emulsified fats we calculated $\alpha = 1$ (Kloek (1998), chapter 3) when nucleation was assumed to occur in the α polymorph. It is likely that for nucleation in the β' polymorph this value will be about the same.

Since the nucleation rate and the supersaturation are known as function of time, it is possible to calculate the crystal growth rate G_c as function of time or supersaturation. This was achieved by calculating the number of nuclei $J \cdot \Delta t$ produced in every time step Δt and by how much crystalline material, produced in previous time steps had to grow ($G_c \cdot \Delta t$) to yield the fraction of crystallized material as given by Equation 4-12. After every time step, the nucleation rate corresponding to the new supersaturation was calculated and the whole procedure was repeated. So after every time step a new crystal size interval was created. The size of the crystal at time t that is nucleated on time z is given by $\sum_{i=z}^{i=t} G_{c,i} \cdot \Delta t$.

It is assumed that the crystals are spherical. In reality, the crystals are needles or platelets having more than one growing face and each having its own growth rate. The ratio of growth rates of the various faces equals the ratio of the crystal dimensions perpendicular to the faces. Supposing the crystals to be rectangular and having three pairs of growing faces x, y and z with linear growth rates of G_x, G_y and G_z and furthermore $G_x/G_y = a$ and $G_x/G_z = b$. The volume of the crystal in time can be expressed as function of one growth rate and is for instance given by $(a \cdot b)^{-1} \cdot G_x^3 \cdot t^3$. If the ratio of the growth rate of the various faces remains constant, the volume of a crystal and thereby the crystallization curves can be fitted using only one crystal growth rate.

Because the modified Gompertz-equation does not fit the part of the crystallization curve between $t = 0$ and $t = \lambda$, which is because the fraction solid fat could not be determined accurately enough, the growth rate in this time interval has been calculated using the Avrami equation (Avrami (1939a,b)). The Avrami equation gives the fraction solids as function of time for a constant J and G_c. Both parameters are constant for a constant supersaturation. This will be approximately the case between $t = 0$ and $t = \lambda$ and then the Avrami equation can be used to calculate the initial G_c, since the nucleation rate J is known. Thereto, we calculated the time after which 0.5 % solids would be present using Equation 4-13, and substituting this time in the Avrami equation. In the case of no impingement of crystals, the Avrami equation for spherical crystals is given by:

$$s(t) = \tfrac{1}{3}\pi \cdot G_c^{\,3} \cdot J \cdot t^4 \qquad \textbf{(4-15)}$$

After crystallization of 0.5 % HP in a 10 % HP/SF mixture, the supersaturation ratio is about 95 % of its initial value. We neglect the effect of this decrease on the nucleation rate. At $t > \lambda$, the modified Gompertz equation was used to describe the amount of solid fat.

Figure 4-8 shows the fitted growth rate as a function of supersaturation for 12 % HP/SF dispersions during crystallization at various initial supersaturations. These growth curves coincide for $\gamma = 3.8$ mJ.m^{-2} while for higher values of γ the growth curves strongly deviate from each other.

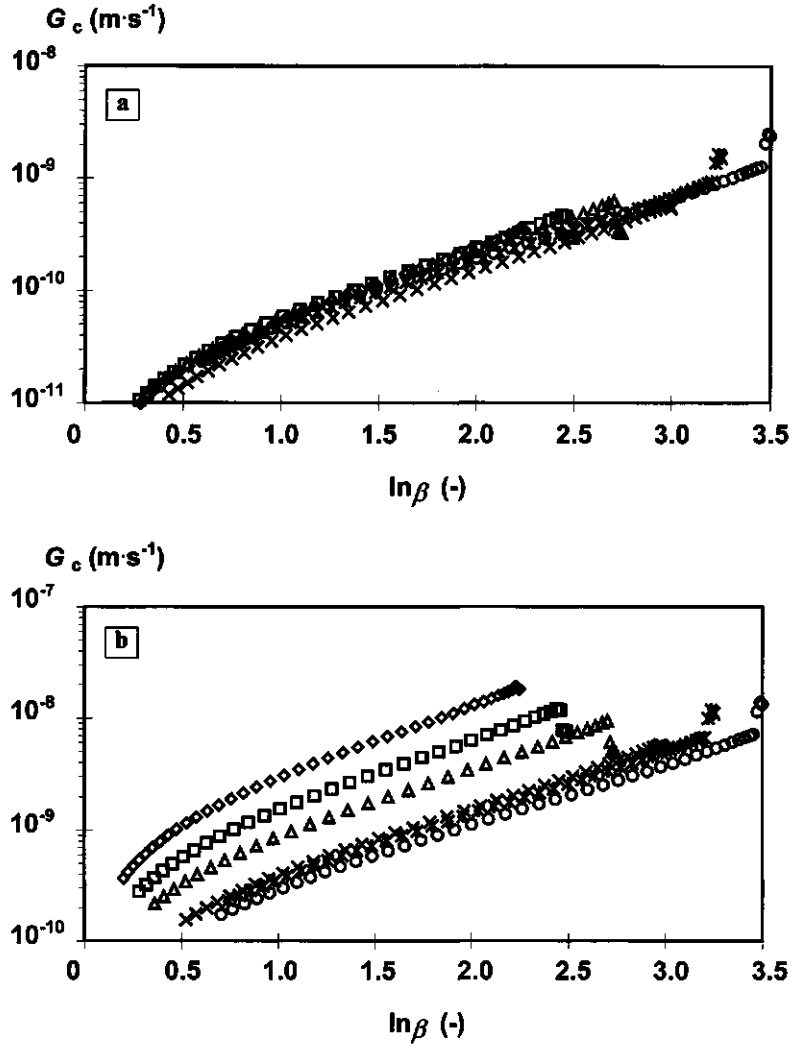

Figure 4-8. *Growth rate (G_c) curves calculated from crystallization curves of 12 % HP/SF dispersions for various initial supersaturations.* $\ln\beta_0$: ◊:*2.25* , □:*2.50*, Δ:*2.75*, ×:*3.00*, *:*3.25*, o:*3.50*. *Nucleation parameters:* α = *0.8; (a):* γ = *3.8* mJ.m^{-2}*; (b):* γ = *5.0* mJ.m^{-2}.

The growth rate curves show some irregularities at the beginning of the crystallization process, *i.e.* at the right hand side of the growth rate curves. This may be due to the change from the Avrami equation to the modified Gompertz equation at $t = \lambda$. As the increase rates of the fraction solid at a solids percentage of 0.50 % differ for both equations, the calculated growth rate curve

cannot be continuous at that point. Figure 4-8 shows that for supersaturations higher than 1, $\log G_c$ is linear with $\ln\beta$, so the growth rate curves can be described by a relation of the following form:

$$\ln G_c = \ln A_g + b_g \cdot \ln\beta \quad \text{or} \quad G_c = A_g \cdot \beta^{b_g} \tag{4-16}$$

This type of equation is not equivalent to one of the theoretical growth rate equations given in paragraph 4.1.4. I come back on this point later

Since now a function is known (4-16) that empirically describes the growth rate as function of supersaturation, the crystallization curves can be fitted by varying only A_g and b_g for a given α and γ. Only the last part of the crystallization curve, corresponding to supersaturations below 0.8, cannot be fitted. At a supersaturation of 1, only a fraction $c_{0,HP}\cdot\exp(1-\beta_0)$ of the HP is soluble. There are two main advantages of using Equation 4-16: only two parameters are needed to describe the growth rate as function of supersaturation and there is no discontinuity by going from the Avrami equation to the modified Gompertz equation.

The measured data were fitted to Equation 4-16 by minimizing the sum of the squares of the differences between the fitted and the measured fractions solid fat. Figure 4-9 shows the fitted lines. There are some small differences compared to the fits obtained using the Gompertz equation (Figure 4-6).

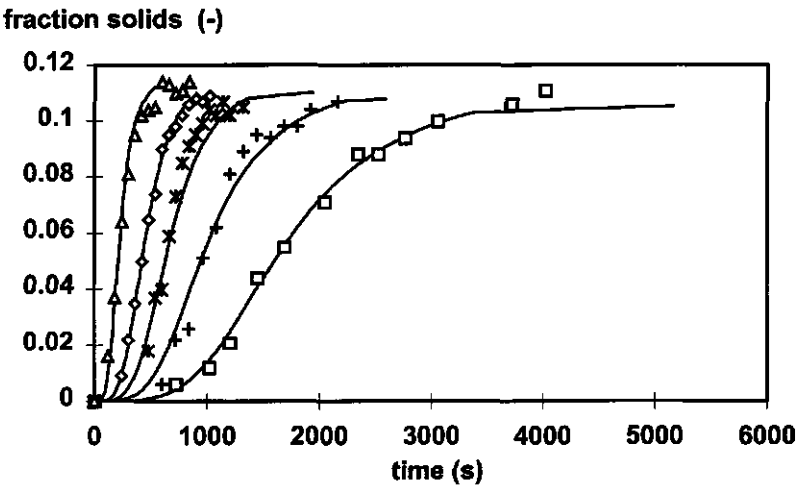

Figure 4-9. *Measured and fitted crystallization curves of 12 % HP/SF dispersions crystallized at various initial supersaturations. The fits were obtained using growth rate Equation 4-16. Initial supersaturations:* □ *2.25,* + *2.50,* * *2.75,* ◊ *3.00,* Δ *3.25.*

Table 4-3. *Coefficients A_g and b_g from growth rate Equation 4-19 obtained from a fit of isothermal crystallization curves of 12 % HP/SF dispersion at various initial supersaturations.*

$\ln\beta_0$ (-)	A_g ($m.s^{-1}$)	b_g (-)
2.25	$1.4 \cdot 10^{-11}$	1.50
2.50	$1.1 \cdot 10^{-11}$	1.50
2.75	$1.39 \cdot 10^{-11}$	1.31
3.00	$1.24 \cdot 10^{-11}$	1.31
3.25	$1.78 \cdot 10^{-11}$	1.31
3.50	$1.80 \cdot 10^{-11}$	1.31

The fit coefficients in Table 4-3 show that for supersaturations below 2.75, slope b_g is about 1.5. For supersaturations of 2.75 and higher the slope decreases to a value of about 1.3. The same slopes were determined for dispersions containing various fractions of HP. The sudden change of b_g is probably related to the morphology of the crystal structures. From microscopic observations it was clear that at supersaturations below 2.75, spherulitic structures were formed.

As mentioned, the growth rate can also be given by a power-law with the supersaturation ratio β as the independent parameter rather than the supersaturation $\ln\beta$ (Equation 4-16). These type of engineering-equations are often used to describe crystal growth rate as function of the concentration difference Δc between a supersaturated and a saturated solution ($\Delta c = c_{0,HP} - x_{HP}$). The supersaturation ratio, which is equal to $c_{0,HP}/x_{HP}$, is about proportional to the concentration difference for supersaturations that are much greater than unity. This is true in the range of supersaturations we studied. The scaling exponent b_g in Equation 4-16 ranges from 1.3 to 1.5. These values are often found when scaling relations like $G_c \propto (\Delta c)^a$ are used (Garside (1987)). For constant b_g, A_g was about proportional to the initial fraction HP.

As mentioned, it was not possible to fit the crystallization curves by using one of the theoretical growth rate equations. Possible explanations for this observation are:

- The growth models normally used, are only suited for dispersions that are only slightly supersaturated, say $\ln\beta$ of about 0.01 to 1. At higher supersaturations, their applicability is limited because: (i) heat of crystallization has to be removed and (ii) molecules must be able to diffuse fast enough to reach the crystal surface. Both phenomena can result in an effectively lower supersaturation at the solid-liquid interface then is calculated on base of the amount of crystallized material. (i): Assuming a heat diffusion coefficient D^* of 10^{-7} $m^2 \cdot s^{-1}$ and a diffusion length $x_{0.5}$= 4 mm (width of p-NMR tube) yields a characteristic time $t_{0.5,h}$ during which the amount of heat is halved of 160 s according to $x_{0.5} = (D^* \cdot t_{0.5,h})^{1/2}$. A maximum crystallization rate of $6 \cdot 10^{-4}$ s^{-1} (μ in Equation 4-12; 12 % HP/SF, $\ln\beta_0 = 3.50$), corresponds to a temperature increase rate of 0.027 $K \cdot s^{-1}$, assuming a specific heat capacity of 4 $kJ \cdot kg^{-1} \cdot K^{-1}$ and no heat loss. In $t_{0.5,h}$ the temperature increase would be about 4 K, which will certainly effect the real supersaturation.

Near the crystal surface this increase rate will be even higher, so that a lower effective supersaturation near the solid - liquid interface due to crystallization heat seems likely. (ii): The diffusion length of a triglyceride molecule using $D^* = 10^{-10}$ m^2·s^{-1} is about 10^{-5} m for $t_{0.5,d} = 1$ s. This distance is very much larger than the displacement of the solid - liquid interface in 1 s.

- Since HP consists of various triglycerides, the supersaturation, which determines the magnitude of the nucleation rate, is a rather ill-defined term. The supersaturation is calculated for the mean thermodynamic bulk properties of HP/SF dispersions while during crystallization a kind of fractionation of triglycerides may occur. Due to the variety of triglycerides, crystal defects will form that can influence the incorporation of other triglycerides to the crystal surface.
- The anisometric shape of the triglyceride molecule and of the crystal will greatly hamper the microscopic description of the incorporation process of a triglyceride molecule. It is not unlikely that the activity coefficient depends on the supersaturation for each crystal face in a different way
- It is assumed that the nucleation rate can be described by the classical nucleation rate equation although it is by no means sure that it is allowable. For instance, no direct account is made for the occurrence of secondary nucleation. However, it may be incorporated in the surface free energy for nucleation which could than be seen as a kind of apparent surface free energy that also includes other supersaturation dependent processes like secondary nucleation.
- Aggregation and sintering of crystals will lead to a decrease in the effective crystal surface and therefore to a lower crystallization rate. This will become more pronounced if strong clustering of crystals to compact aggregates or thickened crystal strands occurs.

4.3.4 Aggregation times

Although, as discussed above, there are many uncertainties in describing the crystal growth rate as a function of supersaturation, it may provide important information about the crystal size distribution as function of time, which can be used to estimate flocculation or gelling times. According to Smoluchowski, the number of collisions per unit time due to Brownian motion between spherical particles in a system containing c particles per unit volume is given by

$$J_{coll} = -\frac{dc}{dt} = K \cdot c^2 \quad \text{with } K = 8\pi \cdot D \cdot a \tag{4-17}$$

The rate constant K depends on the diffusion constant D and the particle radius a. From this equation the flocculation time for spherical particles, this is the time to decrease the number of particles to half its initial value, can be derived and is given by:

$$t_{0.5} = \frac{3 \cdot \eta_0}{4 \cdot k_b T \cdot c_0} = \frac{\pi \cdot \eta_0 \cdot a^3}{k_b T \cdot \phi} \tag{4-18}$$

Aggregation will already occur at low volume fraction of solid fat. During the initial stage of the crystallization process, the amount of solid fat can be approximated with Avrami's equation (4-15). This approximation is only valid if the nucleation rate and the crystal growth rate are constant in this stage of the crystallization process. The volume surface averaged radius a_{32} of the crystals formed is given by:

$$a_{32}(t) = \frac{\text{total volume}}{\text{total surface}} = \frac{\frac{4}{3}\pi \int_0^t G_c^{\,3}(t-z)^3 \mathrm{d}z}{4\pi \int_0^t G_c^{\,2}(t-z)^2 \mathrm{d}z} = \tfrac{1}{4} G_c t \qquad \textbf{(4-19)}$$

where z is the time at which a nucleus is formed.

The flocculation time can be estimated as function of the time t that crystallization proceeds by substituting Equations 4-15 and 4-19 into 4-18.

$$t_{0.5} = \frac{3 \cdot \eta_0}{64 \cdot k_b T \cdot J \cdot t} \qquad \textbf{(4-20)}$$

This equation shows that for a constant nucleation rate, the flocculation time decreases with crystallization time t. At the time that $t_{0.5}/t < 1$, the time scale of flocculation is smaller than the time scale of crystallization and flocculation becomes important. This 'flocculation time' is given by:

$$t_{0.5} = \sqrt{\frac{3 \cdot \eta_0}{64 \cdot k_b T \cdot J}} \qquad \textbf{(4-21)}$$

One should keep in mind that the calculated time is not a real flocculation time in the sense of a time to half the number of initial particles, as there are no particles present at $t = 0$.

Using $\alpha = 0.8$ and $\gamma = 3.8$ mJ.m^{-2}, obtained from the crystallization kinetics, yields for 12 % HP/SF dispersion at a $\ln\beta = 3.5$ a nucleation rate of about $4 \cdot 10^{16}$ m^{-3}.s^{-1} which corresponds to a 'flocculation time' of about 4 seconds. For $\ln\beta = 2.75$, a flocculation time of 13 seconds is calculated. After these times, hardly any solid fat had crystallized. Very short time scales for aggregation were indeed observed from steady shear viscosity measurements during the aggregation of fat crystals in low volume fraction solids dispersions (Kloek (1998)), chapter 5). A rule of thumb is that the gelling time is about ten times the flocculation time. The order of magnitude agrees well with gelling times of 40 and 330 s as determined by dynamical rheological measurements of 12 % HP/SF dispersions at initial supersaturations of 3.50 and 2.75 respectively (Kloek (1998), chapter 6).

Figure 4-10 shows the effect of the fit parameters α and γ on the calculated 'flocculation times'. According to Equation 4-21, 'flocculation time' only depends on the nucleation rate. For

given experimental conditions, nucleation rates only depend on the values of α and γ. The grey band in Figure 4-10 shows the expected range of 'flocculation times'. This shows that not much variation in the values of α and γ is allowed to obtain realistic 'flocculation times'.

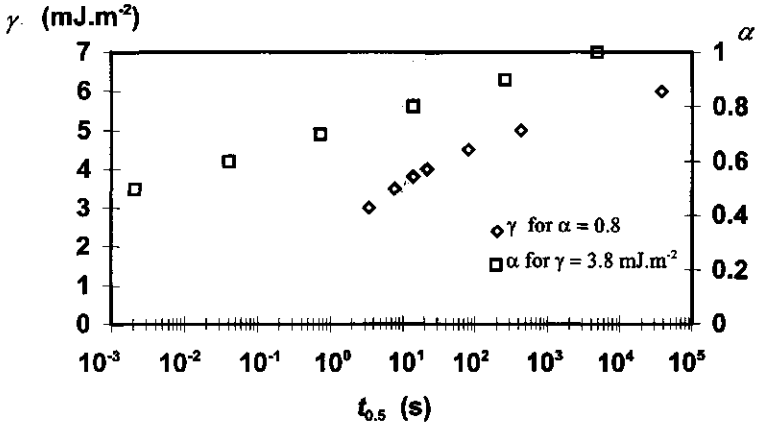

Figure 4-10. *'Flocculation time' $t_{0.5}$ as calculated from Equation 4-21 for various values of the nucleation parameters α and γ for a 12 % HP/SF dispersion at an initial supersaturation of 3.00. The grey band indicates the expected flocculation times.*

4.3.5 Crystal sizes after complete crystallization

Besides 'flocculation time' it is also possible to estimate the mean crystal size from the fits after (primary) crystallization has completed. The mean volume per crystal was calculated by dividing the maximum fraction solids ($c_{0,HP}$-x_{HP}) by the total number of produced nuclei ($\sum_i J_i \cdot \Delta t$). From this value, the average crystal radius was calculated.

The mean crystal size decreased on increasing initial supersaturation (Figure 4-11). The effect was most clear between supersaturations of 2.25 and 3.0. At higher supersaturations, the effect of supersaturation on the mean crystal size was not so pronounced. The mean crystal size increased slightly when dispersions with increasing amount of HP were crystallized at the same initial supersaturation.

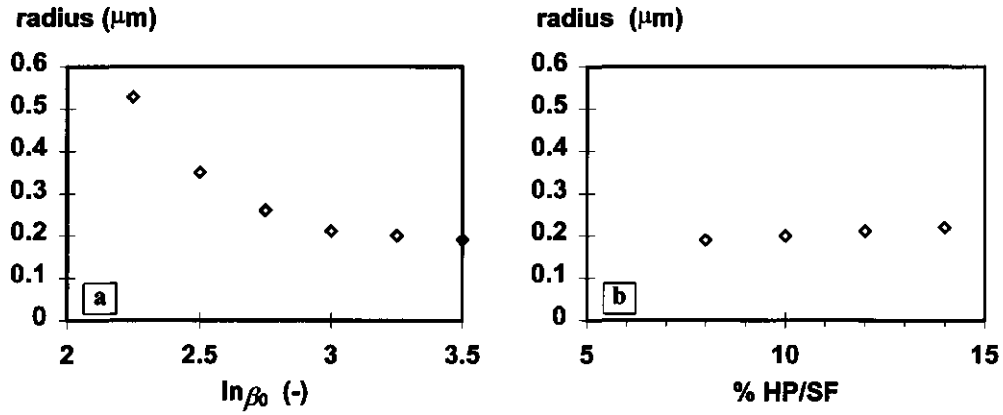

Figure 4-11. *Calculated number average crystal size after completed crystallization of HP/SF dispersions.* ***a****: for a 12 % HP/SF dispersion as function of initial supersaturation.* ***b****: for various HP/SF dispersions crystallized at* $\ln\beta_0 = 3.00$.

How realistic are the obtained crystal sizes? First, fat crystals are not spherical but have anisometric shapes. Suppose the length-width-thickness scales with ratios 50:10:1 and it is assumed that an equivalent average volume can be used, then a radius of 0.3 μm corresponds to a length of 3.0 μm. This length scale corresponds well with the size of the average longest crystal dimension that was observed in electron micrographs for similar dispersions (Heertje *et al.* (1988)).

It is very difficult to obtain experimentally a mean crystal size by other methods then EM. A method that often has been used is by determining the permeability coefficient B and relating B by the Kozeny-Carman relation to an average size of the crystal clusters. The Kozeny-Carman relation for spherical particles is given by:

$$B = \frac{a^2}{45} \cdot \frac{(1-\phi_0)^3}{\phi_0^2} \qquad \textbf{(4-22)}$$

Dispersions of 10 % HP/SF, crystallized at initial supersaturations of 2.75, 3.50 and 4.00 had permeability coefficients of respectively $2.7 \cdot 10^{-12}$, $1.2 \cdot 10^{-12}$ and $2 \cdot 10^{-13}$ m^2 (Kloek (1998), chapter 6). These permeabilities correspond to particle radii of 1.3 μm, 0.86 μm and 0.35 μm. These sizes are respectively a factor 7, 5 and 2 larger than the crystal sizes as calculated from the crystallization kinetics. This suggests that at low supersaturations, compact crystal clusters are formed with big pores in between. The size of these clusters decreased when crystallizing at higher supersaturation. This is probably related to the aggregation and crystallization kinetics.

A complication is that the Kozeny-Carman yields a volume-surface averaged 'crystal size' while the crystallization kinetics yields a number averaged crystal size.

4.4 Conclusions

Thermal behaviour of fully hydrogenated palm oil (HP) in sunflower oil (SF) shows that if HP has crystallized in the α polymorph a transition to a mixture of the β' and the β polymorph occurs. This transition takes place much more rapidly if SF is present. When crystallized in the β' polymorph, the dispersions are stable in this polymorph. The mixing behaviour in the β' polymorph seems to be much less ideal than mixing in the α polymorph, although for both polymorphs the melting temperature as function of the fraction HP could be described well with the Hildebrand-equation.

The crystallization kinetics at different initial supersaturations, $\ln\beta$, in the β' polymorph of dispersions containing various fractions of HP were described using the classical nucleation theory and a growth rate equation with the following form: $\log G_c = \log A + b \cdot \ln\beta$. This growth rate equation is equivalent to an often-used engineering equation but does not correspond to theoretical growth rate models. From the induction times for crystallization, we derived a surface free energy of about 3.4 - 3.9 $mJ.m^{-2}$ for cubic nucleus formation. For such a surface free energy, the crystallization curves could be fitted well by assuming that a fraction of about 0.8 of the triglyceride molecule should be in the right conformation before incorporated in the nucleus. For the growth rate equations, values of $A \approx 10^{-11}$ $m.s^{-1}$ and $b = 0.57$ to 0.65 were obtained. For $\ln\beta < 2.75$, b was about 0.65 and for $\ln\beta \geq 2.75$, b was about 0.57.

'Flocculation times' derived from the crystallization kinetics corresponded well with flocculation times measured in rheological measurements. Also the calculated mean crystal size after crystallization was completed, agreed well with crystal sizes observed on EM-graphs and from permeability coefficients.

4.5 Acknowlegdements

We thank Dr. R. Leloux and Prof. H. Schenk from the University of Amsterdam for allowing us to use the time-resolved X-ray diffraction equipment.

4.6 References

Avrami, M. (1939a) Kinetics of Phase Change. I- General Theory, *J. Chemical Physics* **7**, 1103

Avrami, M. (1939b) Kinetics of Phase Change. II- Transformations - time relations for random distribution of nuclei, *J. Chemical Physics* **8**, 212

Bennema, P. (1992) Growth forms of crystals: possible implications for powder technology, *KONA Powder and particle* **10**, 25

Boekel, M.A.J.S. van (1980) *Influence of fat crystals in the oil phase on stability of oil-in-water emulsions*, Ph.D. thesis Wageningen Agricultural University, Wageningen, the Netherlands

Boistelle, R. (1988) Fundamentals of nucleation and crystal growth, In *crystallization and polymorphism of fats and fatty acids*, Eds: N. Garti, K. Sato, Marcel Dekker, New York

Garside, J. (1985) Industrial crystallization from solutions, *Chem. Engineering Sci.* **40**, 3

Garside, J. (1987) General principles of crystallization, In *Food structure and behaviour*, Eds: J.M.V. Blanshard and P. Lillford, Academic Press, London, pp. 35

Hannewijk, J. (1964) Kristallisatie van vetten I, *Chemisch Weekblad* **60**, 309. (in dutch)

Heertje, I and Pâques, M. (1995) Advances in electron microscopy, In *New physoco-chemical techniques for the characterization of complex food systems*, Ed E. Dickinson, Chapman and Hall, London, pg 1-52

Heertje, I., Eendenburg van, J., Cornelissen, J.M. and Juriaanse, A.C. (1988) The effect of processing on some microstructural characteristics of fat spreads, *Food Microstructure* **7**, 189

Jackson, K.A. (1958) *Mechanisms of crystal growth in liquid metals and solidification*, Amm. Soc. Metals, Cleveland, pg 174

Kloek, W. (1998) *Mechanical properties of fats in relation to their crystallization*, PhD thesis, Wageningen Agricultural University, the Netherlands

Liu, X-Y, Bennema, P. and Eerden, J.P. van der (1992) Rough-flat-rough transition of crystal surfaces, *Nature* **356**, 778

Phipps, L.W. (1964) Heterogenous and homogeneous nucleation in supercooled triglycerides and n-paraffins, *Trans. Faraday Soc.* **60**, 1873

Skoda, W. and Tempel, M. van den (1963) Crystallization of emulsified triglycerides, *J. Colloid Sci.* **18**, 568

Skoda, W. and Tempel, M. van den (1967) Growth kinetics of triglyceride crystals, *J. Crystal Growth* **1**, 207

Smoluchowski, von M. (1917) Versuch einer mathematischen Theorie der Kogulationskinetik kolloider Lösungen, *Z. Physik. Chem.* **92**, 129

Tempel, van den M. (1961) Mechanical properties of plastic-disperse systems at very small deformations, *J. Colloid. Sci* **16**, 284

Walstra, P. and Beresteyn, E.C.H. van (1975) Crystallization of milk fat in the emulsified state, *Neth. Milk Dairy J.* **29**, 35

Walstra, P. and Jennes, R. (1984) *Dairy chemistry and physics*, Wiley, New York

Walstra, P. Fat crystallization, In *Food Structure and Behaviour*, Eds. Blanchard, J.M.V. and Lillford, P., Academic Press, London, 1987, pg. 67

Walstra, P., Vliet, van T. and Kloek, W. (1995) Crystallization and rheological properties of milk fat, In *Advanced Dairy Chemistry Vol. 2; Lipids* 2nd *ed.*, Ed. P.F. Fox, Chapman & Hal, London, pg.179

Wesdorp, L.H.(1990) Liquid - multiple solid phase equilibria in fats - theory and experiments, *Ph.D. Thesis*, Technical University Delft, the Netherlands

Zettlemoyer, A.C. (1969) *Nucleation*, Marcel Dekker, New York

Zwietering, M.H., Jongenburger, I., Rombouts, F.M. and Riet, K. van 't (1990) Modelling of the bacterial growth, *Appl. Environ. Microbiol.* **56**, 1875

Chapter 5

Structure of Fat Crystal Aggregates in Low Volume Fraction Dispersions

5.1 *Introduction*

5.1.1 General

One of the main functions of fats in food products like margarine is its contribution to the structure of the product. This structure results from a fat crystal network that is formed as a result of aggregation of fat crystals by van der Waals attraction (Walstra *et al.* (1995), van den Tempel (1961)). During food manufacture, melted fats are cooled to below their final melting temperature and nucleation is initiated. The formed nuclei, grow out into crystals, and volume fraction of crystals and the average crystal size increase. Fat crystals already start to aggregate at low volume fractions of crystallized fat forming voluminous aggregates, while nucleation and crystal growth still go on (Walstra *et al.* (1995), Kloek (1998) chapter 4). As will be shown later, a continuous crystal network already can be formed at a volume fraction of about 0.02. At this stage, a large amount of fat has still to crystallize. Such ongoing crystallization after formation of a network can strongly influence the mechanical properties of the final systems.

5.1.2 Aggregation

As every collision between two particles or aggregates leads to a permanent contact, perikinetic aggregation rate would be given by Smoluchowski's equation (Smoluchowski (1917)):

$$\frac{dc_k}{dt} = \frac{1}{2}\sum_{i+j=k} K_{i,j} \cdot c_i \cdot c_j - c_k \sum_{j=1}^{\infty} K_{k,j} \cdot c_j \qquad \textbf{(5-1)}$$

where c_k is the number concentration of aggregates containing k particles and $K_{i,j}$ the collision kernel for 2 aggregates containing i and j particles, respectively. Smoluchowski has derived an expression for the collision kernel for perikinetic aggregation, assuming that every collision is effective:

$$K_{i,j} = 4\pi \cdot (R_i + R_j) \cdot (D_i + D_j) \qquad \textbf{(5-2)}$$

where R_x and D_x are the collision radius and the diffusion coefficient, respectively, of an aggregate containing x particles. The diffusion coefficient of aggregates can be estimated by :

$$D_x = \frac{k_b T}{6\pi \cdot \eta_0 \cdot R_x} \qquad \textbf{(5-3)}$$

where k_b is the Boltzmann constant, T the absolute temperature and η_0 the viscosity of the continuous phase. In this equation, R_X is the hydrodynamic aggregate radius rather than the collision radius.

During the initial stage of perikinetic aggregation the change of the number concentration of aggregates and particles c_p in time is approximated by (Bremer (1992):

$$\frac{dc_p}{dt} = -\frac{4 \cdot k_b T \cdot c^2}{3 \cdot \eta_0} \qquad \text{with} \quad c = \sum_{i=1}^{\infty} c_i \tag{5-4}$$

From this equation it is easy to estimate the time needed to reduce the initial number of particles c_0 to half its value. This so-called flocculation time $t_{1/2}$ is given by:

$$t_{1/2} = \frac{3 \cdot \eta_0}{4 \cdot k_b T \cdot c_0} = \frac{\pi \cdot \eta_0 \cdot a^3}{k_b T \cdot \phi_0} \tag{5-5}$$

where ϕ_0 is the volume fraction of dispersed particles.

The flocculation time is an indication for the time scale at which aggregation takes place and can be compared with the time scale at which the mass crystallization of the fat takes place. For a dispersion of spherical particles with a volume fraction ϕ_0 of 0.01, an average particle size a of 0.1 μm and η_0 = 60 mPa.s (viscosity of oil at room temperature, T = 298 K), Equation 5-5 gives a flocculation time of about 4.5 s.

If effective particle motion is only due to an applied shear rate $\dot{\gamma}$, the collision frequency kernel can be written as (Smoluchowski (1917)):

$$K_{i,j} = \frac{4}{3} \cdot \dot{\gamma} \cdot (R_i + R_j)^3 \tag{5-6}$$

This is called orthokinetic aggregation and the change in the number concentration of aggregates and particles, c_o, in time is approximated by:

$$\frac{dc_o}{dt} = -\frac{16 \cdot \dot{\gamma} \cdot R^3 \cdot c^2}{3} \qquad \text{with} \quad c = \sum_{i=1}^{\infty} c_i \tag{5-7}$$

The orthokinetic and perikinetic aggregation rates are approximately additive. Whether the application of shear rate will enhance aggregation can be estimated by comparing both rates. Orthokinetic aggregation cannot be neglected if the following condition for the aggregate radius R is fulfilled:

$$R > \left(\frac{k_b T}{4 \cdot \dot{\gamma} \cdot \eta_0} \right)^{1/3} \tag{5-8}$$

At room temperature (T = 298 K), critical shear rates for spherical crystals aggregates in oil (η_0 = 60 mPa.s) of sizes 0.1 and 1 μm are 17 and 0.02 s^{-1}, respectively.

In the above considerations it is implicitly assumed that at t = 0, all the primary particles are present. To account for the production of particles by nucleation, a nucleation rate J should be added to the equations for the aggregation rates (Meeussen (1995)). In the case of perikinetic aggregation, Equation 5-4 becomes:

$$\frac{dc_{p,J}}{dt} = J - \frac{4 \cdot k_b T \cdot c^2}{3 \cdot \eta_0} \qquad \text{with} \quad c = \sum_{i=1}^{\infty} c_i \tag{5-9}$$

It is assumed that the nucleation rate is constant. This will only be true during the initial stage of the crystallization process in which the supersaturation will not decrease significantly. Furthermore, it is assumed that secondary nucleation, this is additional nucleation due to the presence of crystal surfaces, can be neglected. It is also assumed that after nucleation, particles directly obtain their final size. Integration with respect to c and t gives the number density of aggregates and particles as a function of time.

$$c_{p,J} = \frac{3}{2} \cdot \sqrt{\frac{J \cdot \eta_0}{3 \cdot k_b T}} \cdot \tanh\left(2 \cdot t \sqrt{\frac{J \cdot k_b T}{3 \cdot \eta_0}} \right) \tag{5-10}$$

This function is plotted in Figure 5-1 for some realistic nucleation rates and shows that the number of aggregates increases with time until a steady state is reached. The initial slope of these curves equals the nucleation rate as can be seen directly from Equation 5-9. After reaching the steady state, newly produced particles will aggregate with existing aggregates. In the steady state the number of aggregates is given by:

$$c_s = \frac{3}{2} \cdot \sqrt{\frac{J \cdot \eta_0}{3 \cdot k_b T}} \tag{5-11}$$

As is clear from Figure 5-1, the aggregation rate strongly depends on nucleation rate. For higher nucleation rates or crystallization at higher initial supersaturations, aggregation occurs more rapidly as is clear from c becoming constant sooner.

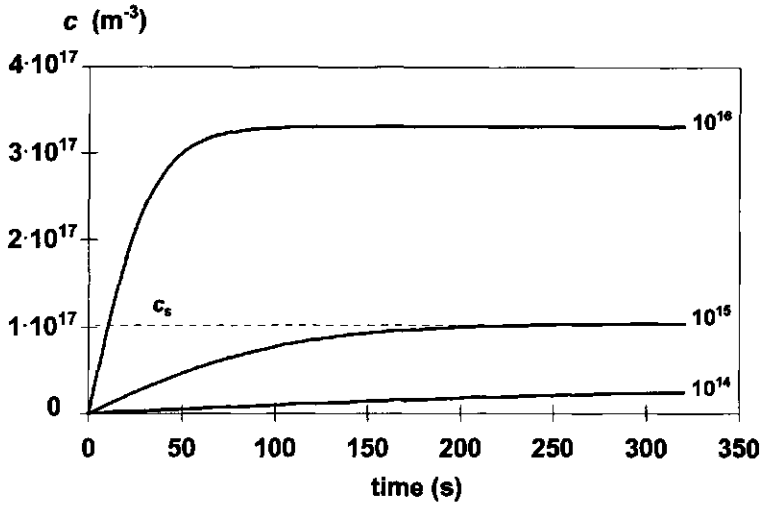

Figure 5-1. *The number density of aggregates according to Equation 5-10 at various nucleation rates (indicated as numbers in* $m^{-3} \cdot s^{-1}$ *near the curves).* $T = 298$ K, $\eta_0 = 60$ mPa.s.

5.1.3 Viscometry

One way to estimate the degree of aggregation is by means of viscometry. On aggregation, the volume fraction of aggregates increases, leading to an increase in viscosity. The extent to which the volume fraction aggregates increases, depends on the arrangement of the particles in an aggregate. Since the fractal approach to aggregate structure has been introduced, considerable progress has been made in treating aggregation processes. According to the fractal concept, the number of particles per aggregate N_p is related to its radius R by (Jullien *et al.*(1984)):

$$N_p \propto \left(\frac{R}{a}\right)^D \tag{5-12}$$

where a is a primary particle size and D the fractal dimensionality. From computer simulations in a 3-dimensional space, values for D were obtained ranging from 1.7 for rapid diffusion-limited aggregation to 2.1 for reaction limited aggregation (Kolb *et al.* (1983), Meakin (1984)). Since these numbers are smaller than 3, the volume fraction of particles in an aggregate decreases on aggregate growth.

The internal volume fraction particles ϕ_{int} in a fractal aggregate is given by the ratio between the number of particles N_p and the total number of volume elements in one aggregate N_{tot}. The latter scales with the dimensionless aggregate radius in a three dimensional space as:

$$\phi_{int} = \frac{N_p}{N_{tot}} = \left(\frac{R}{a}\right)^{D-3} \tag{5-13}$$

A dispersion containing a volume fraction ϕ_0 of primary particles that have formed monodisperse aggregates, will have a total volume fraction of aggregates given by:

$$\phi_a = \frac{\phi_0}{\phi_{int}} = \phi_0 \cdot \left(\frac{R}{a}\right)^{3-D} \tag{5-14}$$

In modelling the viscosity as a function of shear rate, we shall follow the theory presented by Potanin (1991,1992,1993). It is assumed that the dispersion consists of monodisperse aggregates and the viscosity is determined by hydrodynamic contributions only. So possible elastic inter-aggregate interactions are neglected.

Potanin showed from computer simulations that the aggregate radius can be related to the shear rate by the following proportionality:

$$R \propto \dot{\gamma}^{-m} \tag{5-15}$$

where m is a shear rate thinning exponent. This scaling relation was observed experimentally by Sonntag and Russel (1986). Rewriting Equation 5-15 in a dimensionless form yields:

$$\frac{R}{a} = C \cdot G^{-m} \tag{5-16}$$

where $C = (5/2)^m$ is a constant related to the break-up criterion for an aggregate and G the dimensionless shear rate. For a single aggregate the latter is given by:

$$G = \frac{\eta_0 \cdot \dot{\gamma}}{\sigma_m} \tag{5-17}$$

The interparticle bond strength σ_m can be estimated from the interaction potential between the particles divided by the cross section on which it acts. For a dispersion of aggregates, the assumption is made that the viscosity of the whole dispersion surrounding the aggregate equals the viscosity of the dispersion η (mean field approach) so that Equation 5-14 can be rewritten as:

$$\frac{R}{a} = \left(\frac{\eta_0}{\eta}\right)^m \frac{C}{G^m} \tag{5-18}$$

It should be pointed that the validity of the mean field approach is not clear.

The viscosity of dispersions can often be well described by the semi-empirical Krieger relation (Krieger (1972)):

$$\eta = \eta_0 \cdot \left(1 - \frac{\phi_a}{\phi_m}\right)^{-[\eta]\phi_m} \tag{5-19}$$

where ϕ_a is the volume fraction of aggregates and ϕ_m their volume fraction at random close packing, the latter being 0.63 for monodisperse, hard spheres in a 3-dimensional space and $[\eta]$ the intrinsic viscosity which is 2.5 for spheres. To model the viscosity of a dispersion as function of the shear rate, only a relation between the volume fraction of aggregates and the dimensionless shear rate is needed.

The shear rate dependency of the viscosity of dispersions containing fractal aggregates can be modelled by fitting measured viscosities to Equations 5-14, 5-18 and 5-19. Fit parameters are m, D and σ_m. Below we shall examine the shear rate exponent m in more detail.

The shear rate exponent m depends on the type of interaction between two particles. If the particles are aggregated in a deep primary minimum, its structure responds elastically to small deformations. These aggregates are said to be rigid (Potanin (1992,1993)). The yield stress of such an aggregate is proportional to the elastic modulus which, in turn, scales with the volume fraction of particles in an aggregate with an exponent μ or with the aggregate radius with an exponent $-x$. The exponent μ is defined as:

$$\mu = \frac{x}{3 - D} \tag{5-20}$$

The constant x depends on the geometry of the stress carrying strands in the aggregate. It may vary from 2 for straight strands to higher than 4 for completely flexible strands (Bremer (1990,1992)).

As a break-up criterion, one may equal the shear stress $\eta \cdot \dot{\gamma}$ to the aggregate yield stress σ_a. Since the yield stress would scale with the aggregate radius to the power $-x$, the shear rate exponent m would equal $1/x$. This relation can be useful, because it relates the aggregate structure to properties like yield stress and elastic modulus of gelled dispersions. For rigid aggregates values for m are known to range from 0.2 to 0.4. These values compare well with exponents that were determined from the dependency of elastic moduli on the volume fraction of particles. Potanin showed by computer simulation for particles that are aggregated in a weak secondary minimum, that the shear rate exponent m would be of about 0.5.

5.1.4 Light scattering

Another way to determine the structure of aggregates is by measuring the scattered intensity I of light by the aggregate as function of the scattering angle θ. The scattered intensity as function of the wave vector q, which is related to θ, is proportional to the particle form factor P (intra-particle factor) and structure factor S (inter-particle factor):

$$I(q) \propto P(q,a) \cdot S(q) \tag{5-21}$$

The wave vector q depends on the refractive index of the continuous phase n_0 and the wave length λ and is given by:

$$q = \frac{4\pi \cdot n_0}{\lambda} \cdot \sin\left(\frac{\theta}{2}\right) \tag{5-22}$$

If there is no correlation between the position of the primary particles, $S(q)$ equals unity and the scattered intensity is proportional to $P(q,a)$ which can be calculated for a given particle size and geometry.

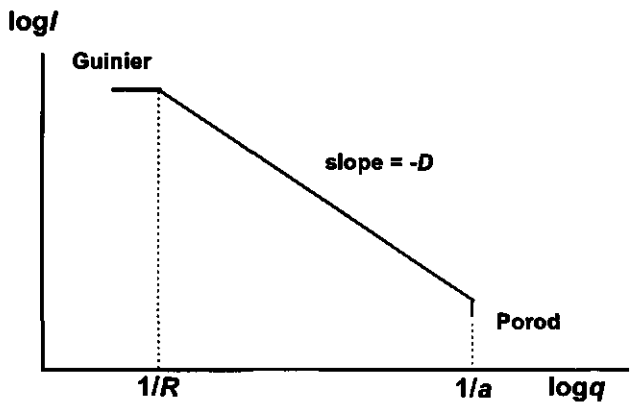

Figure 5-2. *Scattered intensity I as a function of the wave vector q for a fractal aggregate at different wave vector regions. R and a indicate the aggregate size and the particle size respectively*

At very small scattering angles and small particle size, P equals unity and the correlation between the position of the particles can be extracted from the angular dependency of the scattered intensity. $S(q)$ is related to the distribution function $g(r)$ that gives the probability of finding a particle at a distance r from a reference particle. The distribution function is proportional to r^{D-3}. It can be shown that $S(q) \propto q^{-D}$ (Werff and Ackerson (1986)). This relation is only valid if the wave vector is within the Guinier-Porod region. In the Guinier region the scattering of the whole

aggregate is seen while in the Porod region the scattering of the primary particles is seen (Figure 5-2). In the intermediate Guinier-Porod region the structure of the fractal aggregate is seen (Werff and Ackerson (1986)).

5.2 *Materials and methods*

5.2.1 Materials

A description of the physical properties and the triglyceride composition of the model system is given in chapter 2 of this thesis. The solubility of HP in SF is given by the Hildebrand equation (Hannewijk (1964), Wesdorp (1990)):

$$\ln x_{HP} = \frac{\Delta H_{f,i}}{R_g} \cdot \left(\frac{1}{T_{m,i}} - \frac{1}{T} \right) \tag{5-23}$$

Here, x_{HP} is the mole fraction of dissolved HP in polymorph i at temperature T, R_g the gas constant, $\Delta H_{f,i}$ the molar enthalpy of fusion of HP in polymorph i and $T_{m,i}$ the melting temperature of HP in polymorph i. The Hildebrand equation can be used for systems in which the liquid phase and the solid phase have a similar chemical structure and which differ considerably in peak melting temperature.

The driving force for crystallization is the difference in chemical potential $\Delta\mu$ between a supersaturated dispersion and a saturated dispersion:

$$\Delta\mu = R_g T \cdot \ln \frac{c_{HP}}{x_{HP}} = R_g T \cdot \ln \beta \tag{5-24}$$

c_{HP} is the mole fraction HP and x_{HP} is given by Equation 5-24, β is the supersaturation ratio and $\ln\beta$ is called the supersaturation.

5.2.2 Methods

Prior to any experiment, the HP/SF mixtures were first heated to 80 °C for 10 minutes to destroy any crystal memory.

Low volume fraction HP/SF solutions ($\phi_0 \leq 0.01$) had crystallized at a shear rate of 460 s^{-1} in a concentric cylinder device for 30 min at various initial supersaturations in the β' polymorph. After crystallization, the dispersions were allowed to aggregate at various lower shear rates during which the viscosity was determined as a function of time. After aggregation, a shear rate sweep was applied. The rheometer used was a strain rate controlled Bohlin VOR and the temperature was controlled using a Julabo water bath. During crystallization of the dispersions in the rheometer, the

torque bar was fixed to prevent the software to stop the shearing due to an overload message. The temperature dependency of the viscosity of sunflower oil was determined at a shear rate of 4.6 s^{-1}. Sunflower oil behaves Newtonian.

Figure 5-3 shows the set-up of the light scattering equipment. Two-dimensional light scattering of a few dispersions was monitored during crystallization and aggregation, using a special glass-made concentric cylinder geometry with an inner gap of 1 mm.

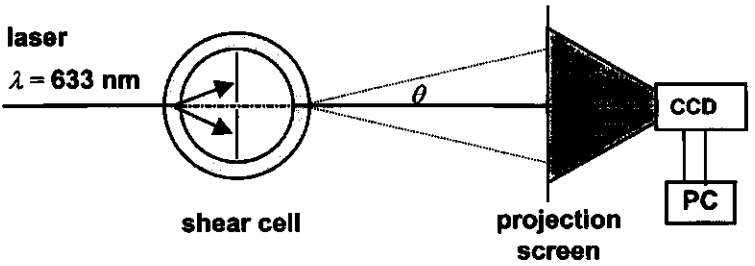

Figure 5-3. *Experimental set-up of the shear - light scattering equipment.*

The inner cylinder rotated, yielding shear rates ranging from 0.04 to about 400 s^{-1}. As a light source, a He-Ne laser with a wavelength of 633 nm was used. The concentric cylinder device was thermostatted by a glass made toluene bath. Photographs of the two-dimensional scattering patterns were made using a CCD camera with 165 x 192 light sensitive pixels (resolution 2^8) and converted to intensity-wave vector curves by home-made software. Corrections were made for refraction of the light when passing the glass-air interface. With the experimental set-up, scattering angles ranging from 0.5 to 18° could be obtained.

5.3 *Results and discussion*

5.3.1 Viscometry

gelled dispersions

Figure 5-4 shows the viscosity - time profile of a 0.5 % HP/SF dispersion crystallized at rest for 30 min. Afterwards, it was subjected to a constant shear rate and the stress or the viscosity was monitored in time. Every shear curve was obtained on using a freshly crystallized dispersion. The viscosity or stress profiles look very irregular. At the lowest shear rate (Figure 5-4a), yielding is clearly visible from the stress overshoot that occurs two times. The viscosity, which is proportional to the shear stress, became constant after some time. At higher shear rates, yielding was less pronounced, but there was still a considerable stress increase. The stresses after one hour of shearing increased with increasing shear rate. The final stresses at shear rates of 0.0146, 0.073 and

0.146 s^{-1} were 0.055, 0.15 and 0.88 $N.m^{-2}$ respectively. The stress overshoot indicates that the dispersions were gelled.

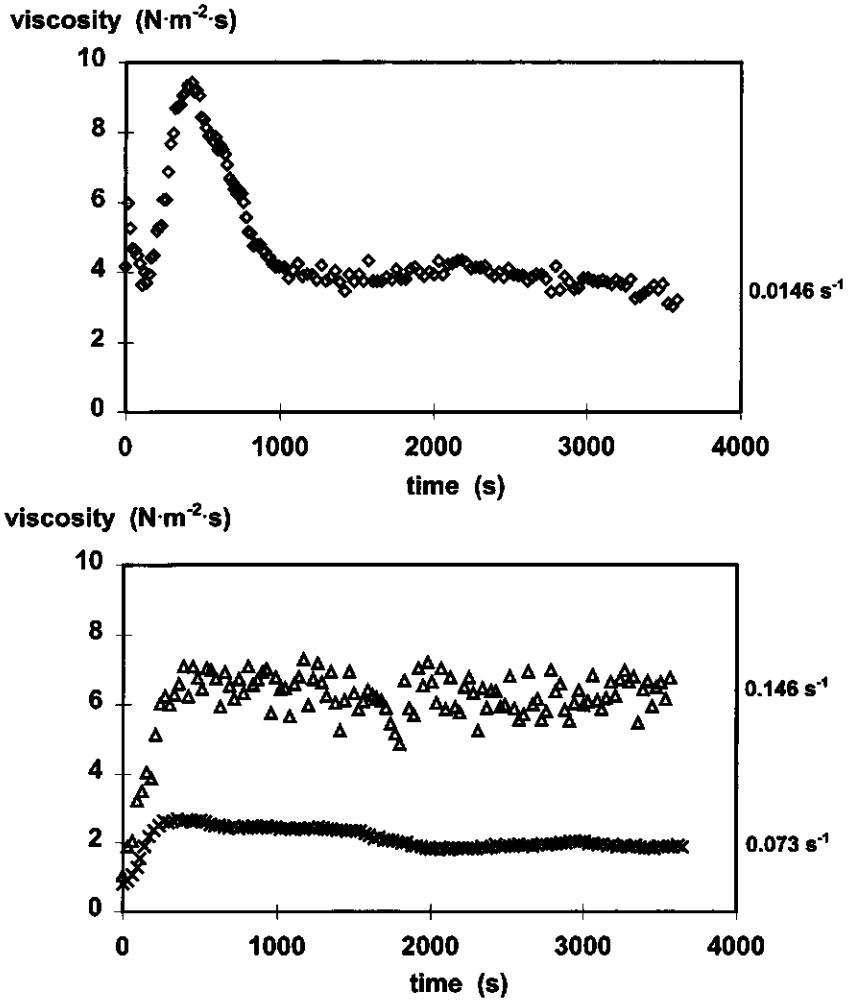

Figure 5-4. *Viscosity of a 0.5 % HP/SF dispersion after crystallization at 5 °C at rest, as a function shearing time for various shear rates. Shear rates are indicated.*

When the gel was a sheared, fairly strong van der Waals bond and possibly much stronger sintered crystal bridges have to be broken. Inhomogeneous structures and different bond strengths between crystals will lead to an inhomogeneous stress distribution and therefore cause the formation of shear planes with solid aggregates in between. The local stress needed for further deformation will decrease as soon as somewhere in the fat yielding occurs. This causes the flow to become even more inhomogeneous. The end viscosities from Figure 5-4 do not show an over all shear rate

thinning effect. This may be due to the time and shear rate dependent and uneven way of shear plane formation: at a low shear rate the formation of slip planes may be pronounced, giving low viscosities while at higher shear rates a more homogeneous yielding can occur, which could lead to a higher measured viscosity than in case of few shear planes.

Whether a gel can be formed within 30 min due to perikinetic aggregation, even at a volume fraction primary particles as low as 0.005, can be estimated using the equation for the gel time t_g as given by Bremer (1992). This equation assumes fractal aggregation, which is true for the present system as will be shown.

$$t_g = z^{D-1} \cdot \left(1 - \frac{6D}{2D+3} + \frac{3D}{D+6}\right) \cdot \frac{\pi \cdot \eta_0 \cdot a^3}{k_b T} \cdot \phi_0^{\frac{3}{D-3}} \qquad \textbf{(5-25)}$$

where z is a constant depending on the fractal dimensionality D. If we assume diffusion-limited aggregation, then D would be 1.7 ($z = 0.884$); $\eta_0 = 0.120$ Pa·s at $T = 278$ K, and for $a = 0.1$ μm, a gel time of about 21 min is obtained. So it is theoretically possible that over a time scale of 30 min a gel is formed, even at these low volume fractions. In reality, this time may even be much shorter because the crystals are anisometric and will therefore have a higher collision probability. At the other hand, if $D = 2$, the calculated gel time would be several hours. Since the experiments show that a gel is formed within 30 min, it is likely that it exist of aggregates of small D.

Whether a gel can be formed in the measuring body of the rheometer also depends on the width of the gap: it should be wide enough to allow growth of the aggregates to such a volume fraction that a gel is formed. For fractal aggregates, that will be the case at the moment the internal volume fraction particles in an aggregate, as given by Equation 5-13, equals about the volume fraction of primary particles present at gelling conditions. Substituting $\phi_{gel} = \phi_{int} = 0.005$ and $D = 1.7$, yields a dimensionless aggregate radius R/a at the gel point of 59. For a primary particle size of 0.1 μm, this yields an aggregate radius of 5.9 μm which is much smaller than the gap size of the measuring geometry; hence, a gel can be readily formed.

Presheared dispersions

It is clear that crystallization, aggregation and network formation are processes that occur simultaneously when fat solutions have crystallized in rest. This can have important consequences for the interaction between crystals. Firstly, crystals will aggregate due to van der Waals forces. These aggregated crystals are close to each other. Separation distances of about 10 Å or lower are reported. These are distances close to the molecular dimensions of triglycerides. The formation of solid crystal bonds (sintering) between aggregated crystals is therefore expected (Walstra (1987), Johannson (1994)). I come back to this point in chapter 6.

To study the aggregation process, it is necessary to separate crystallization and aggregation processes. To this end, mixtures were crystallized while being sheared at a rate of 460 s^{-1}. In this

way, very small crystal aggregates or single crystals were produced which could be considered as primary particles. Due to the high shear rate during crystallization, contact times between crystals will be so short that sintering of crystals will not occur. When the crystallization process was finished, a lower shear rate was applied, allowing the primary particles to aggregate to more voluminous aggregates. Since all dispersion had crystallized at a shear rate of 460 s^{-1}, the starting conditions were the same for each aggregation shear rate.

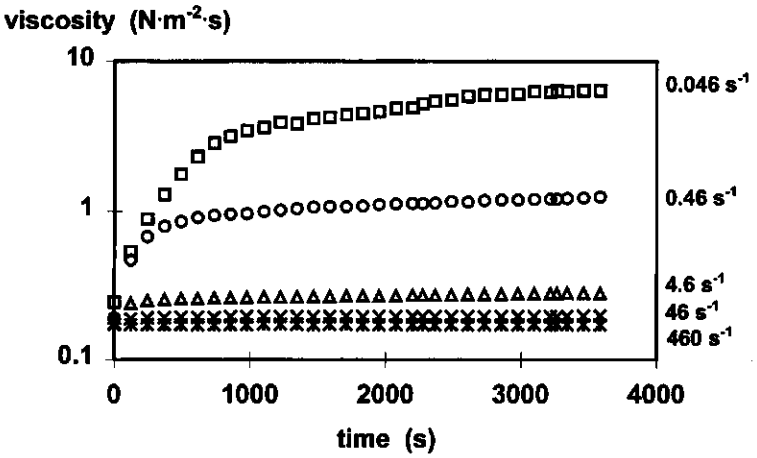

Figure 5-5. *Viscosity of 0.5 % HP/SF dispersions, crystallized at 5 °C at a shear rate of 460* s^{-1}*, as a function of shearing time for various shear rates. Aggregation shear rates are indicated.*

Figure 5-5 shows the viscosity during aggregation at various shear rates. The viscosity increases from roughly that of the continuous phase to values several times higher. The viscosity increase can be explained from the increase of the volume fraction of aggregates. Directly after crystallization this volume fraction would roughly equal the initial volume fraction HP ($\phi_0 = 0.005$) assuming that no or only very dense aggregates had been formed. At shear rates of 0.046 and 0.46 s^{-1}, the time scale over which the steepest increase in viscosity took place was about 200 s. This indicates that at these shear rates the aggregation process was a diffusion-limited process. This can be checked by calculating the critical shear rate above which perikinetic aggregation cannot be neglected from (Equation 5-8). Substituting $T = 278$ K, $\eta_0 = 120$ mPa.s and $R = a = 10^{-7}$ m, yields a critical shear rate of 8 s^{-1}. The order of magnitude corresponds well with the experimental result, which shows that at shear rates higher than 4.6 s^{-1} the final viscosity was reached much sooner than at lower shear rates.

After one hour, the viscosity was almost constant: an equilibrium situation had more or less been reached, in which the growth rate of the aggregates would equal the break down rate of the aggregates. The viscosity after one hour of aggregation decreased with increasing shear rate. This can be explained by the increasing shear stress applied on the aggregates which causes them to

become smaller and or more dense and therefore causes the volume fraction of aggregates to decrease. Figure 5-6 shows the measured relative viscosities after one hour of aggregation for dispersions containing various volume fraction of HP that had crystallized at a $\ln\beta = 5$. The relative viscosities were fitted by Equations 5-14, 5-18 and 5-19, by minimizing the following equation (Potanin (1992):

$$\frac{1}{N}\sum_{i=1}^{N}(\zeta_i^{\lambda} + 2\cdot k_i\cdot\zeta_i - 1)^2 \qquad \textbf{(5-26)}$$

where $\zeta = \left(\frac{\eta_0}{\eta}\right)^{m(3-D)}$, $\lambda = \frac{1}{2.5\cdot m\cdot\phi_m\cdot(3-D)}$, $k = \frac{\phi_0}{\phi_m}\cdot\frac{C^{3-D}}{G^{m\cdot(3-D)}}$

and N is the number of measurements.

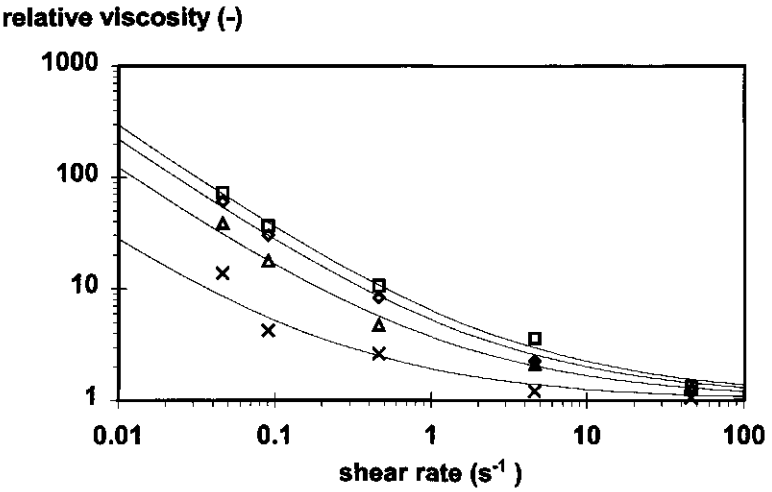

Figure 5-6. *Measured (markers) and fitted final viscosities (curves) as function of the shear rate during aggregation of HP/SF dispersions crystallized at* $\ln\beta = 5$. *Volume fractions of HP: × 0.0020; Δ 0.0050; ◊ 0.0075; □ 0.01.*

The fitted lines show that the viscosities after one hour of aggregation as function of shear rate can be fitted satisfactorily assuming a fractal geometry of the fat crystal aggregates. Table 5-1 gives a compilation of the fit parameters for the various volume fractions. For low dimensionless shear rates, m and D were directly related to each other by the relation $m\cdot(3\text{-}D)$ = constant; consequently m and the breaking stress σ_m were used as fit parameters for some realistic values of D (Potanin (1992)). Values taken for D ranged from 1.7 for the case of diffusion-limited aggregation to 2.3 for

reaction limited aggregation with some compaction due to rearrangements, for instance due to shear.

Table 5-1. *Fitted m values for a number of fractal dimensionalities D as determined from the final viscosities as function of shear rate at various fractions HP. Also the optimum σ_m is given. Dispersions had crystallized in the β' polymorph at an initial $\ln\beta = 5$.*

ϕ_0	m				σ_m
	$D = 1.7$	$D = 1.9$	$D = 2.1$	$D = 2.3$	
(-)					($N.m^{-2}$)
0.002	0.38	0.45	0.55	0.70	10^4
0.005	0.36	0.43	0.53	0.68	10^4
0.0075	0.38	0.45	0.55	0.71	$5 \cdot 10^3$
0.01	0.34	0.40	0.48	0.63	10^4

Assuming a constant D, the shear rate exponent m increased slightly with decreasing volume fraction HP or assuming a constant m, the dimensionality D decreased slightly with decreasing volume fraction HP. The somewhat deviating results for $\phi_0 = 0.0075$ can be explained by the lower optimum value of the interparticle bond strength σ_m: an increasing σ_m results in a decreasing m or D. It is surprising that the value of σ_m is independent on ϕ_0 since it is expected that crystallization at a constant initial $\ln\beta$ for various fractions HP would result in dispersions with different crystal sizes.

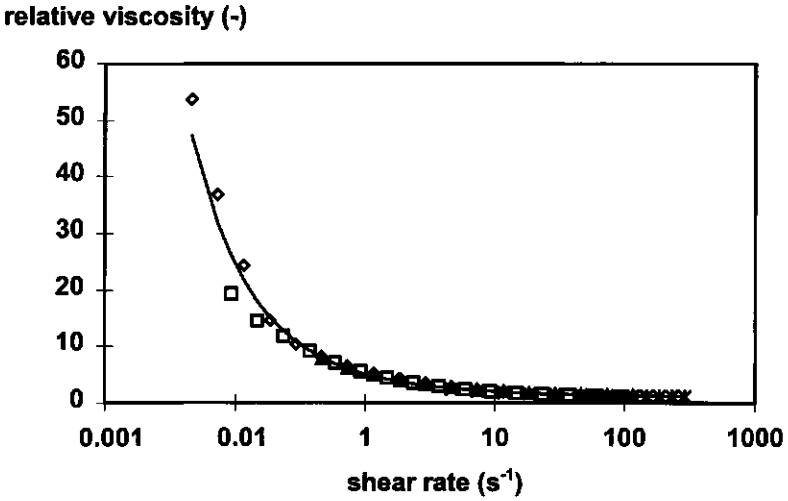

Figure 5-7. *The relative viscosities measured in a shear rate sweep starting at the aggregation shear rate of a 0.75 % HP/SF dispersion at $\ln\beta = 5$. The solid line is fitted according the model of Potanin. Aggregation shear rates: ◊ 0.046 s^{-1}; □ 0.092 s^{-1}; Δ 0.46 s^{-1}; × 4.6 s^{-1}; * 46 s^{-1}.*

Figure 5-7 shows the viscosities of 0.75 % HP/SF dispersions, measured in a shear-rate sweep applied after the aggregation step at a certain shear rate. The fitted curve is also given. The shear-rate dependency of the viscosity did not significantly depend on the aggregation shear-rate. Therefore, all the results of the various shear-rate sweeps at one volume fraction were treated as one group. The fit results are given in Table 5-2. The same trends are observed as from the fits of the final viscosities: m slightly increases or D slightly decreased with decreasing volume fraction HP. Higher values for σ_m go along with lower values for m. The obtained values for m ranged from 0.3 to 0.4 for $D = 1.7$ and from 0.5 to 0.7 for $D = 2.3$ (Tables 5-1 and 5-2).

Table 5-2. *Fitted m values for a number of fractal dimensionalities D as determined from the viscosities measured in a shear rate sweep after aggregation at various shear rates for various fractions HP. Also the optimum σ_m is given. Dispersions had crystallized in the β' polymorph at an initial $\ln\beta = 5$.*

ϕ_0	m				σ_m
	$D = 1.7$	$D = 1.9$	$D = 2.1$	$D = 2.3$	
(-)					($N.m^{-2}$)
0.002	0.34	0.40	0.49	0.62	$4 \cdot 10^4$
0.005	0.32	0.37	0.46	0.59	$4 \cdot 10^4$
0.0075	0.32	0.38	0.47	0.60	$2 \cdot 10^4$
0.01	0.28	0.34	0.41	0.53	$4 \cdot 10^4$

Aggregation of fat crystals is a rapid diffusion-limited process because no steric- or electrostatic barriers are present (if no emulsifiers are adsorbed on the crystal surface). For rapid diffusion-limited aggregation, a D of 1.7 is expected. This would correspond to low m values ranging from 0.3 to 0.4. According to Potanin (1991, 1992, 1993), these values are indicative for rigid and irreversible bonds. This agrees well with the deep potential well that was estimated to be about 30 kT by van den Tempel.

The order of magnitude of σ_m that gave the best fit, is reasonable for van der Waals attraction. The van der Waals attraction force F_w between spherical particles is approximated by:

$$F_w = \frac{A_h \cdot a}{12 \cdot H^2} \tag{5-27}$$

where A_h is the Hamaker constant en H the separation distance between the particles. The separation distance between the particles will be between 4 Å, roughly the spacing between two paraffin chains in a crystal, and 10 Å, a value estimated from shear moduli of fat dispersions by van den Tempel (1961). A reasonable estimate for $A_h = 2.5 \cdot 10^{-20}$ J (6.5 k_bT for $T = 278$ K) (van den Tempel (1961)). Assuming an average $H = 7$ Å and $\sigma_m = F_w/(\pi \cdot a^2)$, yields for σ_m 10^4 and 10^5 $N \cdot m^{-2}$ for particle radii of 140 nm and 14 nm respectively. These values sound realistic, although one should be careful

applying these equations since the particles are strongly anisometric. The anisometric nature of fat crystals will probably give an underestimation of the calculated a. Furthermore the anisotropicity of the crystals will cause A_h to be dependent on the crystal plane.

The bond strength between the crystals should be influenced by particle size, as indicated by Equation 5-27 and the relation $\sigma_m = F_w/(\pi \cdot a^2)$, and should therefore be sensitive to the initial supersaturation at crystallization. Figure 5-8 shows the viscosities obtained from a shear-rate sweep of 0.5 % HP/SF dispersions that had crystallized at various initial supersaturations. The dispersions were aggregated at a shear rate of 0.046 s^{-1} after which the shear-rate sweep was applied.

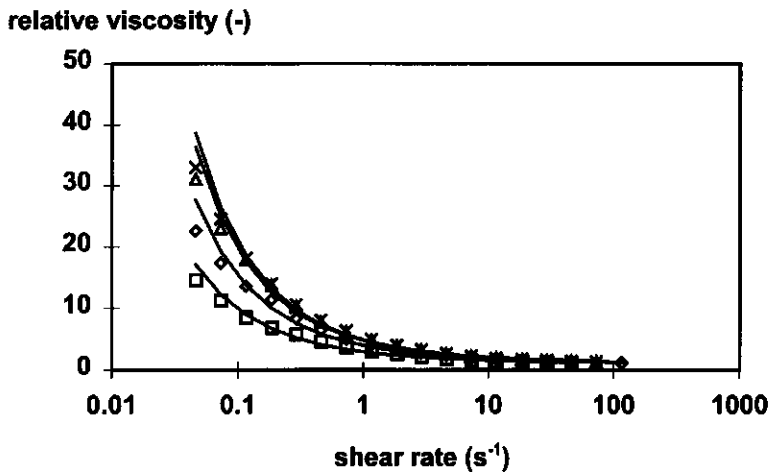

Figure 5-8. *The measured (markers) and fitted (lines) relative viscosities of 0.5 % HP/SF dispersions crystallized at various initial supersaturations (lnβ). Viscosities are determined in a shear-rate sweep after aggregation at 0.046* s^{-1}. *lnβ: □ 4.5; ◊ 5.0; Δ 5.5; × 6.0.*

The fitted values are compiled in Table 5-3. The bond strength seems to increase with increasing initial supersaturation, indicating that the average particle dimension decreased with increasing supersaturation. This is expected when considering the crystallization kinetics (Kloek, chapter 4). The nucleation rate is much more temperature dependent than the crystal growth rate. Due to the higher nucleation rates, more particles will be produced that grow to a lesser extent as the amount of HP is limited. As the σ_m is inverse proportional to the particle size, the particle size should be reduced by a factor 7 when the lnβ is increased from 4.5 to 5.5. It should be remarked that that when assuming a linear relation between lnβ and σ_m, the differences in σ_m are not significant at a probability level of 95 %.

The deviating value of σ_m for the dispersion crystallized at $\ln\beta = 6$ may possibly be explained by some crystallization occurring in the α polymorph, because at a supersaturation of 6.0 in the β' polymorph, the bulk phase of this polymorph is almost supersaturated. As the HP consists of numerous triglycerides, at least a small proportion of them would be supersaturated in the α polymorph. The crystals in the α polymorph will transform rapidly into a mixture of mainly the β polymorph and some in the β' polymorph (Kloek, chapter 4). This transformation is accompanied by a coarsening of the crystals.

Since shear rate sweeps of dispersions, crystallized at various supersaturations, were only performed on dispersions aggregated at a shear rate of 0.046 s^{-1}, somewhat higher values for σ_m were found. By combining several shear rate sweeps, starting at a shear rates that are equal to the various aggregation shear rates, the viscosities obtained at higher shear rates are weighted more than in these experiments. This difference in weighting would also be the reason for the somewhat lower values of m in comparison with the experiments in which dispersions were aggregated at various shear rates prior to the shear-rate sweeps.

Table 5-3. *Fitted m values for fractal dimensionalities (D) of 1.7 and 2.3 as determined from the viscosities measured in a shear rate sweep after aggregation at a shear rate of 0.046 s^{-1}. Also the best fit for σ_m is given. Solutions of 0.5 % HP/SF were allowed to crystallize in the β' polymorph at various initial $\ln\beta$. Exponent μ relates the elastic moduli to the volume fraction of particles according to Equation 5-20.*

$\ln\beta$	m		$\mu = \frac{1}{m \cdot (3 - D)}$	σ_m
	$D = 1.7$	$D = 2.3$		
(-)	(-)	(-)	(-)	($N \cdot m^{-2}$)
4.5	0.28	0.52	2.77	$1 \cdot 10^5$
5.0	0.27	0.50	2.85	$3 \cdot 10^5$
5.5	0.26	0.49	2.94	$7 \cdot 10^5$
6.0	0.28	0.51	2.80	$4 \cdot 10^5$

5.3.2 Light scattering

Since it was not possible to distinguish between m and D by viscometry, light scattering was used to estimate D. The dispersions (ϕ_0 = 0.0025) had crystallized in a glass-made shear cell at a shear rate of about 460 s^{-1} and were subsequently allowed to aggregate at a shear rate of 0.04 s^{-1}. The two-dimensional scattering profiles were measured during shearing. Figure 5-9 shows the scattering profiles as seen on the projection screen directly after crystallization and after 40 min of aggregation at 0.04 s^{-1}. The scattering patterns show that directly after crystallization, light was

scattered up to relative high θ. The crystallization process it self could also be monitored by the increase of the intensity in time. As soon as the shear rate was lowered to the aggregation shear rate, scattering became more concentrated to lower θ. This indicates that the scattering structures were increasing in size. After correction for the refraction of light by the glass/air interface, the scattering patterns did not show any anisometry.

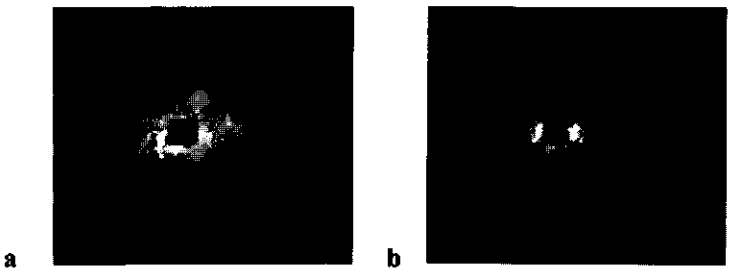

Figure 5-9. *Scattering patterns (not corrected for refraction at glass/air interface) of a 0.25 % HP/SF dispersion.* ***a:*** *after crystallization at a shear rate of 460* s^{-1} *at* $\ln\beta = 5$. ***b:*** *after 40 min of aggregation at 0.04* s^{-1}. *Black square in centre is a piece of paper to protect CCD from overexposure.*

Verduin (1996) found, for a weakly aggregating system, a bright vertical line on the scattering pattern, perpendicular to the flow direction during shearing of the system. Cessation of the shear caused this line to disappear. The line was explained by the influence of the shear rate on the structure factor $S(q)$ as the pair correlation function becomes direction dependent in a flow field. In aggregating HP/SF dispersions no bright vertical line could be observed, which suggests that the aggregate structure did not become strongly anisotropic. This could have been due to the strong attractive forces between the fat crystals. Figure 5-10 shows the calculated I-q curves after various times of aggregation.

Fractal aggregates should yield straight lines for $\log I$ versus $\log q$. Directly after crystallization was completed, such a power-law relation was not observed. At the shearing during crystallization, the primary particles are expected to be "seen" by light scattering. The angular dependency of intensity is determined by the particle form factor only if there is no correlation between the positions of the primary particles. From this factor it is possible to calculate the particle size. However, the intensity at $\theta = 0$ is not known and also the anisotropic nature of the fat crystals interferes with particle size calculations.

After 1 min of aggregation the relationship was still curvilinear but after longer times the slopes became nearly linear. After 5 min, an average slope of -1.6 was obtained. After longer times, correlation coefficients became higher with a final slope of about -1.7 to -1.8 (Table 5.4). Fitted slopes would correspond to fractal dimensionalities of 1.7 to 1.8. These slopes correspond well to the results obtained by Vreeker *et al.* (1992) for tristearate crystals in olive oil.

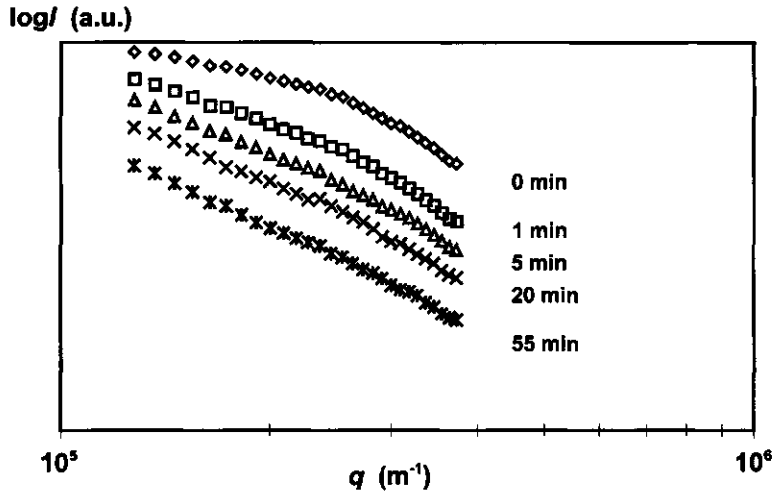

Figure 5-10. *Scattered intensity (shifted along the I-axis for clarity) as a function of the wave vector q of an aggregating 0.25 % HP/SF dispersion after shearing for various times at 0.04* s^{-1}. *Shearing times are indicated near the curves.*

Table 5-4. *Slopes obtained from the power-law dependency of the scattered intensity as function of wave vector of an aggregating 0.25 % HP/SF dispersion at a shear rate of 0.04* s^{-1} *after various times.*

time (min)	slope (= -D) (-)	r^2 (-)	time (min)	slope (= -D) (-)	r^2 (-)
0	-	-	30	-1.75	0.995
1	-	-	35	-1.69	0.996
5	-1.57	0.995	40	-1.68	0.996
10	-1.58	0.995	45	-1.73	0.999
15	-1.76	0.996	50	-1.78	0.997
20	-1.62	0.993	55	-1.75	0.997
25	-1.67	0.998			

Dimensionalities of 1.7 - 1.8 are expected for aggregates that are formed due to rapid diffusion-limited aggregation in the absence of shear. However, the aggregates were grown under shear. This can cause rearrangements of the particles in the aggregates, leading to compaction of the aggregates and therefore higher dimensionalities. Dimensionalities up to 2.1 are expected when aggregates are grown under shear (Hoekstra *et al.* (1992)). On the other hand, rotational diffusion of the anisotropic crystals would lead to a smaller dimensionality. Whether rotational diffusion is

important compared to the effect of shearing can be examined by calculating the rotary Peclet number Pe_r:

$$Pe_r = \frac{a_a \cdot \dot{\gamma}}{D_r} \quad \text{with} \quad D_r = \frac{k_b T}{8\pi \cdot \eta_0 \cdot a^3} \tag{5-28}$$

where a_a is a constant depending on the axis size ratio of the particle and D_r the rotational diffusion coefficient. For $Pe_r \leq 1$, the rotational component cannot be neglected compared to aggregate movement due to shear. To calculate the rotational diffusion coefficient, a particle size has to be known. However, the primary particles were too small to be sized by light microscopic observations. Therefore, the particle size was estimated from the flocculation times. From viscometric data, it was concluded that growth of aggregates took place during, say, during the first 200 s. Before aggregate growth becomes detectable by an increase in viscometry, aggregates must have grown to rather high dimensionless radii. The flocculation time will thus be much smaller than 200 s. The greatest change in the light scattering patterns on cessation of shear took place during 10 to 60 s. Substituting $\phi_0 = 0.0025$, $T = 278$ K, $\eta_0 = 0.120$ N·m^{-2}·s^{-1} and flocculation times of 10 and 60 s in Equation 5.5 yields as estimate for the average particle sizes 63 and 120 nm respectively. These sizes correspond to diffusional rotation coefficients of 5.09 and 0.74 s^{-1} respectively. Assuming $a_a = 1$ and substituting $\dot{\gamma} = 0.04$ yields $Pe_r \ll 1$. Therefore, rotational diffusion may be important and can possibly explain the low dimensionalities obtained.

If the aggregates grow, its "particle size" increases and already at low dimensionless radii (about 5), Pe_r will be larger then 1. This would lead to an increase of the dimensionality since time-dependent rearrangements become important.

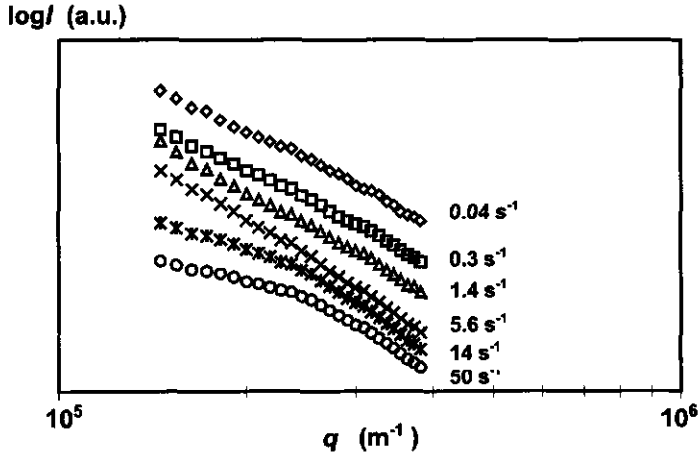

Figure 5-11. *Scattered intensity as a function of wave vector q of an 0.25 % HP/SF dispersion aggregated at 0.04* s^{-1} *of the aggregates remaining after subjecting them for 3* min *to various shear rates. Shear rates are indicated near curves.*

Table 5-5. *Slopes obtained from Figure 5-11.*

shear rate s^{-1}	slope (-)	r^2 (-)	shear rate s^{-1}	slope (-)	r^2 (-)
0.04	-1.75	0.995	5.6	-2.21	0.997
0.3	-1.79	0.997	14	-	-
1.4	-1.91	0.998	50	-	-

After aggregation at a shear rate of 0.04 s^{-1}, the dispersions were subjected to a shear rate sweep. Every shear rate was applied for about 3 minutes. This time was sufficient to reach an equilibrium situation. Figure 5-11 shows the *I-q* curves at the various shear rates and Table 5-5 compiles some correlation results.

On increasing the shear rate in the range from 0.04 to 5.6 s^{-1}, a power-law relation remains valid. Assuming the slope of the power-law equals *-D*, it can be concluded that the dimensionality increases more strongly at shear rates of about 1 s^{-1} and higher. These are shear rates at which rotational diffusion can be neglected, so that higher dimensionalities are expected due to rearrangements.

At a shear rate of 14 s^{-1}, the results could not be fitted to a power-law. This may be due to the effect of shear rate on the form factor. Another explanation may be that the aggregate size becomes so small that the wave vector is outside the Guinier-Porod region. At a shear rate of 14 s^{-1}, the lower limit of the Guinier-Porod region is at $q \approx 3 \cdot 10^5$ m^{-1}. This limit should correspond with the reciprocal aggregate radius (Figure 5-2). For $m = 0.3$, $\sigma_m = 10^5$ and $\eta/\eta_0 = 2$, Equation 5-18 yields an dimensionless aggregate radius R/a of 17. Combining $R/a = 17$ with $q = 3 \cdot 10^5$ $m^{-1} = 1/R$ yields a particle size of 200 nm, which is somewhat larger than the size obtained from flocculation times. For $m = 0.5$ a particle size of 30 nm is obtained which is somewhat smaller then the size obtained from flocculation times.

If compaction of the aggregates occurs at shear rates higher than a certain critical shear rate, this may somewhat affect fit parameter m obtained by viscometry. How big this effect will be is not clear.

5.4 *Conclusions*

The aggregate structure of low volume fraction HP/SF dispersions can be described well using a fractal approach. Light scattering of dispersions aggregated at low shear rates yielded fractal dimensionalities of about 1.7 - 1.8, which is indicative for rapid diffusion-limited aggregation. From viscometric data at these shear rates, a shear rate exponent $m = 0.3$ - 0.4 could be derived. The bond strengths between the primary particles could be explained by van der Waals attraction. The bond strength increased with increasing initial supersaturation on crystallization, which is explained by a decreasing particle size. Shearing these aggregated dispersions at higher shear rates lead to higher

dimensionalities which can be explained by rearrangements becoming more important than rotational diffusion.

5.5 *Acknowledgements*

We thank Dr. J. Dhont and Dr. H. Verduin (Laboratory of Physical Chemistry, University of Utrecht, the Netherlands) for the use of their 2*D* light scattering-shear cell set-up and the valuable discussions.

5.6 *References*

Bremer, L.G.B. (1992) *Fractal aggregation in relation to formation and properties of particle gels*, Ph.D. Thesis, Wageningen Agricultural University, the Netherlands

Bremer, L.G.B., Bijsterbosch, B.H., Schrijvers, R., Vliet, van T. and Walstra, P. (1990) On the fractal nature of the structure of acid casein gels, *Colloids and Surfaces* **15**, 159

Hannewijk, J. (1964) Kristallisatie van vetten I, *Chemisch Weekblad* **60**, 309. (in dutch)

Hoekstra, L.L., Vreeker, R. and Agterof, W.G.M. (1992) Aggregation of colloidal nickel hydroxycarbonate studies by light scattering, *J. Colloid Interface Sci.* **151**, 17

Johansson, D. (1994) *Colloids in fats: the fat crystal as a functional particle*, Ph.D. Thesis, Lund University, Sweden

Jullien, R., Kolb, M. and Botet, R. (1984) , In *"Kinetics of aggregation and gelation"*, Eds. F.Family and D.P. Landau, Elsevier, Amsterdam/New York

Kolb, M., Botet, R. and Jullien, R. (1983) Scaling of kinetically growing clusters, *Phys. Rev. Lett.* **51**, 1123

Krieger, I.M. (1972) Rheology of monodispersed lattices, *Adv. Colloid Interface Sci.* **3**, 111

Meakin, P. (1984) Diffusion-controlled aggregation on 2-dimensional square lattices, *Phys. Rev. B*, **29**, 2930.

Meeussen, W. (1995) personal communication

Potanin, A.A. (1991) On the mechanism of aggregation in the shear flow of suspensions, *J. Colloid Interface Sci.* **145**, 140

Potanin, A.A. (1992) On the microrheological modeling of aggregating colloids, *J. Dispersion Sci. and Technology* **13**, 527

Potanin, A.A. (1993) On the computer simulation of the deformation and breakup of colloidal aggregates in shear flow, *J. Colloid Interface Sci.* **157**, 399

Smoluchowski von, M. (1917) Versuch einer mathematischen Theorie der Kogulationskinetik kolloider Lösungen, *Z. Physik. Chem.* **92**, 129.

Sonntag, R.C. and Russel, W.B. (1986) Structure and breakup of flocs subjected to fluid stresses -1 - shear, *J. Colloid Interface Sci.* **113**, 399

Tempel, van den M. (1961) Mechanical properties of plastic-disperse systems at very small deformations, *J. Colloid. Sci* **16**, 284

Verduin, H. (1996) *The shear-distorted long range microstructure of colloidal dispersions*, PhD Thesis, University of Utrecht, The Netherlands

Vreeker, R., Hoekstra, L.L., Boer, den D.C. and Agterof, W.G.M. (1992) The fractal nature of fat crystal networks , *Colloids Surf.* **65**, 185

Walstra, P. (1987) Fat crystallization, In *Food Structure and Behaviour*, Eds. J.M.V. Blanchard and P. Lillford, Academic Press, London, pg. 67

Walstra, P., Vliet, van T. and Kloek, W. (1995) Crystallization and rheological properties of milk fat, In *Advanced Dairy Chemistry Vol. 2; Lipids* 2nd *ed.*, Ed. P.F. Fox, Chapman & Hal, London, pg.179

Werff, J. van der and Ackerson, B.J. (1986) Selected topics in static and dynamic light scattering, *Lecture notes Van 't Hoff Laboratory,* University of Utrecht, The Netherlands, chapter III

Wesdorp, L.H. (1990) *Liquid - multiple solid phase equilibria in fats - theory and experiments*, Ph.D. Thesis, Technical University Delft, the Netherlands

Chapter 6

Structure of Fat Crystal Networks: Mechanical Properties at Small Deformations

6.1 Introduction

6.1.1 General

Fats are important components in food products due to their sensorial and structural properties. They can occur as a liquid oil phase or a solid crystal phase, depending on composition, temperature and pressure. In dispersions of fat crystals in oil, the structural properties arise from the presence of aggregated fat crystals. The continuous fat crystal network determines the mechanical properties of products like margarine and butter. A high percentage of solid fat yields a hard product with undesirable brittle properties. Lower amounts of solid fat can give a more spreadable product but may also result in undesirable oiling-off: the crystal network is to weak to carry its own weight and liquid oil can permeate through the pores in the crystal network.

From a nutritional point of view fats act as suppliers of energy and essential fatty acids and as a solvent for some vitamins. It is recommended that the intake of fats, especially those containing a proportion of saturated fatty acids, is reduced. However, triglycerides containing saturated fatty acids are the ones that crystallize under conditions as applied in food processing. A reduction of triglycerides containing saturated fatty acids will reduce the amount of solid fat and therefore will affect mechanical properties. The latter properties depend on the geometrical structure of the fat crystal network *i.e.* how are the fat crystals distributed in space, the number of crystals and on the interaction forces between crystals. A better understanding of how crystals are arranged and how they interact with each other can provide tools to optimize the mechanical properties of fat continuous systems using as little solid fat as possible.

The aim of this research is to determine the mechanical properties of fat dispersions at small deformations as a function of the crystallization conditions and to interpret the results in terms of interaction between the crystals and the spatial distribution of the crystals.

6.1.2 Crystallization

Fats can only crystallize if the triglycerides are supersaturated: then the solubility of a group of triglycerides at certain conditions is lower than the fraction present. For a given liquid triglyceride blend this can be achieved by increasing the pressure or by lowering the temperature. The latter is most common in food industry although also pressure treatments are gaining interest.

Crystals can only grow after nuclei have been formed. So the number density of crystals and the crystal size distribution will be directly related to the nucleation rate. Nucleation is the process in which embryos *i.e.* aggregates of molecules are formed as a result of addition of monomers. If the embryo exceeds the critical size defined by the Gibbs-Thomson relation, it is called a nucleus. Homogeneous nucleation, which is nucleation in the absence of any external structured surface, is very strongly temperature dependent and only occurs at considerable supercooling (20 - 40 K). In fats, homogeneous nucleation can only be achieved if the fat is finely dispersed, for example

emulsified. In bulk fats heterogeneous nucleation, which occurs at higher temperatures, will be predominant. This type of nucleation is catalyzed by foreign surfaces like micelles of monoglycerides and walls of equipment used. It is also very temperature dependent, though less than for homogeneous nucleation.

By changing the temperature of crystallization or the applied supersaturation, it is possible to influence the nucleation rate and therefore the number of crystals; the number of catalytic impurities increases with decreasing temperature and nucleation rate is much more temperature dependent than the crystal growth rate. As soon as a nucleus is formed it will grow out to form a crystal. Fat crystals are anisometric and their dimensions depend on the polymorph in which they have crystallized. Every crystal face has a different growth rate and the differences are large because of the anisometry of a triglyceride molecule. The linear growth rate of a crystal face is supersaturation dependent, but not as strong as the nucleation rate. If the temperature dependencies of nucleation rate and growth rate are known, it is in principle possible to calculate at every time the number density of crystals and their size distribution, as long as no fusion of crystals or secondary nucleation occurs. At the initial stage of isothermal crystallization, both nucleation rate J and crystal growth G_c rate would be constant. During this stage the fraction solid $\phi(t)$ may be calculated as a function of time t by the Avrami-equation (Avrami (1939) *a* and *b*). For the hypothetical case of spherical crystals the Avrami-equation is given by:

$$\phi(t) = \tfrac{1}{3}\pi \cdot G_c^{\,3} \cdot J \cdot t^4 \qquad \textbf{(6-1)}$$

6.1.3 Aggregation

Fat crystals in oil exhibit Brownian motion and thus can meet each other. As they are attracted to each other by van der Waals forces, they can aggregate forming voluminuous aggregates and finally a continuous crystal network. The collision frequency J_{coll} of a dispersion containing c spherical particles per m^3 due to Brownian motion is given by (Smoluchowski (1917)):

$$J_{coll} = \frac{dc}{dt} = \frac{4 \cdot A \cdot k_b \cdot T \cdot c^2}{3 \cdot \eta_0} \qquad \text{with} \quad c = \sum_{i=1}^{\infty} c_i \qquad \textbf{(6-2)}$$

where k_b is the Boltzmann constant, T temperature, η_0 the viscosity of the continuous phase and A a constant depending on the type of colloidal interaction between the particles, hydrodynamic interactions and polydispersity (Bremer *et al.* (1995)). For particles that are only subject to van der Waals forces, like fat crystals (*i.e.* fast diffusion-limited aggregation), A is about unity. This means that every collision is effective in creating a permanent bond between two particles and that every new cluster may be considered as a particle having the same collision probability. The time needed to reduce the particle number to half its initial value then is given by:

$$t_{1/2} = \frac{3 \cdot \eta_0}{4 \cdot k_b T \cdot c} = \frac{\pi \cdot \eta_0 \cdot a^3}{k_b T \cdot \phi_0} \qquad \textbf{(6-3)}$$

where a is the particle radius and ϕ_0 the volume fraction of particles. A requirement for aggregation is that the van der Waals attractional energy, which depends on the particle size, is larger than the thermal energy *i.e.* is larger than k_bT. As can be seen from Equation 6-3 this "flocculation time" time is very sensitive to the particle size. An order of magnitude calculation for a dispersion of spherical crystals (a = 0.1 μm; ϕ_0 = 0.10) in an oil phase of η_0 = 60 mPa.s at T = 298 K yields a flocculation time of about 0.5 s. For anisotropic fat crystals this time will be even smaller due to their higher collision probability. As aggregation proceeds, the aggregates become more polydisperse. This would further enhance flocculation rate. The 'flocculation time' as calculated from Equation 6-3 would therefore be overestimated.

During crystallization both crystal size and volume fraction of crystals are increasing. During the initial stage of isothermal crystallization, the average crystal size would increase linearly in time and the volume fraction of solids would be proportional to t^4. As a result, the flocculation time therefore decreases as crystallization proceeds. 'Flocculation times' would even be shorter if secondary nucleation is taken into account.

From modelling the crystallization kinetics of fat dispersions, it appeared that already at volume fractions below 0.01, the time scale of crystallization is longer than the time scale of flocculation. This would mean that already in the beginning of the crystallization process considerable flocculation occurs (Kloek (1998), chapter 4).

The simultaneousness of nucleation, crystal growth and aggregation has important consequences for describing and modelling crystallization and aggregation kinetics. As soon as considerable aggregation of crystals occurs, the crystal surface that is available for growth decreases. This will slow down the crystallization rate.

Equations 6-2 and 6-3 assume that at t = 0 the volume fraction of particles is ϕ_0. However, at t = 0 no crystals are present (ϕ_0), so the nucleation rate J has to be taken into account to calculate the number of particles and aggregates. If a dispersion of say 10 % potential solids is supersaturated and secondary nucleation is neglected, J may be considered constant during the crystallization of the first one percent of solids (Meeussen (1995)).

$$\frac{dc}{dt} = J - \frac{4 \cdot k_b T \cdot c^2}{3 \cdot \eta_0} \qquad \textbf{(6-4)}$$

Integrating this equation with boundary condition $c_{t=0} = 0$ and solving for c yields:

$$c = \frac{3}{2} \cdot \sqrt{\frac{J \cdot \eta_0}{3 \cdot k_b T}} \cdot \tanh\left(2 \cdot t \sqrt{\frac{J \cdot k_b T}{3 \cdot \eta_0}}\right) \qquad \textbf{(6-5)}$$

This equation is plotted in Figure 6-1, together with the total number of potential crystals ($J \cdot t$) that could be produced by primary nucleation. After a certain time the total number of particles is constant: the decrease of its number by aggregation is compensated by the production of particles by nucleation. So the number of aggregates is determined in the initial stages of the crystallization process.

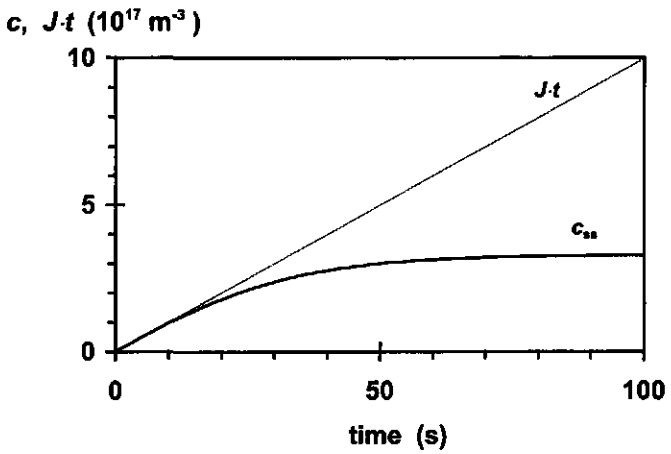

Figure 6-1. *The number density of aggregate and crystals c and the maximum number density of crystals as function of time during simultaneous nucleation and aggregation according to Equation 6-5.* $J = 10^{16}$ $m^{-3} \cdot s^{-1}$, $\eta_0 = 60$ mPa·s *and* $T = 298$ K.

The number concentration of aggregates and crystals in the steady state (c_{ss}) would be given by:

$$c_{ss} = \tfrac{3}{2} \cdot \sqrt{\frac{J \cdot \eta_0}{3 \cdot k_b T}} \qquad \textbf{(6-6)}$$

The time at which half of this steady state number density is reached is at:

$$t_{\frac{1}{2}c} = \tfrac{1}{2} \cdot \operatorname{arctanh} \tfrac{1}{2} \cdot \sqrt{\frac{3 \cdot \eta_0}{J \cdot k_b T}} \qquad \textbf{(6-7)}$$

The average number of particles in an aggregate N_p is simply calculated by dividing the number density of crystals ($J \cdot t$) by the number density of aggregates. This gives the relation:

$$N_p = k \cdot \tanh k \qquad \text{with} \qquad k = \frac{t}{t_{\frac{1}{2}c}} \cdot \operatorname{arctanh} \tfrac{1}{2} \approx 0.55 \cdot \frac{t}{t_{\frac{1}{2}c}} \qquad \textbf{(6-8)}$$

For $t > 5 \cdot t_{½,c}$, the average number of particles per aggregate would roughly be given by $t/t_{½c}$ which is proportional with time.

The consideration of simultaneous aggregation and crystallization given above assumes that the particles produced by nucleation directly have their final size. However, the crystals grow in time. An increase of particle size will delay aggregation of crystals but it is not clear to what extent. Another consequence of simultaneous crystallization and aggregation is that solid bridges can readily be formed between aggregated crystals (sintering) since these are in very close contact (Walstra *et al.*(1995)). The separation distance between two aggregated crystals is of the order of 1 nm which is comparable with the dimension of a triglyceride molecule. Sintering may markedly influence the mechanical properties of the aggregates and the network.

6.1.4 Network models

When aggregation proceeds, a continuous crystal network will generally be formed. The mechanical properties of the network depend on the amount of solid fat, the spatial distribution of the fat crystals, the interaction forces between the crystals and the size and the shape of the crystals.

If an elastic network is deformed, energy is applied to the structural units. The change in Gibbs energy ΔA on deformation can be stored enthalpically (ΔH) or entropically ($T \cdot \Delta S$) :

$$\Delta A = \Delta H - T \cdot \Delta S \qquad \textbf{(6-9)}$$

In case of macromolecular gels the deformation energy is mostly stored in an entropic way. On deformation the chains between junctions are straightened and they lose part of their entropy. In case of particle gels, like fat crystal networks, there is hardly any loss of entropy so the main energy change is enthalpic. The shear modulus G of a network is given by (van Vliet and Walstra (1985)):

$$G = C \cdot N \cdot \frac{d^2 A}{dx^2} \qquad \textbf{(6-10)}$$

where $C = \Delta x/\gamma$ is a constant relating the macroscopic strain γ to the displacement Δx of two structural elements with respect to each other and N is the number of effective strands per unit cross section of the gel.

Van den Tempel (1961) was the first to try and explain the shear modulus G of a fat crystal network (tristearate in oil) on the basis of van der Waals attraction, assuming a linear arrangement of spherical crystals parallel to the three axes of an orthogonal co-ordinate system (Figure 6-2).

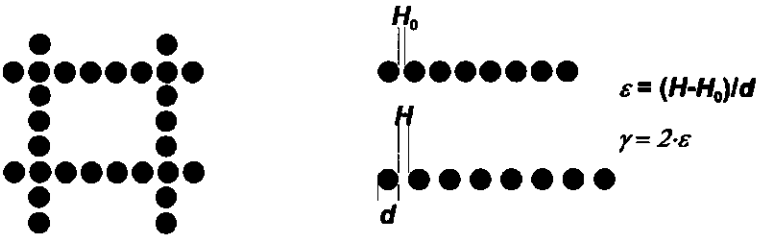

Figure 6-2. *Arrangement of fat crystal in a network according to van den Tempel (1961). Particles incorporated in stress-carrying strands are filled.*

In a dispersion of spherical crystals of diameter d and volume fraction ϕ_0, the total length of the crystal chains per unit volume equals $6\cdot\phi_0/(\pi\cdot d^2)$. Then stretching the network, a third of the chains will carry the stress so that N equals $2\cdot\phi_0/(\pi\cdot d^2)$. Van den Tempel assumed van der Waals attraction to be the only interaction force. To correct for the non-spherical shape of the crystals, it was assumed that the interaction energy could be considered as an intermediate between for that of spheres and cubes. This yielded for the interaction energy $A = A_h\cdot d^{1.5}/(12\cdot H^{1.5})$ where A_h is the Hamaker constant and H the distance between the crystals. The stress per unit cross-section σ_c is given by $N\cdot(dA/dH)$ and the shear modulus of the unstrained network is then given by $(1/3)\cdot(d\sigma_c/d\varepsilon)$. Converting the relative extension ε to a shear strain γ by $\gamma = 2\cdot\varepsilon = 2\cdot(H-H_0)/d$, it finally yields for the shear modulus at very small deformations:

$$G = \frac{5\cdot A_h\cdot\phi_0\cdot d^{0.5}}{24\pi\cdot H_0^{3.5}} \qquad \textbf{(6-11)}$$

This equation is equivalent to Equation 6-10, for $C = d/3$.

Van den Tempel obtained reasonable values for the shear moduli. A consequence of this equation is that the modulus is proportional to the amount of solid fat, and is slightly dependent on the crystal size. According to the derivation of Equation 6-11 there would be no region of linear deformation. From the literature it is known that the modulus scales with the amount of solids with an exponent of 4 to 8. It is also known that the crystal size has a large effect on the modulus: an increase of the particle size lead to a decrease of the modulus (Tempel (1979)). Furthermore, linear regions of deformation of about 10^{-4} to 10^{-3} are observed.

Nederveen assumed a similar geometrical model but calculated the interaction on the base of spherical particles and took into account van der Waals attraction and Born repulsion so that $N = 2\cdot\phi_0/(\pi\cdot d^2)$ and $A = ((A_h\cdot d/24\cdot H)\cdot(1-(1/7)\cdot(H_0/H)^6))$. In this case the shear modulus for small deformations would be:

$$G = \frac{A_h \cdot \phi_0}{6\pi \cdot H_0^3} \cdot \left(1 - \frac{11d\varepsilon}{2 \cdot H_0}\right) \qquad \textbf{(6-12)}$$

which is equivalent to Equation 6-10, for $C = d$.

Also this model shows linear scaling of the modulus with the volume fraction of solids. It predicts a decrease of the modulus with increasing particle size. The term in brackets gives the deviation of the modulus from the linear region and is introduced by taking into account Born repulsion. Assuming a particle diameter of 0.1 μm, a distance between the particles at equilibrium of 0.5 nm and an allowable deviation of the modulus of 10 % yields a linear elongation of about $9 \cdot 10^{-5}$. This corresponds with a linear strain of about $2 \cdot 10^{-4}$. This value compares rather well with experimental values.

The network models described so far assumed that all the solid fat is present in stress-carrying chains. This seems not very realistic. Papenhuijzen assumed that only a fraction α was effective in contributing to the modulus so that N equals $2\alpha \cdot \phi_o/(\pi \cdot d^2)$. Assuming spherical crystals and van der Waals attraction only then yields:

$$G = \alpha \cdot \frac{\phi_0 \cdot A_h}{6\pi \cdot H^3} \qquad \textbf{(6-13)}$$

For a dispersion containing 7 % solids it was calculated that only 4 % of the solid fat was effective. This was translated to a geometrical model as given in Figure 6-3. Linear chains of crystals connect big clusters of fat crystals to each other.

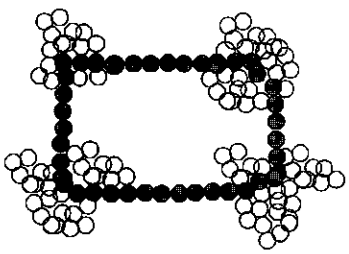

Figure 6-3. *Cross-section of the arrangement of crystals in clusters and linear chains according to Papenhuijzen. Particles incorporated in stress-carrying strands are filled.*

The models of van den Tempel, Nederveen and Papenhuijzen assume that the crystal chains are oriented parallel to the axis of an orthogonal co-ordinate system and that only the chains in one direction are stress carrying.

Kamphuis put forward an isotropic network model; a model in which the probability to find a chain is equal for all directions. In this model also breaking and formation of bonds due to thermal movement was incorporated. The result of that analysis was:

$$G = \frac{A_h \cdot \phi_0}{20\pi \cdot H_0^3} \tag{6-14}$$

This result is close to the result of the earlier mentioned models, except for a numerical coefficient. The difference in this coefficient is about a factor 3 and can be explained by the use of an isotropic network model in stead of a network in which there are only chains in three mutually perpendicular directions. The models of Kamphuis and Papenhuijzen yield the same equation for G when $\alpha = 0.3$ in Equation 6-13. Bremer (1992) performed a similar analysis but in a much less complicated way and found an equation similar to that of Kamphuis :

$$G = \frac{6}{\pi^3} \cdot (1 - \ln 2)^2 \cdot \frac{A_h \cdot \phi_0}{H_0^3} \tag{6-15}$$

The numerical front factors found by Bremer and Kamphuis hardly differ.

Large progress in describing mechanical properties of particles gels as function of volume fraction particles has been made after the introduction of the fractal concept (Bremer *et al.* (1989), Bremer (1992) and de Rooij (1996)). By using the fractal concept it is possible to describe the geometric distribution of particles in space. This distribution can be incorporated into equations for elastic moduli via N and C (Equation 6-10).

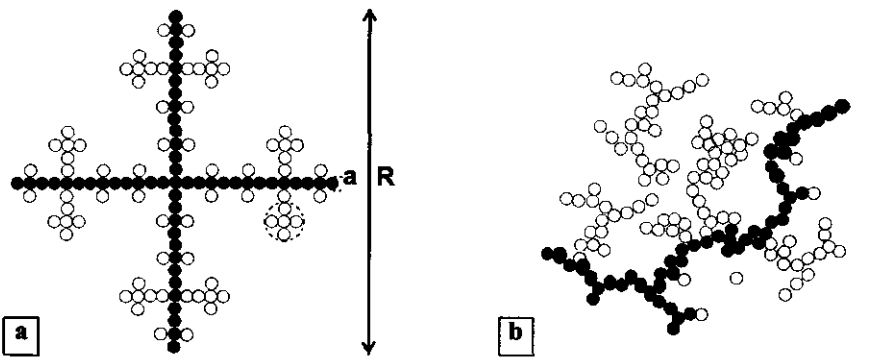

Figure 6-4. *Example of a deterministic fractal aggregate (a) and a stochastic fractal aggregate (b). Particles incorporated in stress-carrying strands are filled.*

A fractal is a structure that is repeated at different length scales. A deterministic fractal is built of structures that are connected to each other as a result of transformations according to strict rules (*e.g.* Figure 6-4a). A stochastic fractal is build up of structures connected to each other as a result of a random process (Figure 6-4b). Many aggregates formed during aggregation can on average be modelled as a fractal. The number of particles N_p in a fractal aggregate scales with the dimensionless radius (R/a) with an exponent D, the fractal dimensionality:

$$N_p = \left(\frac{R}{a}\right)^D \tag{6-16}$$

D is a characteristic parameter describing the structure of the aggregate. The primary particle size a may be the size of a crystal, or the radius of a small, compact aggregate of crystals. The number of volume elements in a three-dimensional space N_{tot} scales with an exponent of 3 with the dimensionless radius. The volume fraction of particles in an aggregate is thus given by:

$$\phi_{int} = \frac{N_p}{N_{tot}} = \left(\frac{R}{a}\right)^{D-3} \tag{6-17}$$

An important consequence of this equation is that the volume fraction of particles in an aggregate decreases with increasing radius. As aggregation proceeds, the aggregates become more tenuous. At the moment the volume fraction of particles in the aggregate equals the volume fraction of primary particles, a three-dimensional network is formed. At the gel point, the radius of an aggregate equals $a \cdot \phi_0^{1/(3-D)}$. The number of stress-carrying chains N in a network consisting of fractal aggregates depends on the size of the aggregates and is inversely proportional to the surface area of an aggregate. This is because the number of contact points between two aggregates will be constant and independent on the aggregate size, as follows from the scale invariance of aggregate structure. For N the following relation holds:

$$N \propto \left(\frac{R}{a}\right)^{-2} = \phi_0^{2/(3-D)} \tag{6-18}$$

If chains between the aggregates are straight, the deformation of the chains is independent of the aggregate size so that C is independent on the aggregate size. For hinged chains C depends on the aggregate size and scales with $(R/a)^{-1}$ (Bremer (1992)). For chains that have a fractal backbone of dimensionality $(1+x)$, C is proportional to $(R/a)^{-2-x}$ (Brown and Ball (1985)). Inserting 6-18 in 6-10 and using the appropriate equations for C yields the following proportionalities between G and ϕ_0 (Bremer (1992)):

$$\begin{aligned}
&\text{straight chains} && G \propto \left(\frac{R}{a}\right)^{-2} = \phi_0^{\,2/(3-D)} \\
&\text{hinged chains} && G \propto \left(\frac{R}{a}\right)^{-3} = \phi_0^{\,3/(3-D)} \\
&\text{'flexible chains'} && G \propto \left(\frac{R}{a}\right)^{-4} = \phi_0^{\,(4)/(3-D)} \\
&\text{fractal chains} && G \propto \left(\frac{R}{a}\right)^{-4+x} = \phi_0^{\,(4+x)/(3-D)}
\end{aligned} \qquad \textbf{(6-19)}$$

The fractal network models can explain the observed power-law scaling between elastic moduli and volume fraction solids. It has been used with success to explain mechanical properties of particle gels. From the slope of a log - log plot of G against ϕ_0, the fractal dimensionality can be obtained if the geometry of the stress-carrying strands is known. The intercept of this plot is a measure of the interaction force between the particles at $\phi_0 = 1$

The fractal dimensionality can also be determined from other physical parameters, like yield stress, permeability, viscosity, if these are determined as function of the volume fraction particles. A very powerful technique to determine the geometric distribution of particles is Confocal Scanning Laser Microscopy (Bremer (1992)). From a single micrograph of a dispersion at one volume fraction it is possible to determine the fractal dimensionality by calculating the distribution function. From these type of experiments it became clear that a distribution of dimensionalities may occur in several systems (Bos, 1997). The dimensionality may vary among aggregates in the same dispersion, but it may also vary among regions in an aggregate. Determining the fractal dimensionality from physical parameters would therefore yield an average dimensionality that will depend on the way it is determined. It is likely that elastic moduli will yield other dimensionalities than the values obtained from permeabilities, since parameters determined by the properties of the strands and of the pores are measured, respectively.

6.1.5 Particle interactions

The interaction energy between aggregated fat crystals in oil can be described well by a Lennard-Jones type equation which gives the energy content ΔA of a bond between two spherical non-polar particles (van den Tempel (1961), Kamphuis (1984)). It contains a van der Waals attraction and a hard core repulsion term. The integrated form of the original equation is given by:

$$\Delta A = \frac{-A_h \cdot d}{24 \cdot H} \cdot \left(1 - \frac{1}{7} \cdot \left(\frac{H_0}{H}\right)^6\right) \qquad \textbf{(6-20)}$$

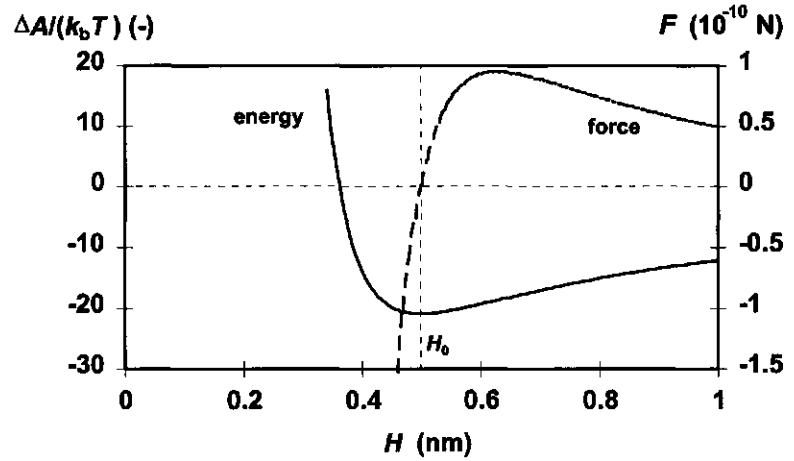

Figure 6-5. *Lennard-Jones potential and the corresponding attractive interaction force as a function of the separation distance H for two spherical particles with* $a = 10^{-7}$ m, $A_h = 2 \cdot 10^{-21}$ J *and* $H_0 = 5 \cdot 10^{-10}$ m.

When the energy content is differentiated with respect to the interparticle distance H, the interaction force F_w is obtained:

$$F_w = \frac{A_h \cdot d}{24 \cdot H^2} \cdot \left(1 - \left(\frac{H_0}{H}\right)^6\right) \qquad \textbf{(6-21)}$$

Both equations are plotted in Figure 6-5. At a separation distance H_0, the interaction force is zero. Moving the particles from this equilibrium situation to each other causes a net repulsive force, while moving the particles away from each other causes an attractive force. The maximum attractive force is at a separation distance of $2^{1/3} \cdot H_0$.

By using this analysis, it is implicitly assumed that the particles are undeformable. In reality, fat crystals are strongly anisometric and can be subject to bending. The resistance to bending will depend on the length to thickness ratio and the bending modulus of the crystal E_b. If two crystals are situated perpendicular to each other and one crystal is moved, several things can occur: the separation distance remains constant but the crystal bends, the crystal does not bend but the separation distance increases or something intermediate occurs (Figure 6-6). The deflection x_c at the non fixed end of a cantilever with length l_c, width w_c and thickness t_c is given by (Roark (1985)):

$$x_c = -\frac{F}{3 \cdot E_b \cdot I} \cdot l_c^3 \qquad \textbf{(6-22)}$$

where I is moment of inertia, which is given by $w_c \cdot t_c^3/12$, and F is the force acting on the non fixed end.

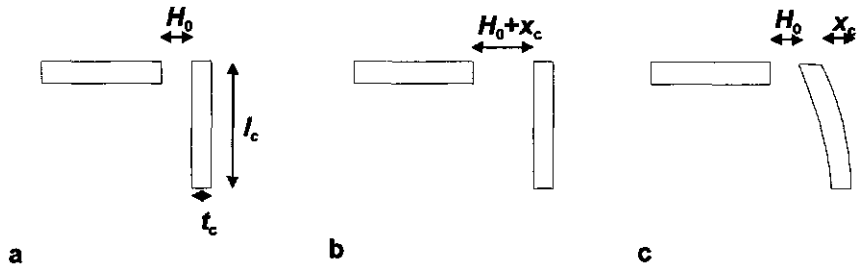

Figure 6-6. *Possible deformation of anisotropic crystals:* **a;** *no deformation* **b;** *displacement over a distance x_c if the van der Waals attraction is weak compared to the stiffness of the crystal* **c;** *deflection over a distance x_c if the van der Waals attraction is strong compared to the stiffness of the crystal.*

The maximum attractional force occurs at $H = 2^{1/3} \cdot H_0$. If this force is taken as the load on the end of the cantilever and taking $d = (w_c \cdot t_c)^{1/2}$ in Equation 6-21, the following relation for the deflection x_c is found:

$$x_c = \frac{2^{1/3}}{16} \cdot \frac{A_h}{H_0^2 \cdot E_b} \cdot \frac{l_c^3}{t_c^2 \cdot \sqrt{w_c \cdot t_c}} \qquad \textbf{(6-23)}$$

The macroscopic strain γ of the crystal is estimated by x_c/l_c. Inserting crystal dimensions of l_c = 1 μm, w_c = 0.2 μm and t_c = 0.05 μm and using $A_h = 2 \cdot 10^{-21}$ J, $H_0 = 5 \cdot 10^{-10}$ m and $E_b = 10^9$ N·m^{-2}, yields a macroscopic strain of $2.5 \cdot 10^{-3}$. This shows that fairly high macroscopic strains can be reached due to attractional forces between crystals required to separate them from each other. Especially the dimensions of the crystal (last term in Equation 6-23) will determine to which extent it will bend.

Figure 6-7 shows the deflection of the one-side fixed crystal as a function of the displacement between the two crystals for various bending moduli of the crystals. On moving the crystals from each other, the deformation of the fixed crystal increases and reaches a maximum deflection at a separation distance between the crystals of $2^{1/3} \cdot H_0$. This is the distance at which the van der Waals attractional force is highest. On further separation of the crystals, the deflection of the fixed crystal decreases since the attractional force decreases.

Bending of the crystals by moving these away from each other will become more difficult if more crystals are present or if crystals are not rectangular but somewhat curved and twisted. Such crystals will only bend easily if the force is perpendicular to the direction of the curvature. Bending

of a crystal also becomes more difficult if both crystal ends are non-fixed *i.e.* if they are free to move. In this case, external forces can result in a sliding movement over the crystal surface.

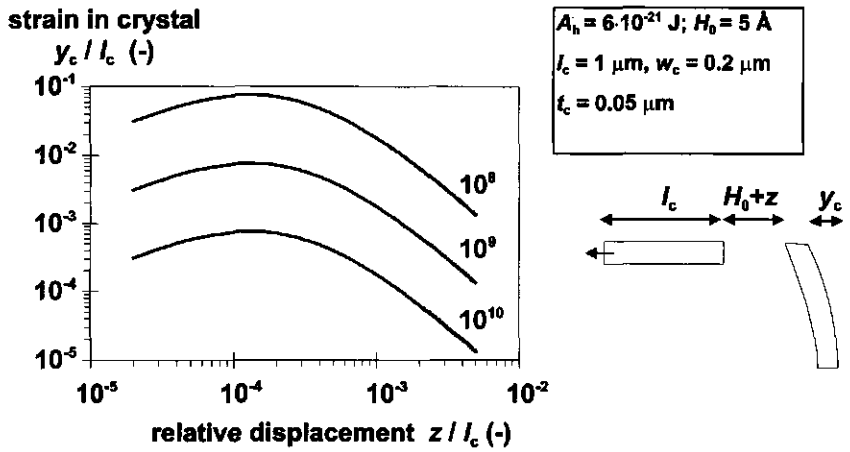

Figure 6-7. *Relative bending deformation (y_c / l_c) of a crystal that is attracted due to van der Waals attraction of a crystal as function of the relative displacement (z/l_c) between the crystals (see diagram at right). Bending moduli of the crystal* ($N \cdot m^{-2}$) *are indicated near the curves.*

If fat crystals are sintered due to simultaneous aggregation and crystallization or by recrystallization of thermodynamically unstable crystals, the bonds between the crystals are very stiff. Therefore, the deformation behaviour of such a sintered dispersion at strains smaller than the yield deformation, will be determined by the bending modulus of the crystals and their dimensions.

If emulsifiers adsorb onto the crystal surface there may be an additional repulsive term due to steric or electrostatic repulsion. This would slow down the aggregation process (reaction limited aggregation) and may result in more compact aggregates. Johannson and Bergenståhl (1992[a]) showed by sedimentation studies that emulsifiers adsorb weakly onto fat crystals; they formed tight monolayers at high and loosely packed layers at low emulsifier concentrations. Loosely packed monolayers appeared to lead to a weaker crystal network and tight layers lead to an increased strength.

Addition of a small amount of water (0.2 %) to tristearate crystals in soy bean oil dispersions did not affect the elastic moduli of the dispersion, but it increased the yield stress by a factor 4. Also the region of linear deformation was extended from $1.2 \cdot 10^{-3}$ to $5 \cdot 10^{-3}$ by the addition of water (Johansson *et al.* (1992[c])). Johansson *et al.* (1992[b]) calculated that formation of water bridges between fat crystals may yield adhesive forces of a magnitude comparable to or higher than van der

Waals forces. It should be kept in mind that the authors used a Hamaker constant of $2 \cdot 10^{-22}$ J (0.05 k_bT), calculated from dielectric permitivities and refractive indices. For this estimate, they used a refractive index for the fat crystal of 1.45 (smaller than the refractive index of the oil phase). If a refractive index of 1.56 is used (Meeussen (1995)), we calculate a more reasonable Hamaker constant of $2 \cdot 10^{-21}$ J, which is about ten times higher.

The results of Johansson can also be explained by assuming the crystals to bend. Adding traces of water leads to stronger bonds between the fat crystals compared to van der Waals bonds due to formation of water bridges. Assuming the van der Waals bonds are stiff compared to the bending modulus of the crystals, the crystals will bend on small deformations but the separation remains the same; the elasticity modulus is the same as for a dispersion that contains no water. At larger deformations around the yield point, the crystals bend so much that the force at the end of the crystal becomes so high that the water bridge is broken. Since for larger strains the water bridge is stronger than the van der Waals force, a higher stress is necessary to break the bond (higher yield stress). This higher stress can only be obtained by deforming the crystal to a greater extent which explains the larger region of linear deformation.

6.2 *Materials and methods*

6.2.1 Materials

A description of the physical properties and the triglyceride composition of the model system is given in chapter 2 of this thesis. Due to the large number of different triglycerides, many crystal defects will be formed and considerable recrystallization is expected to occur. Both factors will probably promote sintering of aggregated crystals.

Also solid phases with a much more homogeneous triglyceride composition were used. The first was tripalmitate (PPP). Moreover, a PSP-rich fat was used that had been obtained by hydrogenation of POP (glycerol 1-3 dipalmitate 2-oleate); it will be referred to as PSP. The main triglycerides in "PSP" are: PPP (0.7 %); PSP (70.4 %); PSS/SSP (19.2 %) and SSS (3.3 %).

Table 6-1 gives some characteristics of PSP.

Table 6-1. *Some properties of PSP and PPP.*

component	molar mass ($g.mol^{-1}$)	$T_{m,\alpha}$ (°C)	$T_{m,\beta'}$ (°C)	$\Delta H_{f,\alpha}$ ($J.mol^{-1}$)	$\Delta H_{f,\beta'}$ ($J.mol^{-1}$)
PPP	807	44.7	55.7	$9.5 \cdot 10^4$	$1.26 \cdot 10^5$
PSP	821	42.4	62.2	$8.7 \cdot 10^4$	$1.57 \cdot 10^5$

The solubility of HP or another high melting fat in SF is given by the Hildebrand equation assuming ideal mixing behaviour (Hannewijk (1964); Wesdorp (1990)).

$$\ln x_{HP} = \frac{\Delta H_{f,i}}{R_g} \cdot \left(\frac{1}{T_{m,i}} - \frac{1}{T} \right) \tag{6-24}$$

where x_{HP} is the mole fraction soluble HP in polymorph i at temperature T, $\Delta H_{f,i}$ the molar enthalpy of fusion of polymorph i, R_g the gas constant and $T_{m,i}$ the absolute melting temperature of polymorph i.

The driving force for crystallization is the chemical potential difference $\Delta\mu$ between a supersaturated solution and a saturated solution:

$$\Delta\mu = R_g T \cdot \ln \frac{c_{HP}}{x_{HP}} = R_g T \cdot \ln \beta \tag{6-25}$$

where c_{HP} is the mole fraction crystallizing component, x_{HP} the solubility given by 6-24, β the supersaturation ratio and $\ln\beta$ the supersaturation. If the mole fraction crystallizing component is known, the crystallization temperature T can be calculated for every initial supersaturation. As the crystallizing component, the whole group of "solid" triglycerides present will be taken. They are treated as a one-component system.

6.2.2 Methods

6.2.2.1 Rheology

Mixtures of the model system were made by weighing the fats in the liquid state. Prior to rheological measurements, the mixtures were kept at 80 °C for 10 minutes to destroy all possible crystal memory. The melted dispersion was introduced into the rheometer that was set to the desired crystallization temperature. During crystallization, the dynamic moduli were determined at a frequency of 0.10 Hz and a maximum strain of $5 \cdot 10^{-4}$. This strain was within the linear region of crystallized fat dispersions. Strain sweeps were performed at a frequency of 0.1 Hz.

Frequency spectra were determined at a maximum strain of $5 \cdot 10^{-4}$. The lowest applied frequency was 0.001 Hz. At high frequencies problems occurred with very stiff samples using a strain-controlled rheometer. Due to the stiffness of the sample, the measured storage moduli decreased with increasing frequency above a critical frequency. This is physically not possible and is explained by deformation of the driving gear of the rheometer. This deformation causes some energy uptake that is not accounted for in the software. This leads to an apparent decrease in G' and increase in loss tangent with increasing frequency. The critical frequency decreased with increasing modulus. For a 10 % HP/SF dispersions, having a storage modulus of about $7 \cdot 10^5$ N·m^{-2} and a very low loss tangent (< 3°), the critical frequency was about 0.4 Hz.

The rheological measurements were performed using a strain-controlled Bohlin VOR or a stress-controlled Bohlin CS. In case of isothermal crystallization in the β' polymorph, a concentric cylinder geometry (code C14) was used. In the case of crystallization in the α polymorph or measurements on mechanically treated dispersions, a parallel plate geometry with roughened plates was used.

6.2.2.2 Permeability

Permeability coefficients were determined by measuring the volume flow rate Q of sunflower oil through crystallized HP/SF dispersions. The flow rate is related to the permeability coefficient B according to the Darcy relation:

$$Q = \frac{B \cdot A_c}{\eta_0} \cdot \frac{\Delta P}{l} \tag{6-26}$$

where A_c is the cross-sectional area of the dispersions through which the oil is permeating, ΔP the applied pressure difference over a distance l and η_0 the viscosity of the oil.

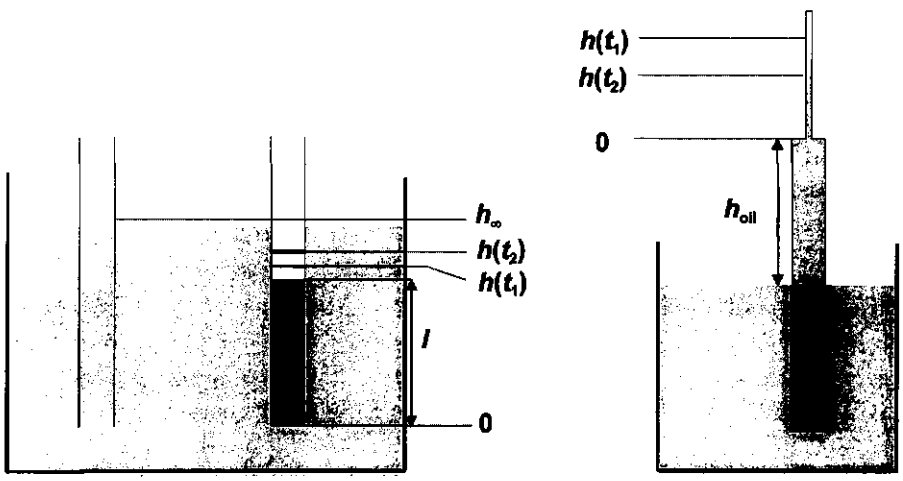

Figure 6-8. *Schematic representation of the permeability set-up using the normal method (left) and the capillary method (right).*

The HP/SF dispersions had crystallized in open-end permeability tubes (diameter 4 mm) for one hour at the appropriate temperature. The tubes were placed in a bath thermostatted at the crystallization temperature that was filled with sunflower oil. The pressure difference over the fat plug could be changed by varying the depth of the tube in the bath (Figure 6-8, left). The flow rate

was determined by monitoring the level of the permeating liquid in time with a travelling microscope. This was our normal method (van Dijk (1986)).

For low permeabilities, the flow rates were too low to be determined by the above-mentioned method. In this case, the flow rate was determined by measuring the linear speed of the oil-air interface in a vertical capillary. To this end, the permeability tube that contained the crystallized fat dispersion was further filled with oil and a thin capillary was fitted on top of the permeability tube (Figure 6-8, at right). The ratio between the cross-sectional surfaces of the permeability tube and the capillary was about 22.5. The capillary rise h_{cap} was taken into account. The permeabilities were calculated by inserting the measured oil levels at different times in the following equations:

$$B = \frac{1}{t_2 - t_1} \cdot \frac{\eta_0 \cdot l}{\rho \cdot g} \cdot \ln\left[\frac{h_\infty - h(t_1)}{h_\infty - h(t_2)}\right] \qquad \text{normal method}$$

$$B = -\frac{1}{t_2 - t_1} \cdot \frac{\eta_0 \cdot l \cdot c}{\rho \cdot g} \cdot \ln\left[\frac{h(t_2) + h_{oil} - h_{cap}}{h(t_1) + h_{oil} - h_{cap}}\right] \qquad \text{capillary method} \qquad \textbf{(6-27)}$$

where c is the ratio between the cross-sectional surfaces of the permeability tube and the capillary.

6.3 Results and discussion

6.3.1 Elastic moduli during crystallization

Figure 6-9 shows the storage modulus during the isothermal crystallization of 12 % HP/SF dispersions at various initial supersaturations in the β' polymorph. Under the applied conditions, the α polymorph was not supersaturated.

As a supersaturation is applied, crystals are produced by nucleation and crystal growth. After a certain induction time, the storage modulus starts to increase. This induction time depends on the initial supersaturation. The induction can be seen as the time needed for crystals to be formed and to flocculate to aggregates that are space filling *i.e.* the time needed to form a gel. For high supersaturations ($\ln\beta = 4$) the induction time was a few seconds while for low supersaturations the induction time was a few hundreds of seconds. This is in agreement with expectations: at a high supersaturation, both nucleation and crystal growth rate are fast. Because there is no energy barrier to aggregation of crystals, the crystals will rapidly form aggregates and subsequently a gel.

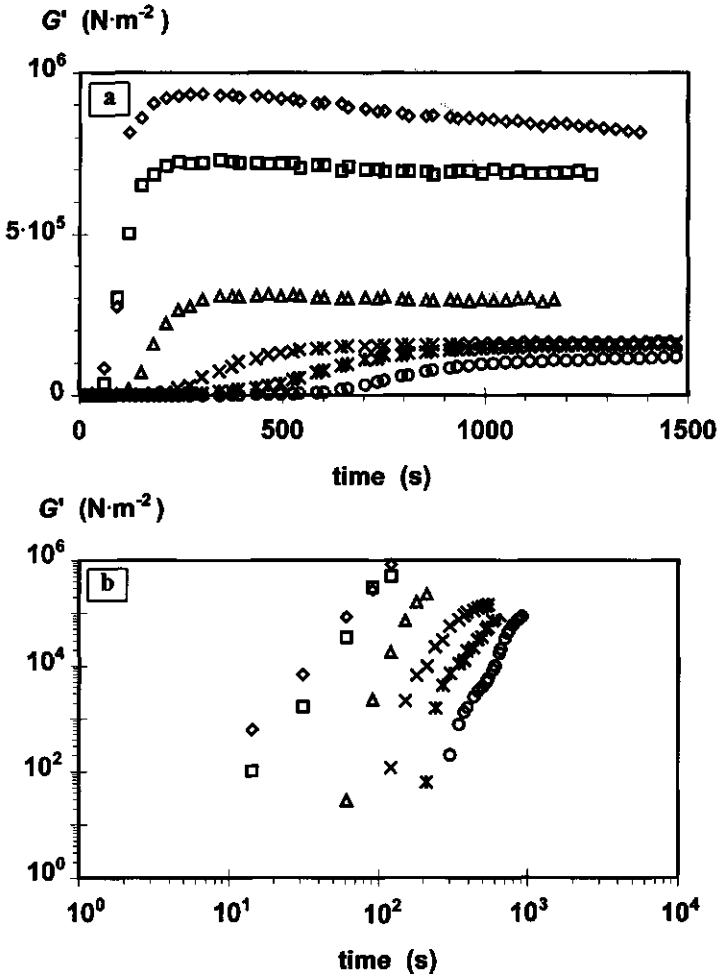

Figure 6-9. *Storage moduli of 12 % HP/SF as function of time during isothermal crystallization at various initial supersaturations plotted on linear scales (a) and the initial part on log-log scales (b).* ◊: $\ln\beta=4.0$, □:$\ln\beta=3.75$, Δ:$\ln\beta=3.50$, ×:$\ln\beta=3.25$, *:$\ln\beta=3.0$, o:$\ln\beta=2.75$.

Bremer (1992) derived an equation to estimate gel time t_g; *i.e.* the time needed to form a space filling network assuming fractal aggregation:

$$t_g = z^{D-1} \cdot \left(1 - \frac{6D}{2D+3} + \frac{3D}{D+6}\right) \cdot \frac{\pi \cdot \eta_0 \cdot a^3}{k_b T} \cdot \phi_0^{3/(D-3)} \qquad \textbf{(6-28)}$$

where z is a factor ranging between 0.85 and 1 depending on the value of D. This equation assumes that at $t = 0$ already a volume fraction ϕ_0 of particles with radius a is present. Although strictly speaking not valid for the case of simultaneous crystallization and aggregation, this equation can be used to estimate the order of magnitude of the gel time. Assuming D = 1.7 for aggregates at small volume fraction of solid (Kloek (1998), chapter 5), a particle radius of about 10^{-7} m (Kloek (1998), chapter 4) and a volume fraction of solid at the gel point ϕ_{gel} of about 0.02, would yield a gel time of 24 s. At a $\phi_{gel} = 0.01$ the gel time would equal 120 s. These times correspond well with the times at which storage moduli obtain significant values (10-100 $N \cdot m^{-2}$, Figure 6-9b). The calculated gel times may be overestimated by the anisometric nature of fat crystals.

For a given dimensionality, the gel time according to Equation 6-27 is very sensitive to both particle size ($\propto a^3$) and fraction solid ($\propto \phi^{2.31}$ for $D = 1.7$). During the initial stage of crystallization, both nucleation rate and crystal growth rate are constant so that the volume fraction solid would be given by Avrami's equation 6-1, where the fraction solid is proportional to t^4. The volume-surface average crystal size then is only proportional to t so that the gel time would be mainly determined by the fraction solid. The influence of initial supersaturation on the gel time is therefore primarily due to the effect of supersaturation on the crystallization kinetics.

After the induction period, the storage modulus increased rapidly. At high supersaturation, the storage modulus reached a maximum, while at lower supersaturation the modulus became constant. At very low supersaturations ($\ln\beta \leq 2.75$), the storage modulus kept increasing over the time span studied. Interpretation of the results for dispersions crystallized at $\ln\beta \leq 2.75$ is somewhat cumbersome, because at these low supersaturations spherulitic structures with sizes up to 100 μm were often formed, as noticed by microscopic evaluation. These structures are too large, compared to the gap size of the measuring body, to allow accurate rheological measurements.

The initial rate of increase of the storage modulus (in the range $10^2 < G' < 10^3$) is very high. Scaling relations of $G' \propto t^p$ with p varying between 15 and 20 can be obtained for initial supersaturations smaller than 3.75. At these supersaturations it was experimentally possible to perform the first measurement while no solid fat was present. This was not possible at initial supersaturations of 3.75 and 4. The scaling exponent p decreased to roughly 4 - 6 after considerable crystallization has occurred. During the initial stage of crystallization the fraction solids is given by Avrami's equation and scales with t^4. If the relations $G' \propto t^p$ with $p \approx 15$-20 and $\phi \propto t^4$ are combined, G' would be proportional to $\phi^{3.8-5}$. This range of scaling exponents is often observed and can be explained well by assuming that the gel is built of fractal aggregates (Equation 6-19). This will be discussed later. The lower value of scaling exponent p, that prevails later on in the crystallization process, can be due to two mechanisms. Firstly, supersaturation has decreased and therefore the fraction solids is not proportional anymore to t^4 but to t to a smaller exponent. Secondly, the crystals that aggregate onto an existing network will probably be less effective in contributing to the network modulus than the crystals that form the primary network.

Figure 6-10 shows that during crystallization the loss modulus follows the same pattern as the storage modulus. After a certain induction time, the loss modulus increases rapidly. At a certain

stage the loss modulus reaches a maximum value, while the storage modulus still increases. A decrease of the loss modulus will be due to relatively less energy dissipation during deformation. A possible explanation for a maximum in the loss modulus can be a gradual change in the type of interaction.

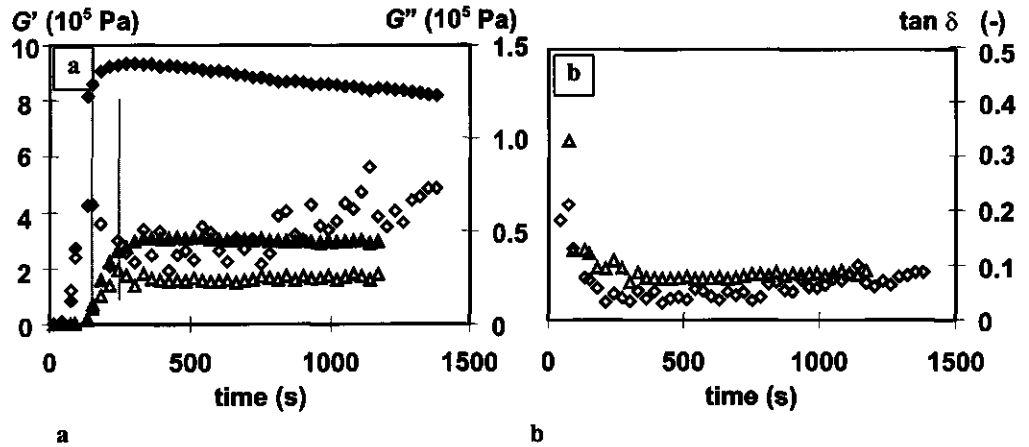

Figure 6-10. *The storage modulus (closed symbols), the loss modulus (open symbols) (a) and the loss tangent (b) during the crystallization of 12 % HP/SF at supersaturations of ◊ 4.00 and Δ 3.50. Vertical lines indicate the time at which the loss modulus obtains a maximum value.*

During the initial stage of crystallization, the crystals are attracted to each other by van der Waals forces. These bonds may exhibit considerable relaxation and therefore cause energy dissipation. If these bonds become sintered due to ongoing crystallization or recrystallization, much less energy relaxation will occur. This would result in a decrease of the loss modulus.

For intermediate initial supersaturations, the loss modulus was almost constant after crystallization was about finished. Since also the storage modulus was constant, so was the loss tangent. For the highest supersaturation ($\ln\beta = 4$), the storage modulus decreased and the loss modulus increased with time. Ostwald ripening of the small crystals produced at high supersaturations can possibly explain the decrease of the storage modulus. These crystals will have irregular shapes. Local radii of curvature will be very small and therefore the local solubility will be high. This would result in dissolution of the irregular-shaped structures and recrystallization to form larger crystals. Structures with larger crystals but with about the same spatial distribution of the crystals would result in lower storage moduli if the particles are bendable, because there is less resistance to bend a longer crystal. Furthermore, the dissolving triglyceride may move to places where it is elastically less effective.

Dispersions that had crystallized at $\ln\beta = 4$ were almost supersaturated in the α polymorph. Because the HP consists of various triglycerides each having its own melting temperature and

melting enthalpy, some triglycerides may have been supersaturated in the α polymorph as the value of $\ln\beta$ was calculated using the "average" bulk properties of the HP. Time resolved X-ray diffraction experiments have shown that an α → β' /β polymorphic transition occurs when HP/SF dispersions have crystallized in the α polymorph. This transition is accompanied by a coarsening of the crystals. So both Ostwald ripening and polymorphic transitions can be the reason for the decrease of the storage modulus of HP/SF dispersions when crystallized at a high supersaturation for the β' polymorph.

6.3.2 Elastic moduli as a function of volume fraction solids

From the elastic moduli as a function of the volume fraction maximal achievable solid (ϕ_0), information can be obtained about the geometrical structure of the network and the interaction parameter A between the structural elements by using the scaling $G' = A \cdot \phi_0^{\mu}$. We took the moduli at the time that the maximum amount of solids was obtained (as determined by p-NMR). When using the final values of the moduli instead, this did not strongly influence the results. Figure 6-11 shows that for all supersaturations a fairly good power-law relation between the storage moduli and the volume fraction HP is obtained. This suggests that the network properties can be described by a fractal approach. The statistics of the power-law fit are given in Table 6-2. Table 6-2 shows that the slope is almost constant having a value of about 6 up to initial supersaturations of 3.75. The same trend is observed for the interaction parameter A. Dispersions crystallized at an initial supersaturation of 4.00 have a clearly lower slope and interaction term as can also be seen in Figure 6-12.

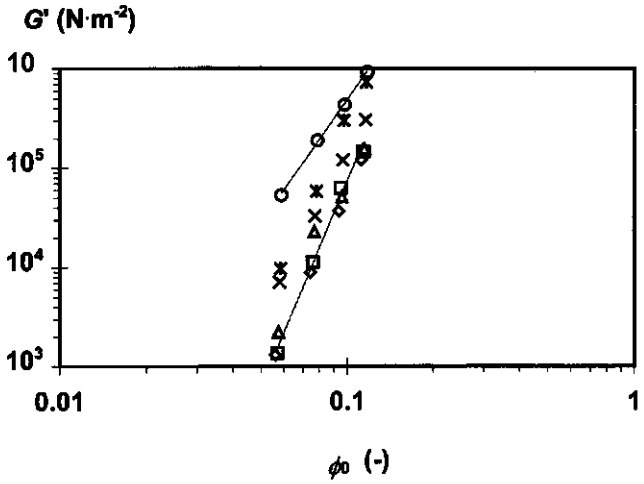

Figure 6-11. *Elastic moduli as function of volume fraction crystallized HP/SF after crystallization at various initial supersaturation.* ◊: $\ln\beta = 2.75$, □: $\ln\beta = 3.00$, Δ: $\ln\beta = 3.25$, ×: $\ln\beta = 3.50$, *: $\ln\beta = 3.75$, o: $\ln\beta = 4.00$.

Table 6-2. *Slopes μ and interaction parameters A obtained from correlation analyses of elastic moduli G' as function of the volume fraction solids ϕ_s according to $G'=A.\phi_s^{\mu}$.*

lnβ	μ	log(A/ Pa)	r^2	ϕ for G'=10 Pa
(-)	(-)	(-)	(-)	(-)
2.75	6.53	11.3	0.9998	0.026
3.00	6.91	11.8	0.9934	0.027
3.25	5.97	10.8	0.9754	0.023
3.50	5.45	10.6	0.9995	0.017
3.75	6.35	11.8	0.9957	0.020
4.00	4.08	9.8	0.9991	0.007

The decrease of both slope and interaction term suggests that the geometrical structure and interaction between the particle changes when crystallizing at higher supersaturations. Most of the slopes are somewhat higher than the slopes of 3.8 - 5 that were determined from the scaling relations between G' and ϕ as function of time during the initial stage of crystallization.

At the moment a gel was formed, the storage modulus started to increase. Already at storage moduli of 1 N·m^{-2} a gel would exist. The lowest detection limit was about 10 N·m^{-2}. At this value also the phase angle became smaller than 45°, *i.e.* the elastic part dominated over the dissipative part. From the slopes and the intercepts in Table 6-2, the volume fraction is calculated at which such a modulus would be obtained. This is the case at volume fractions solids of about 0.02 for supersaturations up to 3.75. At a supersaturation of 4 the calculated volume fraction is lower.

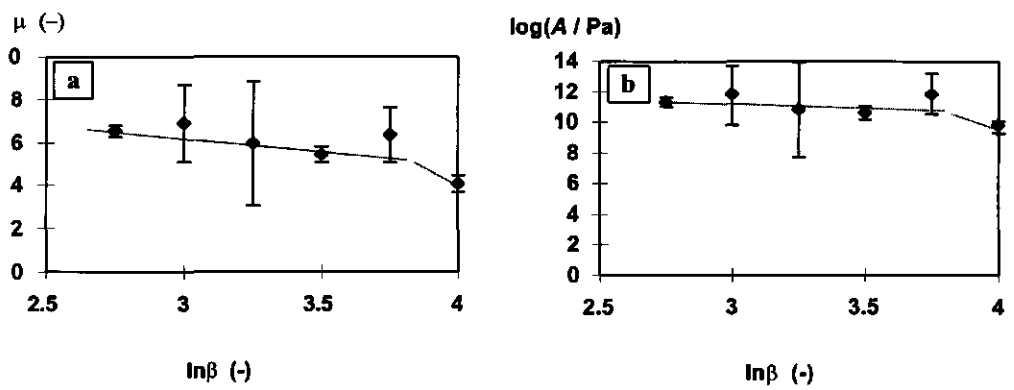

Figure 6-12. *Slopes μ and interaction parameters A and their 95 % confidential limits obtained from correlation analyses of elastic moduli G' as function of the volume fraction solids ϕ_s according to $G'=A.\phi_s^{\mu}$.*

The slope μ can be used to calculate the fractal dimensionality of the network by using Equation 6-19. Depending on the geometry of the backbone of the stress-carrying chains, several dimensionalities can be obtained. A compilation is given in Table 6-3.

Table 6-3. *Calculated fractal dimensionalities of HP/SF networks assuming different geometries of the stress-carrying chains. x refers to the numerator in the exponents of Equation 6-19.*

	scaling exponent	fractal dimensionality D			
	μ	$x=2$	$x=3$	$x=4$	$x=4.3$
low $\ln\beta$: ≤ 3.75	6	2.7	2.5	2.33	2.28
high $\ln\beta$: ≈ 4	4	2.5	2.25	2.00	1.93

Assuming the aggregates to form straight stress-carrying strands (x = 2), very high dimensionalities result. This geometry, however, is not very likely. Presumably, it can only occur if shrinking of the strands takes place after formation of the network, as was shown for aged casein gels (Bremer (1992)). Using a, more likely tortuous arrangement of the stress-carrying strands, smaller dimensionalities result. The highest possible value of the numerator in the exponent μ would be 4.3 (Rooij (1996)). For this geometry, fractal dimensionalities ranging from 2.28 for low supersaturations to 1.93 for high supersaturations were calculated.

Computer simulations for diffusion-limited aggregation (translation diffusion only) showed fractal dimensionalities of about 1.8. By introduction of a sticking probability (energy barrier for aggregation), fractal dimensionalities of about 2.1 were obtained. Taking into account rearrangements would even lead to a higher dimensionality (+ 0.2). The occurrence of rotational diffusion will lead to a lower dimensionality. As the type of interaction between fat crystals in an non-polar medium will be strongly attractive and some rotational diffusion may occur due to the anisometric nature of the fat crystal, it is expected that the primary network consist of aggregates with a low dimensionality. It was shown by light scattering on low volume fraction dispersions that slightly smaller scaling exponents (1.7-1.8) were obtained when correlating the scattered intensity as a function of the wave vector (Vreeker (1992), Kloek (1998) chapter 5)). This may be due to the occurrence of rotational diffusion of the anisometric fat crystals. However, it should be mentioned that this kind of analysis of scattering data on anisotropic particles is questionable.

A possible explanation for the difference in D obtained by light scattering and the analysis of the G' versus ϕ_0 relation is in the strongly different range of ϕ_0 studied. As shown previously, already at very low volume fraction solids, a primary network can be formed with a low fractal dimensionality. Ongoing crystallization will produce more crystals that will aggregate in the pores of the primary network or aggregate to the chains of the primary network. This will compact the

network. If we assume that the primary network is formed at a volume fraction of ϕ_{gel} with a dimensionality of D_{gel}, the dimensionless aggregate radius R/a at the gel point is calculated from $\phi_{gel} = (R/a)^{D_{gel}-3}$. Assuming that the relation $\phi_0 = (R/a)^{D-3}$ remains valid during further crystallization but that the aggregates can not increase in radius so that $R/a = (R/a)_{gel}$, an apparent fractal dimensionality D^* can be calculated as a function of volume fraction for $\phi > \phi_{gel}$:

$$D^* = 3 + (D_{gel} - 3)\frac{\log \phi_0}{\log \phi_{gel}} \qquad \textbf{(6-29)}$$

For $\phi_{gel} = 0.01$ and $D_{gel} = 1.7$, we derive $(R/a) = 34.6$. If an additional 5 % of particles aggregates into existing aggregates, the radius cannot increase, so that a D^* of 2.21 is obtained. At a volume fraction solid of 0.12, $D^* = 2.4$. According to Equation 6-29, D^* should increase with higher volume fractions and therefore a power law relation between G' and ϕ_0 need not hold. However, there are several complicating factors.

- The assumption that aggregates grow not further than to a radius $(R/a)_{gel}$ can be questioned. After the gel point, radial growth of aggregates will be hindered but some interpenetrating of aggregates and therefore growth of aggregates will occur. Neglecting this growth would overestimate D^* since ϕ_{gel} is overestimated.
- The volume fraction at which a space-filling network is formed, depends on the crystallization kinetics of the dispersions. At the same initial supersaturation but varying volume fraction of HP, the crystal growth rate will be constant but the nucleation rate will be higher for a higher volume fraction HP. If the time scale of crystallization is much shorter than the time scale of aggregation, aggregation is rate limiting. Therefore, ϕ_{gel} can increase with increasing ϕ_0. A higher ϕ_{gel} will result in a higher D^*.
- At the gel point, the stress-carrying strands of the network will be tortuous. This corresponds to high x-values in the scaling relation $G' = \phi_0^{\,x/(3-D)}$. On continuous crystallization, the stress-carrying strands will become less tortuous, especially when the new crystals aggregate onto the strands of the primary network. This would result in lower x-values and which may "compensate" for the increase in D^* upon crystallization and thereby result in a power-law scaling between G' and ϕ_0.
- It is not possible to speak about the dimensionality of an aggregate. There will be a distribution of dimensionalities, depending on the length scale considered. On scales smaller than particle size and larger than the aggregate size, the dimensionality will be 3. In intermediate regions D will be smaller than 3. The fractal domain is in between the size region of the crystalline region (primary crystals) and the size region in which the gel is a homogeneous domain. Due to inhomogeneities in the fractal domain, D may locally vary and the D observed by experimental techniques then depends on the physical parameter that is determined.

Table 6-3 shows that, on assumption of a constant x-value, at a high initial supersaturation of crystallization, a lower D is found than at a lower initial supersaturation. This can probably also be explained by differences in ϕ_{gel} due the differences in time scales of aggregation and crystallization. Another parameter that can be important for explaining the difference in scaling exponents for various initial supersaturations is the crystal size. The size (distribution) will depend on the initial supersaturation during crystallization, leading to smaller crystals at higher supersaturations. It was shown that for certain geometrical arrangements, the average size of particles can have an influence on the scaling relations between G' and ϕ (van Vliet and Kloek (1997)).

Furthermore, the type of interaction between the particles can influence the scaling exponent. Non-sintered bonds will be much more flexible than sintered bonds. For a constant dimensionality, more flexible bonds will lead to higher scaling exponents, since the numerator in the exponent μ will be higher. For higher initial supersaturations, the growing crystal surface will probably show more defects, which will promote sintering of crystals. This can probably explain the lower scaling exponents obtained at higher initial supersaturations.

Besides the fractal dimensionality, the scaling behaviour of G' versus ϕ_0 also gives some information about the interaction between the crystals. This interaction term A is given in Table 6-2 and plotted in Figure 6-12. Up to supersaturations of 3.75, A seems to be independent of supersaturation. At a supersaturation of 4, A is, like the scaling exponent μ, markedly lower. If the interaction between the crystals would be van der Waals attraction and the crystals are non deformable, A is expected to increase with increasing supersaturation as the average crystal size decreases with increasing supersaturation. Therefore, it is expected that the crystals are sintered due to simultaneous crystallization and recrystallization or that deformable (thin or long) crystals are kept together by van der Waals attraction. Due to the nature of the fats used, sintering seems most likely.

Figure 6-13 shows storage moduli of HP/SF dispersion that had all crystallized in tubes at a temperature of 20 °C for 20 hours. This means that all dispersions were supersaturated in the α polymorph at various initial supersaturation, and that a polymorphic transition from α to β'/β must have occurred. The elastic moduli were measured using a roughened parallel plate geometry, directly after spreading the sample on the bottom plate with a spatula, as well as 1 hour after this mechanical treatment. The mechanical treatment will break sintered bonds. Scaling exponents of 4.25 and 4.50 and intercepts of $10^{8.03}$ and $10^{8.55}$ were obtained with excellent correlation ($r^2 >$ 0.9998). This is remarkable, as due to the isothermal crystallization process, the initial supersaturation in the α polymorph is different for each dispersion. The scaling exponents are comparable to those obtained for dispersions crystallized in the β' polymorph at high supersaturations (Table 6-2). The increase of the exponent during keeping indicates that some reformation and rearrangement of the broken bonds take place. The increase of the intercept may have been caused by sintering due to Ostwald ripening: due the mechanical treatment, the broken crystals will locally have high radii of curvature. These regions will dissolve and the triglycerides

will recrystallize, forming solid bridges between the crystals.

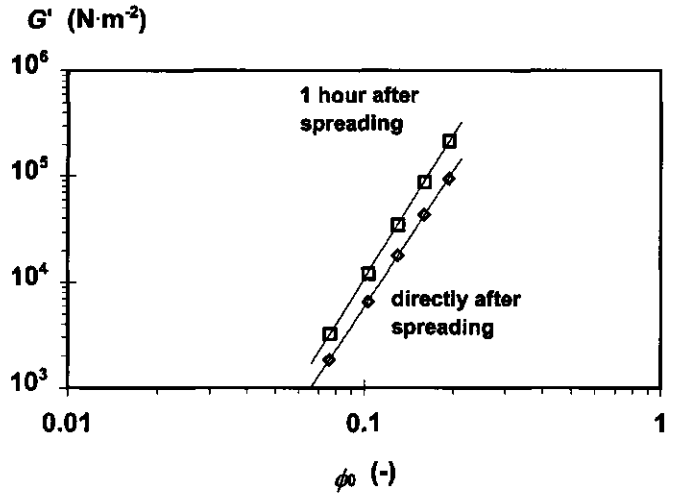

Figure 6-13. *Storage moduli of HP/SF dispersion crystallized in the α polymorph at 20 °C as a function of the fraction HP*

Papenhuijzen measured storage moduli of tristearate in olive oil crystallized in the α polymorph. Storage moduli scaled with the volume fraction tristearate with an exponent of 4.1 and the intercept was $10^{8.0}$. Again the exponent is comparable to that of HP/SF dispersions crystallized at high supersaturations, indicating there is no big difference in the spatial distribution of the solid fat. As the tristearate used was rather pure, sintering of the crystals is not likely and therefore van der Waals attraction is expected to dominate the interaction term. This is consistent with the relatively low intercept. Vreeker analysed the data of Papenhuijzen in the framework of a fractal network model and calculated a fractal dimensionality of 1.95, assuming the crystal aggregates to be arranged in a backbone with a fractal geometry ($x = 4.3$). This analysis may be questioned, because the crystallization and aggregation processes were not separated. In our opinion, it is more likely that the apparent fractal dimensionality will be higher due to formation of crystal aggregates in the pores of a primary network of low dimensionality.

To obtain further information about the structure of the primary network, the dispersions were subjected to a temperature sweep while measuring the storage modulus. As the temperature increases, the solubility of HP in the oil phase increases. The HP that will dissolve first is situated at the boundaries of the crystals. This is presumably the HP containing triglycerides with low melting temperatures and enthalpies. At temperatures at which not many solids are left, the structure of the network may approximate the structure of the original primary network. The storage modulus at temperature T relative to the storage modulus at the starting temperature T_{ref} would then roughly be:

$$\frac{G'(T)}{G'(T_{ref})} = \left(\frac{A_T}{A_{ref}} \cdot (\phi_0 - x_{HP}) \right)^{\mu} \qquad (6\text{-}30)$$

where A_T and A_{ref} are the interaction terms at temperatures T and T_{ref}, respectively, and x_{HP} is the mole fraction of HP soluble given by Equation 6-24. The volume fraction is assumed to be equal to the mole fraction.

The melting curves of dispersions crystallized in the β' polymorph in Figure 6-14 show two regimes. First there is a rapid decrease of the modulus that is associated with the melting of secondary crystallized fat and the becoming thinner of the crystal chains. This is probably related to the change in ratio of the interaction terms. The second part of the melting curve has about the shape of the theoretical curve, also given in Figure 6-14. This part could be associated with the melting of the primary network of low dimensionality. The primary network will only be obtained at low volume fractions solid, *i.e.* rather high temperatures. The storage moduli were correlated with the volume fractions solid at a temperature of 42 °C. At this temperature roughly 5.8 % HP is soluble so that the dispersions studied still contain about 2.2 to 8.2 % solids. Table 6-4 shows that at the supersaturations studied, small values for μ were obtained as compared to those given in Table 6-2, with fairly good correlation coefficients.

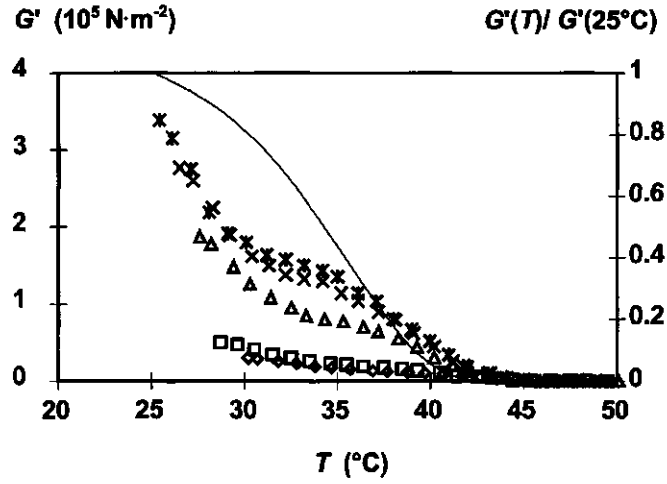

Figure 6-14. *Storage moduli of 10 % HP/SF dispersions crystallized at various initial supersaturations as a function of temperature. Supersaturation: ∗:4.00, ×:3.75, Δ:3.50, □:3.25, ◊:3.00. Also the relative modulus (solid line) as function of temperature calculated by Equation 6-30 is given, assuming a real fractal network with scaling exponent μ = 6, A_T/A_{ref} =1 and T_{ref}=25 °C.*

Small values of μ correspond to low fractal dimensionalities. If it is assumed that the fractal dimensionality of the primary network is 1.75, the numerator x in the expression for μ would equal 4, implying that the stress carrying chains can be bent completely. This does not seem irrealistic. Assuming hinged chains ($x = 3$) would yield dimensionalities ranging from 2.0 to 2.2.

The interaction term A is smaller than the interaction term found for the fully crystallized samples. This may be explained by the more flexible crystal chains if the type of interaction would be the same *i.e.* sintered bonds.

Table 6-4. *Scaling exponent μ from correlation of storage moduli G' and volume fraction solid (ϕ_0-x_{HP}) of a partially melted network at T = 42 °C that had crystallized at various supersaturations. The fractal dimensionality D is calculated assuming $\mu = 4/(3-D)$*

$\ln\beta$ (-)	μ (-)	$\log(A)$ (A/ N·m^{-2})	D (-)	r^2 (-)
4.00	3.16	8.6	1.73	0.9989
3.75	3.30	9.1	1.79	0.9934
3.50	3.74	9.4	1.93	0.9964
3.25	3.87	9.4	1.97	0.9760
3.00	3.28	8.6	1.78	0.9772

6.3.3 Permeability

Another method to observe network structure is by determining permeability as function of the volume fraction solid. Bremer (1992) showed that for a fractal network, the permeability coefficient B scales with the volume fraction of particles with an exponent $2/(D-3)$. According to Darcy's law (Equation 6-26), the permeability is proportional to the flow rate Q through the gel divided by the cross section area A_p of the gel. Poiseuille's law states that the flow rate through a cylinder is proportional to R^4. The total pore area in a cross section of a fat scales with R^2 so that the permeability scales with R^2. At the gel point, the aggregate radius is given by $a.\phi_0^{1/(D-3)}$; hence, the permeability is proportional to $a^2.\phi_0^{2/(D-3)}$:

$$B \propto a^2 \cdot \phi_0^{2/(D-3)} \qquad \textbf{(6-31)}$$

Figure 6-15 shows that for 2 hours old, crystallized HP/SF dispersions, there is a power law relationship between the permeability and the fraction HP. The scaling exponents at supersaturations of 2.75 and 3.50 were -6.0 and -6.7 respectively. These negative slopes are quite high and correspond to very high dimensionalities of 2.67 and 2.70, respectively. Bremer reported scaling exponents of -3.05 in the case of sodium caseinate gels and -2.54 for polystyrene particle gels. These slopes correspond to more realistic dimensionalities of 2.34 and 2.21 respectively.

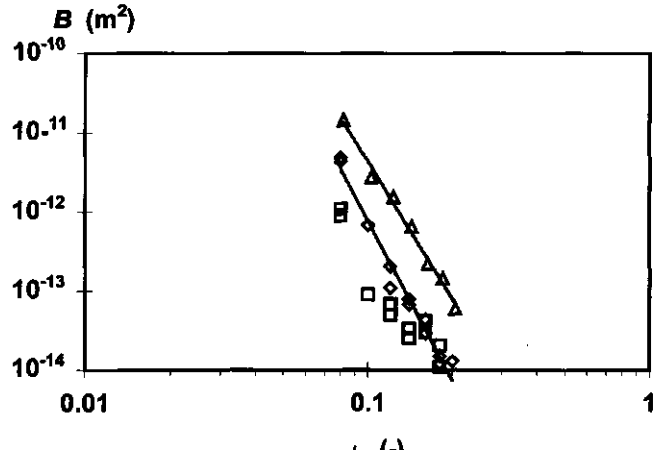

lnβ	slope 2/(D-3)	D
2.75	-6.0	2.67
3.50	-6.7	2.70

Figure 6-15. *Permeability of 2 hours old HP/SF dispersions crystallized at initial supersaturations of 2.75* (Δ) *and 3.50* (◊) *and of 1 day old HP/SF dispersions crystallized at an initial supersaturation of 3.50* (□) *as a function of the fraction solid.*

De Groot *et al.*(1992) determined slopes of about -8 for isothermal crystallized milk fat and commercial fat blends. In these cases, the crystallization rates were lower than in the case of crystallization of HP/SF dispersions. The high negative slopes and thereby high fractal dimensionalities, obtained for crystallized fat dispersions are probably due to the simultaneous crystallization and aggregation. Therefore, Equation 6-29 may be better as an estimate for the apparent dimensionality; it yields $D^* = 2.4$ for $\phi_0 = 0.12$, $D_{gel} = 1.7$ and $\phi_{gel} = 0.01$. This calculated apparent dimensionality is still much smaller than the apparent dimensionality calculated from the permeabilities. Another explanation for the high apparent dimensionality *i.e.* the rapid decrease of permeability on increase of the volume fraction solid fat can be due to the blocking of pores with increase of the fraction solid fat. Blocking of pores, which is more likely at higher volume fraction solid, will lead to lower permeabilities

6.3.4 Interactions between fat crystals

So far, we mainly focused on the geometrical distribution of the fat crystals in space by examining the elastic moduli as a function of the fraction solid. The mechanical properties of fat crystal dispersions are determined by the geometric distribution of the crystals in space and the interaction between the crystals.

Crystals will aggregate due to the attractive van der Waals forces and can sinter due to simultaneous crystallization and aggregation or to recrystallization. Sintering is more likely to occur if the solid phase contains a wide range of triglycerides, since then more crystal defects are formed and more recrystallization can occur. Therefore, we used a second model system, a PSP/SF mixture, that is comparable to the HP/SF system. This system shows the same polymorphic behaviour as the HP/SF system, but the triglyceride distribution is much more restricted. The fat hardly contains any C20 and C22-fatty acid containing triglycerides.

Crystallization of PSP/SF dispersions at a $\ln\beta = 4$ in the β' polymorph, resulted in very large compact crystal clusters with sizes up to 100 μm. This microscopic picture was very different from the HP/SF dispersions, which only showed very small structures. The crystallization rate of the PSP/SF dispersions was also very slow. Similar very small microscopic structures could only be obtained if the PSP/SF dispersions had crystallized in the α polymorph. This indicates that nucleation rates are too slow for the PSP/SF dispersions if crystallized in the β' polymorph. The slower nucleation rates may be due to the more restricted triglyceride distribution of the PSP. Specially the triglycerides containing C20 en C22 fatty acids, which are hardly present in PSP but are present in HP, will have high melting temperatures and high melting enthalpies. At a given temperature the HP/SF dispersions will be supersaturated more than the overall supersaturation and may therefore cause high nucleation rates (Kloek (1998), chapter 4). Furthermore, the crystal growth rate in PSP/SF dispersions will be faster since less crystal defects will be formed that can poison the crystal surface.

To avoid the formation of large compact crystal clusters, HP or glycerol monostearate (GMS) was added to the PSP, to obtain higher nucleation rates in the β' polymorph of these enriched PSP/SF dispersions. Addition of HP to PSP showed a gradual change to smaller structures. Addition of only 1 % GMS to the PSP phase had roughly the same effect as the addition of about 70 % of HP to PSP. GMS has a relative low solubility in the oil and may therefore cause rapid heterogeneous nucleation.

Figure 6-16 shows the storage modulus and phase angle after 1 hour of crystallization of enriched PSP/SF dispersions. It shows that the storage modulus increased and the loss angle decreased on addition of HP to PSP. Addition of GMS to PSP was very effective in obtaining higher storage moduli and lower loss angles. Addition of only 1 % GMS yielded loss angles of about 3°. These small values suggest that even in this situation bonds will be sintered, although the amount of sintering will be less as compared to the HP/SF dispersion which showed loss angles of about 1.5°.

Since it appeared likely that also enriched PSP/SF dispersions showed sintering, it was necessary to use a pure triglyceride. However, crystallization of pure triglycerides in more stable polymorphs than the α polymorph will result in the formation of compact crystal clusters. Therefore it was decided to crystallize all dispersions directly in the α polymorph to obtain high nucleation rates. Tripalmitine (PPP) was used as the pure triglyceride.

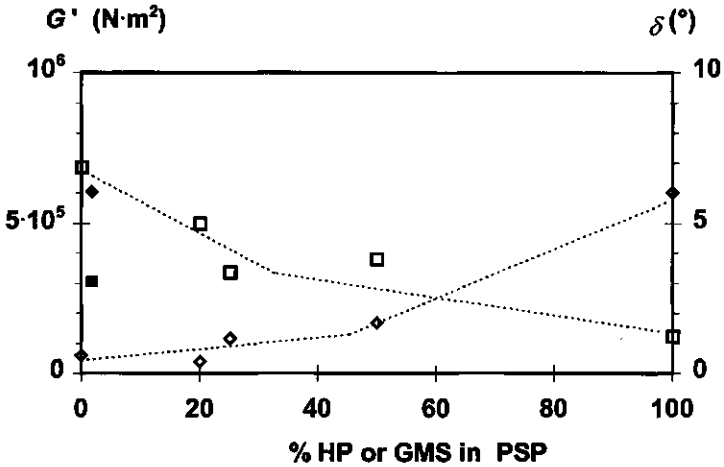

Figure 6-16. *Storage moduli G' (◊) and phase angle δ (□) of crystallized enriched PSP/HP dispersions as function of the percentage additive in PSP. All dispersions had crystallized in the β' polymorph at high* ln*β. The lines are a guide to the eye. Open symbols: HP enriched; closed symbols: GMS enriched.*

All dispersion were crystallized at 10 °C on the lower part of the parallel plate body of the rheometer. At this crystallization temperature it was possible to lower the upper plate of the measuring body to the desired gap size before the sample had completely crystallized. Since the crystallization proceeded rapidly, it was not possible to monitor the crystallization or aggregation kinetics. About 30 minutes after bringing the PPP/SF solution on the plate, the storage modulus was constant in time. To study the type of bonds formed, moduli were also determined after the crystallized dispersion was spread. Spreading will cause sintered bonds to break at certain length scales.

Table 6-5. *Storage moduli G' and loss angles δ at a frequency of 0.1 Hz of crystallized fat dispersions containing 10 % solids. Dispersions had crystallized at 10 °C in rest. Moduli were also determined after spreading and storing for 1 and 20 h.*

dispersion - treatment	G' (0.1 Hz) ($N \cdot m^{-2}$)	δ (°)
10 % HP/SF - at rest	$7.03 \cdot 10^5$	1.22
10 % HP/SF - spread, t = 1 h	$3.87 \cdot 10^4$	5.38
10 % HP/SF - spread, t = 20 h	$1.10 \cdot 10^5$	2.62
10 % PPP/SF - at rest	$3.47 \cdot 10^4$	6.35
10 % PPP/SF - spread, t = 1 h	$2.95 \cdot 10^4$	5.19
10 % PPP/SF - spread, t = 20 h	$3.15 \cdot 10^4$	4.30

Table 6-5 compiles the storage moduli and loss angles of dispersions that had crystallized at rest and of dispersions which had first crystallized and were then allowed to recover for 1 hour and 20 hours after spreading. The non-treated 10 % HP/SF dispersion showed the highest storage modulus and the smallest loss angle. The very small loss angle indicates that the mechanical properties are determined by very elastic bonds that hardly show any relaxation during the time scale of the experiment which was $1/(2\pi f) = 1.6$ s. Because van der Waals bonds can much more easily relax than fixed sintered bonds, sintering of the crystal bonds is very likely in case of HP/SF dispersions.

Spreading of this dispersion led to a decrease of the modulus (work softening) by about 90 % and an increase of the loss tangent. Spreading will lead to partial fracture of the sintered bonds, probably at the length scales of the aggregates. A spread HP/SF dispersion will therefore consist of aggregates that are attracted to each other by van der Waals attraction, while inside the aggregates many of the bonds will probably be sintered. The change from completely sintered to partially sintered can account for the strong decrease of the storage modulus and the increase of the loss tangent. Storing the spread HP/SF dispersion led to an increase of the storage modulus and a decrease of the loss angle. The increase of the storage modulus would be due to recovery of the sintered bonds between the aggregates. Sintering may occur because of recrystallization of compound crystals or recrystallization of crystal regions that have small radii of curvature due to brittle fracture of crystal bonds. These regions have high local solubilities and can therefore enhance sintering of crystals. The storage modulus was not completely recovered compared to dispersions that had crystallized at rest. This can be due to incomplete recrystallization or due to rearrangement of aggregates by the spreading. Rearrangements will lead to a changed geometric distribution of the fat crystals and aggregates. Sintering after spreading can also explain the decrease of the loss angle.

The storage modulus of a non-treated PPP/SF dispersion was much smaller than the storage modulus of a non-treated HP/SF dispersion. This may be due to a larger average crystal size or a weaker interaction between the crystals. Since the average fatty acid length of triglycerides in PPP is shorter than in HP, implying a lower melting temperature and melting enthalpy and therefore a lower initial supersaturation during crystallization and less secondary nucleation, it is expected that the crystal size in the PPP/SF dispersions is somewhat larger. This can lead to lower storage moduli. Since PPP is a relatively pure triglyceride, the extent of sintering in PPP/SF dispersions is expected to be much less. This would also lead to lower storage moduli for PPP/SF dispersions compared to HP/SF dispersions, assuming that van der Waals forces are weaker than the force needed to bend the crystals. The much higher loss angle for PPP/SF dispersions suggests that these dispersions have no or far fewer sintered bonds. Both storage modulus and loss angle of a non-treated PPP/SF dispersion are comparable to the numbers for a spread HP/SF dispersion. Spreading of a crystallized PPP/SF dispersion led to a work softening of 15 % after a storing time of 1 hour, which is much less than the work softening of HP/SF dispersions after the same storing time. This much lower work softening is explained by the smaller number of sintered bonds that are fractured on spreading.

It is remarkable that the loss angle decreased on spreading, although it should be kept in mind that the moduli were determined after one hour after spreading. In this time, broken van der Waals bonds will be recovered for the most part. If the contribution by sintered bonds in non-treated PPP/SF dispersions is very small compared to the contribution by van der Waals bonds, the latter can rearrange during storage and the dispersion becomes more elastic.

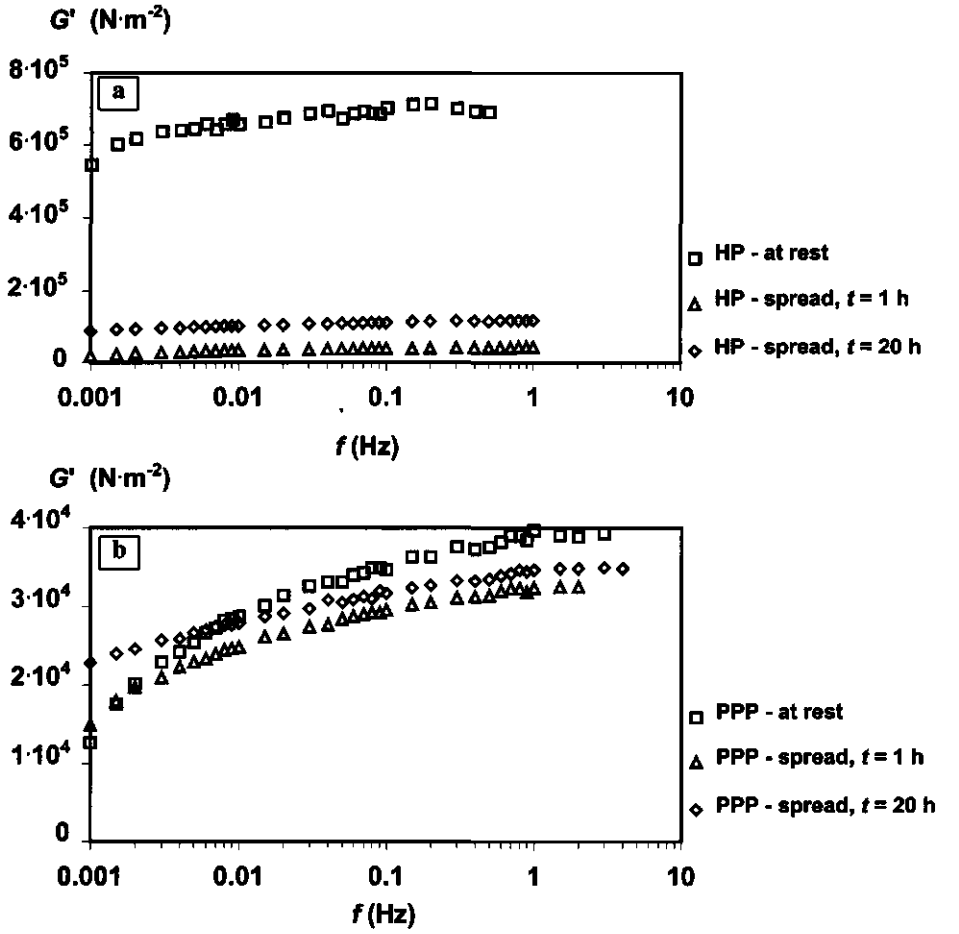

Figure 6-17. *Storage modulus G' as a function of frequency f for 10 % HP/SF dispersions (a) and 10 % PPP/SF dispersions (b) crystallized at 10* °C, *directly after crystallization, 1* h *after spreading and 20* h *after spreading.*

Storing the spread PPP/SF dispersions resulted in an increase of the storage modulus and a further decrease of the loss angle. It seems that the storage modulus almost fully recovers. It is not

clear whether this is the result of rearrangements of crystals or aggregates or the result of some sintering.

The above discussion was limited to the relaxation behaviour of crystallized fat dispersions at a time scale of about 1.6 s since the measurements were carried out at a frequency of 0.1 Hz. The time scale of relaxation of interparticle bonds depends on the type of interaction and on the size of the relaxing structures. Bonds with a high energy content will relax at lower frequencies than bonds with lower energy content. To study the relaxation behaviour at a range of time scales, frequency spectra of the various dispersions were determined.

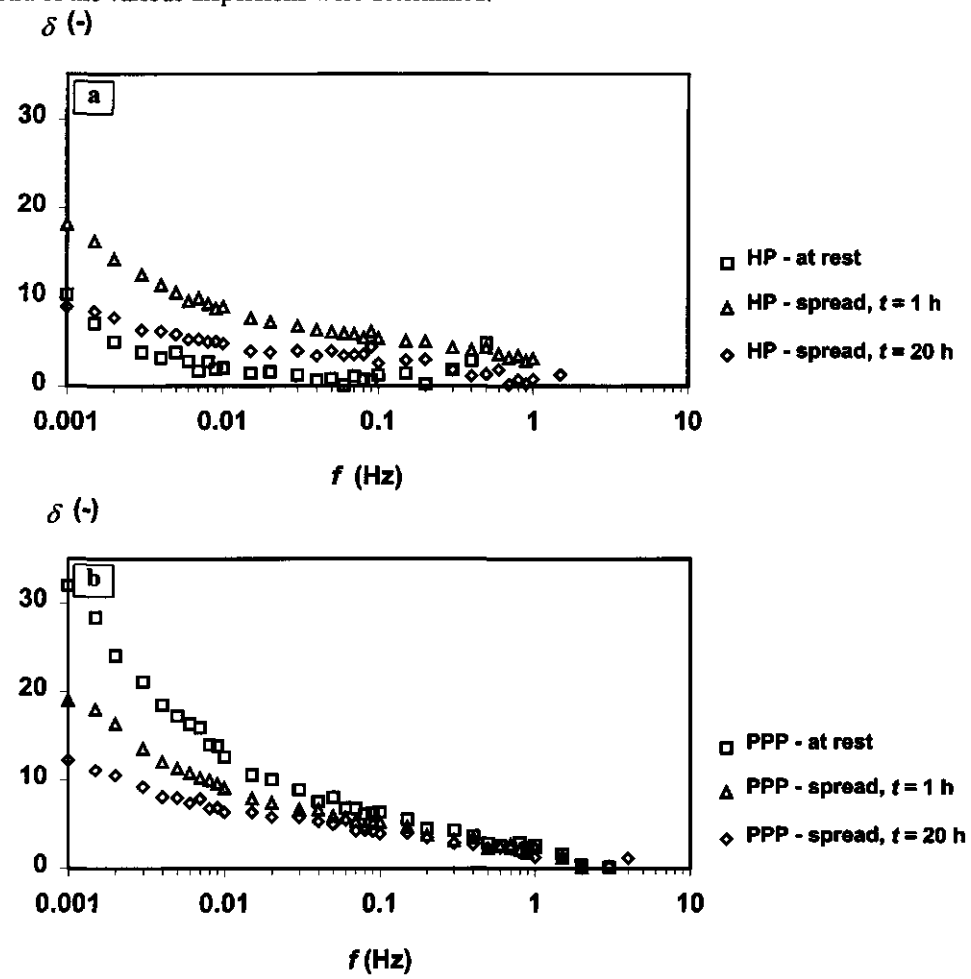

Figure 6-18. *Loss angle δ as a function of frequency f for 10 % HP/SF dispersions (a) and 10 % PPP/SF dispersions (b) crystallized at 10* °C, *directly after crystallization, 1* h *after spreading and 20* h *after spreading.*

Figure 6-17 and 6-18 show the frequency spectra of the storage modulus and the phase angle. Spreading of HP/SF dispersions caused a decrease of the storage modulus over the whole frequency range. Storing the spread dispersions caused an increase of the modulus over the whole frequency range. The loss angle of non-treated HP/SF dispersions indicates that the dispersions were very elastic at frequencies higher than 0.01 Hz. At lower frequencies, the relaxation behaviour was more time dependent, as can be seen from the greater loss angles. This means that non-treated HP/SF dispersions show some relaxation over long time scales. This may be relaxation of van der Waals bonds at a length scale of the aggregate size.

Spreading the HP/SF dispersions led to an increase of the loss angle over the whole frequency range. The increase of the loss angle was somewhat larger at low frequency, which may be explained by the stronger structure breakdown at larger length scales. After storing the spread dispersion for 20 hours, the loss angle decreased over the whole frequency range but most at low frequency. Again, this indicates that most of the changes occur on the level of the aggregates.

The storage moduli were much more frequency dependent for non-treated PPP/SF dispersions than for the non-treated HP/SF dispersion. This was also the case for the dependency of the loss angle on frequency: the loss angle decreased with increasing frequency. It did not show a loss angle plateau as the non-treated HP/SF dispersions did. This may be explained by van der Waals attraction between structures having a very wide range of length scales. It is likely that van der Waals attraction is dominant between aggregates, and also between crystals. Directly after spreading the storage modulus was roughly constant at low frequencies but lower at higher frequencies.

After spreading, the loss angle decreased most strongly at low frequencies and only a little at higher frequencies. After storing the spread PPP/SF dispersions for 20 hours, the storage modulus had increased over the whole frequency range while the greatest decrease of the loss angle occurred at low frequencies. This suggests that bonds with high-energy contents rearrange while hardly any rearrangements occur to bonds with a lower energy content. The bonds with high energy content may be associated with van der Waals bonds between crystal aggregates while lower energy contents may be associated with van de Waals bonds between crystals located in the centre of aggregates

The frequency spectra can also be interpreted in a more quantitative way by fitting them, assuming a certain type of relaxation spectrum. The relaxation spectrum gives the relaxation strength $H(\tau)$ as a function of relaxation time. $H(\tau)$ is a measure for the contribution of relaxation of bonds of relaxation time τ to the overall relaxation. If the relaxation spectrum is known it is possible to calculate the frequency spectra, and vice versa.

For an infinite array of Maxwell elements, the dynamic moduli can be written as a function of $H(\tau)$ and the angular velocity $\omega = 2\pi \cdot f$ (Ferry (1969); Whorlow (1980)):

$$G'(\omega) = G_e + \int_{-\infty}^{\infty} H(\tau) \cdot \frac{\omega^2 \cdot \tau^2}{1+\omega^2 \cdot \tau^2} \mathrm{d}\ln\tau$$
$$G''(\omega) = \int_{-\infty}^{\infty} H(\tau) \cdot \frac{\omega \cdot \tau}{1+\omega^2 \cdot \tau^2} \mathrm{d}\ln\tau \qquad \textbf{(6-32)}$$

where $\tau = 1/\omega$. G_e is the contribution of the permanent bonds to the elasticity modulus, or in experimental cases the contribution of the bonds that do not relax at time scales longer than corresponding to the lowest frequency. It is assumed that the relaxation spectrum is normally distributed around $\ln\tau$ with a width of $\sigma_{\ln\tau}$:

$$H(\ln\tau) = A_0 \cdot \frac{1}{\sigma_{\ln\tau} \cdot \sqrt{2\pi}} \cdot \exp\left(\frac{-0.5 \cdot (\ln\bar{\tau} - \ln\tau)^2}{\sigma_{\ln\tau}^2}\right) \qquad \textbf{(6-33)}$$

A property of this function is that integration between $-\infty < \ln\tau < \infty$ yields A_0 as result. The frequency spectra were fitted to 6-32 and 6-33 using A_0, G_e, $\ln\tau$ and $\sigma_{\ln\tau}$ as fit parameters. The sum of A_0 and G_e equals the storage modulus at high frequencies. In the fat systems, the permanent modulus G_e may be a measure of the contribution of sintered bonds to the storage modulus. Table 6-6 shows the fit results for the various dispersions and the fits are plotted in Figure 6-19.

Table 6-6. *Parameters obtained from the fit of frequency spectra of crystallized fat dispersions by Equations 6-32 and 6-33.*

dispersion	A_0 ($N \cdot m^{-2}$)	τ (s)	$\sigma_{\ln\tau}$ (s)	G_e ($N \cdot m^{-2}$)
HP - at rest	$3.8 \cdot 10^5$	497	0.40	$3.1 \cdot 10^5$
HP - spread, $t = 0$	$4.0 \cdot 10^4$	103	0.023	$5.6 \cdot 10^3$
HP - spread, $t = 20$ h	$7.0 \cdot 10^4$	241	0.088	$4.8 \cdot 10^4$
PPP - at rest	$4.5 \cdot 10^4$	106	0.042	$-3.6 \cdot 10^3$
PPP - spread, $t = 0$	$2.7 \cdot 10^4$	78	0.040	$6.7 \cdot 10^3$
PPP - spread, $t = 20$ h	$3.0 \cdot 10^4$	236	0.019	$6.2 \cdot 10^3$

Figure 6-19 shows that the frequency spectra are described reasonably well by assuming a log-normal distribution of the relaxation strengths. The distributions are rather wide. The fit is poor for the loss modulus of the non-treated HP/SF dispersion at high frequencies, but this is due to the lack of accurate data points at these frequencies. Since crystallized fat dispersions have van der Waals bonds and sintered bonds, it was also tried to fit the frequency spectra with a bimodal distribution function of relaxation times, where one peak would correspond to the van der Waals attraction and the other to the sintered bonds. However, it was not possible to adjust the different fit

parameters independently to obtain the best fit due to the high number of fit parameters. Therefore, it was assumed that the relaxation spectrum could be described by only one type of bond with a wide distribution.

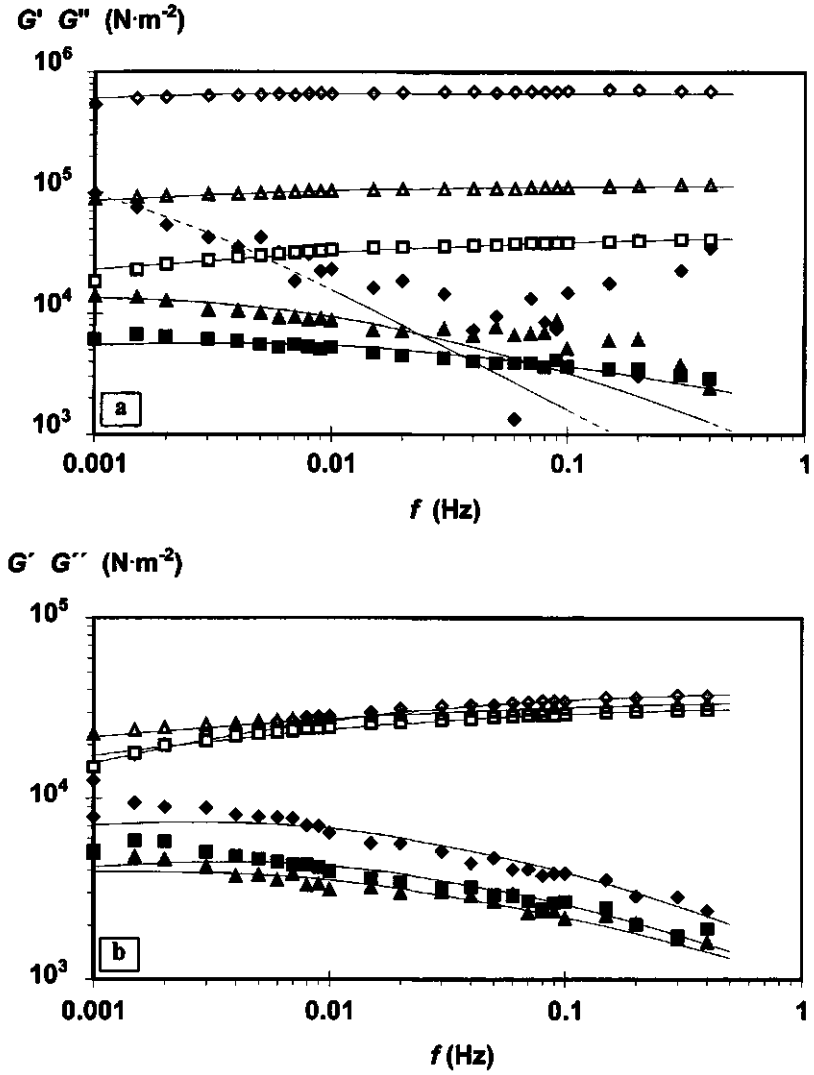

Figure 6-19. *Measured (symbols) and fitted (lines) frequency spectra of crystallized HP/SF dispersions (a) and PPP/SF dispersions (b). G' : open symbols, G'': filled symbols.* ◊: at *rest*, □: *spread, t = 1* h, Δ: *spread, t = 20* h

The average relaxation times show that on spreading the fat dispersions, the relaxation time decreases compared to the non-treated dispersions. Storing the treated dispersions led to an increase

of the relaxation time. The relaxation times of the HP/SF dispersions were higher than the relaxation times of the PPP/SF dispersions. All these results are consistent with a more sintered character of the HP/SF dispersions and much less sintering in PPP/SF dispersions.

The permanent modulus G_e, which will be a measure for the amount of sintered bonds (very long relaxation times) since integration is performed using a lower boundary of $\tau = 10^{-7}$ s, is very high for the non-treated HP/SF dispersions. The decrease of G' on spreading for this dispersion is very strong and considerable recovery occurs after storing the treated sample. This agrees with the occurrence of many sintered bonds that are broken due to spreading, but that partially recover while storing the treated sample.

The permanent modulus of PPP/SF dispersions changes much less and is much lower. The negative value of the PPP/SF dispersion crystallized in rest must be due to the inaccuracy of the fit.

6.4 Conclusions

Interpretation of the mechanical properties of HP/SF dispersions crystallized at rest is hampered by the simultaneousness of crystallization and aggregation. During the initial part of the crystallization process (say the first one or two percent solids), fat crystals already flocculate to form a space filling network. The properties of this primary network can be described by a fractal approach.

Correlating storage moduli with the volume fraction of solid HP in partially melted HP/SF dispersions, assuming completely bendable stress carrying, chains yielded small fractal dimensionalities of 1.7 -1.9. This is consistent with the results obtained for the aggregation of dilute HP/SF dispersions.

Continuous crystallization after formation of the primary network would cause deposition of crystals into the pores of this network and possibly preferentially to the strands of the primary network. The storage moduli of completely crystallized dispersion can be fitted to fractal models, but because crystallization and densification of the primary network proceed simultaneously, this would yield apparent dimensionalities. Assuming that the strands between the aggregates can bend completely, the apparent dimensionality of dispersions crystallized at low supersaturations ($\ln\beta \leq 3.75$) in the β' polymorph would be 2.33, and 2.0 for dispersions crystallized at high supersaturations in the β' polymorph ($\ln\beta > 3.75$). Storage moduli of dispersions crystallized in the α polymorph at 20 °C yield apparent dimensionalities of about 2.1, irrespective of the supersaturation. The lower apparent dimensionalities of dispersions crystallized at high supersaturations may be explained by the shorter time scales of crystallization, leading to a higher volume fraction of solids at which a gel is formed. This also holds for crystallization in the α polymorph.

Due to the simultaneousness of crystallization and aggregation and the wide range of triglycerides that are present in HP, the crystals are sintered when crystallization is finished. This

means that crystals will bend on deformation of the gel rather than separate from each other. The interaction term, which is a measure for the attractive force between crystals and is the proportionality constant in the power-law scaling relation between the storage modulus and the volume fraction of solids, was about constant for dispersions crystallized at supersaturations in the β' polymorph between 2.75 and 3.75. For a supersaturation of 4.0 in the β' polymorph or for supersaturation in the α polymorph, the interaction term decreased, but was still higher than measured for dispersions in which no sintering was expected. Interaction terms obtained from measurements on partially melted dispersions (T = 42 °C) were about the same as found for dispersions crystallized at high supersaturations. The interaction term may be associated with the length/thickness ratio of the crystals. If crystals are thinner, whether due to melting or to the higher number concentration crystals, it must be easier to bend the crystals.

Permeability as a function of the fraction solid can be described well with a power-law relation. Assuming simple fractal aggregation yields very high dimensionalities of 2.67 to 2.70, according to the model chosen. These high dimensionalities may be partially explained by compaction after formation of the primary network, which occurs at a low volume fraction solid. Blocking of the pores, that is more likely to occur at high volume fraction of solids, leads to smaller permeabilities and can therefore also account for the high apparent dimensionalities.

Frequency spectra of dispersions crystallized in rest indicate that HP/SF dispersions have many sintered crystal bonds, whereas the bonds in PPP/SF dispersions are much less sintered. Moduli of HP/SF dispersions are much higher than those of PPP/SF dispersions. The decrease of the modulus on mechanical treatment (work softening), measured after 1 h working, is much stronger for the sintered dispersion, which indicates that sintered bonds are much stronger than van der Waals bonds. Mechanical treatment of sintered dispersions is followed by much stronger recovery of the storage modulus than was found for mechanically treated less sintered dispersions. This would be due to resintering, possibly caused by Ostwald ripening (after short times) and recrystallization (after longer times). It is likely that the propensity of a fat to exhibit sintering is inversely related to the "purity" of the triglyceride in the solid phase.

6.5 References

Avrami, M. (1939 *a*), Kinetics of Phase Change. I- General Theory, *J. Chem. Physics* **7**, 1103

Avrami, M. (1939 *b*), Kinetics of Phase Change. II- Transformations - time relations for random distribution of nuclei, *J. Chem. Physics* **8**, 212

Bos, M.T.A. (1997) *The structure of particle gels as studied with confocal microscopy and computer simulations*, Ph.D. Thesis, Wageningen Agricultural University, the Netherlands

Bremer, L.G.B. (1992) *Fractal aggregation in relation to formation and properties of particle gels*, Ph.D. Thesis, Agricultural University Wageningen, the Netherlands

Bremer, L.G.B., Bijsterbosch, B.H., Schrijvers, R., Vliet, van T and Walstra, P. (1990) On the fractal nature of the structure of acid casein gels, *Colloids and Surfaces* **15**, 159

Bremer, L.G.B., Vliet, van T. and Walstra, P. (1989) Theoretical and experimental study of the fractal nature of the structure of casein gels, *J. Chem. Soc. Faraday Trans I* **85**, 3359

Brown, W.D. and Ball, R.C. (1985) Computed simulation of chemically limited aggregation, *J. Phys. A* **18**, L517

Dijk, H. van and Walstra, P. (1986) Syneresis of curd I: One dimensional syneresis of rennet curd in constant condition, *Neth. Milk Dairy J.* **40**, 3

Family, F. and Landau, D.P. (1984) *Kinetics of aggregation and gelation*, Elsevier, Amsterdam/New York

Ferry, J.D. (1969) *Viscoelastic properties of polymers*, John Wiley & Sons

Groot-Mostert, de A. (1992) *internal report*

Hannewijk, J. (1964) Kristallisatie van vetten I, *Chemisch Weekblad* **60**, 309. (in dutch).

Johansson, D. (1994) *Colloids in fats: the fat crystal as a functional particle*, Ph.D. Thesis, Lund University, Sweden.

Johansson, D. and Bergenståhl, B. (1992[a]) The influence of food emulsifiers on fat and sugar dispersions in oils. I. Adsorption, Sedimentation, *J. Am. Oil Chem. Soc* **69**, 705

Johansson, D. and Bergenståhl, B. (1992[b]) The influence of food emulsifiers on fat and sugar dispersions in oils. II. Rheology, Colloidal forces, *J. Am. Oil Chem. Soc* **69**, 718

Johansson, D. and Bergenståhl, B. (1992[c]) The influence of food emulsifiers on fat and sugar dispersions in oils. III. Water content, Purity of oils, *J. Am. Oil Chem. Soc* **69**, 728

Kamphuis, H. (1984) *The rheological behaviour of structured dispersions*, PhD Thesis Technical University Twente, the Netherlands

Kloek, W. (1998) *Mechanical properties of fats in relation to their crystallization*, PhD thesis, Wageningen Agricultural University, the Netherlands

Kloek, W. and Vliet, T. van, Structure of fat crystal aggregates, *Proc. XIIth Int. Congr. on Rheology*, 1996, Eds: A. Ait-Kadi, J.M. Dealy, D.F. James and M.C. Williams, Laval University, Quebec, pg.791

Meakin, P. (1988) Fractal aggregates, *Adv. Colloid Interface Sci.* **28**, 249

Meeussen, W.(1995) personal communication

Nederveen, C.J. (1963) Dynamical mechanical behaviour of suspensions of fat particles in oil, *J. Colloid Sci.* **18**, 276

Papenhuijzen, J.M.P. (1972) The role of particle interaction in the rheology of dispersed systems, *Rheol. Acta* **11**, 73

Roark, R.J. (1985) *Formulas for stress and strain, 6th Ed.*, McGraw

Smoluchowski von, M. (1917) Versuch einer mathematischen Theorie der Kogulationskinetik kolloider Lösungen, *Z. Physik. Chem.* **92**, 129

Tempel, van den M. (1961) Mechanical properties of plastic-disperse systems at very small deformations, *J. Colloid. Sci* **16**, 284

Tempel, van den M. (1979) Rheology of concentrated dispersions, *J. Coll. Interface Sci.* **71**, 18

Vliet, T. van and Kloek, W. (1997) Rheology of gels and suspensions containing fractal aggregates: perspectives and limitations, *Proc. 1st Int. Symp. on Food Rheology and Structure*

Vliet, T. van and Walstra, P.(1985) Note on the shear modulus of rennet-induced milk gels, *Neth. Milk Dairy J.* **39**, 115

Vreeker, R., Hoekstra, L.L., Boer, den D.C. and Agterof, W.G.M. (1992) The fractal nature of fat crystal networks , *Colloids Surf.* **65**, 185

Walstra, P., Vliet, van T., Kloek, W. (1995) Crystallization and rheological properties of milk fat, In *Advanced Dairy Chemistry Vol. 2; Lipids* 2nd *ed.*, Ed. P.F. Fox, Chapman & Hal, London, pg.179.

Wesdorp, L.H. (1990) *Liquid - multiple solid phase equilibria in fats - theory and experiments*, Ph.D. Thesis, Technical University Delft, the Netherlands

Whorlow, R.W. (1980) *Rheological Techniques*, Ellis Horwood Ltd.

Chapter 7

Large Deformation Behaviour of Fat Crystal Networks

7.1 Introduction

7.1.1 General

The large deformation behaviour of solid and semi-solid food products is an important quality characteristic, yielding information about properties that are relevant to processing, handling and eating. For fat continuous products like margarine, shortenings, spreads and butter, forces needed for cutting and spreadability are especially important.

Most solid food products consist of a large number of different structural elements that interact with each other by different type of bonds of various energy contents. All these bonds have different relaxation times, resulting in a broad relaxation spectrum. This explains the visco-elastic behaviour of food products. By measuring the rheological behaviour at very small deformations as a function of the time scale of deformation, so that the overall structure is not affected, information can be obtained about the geometrical arrangement of the structural elements and the interparticle interaction forces. During these small deformation experiments, part of the bonds may due to thermal motions break and reform, which may result in relaxation of (applied) stresses and flow.

When large deformations are applied to food products, the initial structure is mostly irreversibly changed. This is due to breaking of bonds and rearrangements between structural elements. An example is the work softening occurring when working margarine. Margarine consists of a continuous fat crystal network in which the crystals are partially sintered (Haighton (1965); Walstra *et al.*(1995); Kloek (1997)). When the margarine is subjected to large deformations, part of the solid bonds are broken and the storage modulus decreases. After that, the modulus increases slowly in time. Due to such treatment the product consistency changes from brittle, primarily due the solid bonds, to spreadable, primarily due to the weaker van der Waals forces.

In this chapter the large deformation behaviour of fat crystal networks is discussed with special attention to fracture mechanics.

7.1.2 Fracture mechanics

There is no general definition for fracture. Fracture can be considered to occur if all bonds between structural elements in macroscopic planes break, resulting in a degradation of the structure of the product over length scales much larger than the size of the structural elements and in falling apart of the product (van Vliet and Luyten (1995)). Characteristics of fracture are:

1. All bonds between the structural elements in a macroscopic plane are broken within a relevant time scale.
2. Visual changes in structure over relative long distances like the formation of cracks.
3. Falling apart of the material into smaller pieces or lumps

All of these changes have to occur for fracture. For flow, only change 1 is needed. If only 1 and 2 occur, the material yields.

Fracture mechanics assume that fracture initiates at a defect or inhomogeneity, constituting a "weak spot" in the material. These defects or inhomogeneities can be considered as initial cracks.

There are two prerequisites for growth of an initial crack. First, the stress near the tip of the crack or inhomogeneity should exceed a critical value which corresponds to the counteracting stress due to the interaction forces between the structural elements. Second, the differential energy released in the material due to stress relaxation near the tip on crack growth is larger than the differential energy needed for creation of new surface.

Fracture initiation

The stress distribution in a deformed material depends on the arrangement of structural elements and the interaction forces between them. At places where the structure is most inhomogeneous, stress concentration is greatest, and fracture will probably start at such places. Inhomogeneities in fat dispersions can be fat crystals, fat crystal aggregates or the pores in a fat crystal network. Interactions that should be overcome for fracture to occur are those due to van der Waals-attraction between crystal or aggregates and/or the sintered crystal bonds.

Fracture propagation

On deformation of a linear elastic material with elasticity modulus E, an amount of energy W' is elastically stored that is given by:

$$W' = \int_0 \sigma \, d\varepsilon = \tfrac{1}{2} E \cdot \varepsilon^2 \qquad \textbf{(7-1)}$$

where σ is the stress and ε the strain. The stored energy can be used for formation of new surfaces.

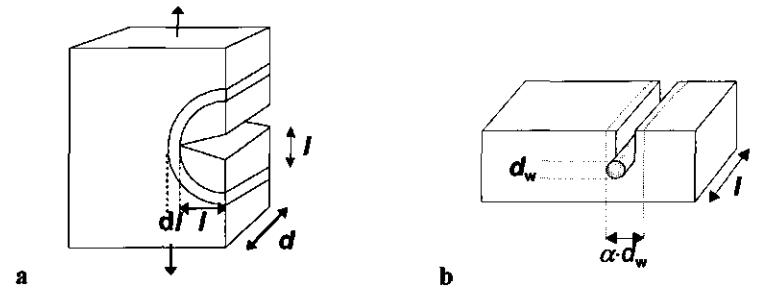

Figure 7-1. ***a:*** *Test piece that is subject to an uni-axial tensile stress, showing strain energy relaxation due to growth of a crack over a distance* dl. ***b:*** *Schematic representation of a wire cutting set-up*

Assuming the geometry drawn in Figure 7-1a, the volume in which the stress relaxes would be proportional to $l^2 \cdot d$ where d is the width and l the length of the crack. The energy needed to

create new surface is proportional to $l \cdot d \cdot R_s$ where R_s is the specific fracture energy. A crack will grow spontaneously over a length dl if the amount of energy released is larger than the amount of energy needed for the creation of the new surface (Luyten (1988)):

$$\tfrac{1}{2} \cdot \pi \cdot d \cdot \left[(l + \mathrm{d}l)^2 - l^2 \right] \cdot W' \geq R_s \cdot d \cdot \mathrm{d}l \tag{7-2}$$

This condition is fulfilled if half the crack length is equal to or greater than a critical length l_c, which is found by neglecting $(\mathrm{d}l)^2$ compared to l and $2 \cdot l \cdot \mathrm{d}l$:

$$l_c = \frac{R_s}{\pi \cdot W'} \tag{7-3}$$

The amount of stored energy W' in a elastic material can be measured relative simply in a compression test in which the compressive stress is measured as function of strain. W' is then obtained by integrating the stress over strain from 0 to the fracture strain ε_f. The specific fracture energy can be obtained from wire cutting experiments in which a controlled amount of surface can be created while measuring the cutting force F_c. Dependent on the diameter of the wire also some energy dissipation of amount W'' due to flow can occur. Therefore the determined specific fracture energy R_s should be extrapolated to wire diameter $d_w = 0$:

$$\frac{F_c}{l} = R_s + (W' + W'') \cdot \alpha \cdot d_w \tag{7-4}$$

where α is a proportionality constant that is related to the width of the disturbed region (Figure 7-1b).

For viscoelastic materials always some energy dissipation takes place due to viscous flow while for inhomogeneous materials also energy dissipates due to frictional movements between structural elements. The energy dissipation can become important for large strains. As a consequence, integration of the compressive stress-strain curve then gives an overestimate of the amount of elastically stored energy.

The aim of this work is to establish which parameters are important for the large deformation behaviour of fat crystal networks and to assign some values to them. This is studied by performing compression experiments and wire cutting experiments, to determine the amount of elastically stored energy and the specific fracture energy, respectively. With these parameters information can be gained about the size of inhomogeneities that can be considered as defects.

7.2 Materials and Methods

7.2.1 Materials

The model system used consists of fully hydrogenated palm oil (HP) in sunflower oil (SF), the first being the solid phase and the latter being the liquid phase. A description of the physical properties and the triglyceride composition of this model system is given in chapter 2 of this thesis.

The solubility of HP in SF is given by the Hildebrand equation (Wesdorp (1990)).

$$\ln x_{HP} = \frac{\Delta H_{f,i}}{R_g}\left(\frac{1}{T_{m,i}} - \frac{1}{T}\right) \tag{7-5}$$

x_{HP} is the mole fraction soluble HP in polymorph i at temperature T, $\Delta H_{f,i}$ the molar enthalpy of fusion of polymorph i, R_g the gas constant and $T_{m,i}$ the absolute melting temperature of polymorph i.

The driving force for crystallization is the chemical potential difference $\Delta\mu$ between a supersaturated solution and a saturated solution:

$$\Delta\mu = R_g T \cdot \ln\frac{c_{HP}}{x_{HP}} = R_g T \cdot \ln\beta \tag{7-6}$$

where c_{HP} is the mole fraction HP, x_{HP} the solubility given by 7-5, β the supersaturation ratio and $\ln\beta$ the supersaturation. When the mole fraction HP is known, the crystallization temperature T can be calculated for every initial supersaturation.

7.2.2 Methods

To obtain samples for compression and cutting experiments, rather big quantities of fat blends had to be crystallized. Since, the crystallization kinetics and therefore the aggregation kinetics are strongly temperature dependent, it was important to have a well-controlled temperature in the crystallization cylinder. Therefore, the crystallization vessel was embedded in a cooling jacket through which thermostatted water was circulated. To obtain temperature homogeneity, a stirrer, rotating at 300 rpm, was placed in the cylinder. The outer part of the stirrer was covered with Teflon so that the cooled wall of the cylinder was scraped to disperse any crystallized material from the wall in the bulk. The stirrer blades were at an angle of about 80° with the wall of the cylinder to obtain better dispersion of the crystallized material.

Prior to crystallization, the fat blends had to be heated to 80 °C for 10 minutes to destroy any crystal memory that could influence the crystallization process. The hot blends were poured in the crystallization cylinder that was precooled and in which the stirrer was rotating. As soon as the blend became turbid and showed considerable thickening the stirrer was removed, the bulk temperature T was measured and the cooling jacket was set at T. The dispersion was kept at T for

one hour to complete crystallization. The water in the double walled jacket was set at such an initial temperature that the resulting T would correspond to a $\ln\beta$ of 4 in the β' polymorph (Equations 7-5 and 7-6).

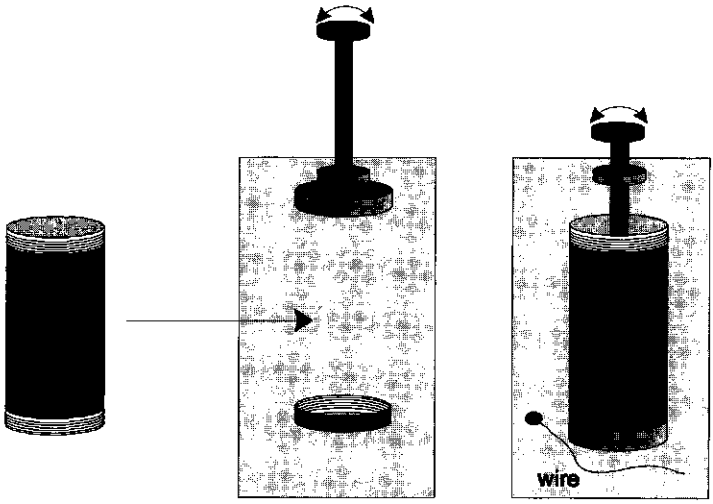

Figure 7-2. *Schematic representation of test piece preparation for compression experiments*

To cut cylindrical test pieces for the compression tests, the crystallization vessel was fixed in a standard by means of a screw thread (Figure 7-2). The sample was pushed out of the cylinder by screwing down the plunger. Every rotation of the screw corresponded to a plunger movement of 1 mm. The part of the sample that was pushed out was cut with a stainless steel wire (0.10 mm diameter) and collected on a piece of parafilm. After cutting the test pieces to be used for compression, they were stored at 20 °C for 20 hours to allow the cutting surface to recover. The top surface of the test piece was also covered with parafilm. The test piece height was approximately 10 mm and measured by a digital gauge meter (Mitutoyo). Compression experiments were performed at 20 °C with a Zwick Material Tester 1425 equipped with a 50 N load cell (resolution 0.001 N). Compression was performed using a perspex compression head having the same diameter as the test piece (30 mm). Parafilm was used to have the same, clean compression surface for every test. The compression speed was 2 mm·min^{-1} in most cases.

For the wire cutting experiments the samples were stored at 20 °C for 20 hours. A wire frame was attached to the Zwick Material Tester. The cylinder with the crystallized fat dispersions was mounted horizontally with the end of the cylinder vertically below the wire frame. The sample was pushed out of the cylinder with the same plunger used for the compression test pieces over a distance of about 20 times the wire diameter. Subsequently the test piece was cut while measuring the required force as a function of cutting distance. No curling of the slices occurred. The friction

force between the wire and the sample was estimated by moving up the wire after cutting off a slice. This friction force could be neglected in all cases. The cutting speed was 20 mm·min^{-1} in all cases.

7.3 Results and Discussion

7.3.1 Compression

7.3.1.1 Calculation of large deformation- and fracture parameters

The force - deformation curves were recalculated to stress-strain curves. The stress σ was calculated by dividing the force F by the contact surface area A:

$$\sigma = \frac{F}{A} \tag{7-7}$$

The Hencky or natural strain ε_h was calculated by:

$$\varepsilon_h = -\ln\frac{h_t}{h_0} \tag{7-8}$$

where h_0 is the initial height of the test piece and h_t the height after a deformation $\Delta h = h_0 - h_t$. The Hencky strain at each moment represents the deformation relative to the actual height of the test piece. The Hencky strain rate $\dot{\varepsilon}_h$ was calculated from the compression speed v using:

$$\dot{\varepsilon}_h = \frac{d\varepsilon_h}{dt} = \frac{v}{h_t} \tag{7-9}$$

Figure 7-3a shows a typical example of a force-deformation curve of a 12 % HP/SF dispersion. The deformation of the test piece over the first 0.2 - 0.3 mm was difficult to determine accurately, due to the non-perfect parallel alignment of the compression plate with the test piece surface and because of local disturbance of the test piece by the wire cutting. At compressions larger than 0.3 mm there was good contact between the test piece and the compression plate.

Figure 7-3b shows the stress-strain curves calculated from the force-deformation curves shown in Figure 7-3a. The stress-strain curve is the starting point for the determination of Young's modulus E, the fracture strain ε_f, the fracture stress σ_f and the apparent uniaxial compression viscosity η_c^*. Young's modulus should be determined in the so-called linear region so that E is independent of deformation:

$$E = \left(\frac{\sigma}{\varepsilon}\right)_{\varepsilon \to 0} \tag{7-10}$$

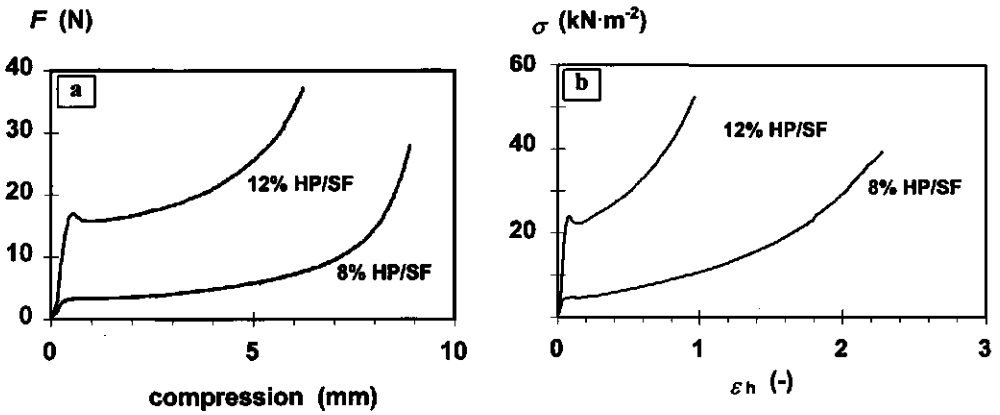

Figure 7-3. *Measured force-deformation (a) and derived stress-strain curves (b) of crystallized HP/SF dispersions. Initial heights are 9.88 and 10.08 mm for 8 and 12 % HP/SF dispersions, respectively.*

By small deformation oscillation experiments it was shown that the linear region of fat dispersions is smaller than a strain of 0.001. This would mean that for initial test piece heights of 10 mm, Young's modulus should be determined at compressions smaller than 10 μm. This is not possible within the given experimental set-up, and only an apparent Young's modulus E^* could be determined. The value of E^* will be smaller than the true E. The true value of E in compression can be calculated from the shear modulus G using the Poisson ratio μ_p that corrects for change of volume (dV/V) on compressive deformations (Ferry (1969)):

$$\mu_p = \frac{1}{2} \cdot \left(1 - \frac{dV}{V d\varepsilon}\right) \tag{7-11}$$

For isotropic, homogeneous materials the values of the shear and Young's moduli are related by (Ferry (1969)):

$$E = 2 \cdot G \cdot (1 + \mu_p) \tag{7-12}$$

If there is no volume change ($dV/V = 0$), $\mu_p = 1/2$ so that $E = 3 \cdot G$.

The measured shear modulus of a 12 % HP/SF dispersion was about $8 \cdot 10^5$ N·m^{-2} (frequency: 0.1 Hz) so that a Young's modulus of about $2.5 \cdot 10^6$ N·m^{-2} would be expected. The determined apparent Young's modulus was about $4 \cdot 10^5$ N·m^{-2} (strain rate: 0.02 s^{-1}) which is about 15 % of the expected value if E would have been determined in the linear region. Although the difference in

time scale may explain a part of the difference, the much lower E will be the result of structure breakdown due to the large deformations applied.

The apparent Young modulus was determined by linear regression in the range of $0.02 < \varepsilon_h < 0.05$ so the regression was not forced through the origin. Correlation coefficients were higher than 0.99 in all cases. Dependent on the shape of the stress-strain curve, the fracture stress was determined in two ways. If the stress-strain curve showed a peak stress, the maximum stress was taken as the fracture stress (Figure 7-4a). The corresponding strain was taken as the fracture strain. These types of stress-strain curves were obtained for dispersions containing 10 % or more solids. The stress-strain curves of dispersions containing less than 10 % solids did not show a peak stress but they exhibited a rather sudden change in the slope of the stress-strain curve. The intersection of the extrapolated straight lines before and after the sudden change was taken as fracture point (Figure 7-4b).

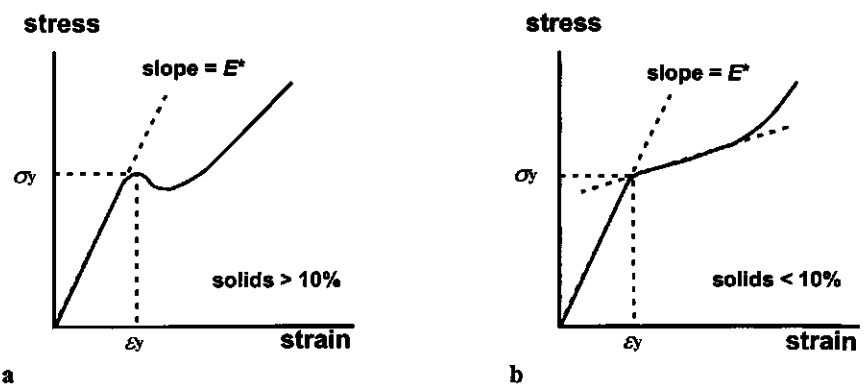

Figure 7-4. *Determination of the fracture or yield point and the apparent Young's modulus E* for different types of stress-strain curves.*

For none of the dispersions studied, the test piece fell apart at fracture, although there was a visual change in structure and formation of cracks. According to the definition of fracture in paragraph 7.1.2, these dispersions would yield rather than fracture. Therefore we will use the terms yield strain (ε_y) and the yield stress (σ_y), rather than fracture strain and stress. Fracture and yielding can occur subsequently, the first at small and the latter at higher deformations.

Whether yielding or fracture occurs will also depend on the fraction of solid fat. On compression, the solid network is deformed and energy is stored in the fat crystal aggregates. If the local stress exceeds a critical value, local fracture of the crystal network will occur. If the energy input near the tip of the crack due to stress relaxation upon crack growth is high enough to create the new surfaces, the crack will propagate. However, since pores around the crystal network are filled with oil, part of the energy near the tip of the crack will dissipate; hence less energy is available for crack propagation. The pores will therefore act like crack stoppers. For a high

proportion of solid fat, less oil is present and less energy is dissipated near the tip of the crack leading to a more brittle appearance.

The formation of macroscopic cracks was most pronounced in dispersions containing more than 10 % solids. It was not possible to study this systematically since the crystallization conditions could not be controlled properly for dispersions containing more than 15 % HP/SF.

7.3.1.2 Effect of fraction solids on parameters obtained from compression

Figure 7-5 shows the apparent Young modulus as a function of the fraction HP. E^* increases with increasing fraction HP. In the range between 6 % HP and 12 % HP the relation can be described well with a power law. The value of E^* for the 15 % HP/SF dispersion deviates from this trend by a factor of 2. This is probably due to the lower initial supersaturation that could be applied during crystallization of this dispersion, because of experimental limitations.

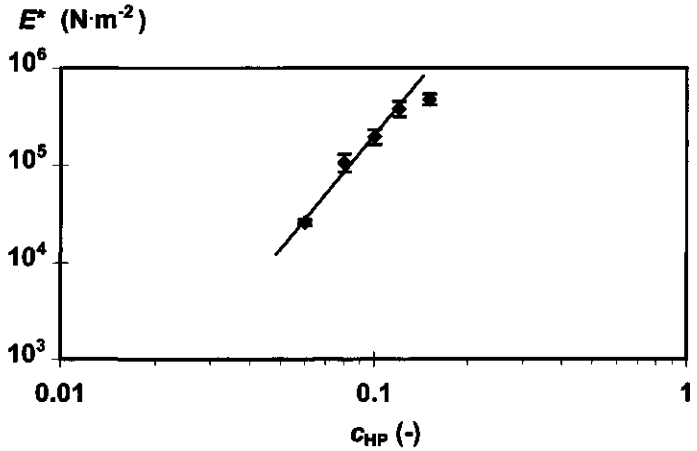

Figure 7-5. *The apparent Young modulus E^* of HP/SF dispersions crystallized at lab scale as a function of the fraction HP. Standard deviations are indicated with vertical error bars. The solid line is the fit according to $E^* = A \cdot c^{\mu}$ excluding the point for 15 % HP/SF.*

If the results for the 15 % HP/SF dispersions are not taken into account, a power-law coefficient μ of 3.82 and an intercept A of $10^{9.1}$ are obtained. This intercept can be interpreted as a measure of the interaction between the particles (it is an extrapolated modulus of a 100 % HP solid). The coefficient does not differ greatly from the coefficient of 4.1 that was found for storage moduli at very small deformations (Kloek (1998), chapter 6). It should be kept in mind that the structural elements that deform will be different for small and large deformation experiments. The intercept found for the low deformation experiments was about $10^{9.8}$. The lower intercept for the larger

deformation results is probably due to the breakdown of structure occurring already at fairly small deformations.

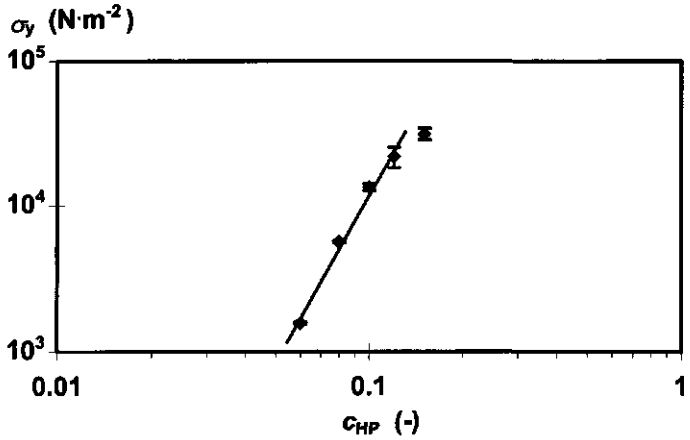

Figure 7-6. *The yield stress σ_y of HP/SF dispersions crystallized at lab scale as a function of the fraction HP. Standard deviations are indicated with vertical error bars. The solid line is the fit according to $\sigma_y = A \cdot c^{\mu}$ excluding the point for 15 % HP/SF.*

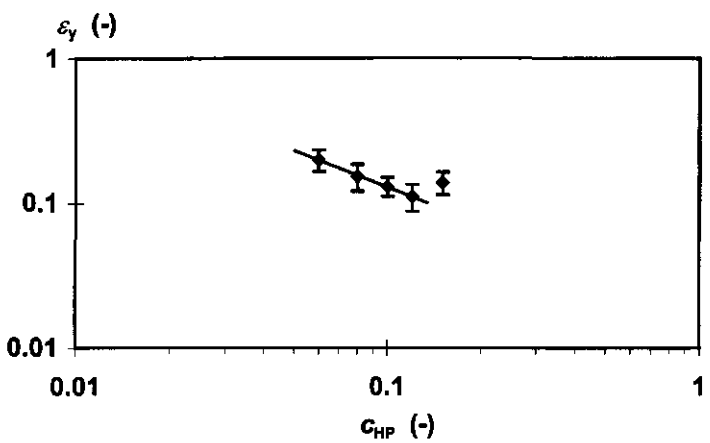

Figure 7-7. *The yield strain ε_y of HP/SF dispersions crystallized at lab scale as function of the fraction HP. Standard deviations are indicated with vertical error bars. The solid line is the fit according to $\varepsilon_y = A \cdot c^{\mu}$ excluding the point for 15 % HP/SF.*

The yield stress (Figure 7-6) shows an identical power-law dependency on the fraction HP as the apparent Young's modulus up to a fraction HP of 0.12. The scaling coefficient is 3.85 and the intercept is about $10^{7.9}$. The yield strain (Figure 7-7) scales with the fraction HP with an exponent -0.83. As can be seen, the scatter in yield strains is appreciable. This is due to the problem of obtaining test pieces with flat and parallel end faces. Despite the spread in the data, the decrease in yield strain with increasing fraction of HP is significant.

The scaling exponents of E^*, σ_y and ε_y can be discussed in terms of fractal aggregate models (Bremer *et al.* (1990, 1992)). These models assume that the network is built of aggregates of which the structure can be described by a fractal approach. For such an aggregate the number of particles in the aggregate N_p scales with the aggregate radius R to an exponent D, which is the fractal dimensionality (Meakin (1988)). If D is smaller than 3 in a 3 dimensional space the aggregate becomes even more tenuous on growth. The higher the value of D, the more compact an aggregate of a given size. The dimensionality of aggregates that are formed due to diffusion limited aggregation is about 1.7 -1.8. For low volume fraction HP/SF dispersions such a D was observed by means of light scattering (Kloek (1998), chapter 5). For high volume fraction HP/SF dispersions, the aggregates are more compact due to simultaneous crystallization and aggregation. The latter causes higher apparent fractal dimensionalities than are observed for the low volume fraction dispersions. From small deformation experiments apparent dimensionalities of about 2.0 - 2.2 were determined (Kloek (1998), chapter 6; Vreeker *et al.* (1992)). Elastic moduli can be discussed in terms of fractal network models (Bremer *et al.* (1990,1992)). The elastic moduli scale with the fraction of particles with an exponent $x/(3\text{-}D)$ where x is a number that depends on the geometric form of the stress-carrying strands. For straight strands $x = 2$, for hinged strands $x = 3$ and for completely bendable strands $x = 4$. A first approximation is hinged strands since the flexible stress-carrying strands of the primary network will become somewhat less flexible due to ongoing aggregation. Then a scaling exponent of 3.82 would correspond to $D = 2.21$.

If the strands are flexible, they can be deformed until they become more or less straight. Further deformation of these strands will result in a strong stress increase and fracture will occur. The yield stress of dispersions with flexible strands would therefore scale with $x/(3\text{-}D)$ where x is smaller than the value obtained for the elastic moduli. However, if the strands are not flexible, but straight or brittle, they cannot be deformed greatly, and fracture will occur at small deformations. Furthermore, the x-value in the scaling relation for the yield stress will then be about the same as that in the scaling relation for the elastic modulus. From the compression experiments, scaling exponents for E^* and σ_y of respectively 3.82 and 3.85 were determined. If the apparent dimensionality would not change on deformation this would mean that the geometry of the stress-carrying strands does not change strongly on deformation. This suggests that the stress-carrying strands are straight or that they are very brittle. In the case of fat crystal networks it is likely that the crystal bonds are very brittle due to sintering of the fat crystals. Since scaling exponents for E^* and σ_y are about equal, the relation given predicts that the yield strain should be almost independent of

the fraction of HP. However, we found a negative correlation, which is more in line with hinged or bendable strands.

One has to keep in mind that on compression, the real linear region of fat crystal dispersions is ignored since it can not be detected. This will make description of fracture in terms of network models more difficult.

Integration of the stress-strain curve according to Equation 7-1 gives the energy input until fracture or yielding of the sample. For linear elastic materials this energy can also be calculated directly from the yield strain, yield stress and Young's modulus. Since the linear elastic region of deformation for fat dispersions is far below the deformation that can be applied accurately, the energy input until yielding occurs is calculated by integration of the stress-strain curve between $\varepsilon =$ 0 and $\varepsilon = \varepsilon_y$. Figure 7-8 shows that a power-law describes the relation between the energy input until yielding and the fraction solid. The scaling exponent is about 2.7. Based on the scaling exponents of the power-law behaviour of the yield stress and the yield strain an exponent of 3.85-0.83 $\approx$ 3 was expected. Deviations will be caused by the non-linear elastic behaviour of the fat dispersion at these deformations and the inaccuracy in determining the scaling exponent of ε_y.

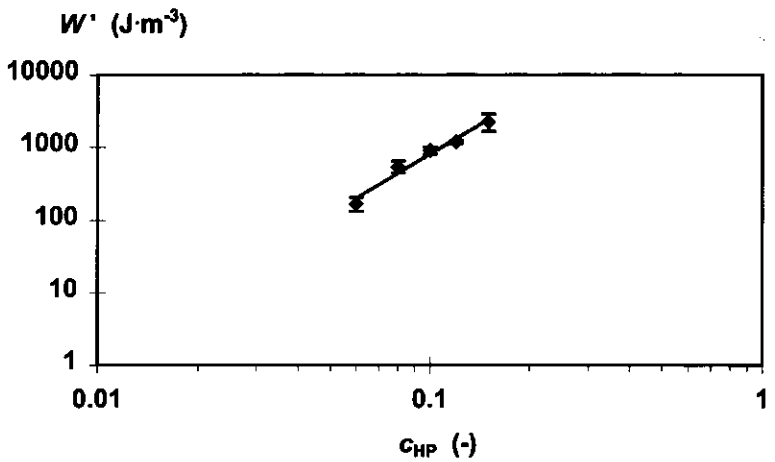

Figure 7-8. *The energy input W until the yield point of HP/SF dispersions crystallized at lab scale as function of the fraction HP. Standard deviations are indicated with vertical error bars. The solid line is the fit according to* $W' = A \cdot c^{\mu}$ *excluding the point for 15 % HP/SF.*

As already was indicated, compression experiments were carried out at deformations much larger than the region of linear deformation. In this region, the dispersions behave elastically: loss tangents, *i.e.* the ratio between viscous energy dissipation and elastic energy storage, are below 0.10. In this region, the elastic moduli are about 6 times as high as the apparent Young's moduli determined at much higher deformations. In the linear region the measured shear modulus of a 12 %

HP/SF dispersion is about $8 \cdot 10^5$ N·m^{-2}. The amount of stored energy in a linear elastic material is given by $\frac{1}{2} \cdot \sigma \cdot \varepsilon = \frac{1}{2} \cdot E \cdot \varepsilon^2$. Up to a shear strain of 0.001 this gives an amount of stored energy for a 12 % HP/SF dispersion of 0.4 J·m^{-3}. Even if the deformation range is extended up to a shear strain of 0.02, the smallest deformation that can be applied accurately in compression, an amount of stored energy of about 160 J·m^{-3} is calculated. In both cases the calculated amount of energy can be neglected compared to the numbers determined by integrating the experimentally obtained compressive stress-strain curves up to macroscopic yielding.

After the dispersions yield, the Bingham apparent extensional viscosity η_{eb} can be determined from the ratio $d\sigma / d\dot{\varepsilon}$. From such an analysis, it appeared that the extensional viscosity scaled with the fraction solids with an exponent 4.15 at a strain rate of approximately $1 \cdot 10^{-2}$ s^{-1} (Figure 7-9).

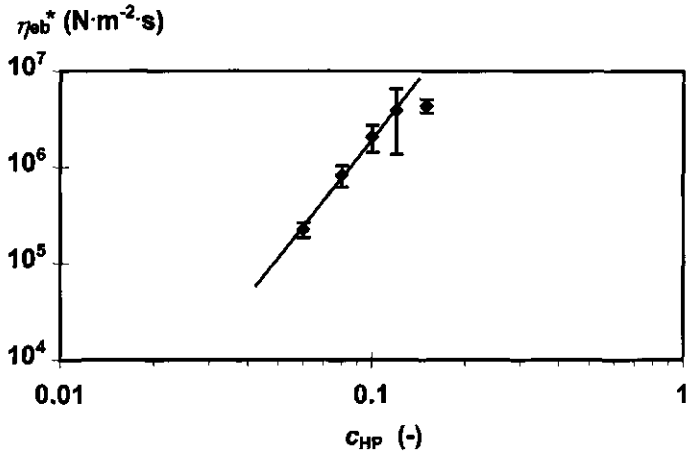

Figure 7-9. *The Bingham apparent extensional viscosity η_{eb}* of HP/SF dispersions crystallized at lab scale as function of the fraction of HP. Standard deviations are indicated with vertical error bars. The solid line is the fit according to $\eta_{eb}^* = A \cdot c^{\mu}$ excluding the point for 15 % HP/SF.*

The calculated coefficients of the power-law relation between the compressive parameters and the fraction solid fat are compiled in Table 7-1.

Table 7-1. *Compilation of coefficients calculated of power-law relations between the compressive parameters and the fraction of solid fat.*

	E^*	σ_y	ε_y	η_{eb}^* ($\dot{\varepsilon} \approx 10^{-2}$ s^{-1})	W^*
log$A$	9.1 ± 0.4	7.9 ± 0.3	-1.7 ± 1.2	10.4	5.7
μ	3.8 ± 0.4	3.9 ± 0.3	-0.83 ± 0.3	4.2	2.7

7.3.2 Wire Cutting

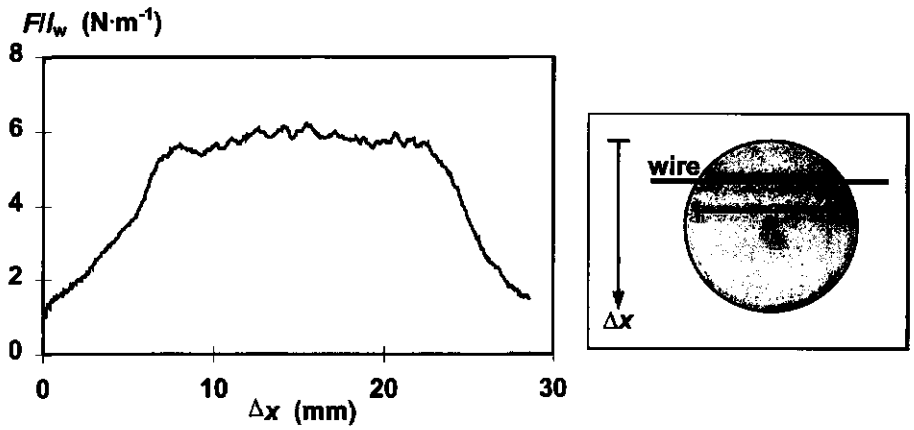

Figure 7-10. *Force F divided by contact wire length l_w as a function of the cutting distance Δx of a 10 % HP/SF dispersion. Wire diameter was 0.1* mm.

Figure 7-10 shows an example of a corrected force - cutting length curve. It shows a much lower resistance against cutting at the outer sides of the cylindrical test piece. This may be due to a temperature gradient over the inner and outer side of the crystallization tube leading to a structural gradient. The higher cutting force per unit length determined for the centre of the sample suggests stronger bonds *i.e.* sintered bonds or higher proportions of solid fat. It is therefore not allowed to average the cutting force over distances at which the force is about constant (8 mm < Δx < 22 mm), but the whole sample should be considered. The properties at the outside of the test piece may be different from those closer to the centre because the sample has been pushed out of the cylinder before cutting it with the wire. This will cause some structure breakdown at the outer side of the sample. When the cutting wire starts penetrating the sample, the accuracy of the force per unit length is low due to the small contact length between the wire and sample and the resolution of the loadcell (0.001 N). In the first few mm the contact length increases rapidly which makes it difficult to calculate the contact length accurately. Taking into account above considerations, the average force per length and the standard deviation have been calculated for cutting distances between 2 and 28 mm.

The average cutting force per unit length was measured with various wire diameters. Figure 7-11 shows the average F/l_w as function of the wire diameter. It shows that the corrected force varied linearly with the wire diameter. In most cases the correlation coefficient was in the range of 0.95 to 0.995. These correlations were only calculated for measurements on test pieces from the same tube. So the cutting force of a fat dispersion was measured with various wire diameters for each tube. From the intercept in Figure 7-11, the specific fracture energy was estimated according to Equation 7-4. For the 10 % HP/SF sample shown, the specific fracture energy was 3.2 $J \cdot m^{-2}$.

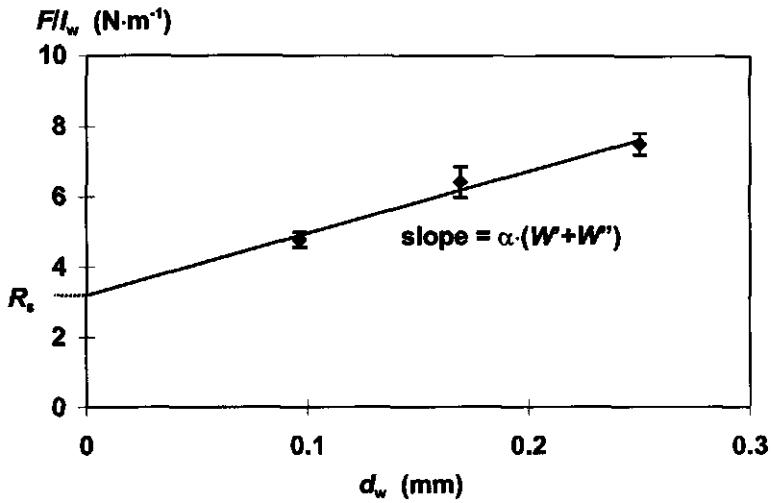

Figure 7-11. *Average force per unit cutting length (F/l_w) as a function of the wire diameter d_w on cutting a 10 % HP/SF dispersion. The solid line is a linear fit; the intercept would equal the specific fracture energy R_s.*

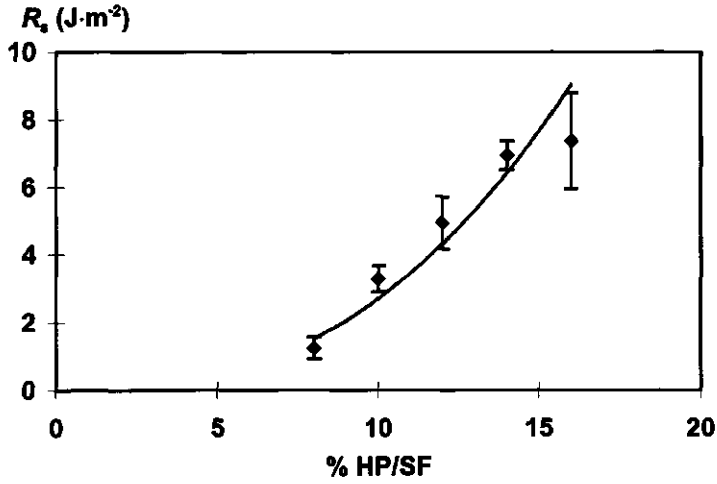

Figure 7-12. *Specific fracture energy R_s as function of the percentage HP for crystallized HP/SF dispersions as determined from wire cutting experiments. Standard deviations are indicated.*

The specific fracture energy was determined for dispersions with various fractions HP. The specific fracture energy increases with increasing fraction HP (Figure 7-12). This is expected since with an increasing amount of solid fat more bonds have to be broken to allow the formation of fracture planes.

Due to the scatter of the data, it is not clear whether the relation between the specific fracture energy and the fraction solids can be described best by a power-law or by a linear correlation. A power-law yielded a scaling exponent of 2.6 and an intercept of $10^{3.0}$ with a correlation coefficient of 0.93, while a linear relation yielded a slope of about 80 J·m^{-2} HP with a correlation coefficient of 0.96.

The standard deviation of R_s as determined when using different tubes (Figure 7-12) is very large compared to the standard deviation for the determination of R_s for a single tube (Figure 7-11). This large difference between R_s for fat dispersions from various tubes will be caused by variations in crystallization conditions. Firstly, there will be variation in the crystallization temperature in one tube. The wall of the tube was cooled to about 10 °C to obtain bulk temperatures that correspond to a supersaturation of about 4 in the β' polymorph. Near the wall of the tube, triglycerides will be supersaturated in the α polymorph. So initially crystallization will occur in the α polymorph. However, the stirrer will scrape the crystallized material from the wall and transport it to the bulk where the temperature is higher and probably part of the crystallized material will dissolve again. This will cause a broad supersaturation range for initial crystallization. As shown by X-ray diffraction, the crystallized dispersions were in the β' polymorph one day after crystallization. This indicates that the dispersions had also crystallized in the β' polymorph and not in the α polymorph, because crystallization in the α polymorph is followed by a polymorphic transition to a mixture of mainly β and some β' polymorph. For every crystallization experiment, the temperature was measured at which crystallization became visible. The corresponding supersaturation did not correlate with R_s. Secondly, the moment at which stirring was stopped was chosen rather arbitrarily. This would cause variation in shearing intensity and time and therefore also variation in the average crystallization temperature.

The slope of the F/l_w - d_w curves is a measure for the energy input of the wire cutting process. This is plotted as function of the percentage solids in Figure 7-13. This figure shows the same trend as the plot of R_s as function of the percentage HP. A power-law fit yielded a scaling exponent of about 3.3 which is higher than the scaling exponent 2.6 found for the power-law relation between R_s and the fraction solids.

A theoretical specific fracture energy can be estimated from the interaction force between the crystals and the size of the crystals. If the crystals are aggregated due to van der Waals forces in a primary minimum of, say, 30 k_bT, the energy per bond is about $1.2 \cdot 10^{-19}$ J. For a spherical crystal with a radius a of 0.1 μm the surface area per bond equals $\pi \cdot a^2 \approx 3 \cdot 10^{-14}$ m^2. For a dispersion of 10 % crystals the energy needed to create a surface of 1 m^2 equals $0.1 \cdot 1.2 \cdot 10^{-19} / 3 \cdot 10^{-14} \approx 4 \cdot 10^{-7}$ J. This value is very small compared to the determined value of about 4 J·m^{-2}. The same calculation can be made by assuming the crystals are sintered. To create new surface, the crystals themselves have to be broken. It is likely that fracture occurs between the aliphatic chains. In a crystal lattice the spacing between two atoms about 4Å. The energy content of the bonds in a crystal lattice is estimated to be 200 kJ·mol^{-1}. Combination of these two numbers yields a specific fracture energy of

0.7 J·m^{-2} for 100 % HP or 0.07 J·m^{-2} for a 10 % HP/SF dispersion. To these theoretical values twice the surface free energy of the oil phase should be added. This will amount to about 0.08 J·m^{-2} for a pure oil.

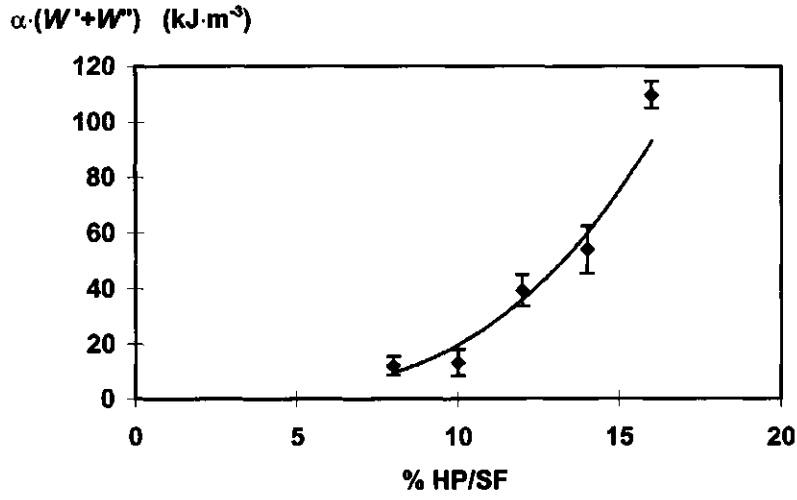

Figure 7-13. *Energy input α·(W'+W") as function of the percentage HP for crystallized HP/SF dispersions as determined from wire cutting experiments. Standard deviations are indicated*

Before sintered bonds will fracture, much deformation energy is stored as bending energy in the crystal. This energy is largely lost on fracture of the sintered bonds. Therefore, calculation of the specific fracture energy on base of bond energies will underestimate the obtained value. The numbers obtained can only be considered as a very rough order of magnitude estimation, nevertheless it is likely that the crystal bonds are to a great extent sintered.

7.3.3 Comparison between compression and cutting experiments

A comparison between the amounts of stored energy as determined from compression tests and cutting tests shows large differences. Integration of the compressive stress-strain curves yields much lower stored energies than obtained from the slope of F/l_w - d_w curves. These values are compared in Table 7-2.

Table 7-2. *Compilation of power-law coefficients of the relations between the energy input W as determined from compression ($\int_0^{\varepsilon_f}\sigma\,d\varepsilon$) or cutting experiments ($\alpha\cdot(W'+W'')$) and the fraction solid fat.*

		compression	wire cutting
$\log A$	(A / J·m^{-3})	5.7	7.6
μ	(–)	2.7	3.3

The difference in the energy input for a 10 % HP/SF dispersion is about a factor 20 (see also Figures 7-8 and 7-13). Since the specific fracture/yield energy is needed to calculate the defect length l_c it is necessary to discuss this difference in more detail. There are several factors that may account for the difference in W:

- There is a large difference in deformation rate. The initial deformation rate on compression was $3.3\cdot10^{-3}$ s^{-1} (Equation 7-9). The deformation rate on wire cutting can be estimated by the following equation $\dot{\gamma} = 3\cdot v / d_w$, where v is the speed of the wire and d_w the diameter of the wire. This equation gives the maximum shear rate at the surface of a sphere with diameter d moving with a velocity v. At a speed of 20 mm·min^{-1} and a wire diameter of 0.1 mm, the deformation rate is 10 s^{-1}. This is a difference in deformation rate by a factor of 3000. Over shorter time scales or for higher deformation rates normally less bonds contribute to stress relaxation leading to higher moduli. However, compression experiments at various deformation rates ranging from $3.3\cdot10^{-3}$ s^{-1} to $3.3\cdot10^{-1}$ s^{-1} did not show significant effect on the apparent Young modulus and the fracture stress, in contrast to the effect of frequency on the storage modulus G' determined in the linear region.
- Compression and wire cutting are different types of tests. On compression, a large test piece is deformed (length scale equals the test piece dimensions; 10 - 30 mm), while on wire cutting only a small part of the sample is deformed (length scale a few times the wire diameter $\approx \alpha\cdot d_w \leq$ 0.5 mm). In compression at deformations outside the linear region, major deformation occurs due to formation of shear planes. In this case only a small new surface area is created per unit volume test piece. In wire cutting experiments much more new surface is created per unit volume. Furthermore, on compression only the energy up to the yield point is considered while on wire cutting also energy dissipations after the yield point are taken into account. This will yield much higher W values from wire cutting experiments.

Since in wire cutting experiments, specific fracture energy and energy input are determined at the same time scales and length scales, it is preferable to compare these figures with each other although it should be kept in mind that the total amount of energy is overestimated.

The energy input until fracture consists of an elastic part W' and a dissipative part W''. The dissipative part arises from flow of the oil through the pores in the fat crystal networks and from

friction due to flow of the aggregates with respect to each other. The amount of energy dissipated due to flow of oil can be estimated using the following equation:

$$W'' = \eta^* \cdot \left(\frac{dv}{dx}\right)^2 \cdot t_{exp} \qquad (7\text{-}13)$$

where η^* is the apparent viscosity of the oil, (dv/dx) the deformation rate or velocity gradient and t_{exp} the experimental time scale. The dissipation arising from flow of oil through the pores, estimated by substituting $\eta^* = 7 \cdot 10^{-2}$ N·m^{-2}·s, $(dv/dx) = 10$ s^{-1} ($\approx 3 \cdot v/d_w$) and $t_{exp} \approx (dv/dx)^{-1}$ yields 0.7 J·m^{-3}. This dissipation is very small compared to the total energy input. The dissipation of energy due to friction between the fat crystal aggregates will be much higher due to the higher viscosity of the whole dispersion. The elongational viscosity at deformation rates of about $5 \cdot 10^{-3}$ s^{-1} for a 12 % HP/SF dispersion was about 10^6 N·m^{-2}·s. Since fat dispersions are highly shear rate thinning, the viscosity at a deformation rate of 10 s^{-1} will be much lower. The shear rate thinning behaviour was shown for low volume fraction HP/SF dispersion by steady shear viscosity measurements (Kloek (1998), chapter 5), and is also observed for high volume fraction dispersions in compression (Figure 7-14).

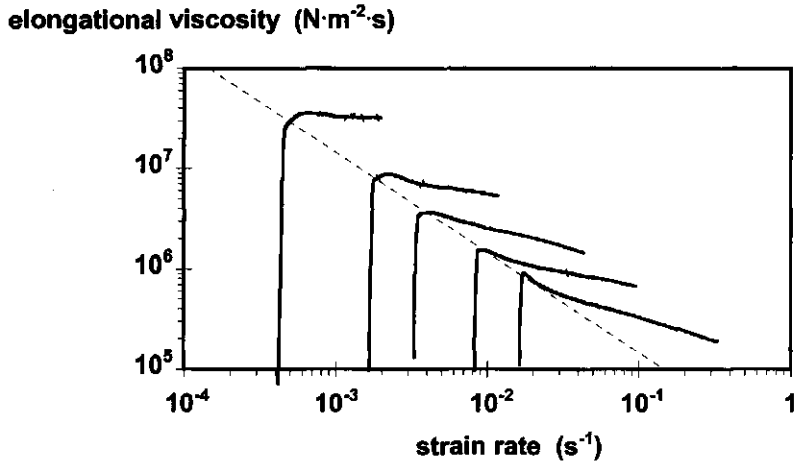

Figure 7-14. *Elongational viscosity (= stress divided by strain rate) of 12 % HP/SF dispersions as function of the initial deformation rate. Every line is one compression curve. The dotted line has a slope of -1.*

Figure 7-14 shows the viscosity (stress over strain rate) as a function of the strain rate of test pieces that were compressed at various initial strain rates. The steep increase of the curves indicates the stage of the compression before yielding and is in fact an elastic effect. The dotted line with a slope of -1, almost precisely crosses the curves at the yield points, which indicates that the yield

stress was independent of the strain rate. After yielding, the viscosity decreased with increasing strain rate. The viscosity after yielding of a test piece scales with the strain rate with an exponent of about -0.2 for low initial strain rates to -0.4 for high initial strain rates. If various test pieces that are compressed at various compression rates, are considered, the elongational viscosity scales with the strain rate for constant overall deformation with an exponent of about -1. This implies that flow probably occurs in shear planes, the number of it depending on the initial shear rate. Extrapolating the dotted line to a strain rate of 10 s^{-1}, predicts a viscosity of approximately $2 \cdot 10^3$ $N \cdot m^{-2} \cdot s$ at the yield point. Combining this viscosity and strain rates yields an energy dissipation of $2 \cdot 10^4$ $J \cdot m^{-3}$. Compared with the total energy input of $4 \cdot 10^4$ $J \cdot m^{-3}$ for a 12 % HP/SF dispersion (Figure 7-13), it can be concluded that a significant amount of energy ($\approx$ 50 %) would be dissipated due to friction between fat crystal aggregates. In fact, the largest part of the energy could be dissipated in this way.

Another way to estimate the contribution of energy dissipation to the total energy input is from the loss tangent $\tan\delta$ at yield deformation. The loss tangent can be determined in oscillatory tests and is defined by the ratio of loss modulus and storage modulus: this equals the ratio of dissipated energy and stored energy. In oscillation tests, a maximum strain of 0.07 could be applied. At this strain the apparent loss angle δ^* was approximately 50° ($\tan\delta^* = 1.2$). The amount of energy that is stored (W') can be expressed as a function of the total energy input W by:

$$W' = \frac{1}{1 + \tan\delta^*} \cdot W \qquad \textbf{(7-14)}$$

This means that roughly 54 % of the applied energy is dissipated and is not available for the creation of new surface. The order of magnitude compares well with the 50 % calculated from the extrapolated viscosities at the yield point

The defect length l_c of inhomogeneities from which fracture initiates, can be calculated from the specific fracture energy R_s and the amount of elastically stored energy W' using Equation 7-3.

$$l_c = \frac{R_s}{\pi \cdot W'} = \frac{R_s}{\pi \cdot \frac{1}{1 + \tan\delta^*} \cdot W} \qquad \textbf{(7-15)}$$

Table 7-3 summarizes the calculated defect lengths from both compression and wire cutting experiments, in the latter case for two fractions of energy stored. The obtained critical defect length using the energy input from compression tests yields an extremely high defect length. This may due to an underestimation of the energy input of the regions where fracture occurs. This could be checked by measuring the elastic recovery after applying a deformation that is close to the yield point. From results from cutting experiments and under the assumption that material is assumed to be completely elastic up to high deformation, a defect length of 40 μm is calculated. Assuming that

only about the half of the input energy is stored elastically, a defect length of 87 μm is calculated. The calculated defect lengths were independent on the fraction HP.

Table 7-3. *Defect length l_c of a crystallized 12 % HP/SF dispersion calculated from the specific fracture energy R_s and the stored energy W' using Equation 7-15. The stored energy is expressed as a function of the total energy W by Equation 7-14.*

W obtained from	tanδ (–)	fraction elastic energy (-)	l_c (m)
compression	0	1	$1.3 \cdot 10^{-3}$
cutting	0	1	$4.0 \cdot 10^{-5}$
cutting	1.2	0.46	$8.7 \cdot 10^{-5}$

There are some uncertainties in the determination of $\alpha \cdot (W'+W'')$ and R_s. Factor α is a proportionality constant that is related to the width of the disturbed region. About a width of two times the wire diameter will be disturbed ($\alpha = 2$) so that W' is in reality only half the value given in Table 7-3. This will increase the value of the calculated defect length. For the determination of R_s, it is assumed that the fracture surface area is a flat plane. In reality it will be uneven and, moreover, some side cracks will be formed so that the real fracture surface area is significantly underestimated. This means also that the specific fracture energy is overestimated. Assuming the fracture to occur around spherical aggregates would give a fracture surface area of four times that of a smooth surface. Together with side cracks the specific fracture energy may well be overestimated by a factor of 10.

These effects on the input energy and the specific fracture energy would result in an overestimation of the calculated defect length from cutting experiments by a factor of 5. The calculated defect lengths from compression experiments will be overestimated by a factor of 10. This leads to defect lengths of 8 and 130 μm, respectively. Both overestimations may be partially compensated by the uncertainty of the contribution of *W''* to the total energy input.

The order of magnitude of the defect lengths may be compared with the size of fat crystal aggregates at the gel point. The gel point is the moment that a space filling network is formed. The size of the aggregates at the gel point can be estimated by assuming that the aggregates have a fractal geometry. A gel is formed at the moment that the volume fraction of particles in an aggregate ϕ equals the total volume fraction of primary particles ϕ_0 (Bremer (1990,1992)). At the moment a gel is formed, growth of the primary aggregates is hindered. The fat crystallizing after a gel is formed, will be deposited within the existing gel and will thereby compact the "aggregates" that formed the gel. Therefore, the size of the aggregate at the gel point could be a measure of the inhomogeneities in aggregated fat crystal networks. For a fractal aggregate ϕ can be written as

function of the radius of the aggregate R and the particles size a using the fractal dimensionality D as a scaling exponent:

$$\phi = \left(\frac{R}{a}\right)^{D-3} \tag{7-16}$$

In chapter 5, we showed that during crystallization at rest already at a volume fraction of fat crystals of 0.005, a gel will be formed. Substituting $\phi = 0.005$, $D = 1.7$ and an average crystal size of 1 μm yields an aggregate radius at the gel point of 59 μm. This is the same order of magnitude as the defect lengths calculated from compression experiments. Since the crystallization of the first few percent of HP occurs under stirring conditions, it is expected that the aggregates are more compact *i.e.* have a higher dimensionality. A higher D leads even to higher R/a values at the gel point for the same ϕ_{gel}.

7.4 Conclusions

Compression tests on dispersions of fully hydrogenated palm oil (HP) in sunflower oil (SF) that have crystallized in the β' polymorph, showed that the apparent Young modulus, the yield stress, the yield deformation and the Bingham extensional viscosity are related to the fraction solid by a power law relation. The scaling exponent of 3.82 found for the apparent Young modulus, compared well with the scaling exponent of 4.1 observed for dynamic moduli, determined within the region of linear deformation. The true Young modulus could not be determined in compression tests, since the surface of the test pieces could not be made flat enough. The yield stress scaled with the same exponent as the apparent Young modulus. In terms of a fractal network approach, this indicates that the stress-carrying strands are either straight, or that they are hinged but very brittle. Solid crystal bonds suggest very brittle bonds, a conclusion which is also supported by the low yield deformations. The scaling exponent for the Young modulus yields for hinged stress-carrying strands an apparent fractal dimensionality of 2.2. This dimensionality predicts a scaling exponent for the yield deformation of -1.25 which deviates somewhat from the determined -0.83.

Crystallized 10 % HP/SF dispersions had a specific fracture energy of about 4 $J \cdot m^{-2}$. This order of magnitude can only be explained by assuming sintering of fat crystals. Mere van der Waals attraction between the crystals would yield much lower specific fracture energies. The specific fracture energy scaled with the fraction solids with an exponent of 2.6.

The critical defect length, which is the length of inhomogeneities that cause local yielding of the network, was calculated from the energy input and the specific fracture energy. When using energy inputs obtained from wire cutting experiments or compression experiments, defect lengths of about 40 and 1300 μm, respectively, are calculated if it is assumed that all the deformation energy is available for fracture. Due to overestimation of the specific fracture energy as a result of rough fracture surfaces and formation of side cracks, the defect length may be smaller than the calculated

ones by a factor of 5 to 10 leading to values of 8 and 130 μm, respectively. The size of 130 μm, obtained from compression experiments, corresponds well to the size of fat crystal aggregates at the gel point.

7.5 References

Bremer, L.G.B., Bijsterbosch, B.H., Schrijvers, R., Vliet, van T and Walstra, P. (1990) On the fractal nature of the structure of acid casein gels, *Colloids and Surfaces* **15**, 159

Bremer, L.G.B., *Fractal aggregation in relation to formation and properties of particle gels*, Ph.D. Thesis, Wageningen Agricultural University, the Netherlands, 1992

Ferry, J.D. (1969) *Viscoelastic properties of polymers*, John Wiley & Sons

Haighton, A.J. (1965), Worksoftening of margarine and shortening, *J. Am. Oil Chem. Soc.* **42**, 27

Kloek, W. (1998) *Mechanical properties of fats in relation to their crystallization*, PhD thesis, Wageningen Agricultural University, the Netherlands

Luyten, H. (1988), *The rheological and fracture properties of Gouda cheese*, PhD Thesis Wageningen Agricultural University, the Netherlands

Meakin, P. (1988) Fractal aggregates, *Adv. Colloid Interface Sci.* **28**, 249

Vliet, T. van and Luyten, H. , Fracture mechanics of solid foods, In *New Physico-Chemical Techniques for the Characterization of Complex Food Systems*, Ed. E. Dickinson, Chapman & Hall, London, 1995, pg. 157

Vreeker, R., Hoekstra, L.L., Boer, den D.C. and Agterof, W.G.M. (1992) The fractal nature of fat crystal networks , *Colloids Surf.* **65**, 185

Walstra, P., Vliet, van T. and Kloek, W., Crystallization and rheological properties of milk fat, In *Advanced Dairy Chemistry Vol. 2; Lipids* 2nd *ed.*, Ed. P.F. Fox, Chapman & Hal, London, 1995, pg.179

Wesdorp, L.H. (1990) *Liquid - multiple solid phase equilibria in fat - theory and experiments-*, Ph.D. Thesis, Technical University Delft, the Netherlands

Chapter 8

Mechanical Properties of Fat Dispersions Prepared in a Votator Line

8.1 Introduction

8.1.1 General

So far, we described the mechanical properties of fat dispersions that had crystallized under non-shearing or weakly shearing conditions. However, in daily practice, fats nearly almost always crystallize under non-quiescent conditions; the flow contains important elongational components but the forces are mainly shear forces. Although it would be more correct to speak about velocity gradients, the term shear is used throughout this chapter. Applying shear during crystallization or during post processing of the crystallized product can have an important influence on the mechanical properties of the final product.

Shearing during the crystallization process can accelerate polymorphic transitions of the α polymorph to the β' or β polymorph (Wesdorp (1992)). Furthermore, shearing during crystallization can lead to fracture of crystals or to enhanced nucleation, both leading to on average smaller crystals. Haighton (1976) showed that crystallization of hydrogenated fish oil in soy bean oil was accelerated by stirring the blend.

Shear will also influence the aggregation process of the crystals. Fat crystals attract each other due to van der Waals forces. Under quiescent conditions, they will meet each other due to Brownian motion. The collision frequency increases if shear is applied and is, in case of orthokinetic aggregation, proportional to the shear rate $\dot{\gamma}$. Above a critical shear rate, which depends on particle size and viscosity, the aggregation of crystals due to shear will dominate. For fat dispersions, taking the particle diameter to be 1 μm and a viscosity of 0.10 Pa·s, the critical shear rate is about 0.08 s^{-1}. During processing of fats, shear rates are generally a few orders of magnitude higher and are very inhomogeneously distributed. In a shear flow, the rotation of the anisometric fat crystals will further increase collision frequencies.

If crystals aggregate, they tend to form voluminous aggregates with a volume that is much greater than the total volume of the primary crystals. This is monitored as an increase in viscosity. However, if the shear rate is increased, the aggregates may break up again due to the shear forces that act on them. This force is proportional to the cross section of the aggregate and therefore scales with the aggregate radius R to a power of 2. Besides the break up of aggregates due to the shear stress, the aggregates may also become more compact due to rearrangement occurring when shear rate is increased (Kloek (1998), chapter 5). When the aggregates have grown so far that a space filling network is formed, applying shear will cause break up of the network and rearrangement of the aggregates.

Due to simultaneous crystallization and aggregation, crystals and aggregates may become sintered (Kloek (1998), chapters 5 and 6). If crystallization is finished and the crystals are sintered, these solid bridges can be broken by the application of shear and the resulting structures are attracted to each other by van der Waals forces. This change of the prevailing interaction between the structural elements can also have a marked effect on the mechanical properties of the fat dispersions.

It is clear that applying shear during the crystallization and structure formation of fat dispersions will have a clear effect on the resulting mechanical properties. The aim of this chapter is to describe the mechanical properties of fat dispersions that had crystallized and aggregated under shearing conditions. The dispersions were processed using a Votator-line which as used for margarine manufacture.

8.1.2 Mechanical Properties

To describe the mechanical properties of a fat dispersion one has to distinguish between properties at small and at large deformations. In this thesis, small deformation properties are defined as the properties at such deformations that the determined parameters do not depend on the applied deformation. Small deformation experiments yield information about the arrangement of the fat crystals and aggregates in space and about the interaction forces between the structural elements. Since for fat dispersions the deformations, at which mechanical characteristics are independent of deformation, are very small (deformation $\varepsilon < 10^{-3}$), these tests are normally carried out using dynamical oscillatory measurements. Parameters that are determined are the storage modulus G' and the loss modulus G''. Also creep tests can be used in this deformation range. The region of linear deformation of fats is so small, that compression tests are not suitable for determination of the mechanical properties of the undisturbed network. This is due to the problem of obtaining test pieces that are flat enough.

Large deformation tests are carried out at deformations outside the linear region. They can be carried out using uni-axial compression tests or creep tests. Creep tests at large deformations are often not accurate since the deformation is not homogeneous over the whole test piece. This has been shown for fat dispersions (Papenhuijzen (1971)), and, for instance, also for concentrated aqueous silica dispersions (Persello *et al.* (1994)). Compression tests are more often used to determine the large deformation behaviour of fat dispersions although they have several drawbacks. One of the main drawbacks is that considerable friction between the test piece and the compression plate can occur. It is possible to correct for friction by performing compression experiments with test pieces of various initial height and extrapolating the results to infinite height (van Vliet (1991)). Large deformation experiments yield parameters like an apparent Young modulus E^*, yield or fracture strain ε_y, yield or fracture stress σ_y and an apparent viscosity η^* (Kloek (1998), chapter 7). Young's modulus is called apparent since it is determined outside the region of linear deformation. Outside this deformation range, bonds between structural elements are broken and considerable rearrangement of structural elements will occur. E^* will therefore be much smaller than 3 times G' of the same dispersion determined in the region of linear deformation. The yield behaviour of fat dispersions at large deformation is largely determined by the occurrence of inhomogeneities. These are spots at which stress will be concentrated if a material is deformed. If the stress exceeds a certain critical value, fracture of the bonds between the structural elements occurs near the inhomogenity. Parameters obtained from large deformation experiments may correlate better with

spreadability than those by small deformation experiments, since then deformations can have the same order of magnitude.

Test pieces that are taken from a mass of fat, cannot be brought in close contact with the parallel plates of a dynamical rheometer without applying a deformation that is outside the region of linear deformation. The critical strain for fat dispersions is smaller than 0.001. For a test piece thickness of 5 mm, this would mean that it should not be deformed by more than 5 μm. It is impossible to prepare test pieces that have a roughness smaller than 5 μm. Therefore, it is impossible to do dynamical measurements on test pieces that are taken from a bulk fat without irreversibly affecting the structure during test piece preparation and bringing it in the rheometer.

Taking the above considerations into account, the fat dispersions obtained from the votator line were mechanically examined by means of compression tests and penetrometer tests. The penetrometer test is a quick and simple test in which a cone of a given angle and weight is allowed to penetrate in the sample for a certain time after free fall from a given height. The penetration depth is a measure of the consistency of the sample. Disadvantages of the penetrometer test are the ill defined deformation and deformation rate near the cone. A test that is used nowadays more often is a penetration of a cylinder of given dimensions at a given speed while measuring the force in time .

8.1.3 Votator Line

Margarine is normally made in a votator line. The three principal processes are emulsification ("droplet disruption"), fat crystallization and working of the partly crystallized water-in-oil emulsion (Young *et al.* (1976)). The aqueous phase and the melted fat phase, together with the additives are mixed, and the resulting emulsion is pumped to a scraped-surface heat exchanger (SSHE, also called A-unit), where the mixture is cooled and further emulsified. Some emulsification will take place in the pump and the tubing between the pump and SSHE. The SSHE normally consists of an inner rotor to which metal blades are attached that scrape the inner surface of the outside wall of the SSHE. This inner surface of the SSHE is cooled by means of liquid ammonia. The rotational speed of the inner rotor can be up to 800 rpm which causes locally high shear rates. Since the cooling surface area is very large compared to dimensions of the gap between the rotor and the cooled surface, the mixture is cooled efficiently. The first SSHE is normally used to cool down the mixture so far that the α polymorph becomes supersaturated and crystallization is initiated. Afterwards the supersaturated emulsion passes a crystallizer (C-unit) in which crystallization can proceed. To keep the material pumpable, the crystallizer contains a rotor fitted with pins. The shear rate in the crystallizer is much smaller than in the SSHE, due to the larger dimensions of the crystallizer. After passing the crystallizer, the emulsion is passed through a second and sometimes even a third SSHE. In these SSHE's the emulsion is further cooled so that crystallization can proceed and water droplets are further divided into smaller droplets. After leaving the last SSHE, the emulsion enters a resting tube (B-unit) in which crystallization is

completed. Often a sieve is placed in the exit of the resting tube, so that the crystallized product is intensively worked. After leaving the resting tube, the product can be packed.

The order and number of SSHE's, crystallizer and resting tubes can be varied, according to the desired product properties and the crystallization kinetics of the fat. The rate of the pump and the rotational speed of the inner rotor of the SSHE can also be varied to influence the consistency of the final product.

8.2 Materials and Methods

8.2.1 Materials

The model system used consists of fully hydrogenated palm oil (HP) in sunflower oil (SF), the first providing the solid phase and the latter remaining the liquid phase. A description of the physical properties and the triglyceride composition of this model system is given in chapter 2 of this thesis.

The solubility of HP in SF is given by the Hildebrand equation (Wesdorp (1990)).

$$\ln x_{HP} = \frac{\Delta H_{f,i}}{R_g}\left(\frac{1}{T_{m,i}} - \frac{1}{T}\right) \qquad \textbf{(8-1)}$$

where x_{HP} is the mole fraction of HP in polymorph i that is soluble at temperature T, $\Delta H_{f,i}$ the molar enthalpy of fusion of polymorph i, R_g the gas constant and $T_{m,i}$ the absolute melting temperature of pure polymorph i. The driving force for crystallization is the chemical potential difference $\Delta\mu$ between a supersaturated solution and a saturated solution:

$$\Delta\mu = R_g T \cdot \ln\frac{c_{HP}}{x_{HP}} = R_g T \cdot \ln\beta \qquad \textbf{(8-2)}$$

where c_{HP} is the mole fraction HP and x_{HP} the solubility given by 8-1; β is called the supersaturation ratio and $\ln\beta$ the supersaturation. If the mole fraction HP is known, the crystallization temperature T can be calculated for every initial supersaturation.

8.2.2 Crystallization in votator

Figure 8-1 illustrates the votator line used in these experiments. It is a very simple set-up, compared to what is normally used during margarine manufacturing. It consists of one storage vessel in which the sunflower oil and the hydrogenated palm oil are mixed and heated to 60 °C. This temperature is roughly 15 K above the final melting temperature of a 10 % HP/SF dispersion.

The storage vessel is a thermostatted double-walled tank of 65 l. The content of the tank is continuously stirred.

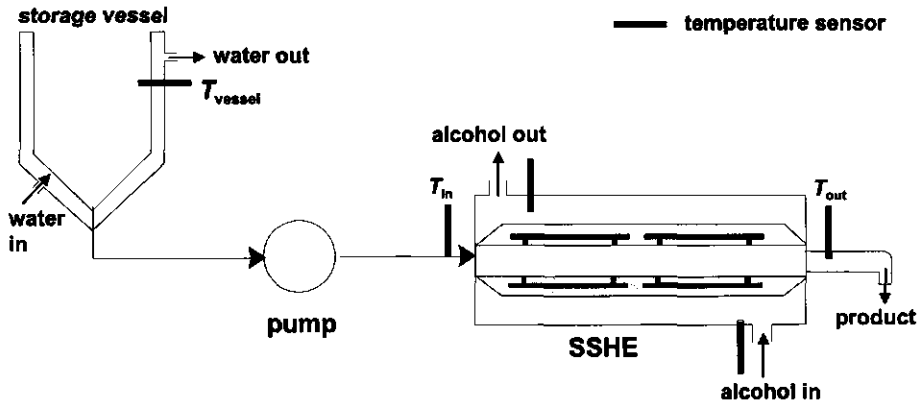

Figure 8-1. *Schematic representation of the votator line*

The melted fat blend is pumped by means of a single worm gear pump, by which the rate can be varied from 20 to 100 kg·h^{-1} to the inlet of the SSHE. The SSHE (Schröder coolers, type UK 01/60 - 400) is cooled by means of alcohol circulation. Some characteristic dimensions of the SSHE are: internal diameter 0.03 m; annular space between rotor and cooled wall 0.005 m, and internal volume 0.41 l. The effective cooling surface area is 0.070 m^2. The rotational speed of the rotor was in all cases 500 r.p.m. The temperature in the storage vessel, the in- and outlet alcohol temperatures and the in- and outlet product temperatures were continuously monitored using a datalogger.

The dispersions were processed at a rate of 20 or 50 kg·h^{-1}. By changing the rate it was possible to switch between complete and partial crystallization of the HP in the votator. The alcohol inlet temperature was so adjusted that T_{out} of the crystallized product would correspond to a $\ln\beta$ of 4 in the β' polymorph (Equations 8-1 and 8-2). Crystallization in the β' polymorph was performed for dispersions containing 8, 10 and 15 % HP/SF. If dispersions were to crystallize in the α polymorph, T_{out} was set at 16 °C. Crystallization in the α polymorph was only performed for 10 % HP/SF dispersions.

The crystallized dispersions were either collected in plastic cups (height: 85 mm , bottom diameter: 40 mm, top diameter: 65 mm) or in tubs (height: 27 mm, bottom diameter: 85 mm, top diameter: 92 mm) and stored at 20 °C.

8.2.3 Analysis

8.2.3.1 Crystallinity

The amount of crystallized fat was determined directly after the product left the votator using a p-NMR (Bruker P20i, 20 MHz) by a direct method (Putte and van Enden (1974)).

DSC melting curves of the crystallized dispersion were recorded on a TA-Instruments type 2910 at a heating rate of 2 $K \cdot min^{-1}$ after the dispersion had been cooled to 15 °C.

X-ray diffraction spectra were recorded on Philips equipment (goniometer PW 1820, control unit PW 18217, Cobalt radiation source (λ = 1.7889 Å)). Radiation was detected using a proportional detector.

8.2.3.2 Mechanical properties

A penetrometer test and a uni-axial compression test were applied. The penetrometer (Sommer & Runge, PNR 10) was equipped with a cone of 40° angle and 80 g falling weight. The penetration could be measured with an accuracy of 0.01 mm in the range of 0 - 10 mm and with an accuracy of 0.1 mm for penetrations larger than 10 mm. The penetration can be converted into a kind of 'yield stress' using the following equation (Haighton (1959)):

$$\text{yield stress} = \frac{K \cdot W}{p^n} \qquad \textbf{(8-3)}$$

where W is the falling weight in g, p the penetration in units of 0.1 mm and n a constant, which is 1.6 for margarine, butter or shortening and K a constant depending on the cone angle and on n. For a 40° cone, K equals 5840. The 'yield stress' is normally expressed in $g \cdot cm^{-2}$ (≈100 Pa) and we will also use this unit. Penetration tests were performed on samples filled in tubs.

Test pieces used for compression tests were prepared 24 hours before the test. The test pieces were cut very slowly out the plastic cup by means of a hollow cylinder. The cylinder was then placed in a specially designed holder and the fat dispersions were pushed out slowly by means of a rotating plunger (see chapter 7, Figure 7-1). The diameter of the test pieces was 30 mm and the height varied from 6 to 10 mm. The test pieces were compressed using a Zwick Material Tester type 1425 equipped with a load cell of 50 N (resolution 0.001 N). The diameter of the compression plunger was also 30 mm. The force-deformation curves were recalculated to stress-strain curves (see chapter 7, section 3.1). The test pieces were compressed at a linear speed of h_0 $mm \cdot min^{-1}$ where h_0 is the initial height of the test piece in mm so that the initial Hencky strain rate equals 0.017 s^{-1}.

8.3 Results

8.3.1 Crystallization

Table 8-1 gives the fraction of solidified fat directly after crystallizing the HP/SF dispersions in the β' polymorph at rates of 20 and 50 $kg \cdot h^{-1}$. If the dispersions had crystallized in the β' polymorph at a rate of 20 $kg \cdot h^{-1}$, crystallization was virtually completed in the SSHE. If the dispersion had crystallized at a rate of 50 $kg \cdot h^{-1}$, about 2 % HP had not crystallized and therefore crystallized in the tub.

Table 8-1. *Fraction crystallized HP after leaving the votator for various HP/SF dispersion crystallized in the β' polymorph at processing rates of 20 and 50* $kg \cdot h^{-1}$.

% HP/SF	fraction solids 20 $kg \cdot h^{-1}$	fraction solids 50 $kg \cdot h^{-1}$
8	0.083	0.062
10	0.098	0.088
15	0.15	0.125

The residence times of the HP/SF dispersions in the SSHE at rates of 20 and 50 $kg \cdot h^{-1}$ can be estimated from the internal volume (0.41 l) and the average density (920 $kg \cdot m^{-3}$) and are about 68 and 27 s, respectively. In isothermal crystallization experiments of 10 % HP/SF dispersions at rest at high supersaturation of the β' polymorph, the maximum amount of solid material was obtained after 5 minutes. After 1 minute of crystallization only about 1 - 2 % of solid material was formed. This indicates that the application of shear accelerates the crystallization of triglycerides. This may be due to enhanced nucleation (Haighton (1976)) or a better heat transport. High shear variations may enhance secondary nucleation.

Since only the input and the output temperature of the product could be monitored it is not clear whether crystallization occurred in the α or the β' polymorph; the α polymorph was supersaturated at the alcohol temperature. Therefore, X-ray diffraction and DSC were applied. Figure 8-2 shows the X-ray diffraction spectra. Their quality is rather poor because of the low amount of crystalline material present, but they are good enough to distinguish different polymorphs.

The dispersion of which the output temperature of the product corresponded to crystallization in the β' polymorph, shows diffraction peaks at 0.37-0.38 and 0.42 nm which are characteristic for the β' polymorph.

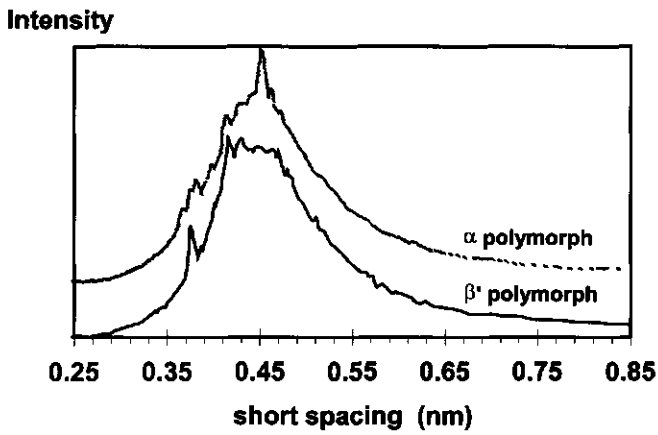

Figure 8-2. *X-ray diffraction spectra of 10 % HP/SF dispersions crystallized in a votator line with product output temperatures corresponding to crystallization in the α and β' polymorphs (indicated).*

The dispersion of which the output temperature of the product corresponded to crystallization in the α polymorph, shows a strong diffraction peak at 0.450 nm and weak peaks at 0.37 and 0.39 nm, which correspond to the β polymorph, and a weak peak at 0.42 nm, which corresponds to the β' polymorph. There was no obvious diffraction peak at 0.415 nm, a spacing characteristic for the α polymorph. The first X-ray spectra were determined 3 days after crystallization. There was no difference between these spectra and spectra determined after 21 days. These results show that dispersions crystallized in the α polymorph transform rapidly to a mixture of mainly β and some β'. We also observed this phenomenon for 10 % HP/SF dispersions that had crystallized in the α polymorph at rest. Time scales of polymorphic transitions at temperatures of 5 °C and 15 °C were 30 and 3 minutes, respectively (Kloek (1998), chapter 4). The results also show that dispersions initially crystallized in the β' polymorph, are stable in the β' polymorph.

In Figure 8-3, the DSC melting curves of 10 % HP/SF dispersions are shown that had initially crystallized in the β' polymorph (Figure 8-3a) or the α polymorph (Figure 8-3b) as function of storage time. For both polymorphs the same trends are observed: the peak temperature slightly increased and the width of the melting peak became smaller on storage. Integration of the melting peak showed that the melting enthalpy increased with time. All effects are associated with recrystallization. Both products had crystallized at high supersaturation, which will cause defects in the crystal lattice. Even more important is the presence of many different triglycerides in the HP, which will lead to the formation of compound crystals. Recrystallization to crystals with fewer defects and demixing of the compound crystals would lead to higher melting temperatures and higher melting enthalpies. The melting peak seems to become narrower due to disappearance of a left-hand shoulder. This would be due to recrystallization of fat crystals containing triglycerides with relative low melting temperature and melting enthalpy.

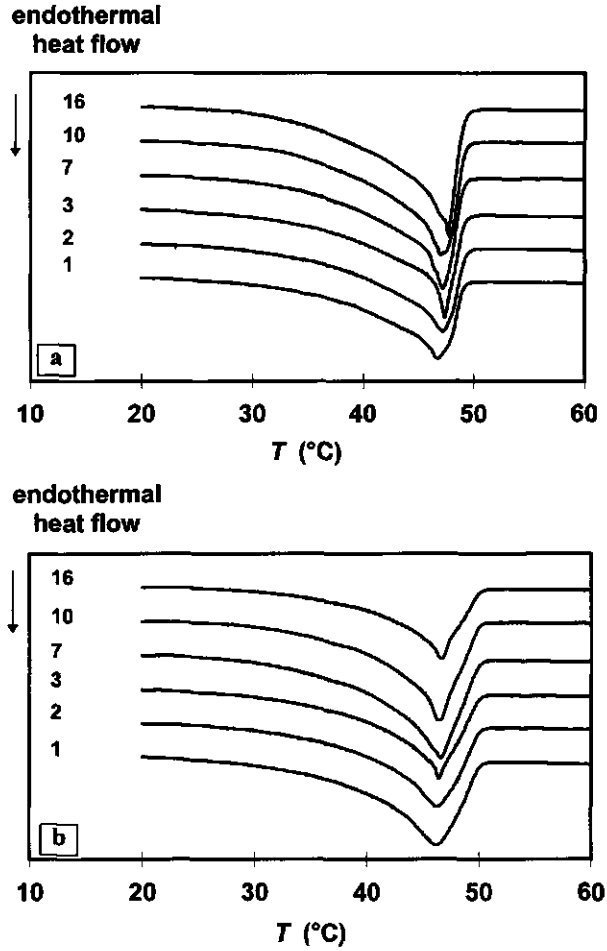

Figure 8-3. *DSC melting curves of 10 % HP/SF dispersions crystallized in the β' polymorph (a) and the α polymorph (b) as function of storage time (indicated in days).*

Integration yields melting enthalpies of 152 kJ·mol^{-1} HP for dispersions crystallized in the β' polymorph and 162 kJ·mol^{-1} HP in the others. These values correspond well with the melting enthalpies of dispersions crystallized in DSC cups (Kloek (1998), chapter 4). The somewhat higher observed melting enthalpy for crystallization in the α polymorph will be due to the presence of a large proportion of the β polymorph, which generally has somewhat higher melting enthalpies than β'. The differences may also be caused by a difference in the extent of compound crystal formation. The peak temperatures of dispersions crystallized in the β' polymorph were in all cases about 0.8 K higher than the peak temperatures of dispersions crystallized in the α polymorph. This may be due

to the triglyceride PSP, which is present at a relative high fraction and which has a higher melting temperature in the β' polymorph than in the β polymorph (Wesdorp (1990)).

8.3.2 Mechanical properties

8.3.2.1 Penetration depths

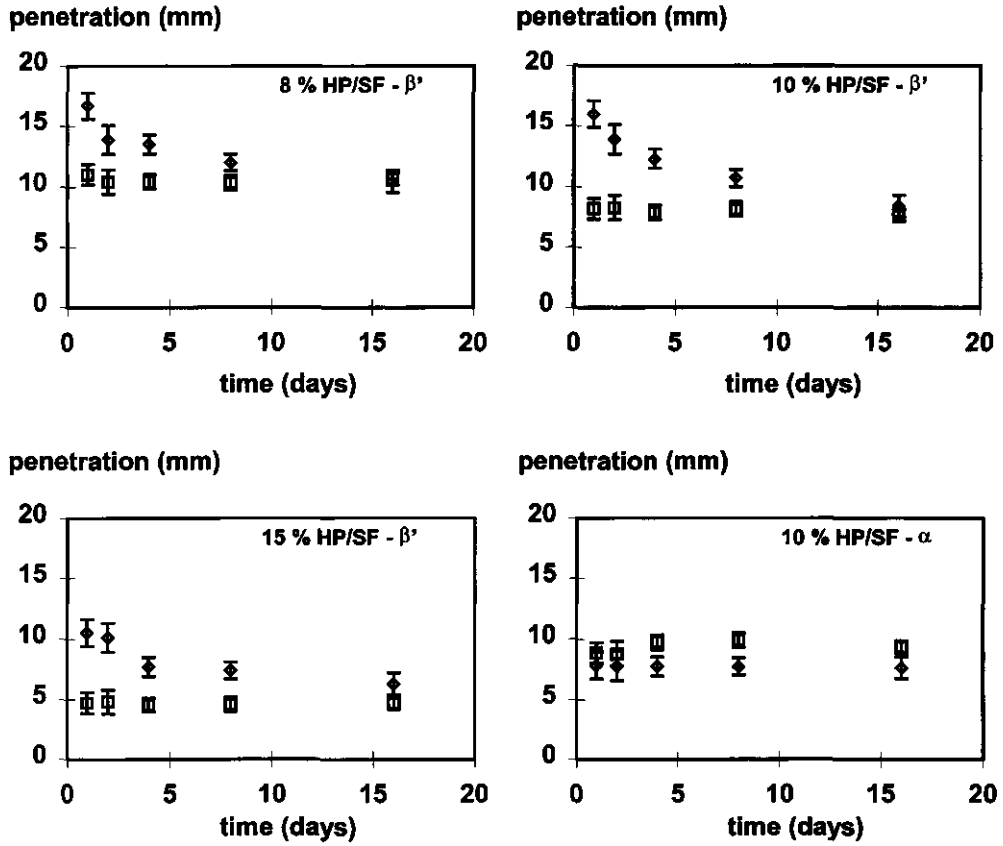

Figure 8-4. *Penetration of a 40° cone in HP/SF dispersions containing various fractions HP, crystallized in either the α polymorph or the β' polymorph in a votator at rates of 20* $kg \cdot h^{-1}$ (◊) *and 50* $kg \cdot h^{-1}$ (□). *Standard deviations are indicated.*

Figure 8-4 shows the penetration depths by the penetrometer cone for HP/SF dispersions initially crystallized at different rates in the α or the β' polymorph as function of storage time; this is to say, both α, β' and β or β' and β polymorphs are supersaturated, respectively.

The penetration depths in dispersions crystallized in the β' polymorph at a rate of 50 $kg \cdot h^{-1}$ were constant as a function of storing time, while the penetration depths in dispersions crystallized at a rate of 20 $kg \cdot h^{-1}$ decreased on storing. After 15 days of storage, the penetration depth was about the same for dispersions crystallized at 20 and 50 $kg \cdot h^{-1}$. These trends were observed for all dispersions containing various fractions HP. As already discussed in the section on solid fat determinations, dispersions that had crystallized at a rate of 50 $kg \cdot h^{-1}$ had not completely crystallized when leaving the votator. An amount of about 2 % HP still had to crystallize in the tub at rest. The setting of the dispersions processed at a rate of 50 $kg \cdot h^{-1}$ was clearly visible when filling the tubs; the dispersion flowed like a liquid during filling but within a few seconds after filling the dispersions set. This rapid setting was confirmed by penetration measurements directly after crystallization (results not shown).

The fat that crystallized in the votator, did so under high shear conditions. Under such conditions, any aggregates formed will be compact. Moreover, any sintered bonds formed between crystals or aggregates may be broken. The product that leaves the votator would get its consistency from 'compact' aggregates that are attracted to each other by van der Waals forces. Despite the high shear rate, the crystals inside fairly small aggregates may be sintered. Crystallization of an additional 2 % solids at rest, which would certainly occur within a day, would cause sintering of the aggregates, resulting in firmer dispersions since the solid bridges are much stronger than van der Waals bonds. Once, the sintered bonds are formed, no further change in firmness was observed because these bonds are too strong to allow any rearrangements of the structure.

The dispersions processed at a rate of 20 $kg \cdot h^{-1}$ had completely crystallized when leaving the votator. When leaving the votator, these dispersions would mainly contain aggregates attracted to each other by van der Waals forces. Since no further bulk crystallization occurred, these dispersions would not become sintered directly after leaving the votator. This implies that aggregates could only become sintered by recrystallization processes (*e.g.* due to demixing of compound crystals). These processes took place over long time scales, as is seen on the DSC melting curves. This can explain the slow decrease in penetration depth as a function of ageing time. The initial high penetration values would be due to the absence of sintered bonds between aggregates. On prolonged storage, the aggregates would become sintered and the dispersion therefore becomes firmer resulting in small penetration depths. After 2 weeks, the extent of sintering between aggregates has apparently become so high that the penetration values in dispersions processed at 20 and 50 $kg \cdot h^{-1}$ were about the same.

Recrystallization should also occur in dispersions processed at a rate of 50 $kg \cdot h^{-1}$, but it would not show up in an increase in firmness on storage. Apparently, the sintering caused by the 2 % fat that crystallizes at rest results in such a firm structure that additional recrystallization does not materially affect it to a measurable extent.

The penetration depth in dispersions decreased with increasing fraction solids present. This is logical since the number of bonds that have to be broken increases with increasing fraction solids.

The penetration depth in dispersions crystallized in the α polymorph did not change on storage and the penetration depths were comparable to those of 10 % HP/SF dispersions that had crystallized in the β' polymorph. The solubility of HP in SF in the α polymorph is about 3 % at a temperature of 16 °C. If the product leaves the votator, the solid phase would still be present in the α polymorph. A polymorphic transition from α to β/β' will lead to crystallization of an additional 3 % HP. Since this transition occurs at rest, this will cause sintering of the aggregates, similar to what happens in the dispersions that had crystallized in the β' polymorph at a rate of 50 $kg \cdot h^{-1}$. Thé time scale of polymorphic transition from α to β/β' at a temperature of 16 °C for 10 % HP/SF dispersions would be about 3 min at rest (Kloek (1998), chapter 4) and about 2 minutes under shearing conditions (Sassen (1996)), which is longer than the residence time in the votator. This means that soon after filling the tubs, the polymorphic transition will be finished. The dispersions that had crystallized in the α polymorph were liquid-like, directly after leaving the votator and set in about 1 min.

Dispersions that had crystallized in the α polymorph showed somewhat higher penetration depths when processed at a rate of 50 $kg \cdot h^{-1}$ compared to a rate of 20 $kg \cdot h^{-1}$. We cannot explain this result.

The appearance of the dispersions crystallized in the β' polymorph was white, turbid like while the dispersion crystallized in the α polymorph looked more glassy and shiny. The white, turbid appearance was more pronounced for dispersions crystallized at a high rate and will be caused by structures of size of the order of a μm that scatter light. These structures may be compact crystal aggregates. It was also noticed that during setting, the appearance of dispersions crystallized in both the α or the β' polymorph became more turbid.

The penetrations can be converted to 'yield stresses' by means of Equation 8-3. Values of 200 to 800 correspond to a product with a satisfactory plasticity and spreadability, values below 100 correspond to very soft, non spreadable products and values over 1000 correspond to too hard and hardly spreadable products (brittle) (Haighton (1959)). The obtained 'yield stresses'(Table 8-2) indicate that all dispersions, except the 15 % HP/SF dispersion, should have good spreadability properties. This was in agreement with visual observation.

Table 8-2. *'Yield stresses' of HP/SF dispersions processed in the α and β' polymorph at a rate of 50* $kg \cdot h^{-1}$ *after 16 days obtained from penetration depths.*

dispersion	"polymorph"	yield stress ($g \cdot cm^{-2}$)
8 % HP/SF	β'	270 ± 20
10 % HP/SF	β'	460 ± 70
15 % HP/SF	β'	1000 ± 165
10 % HP/SF	α	330 ± 60

8.3.2.2 Compression tests

Compression experiments were performed on test pieces of various initial height at the same initial Hencky strain rate to correct for the friction between the compression plate and the test piece. The influence of height can be seen in Figure 8-5a. For small deformations, the stress-strain curves coincide, but at larger strains the stress at the same strain increased with decreasing test piece height.

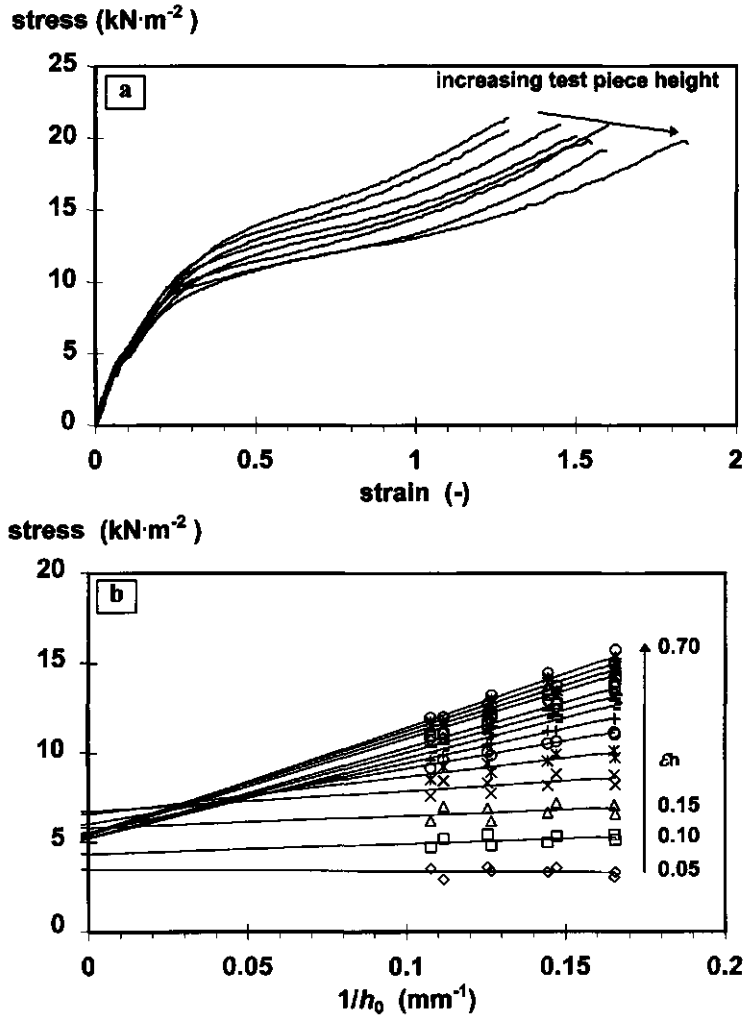

Figure 8-5. *Stress-strain curves in uni-axial compression (a) for various initial test piece heights of 8 % HP/SF dispersions processed in the β' polymorph at a rate of 50* kg·h^{-1} *and the stress as function of the reciprocal test piece height for some constant Hencky strains (b). The intercept of these lines would correspond to the friction-corrected stress.*

For test pieces of small height, the friction layer will contribute more to the total stress than for higher test pieces with the same friction layer. By plotting the stress at a certain strain against $1/h_0$ and taking the extrapolated value at $1/h_0 = 0$, a friction-free stress-strain curve can be constructed (van Vliet (1991)). Figure 8-5b gives the stress - $1/h_0$ curves from the results of Figure 8-5a.

Figure 8-5b shows good linear relations between the stress at a certain strain and the reciprocal initial test piece height. For small strains, the stress is almost independent on the test piece height, indicating that no friction occurs or that the friction is independent on test piece height. For strains larger than 0.25, the stress is strongly dependent on the test piece height. These are strains larger than the yield or fracture strain. This indicates that the apparent Young modulus, the yield stress and the yield strain can be determined from the uncorrected curves. At strains larger than the yield strain, the curves should be corrected for friction.

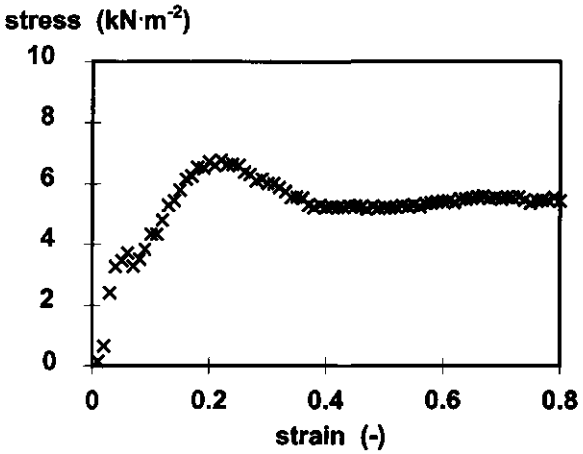

Figure 8-6. *Friction corrected compressive stress-strain curve of 8 % HP/SF dispersions crystallized in the β' polymorph at a rate of 50* kg·h^{-1}.

The corrected stress-strain curve in Figure 8-6 shows that after yielding the stress becomes about constant with increasing strain. These type of figures were also shown by Heertje *et al.* ((1988) for crystallized fat dispersions. The ratio of the corrected stress at large strains and the corrected peak stress is a measure for the degree of worksoftening. Since the reproducibility of the correction method was rather poor, it was decided to use the non-corrected stress-strain curves to determine some characteristics. Only determination of the viscosity after yielding is then subject to large errors.

Figure 8-7 shows apparent Young's moduli as function of time. The scatter in the data is rather large. Therefore it is difficult to indicate trends. Young's moduli of dispersions that had crystallized in the β' polymorph at a rate of 20 kg·h^{-1} increased in time while the moduli of dispersions crystallized in the β' polymorph at a rate of 50 kg·h^{-1} did not show a clear change in

time. For the 15 % HP/SF dispersions it is even more difficult to distinguish a clear trend. This may be due to the brittleness of these dispersions, which makes it difficult to cut the test pieces without disturbing them. These results are similar to those obtained from penetration measurements and can also be explained by part of the crystallization occurring at rest. Young's moduli of dispersions crystallized in the α polymorph seem to decrease on storage although it is hard to explain this observation. A possible explanation would be that recrystallization is accompanied by a coarsening of the crystals, although it may be expected that this does not have much influence on the modulus of an already sintered network.

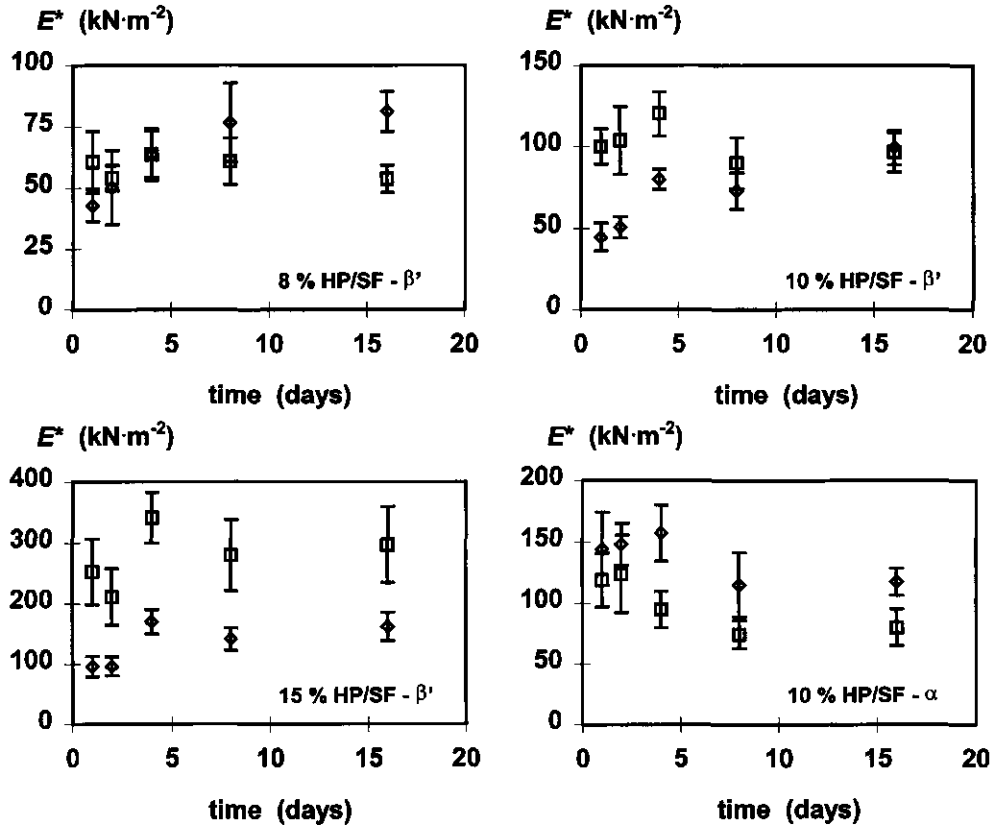

Figure 8-7. *Apparent Young moduli of HP/SF dispersions containing various fractions HP, crystallized in either the α polymorph or the β' polymorph in a votator at a rate of 20* kg·h^{-1} (◊) *or 50* kg·h^{-1} (□).

The yield stresses (Figure 8-8) show a much smaller spread than the moduli. The observed trends are clear. The yield stresses of the 50 kg·h^{-1} dispersions in which some crystallization occurred at rest did not change on storage, whereas the yield stresses of 20 kg·h^{-1} dispersions that

had completely crystallized in the votator showed an increase on storage. The increase of the yield stress is explained by the sintering of aggregates due to recrystallization. The yield stress of the 8 % HP/SF dispersion crystallized at a rate of 20 kg·h^{-1} exceeded after 4 days that obtained at a rate of 50 kg·h^{-1}, For the 10 % HP/SF dispersion the yield stresses equalled each other after 10 days and for the 15 % HP/SF dispersions this apparently took longer than 16 days.

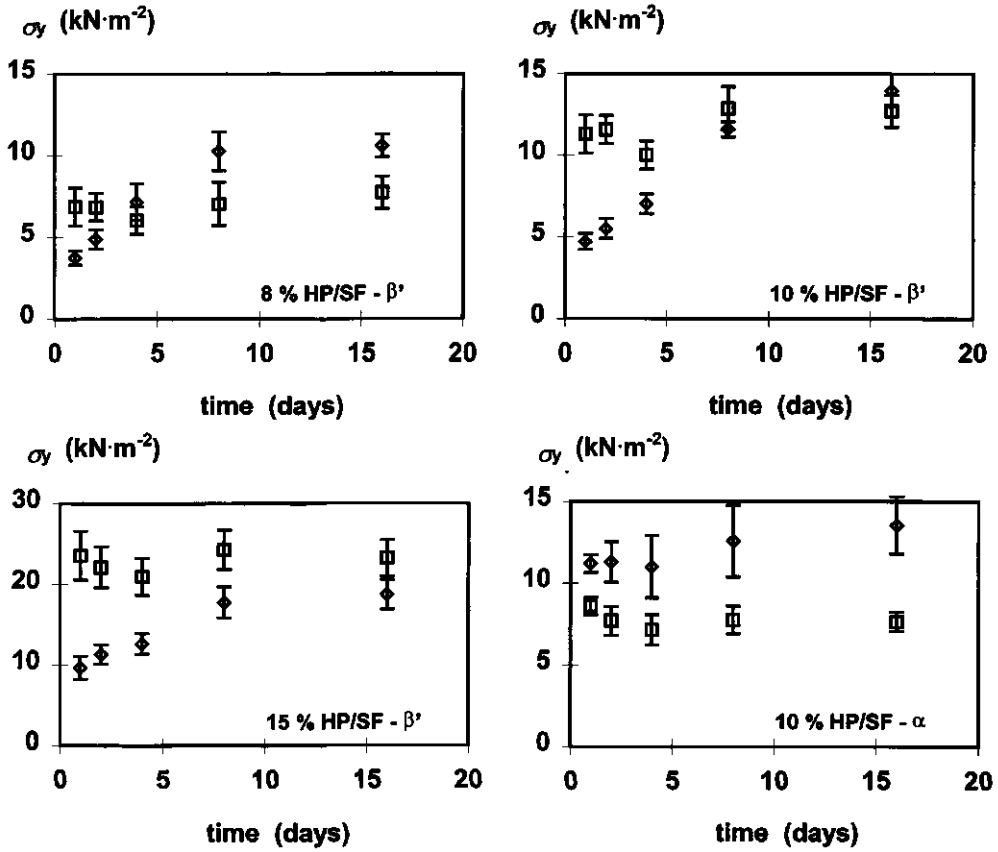

Figure 8-8. *Yield stress of HP/SF dispersions containing various fractions HP, crystallized in either the α polymorph or the β' polymorph in a votator at rates of 20* kg·h^{-1} (◊) *or 50* kg·h^{-1} (□).

The differences for the two rates seem to be caused by the difference in the yield stress directly after crystallization. The difference increased in magnitude with increasing fraction HP. The crystallization rate of HP/SF dispersions that had crystallized at the same supersaturation, increased with increasing fraction HP (Table 8-1). If crystallization occurs more rapidly, aggregates will be formed in an earlier stage of the crystallization process and therefore more at the beginning of the votator line. Since the rate is constant, the aggregates in faster crystallizing dispersions,

would be longer subject to shear after their formation. This extra shear will probably result in a further compaction of the aggregates, so that in dispersions with higher fractions of HP the aggregates would be less efficient in forming a space-filling network. The yield stress of dispersions that had crystallized in the α polymorph showed the same trends as the apparent Young's modulus: the yield stress of dispersions crystallized at a low rate was about constant in time, while at a higher rate it decreased somewhat during the first 4 days. There was no clear influence of storage time and rate on the yield deformations as obtained from the compression tests (data not shown). This is mainly due to the large scatter in these results. Yield deformations were approximately 0.1 to 0.15.

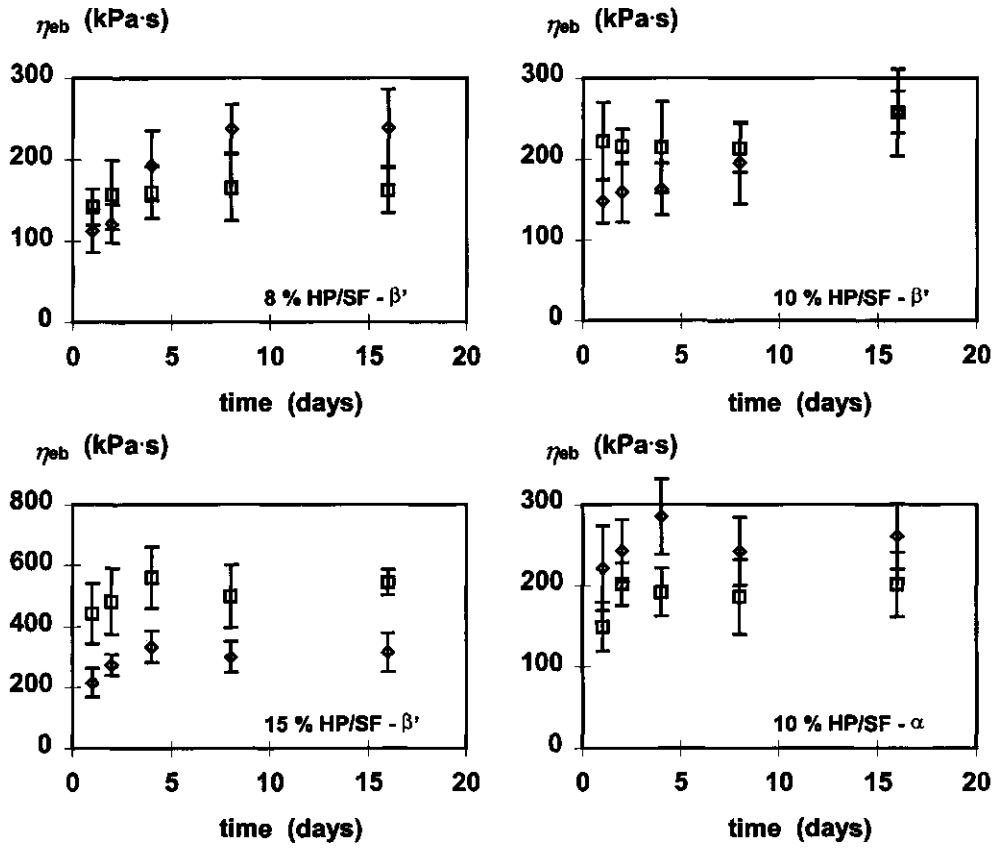

Figure 8-9. *Bingham elongational viscosity η_{be} of HP/SF dispersions containing various fractions HP, crystallized in either the α polymorph or the β' polymorph in a votator at rates of 20* kg·h^{-1} (◊) *and 50* kg·h^{-1} (□).

The viscosity is related to the volume fraction of aggregates and increases with increasing volume fraction aggregates. Figure 8-9 shows the Bingham viscosity (uncorrected for friction) of

the dispersions as a function of storage time. These graphs show again the same trends as found for the apparent Young modulus and the yield stress. This can be explained by the break up process of the network and the aggregates during compression. At strains around and just larger than the yield strain, part of the sintered bonds between the aggregates will be broken. On further compression also the aggregates will be deformed stronger and successively be broken up into smaller aggregates which results in a decrease of the volume fraction aggregates.. These aggregates will be broken up in a similar way but at higher deformations. For the break-up of the aggregates, sintered bonds inside the aggregates have to be deformed and successively be broken. The initial deformation of the sintered bonds is associated with the Young modulus, fracture of the solid bonds is associated with the yield stress. So, on deformation of fat dispersions, the same processes are repeated but on a smaller length scale with increasing deformation. This view is supported by the observed decrease of the Bingham viscosity with increasing strain rate.

8.3.3 General discussion

Both from penetrometer measurements and compression experiments, it is clear that if a HP/SF dispersion has not completely crystallized in the votator line, it obtains its final consistency within one day after crystallization. The part of the solid fat that crystallizes at rest (for instance in a tub) acts as sintering agent for the aggregates. Further recrystallization in time would not change the consistency noticeably, since strong bonds, which do not allow structural rearrangement, have already been formed. The dispersions that had completely crystallized in the votator and that were therefore also mechanically worked in the votator, showed an increase in consistency with ageing over a period of about 10 days. This increase would be due to recrystallization, leading to the formation of sintered bonds between the aggregates that were initially attracted to each other by van der Waals forces. The recrystallization of compound crystals was shown by DSC melting curves: both melting peak temperature and melting enthalpy increased in time.

Penetrometer observations showed that after about 16 days the penetrations were equal for dispersions that had either completely crystallized in shear or partly at rest. However, results of the compression experiments showed that after 16 days the apparent Young modulus, yield stress and Bingham viscosity were not equal for dispersions that had either completely crystallized in shear or partly crystallized at rest. For 8 % HP/SF dispersions completely crystallized in shear, the parameters obtained after 16 days were higher than for dispersions partially crystallizing at rest. For 10 % HP/SF dispersions the values were about the same and for 15 % HP/SF dispersions the values were lower. A possible reason for the differences between the penetrometer measurements and the compression experiments is the difference in deformation rates. In the compression experiments which were performed at a constant compression speed, the Hencky strain rate increased from initially 0.0167 s^{-1} ($\varepsilon = 0$) to about 0.075 s^{-1} at a strain of 1.5. So in compression, macroscopic yielding occurred at a low strain rate while further flow and structure breakdown occurred at somewhat higher strain rates. The speed of an initially free falling cone, on the other hand,

decreased in time. The penetration in the material was reached in less than 0.1 s. For a total penetration of the cone of 10 mm, an average falling speed of 100 mm·s^{-1} is obtained. Suppose, that on average a dispersion layer with a thickness of 1 mm has to flow parallel to the cone. This will cause a strain rate of roughly 100 s^{-1}. These strain rates are much higher than in the compression experiments. Furthermore the cone speed will initially be highest, rapidly decreasing in time. Consequently fracture occurs at much higher strain rates than the subsequent flow of the yielded dispersion. Effects of the strain rate on Young modulus, yield stress and specially on viscosity may be an explanation for the differences between the final consistency as determined with the penetrometer and by the compression test. It is clear that compression tests showed differences between various dispersions that were not observed by the penetrometer test.

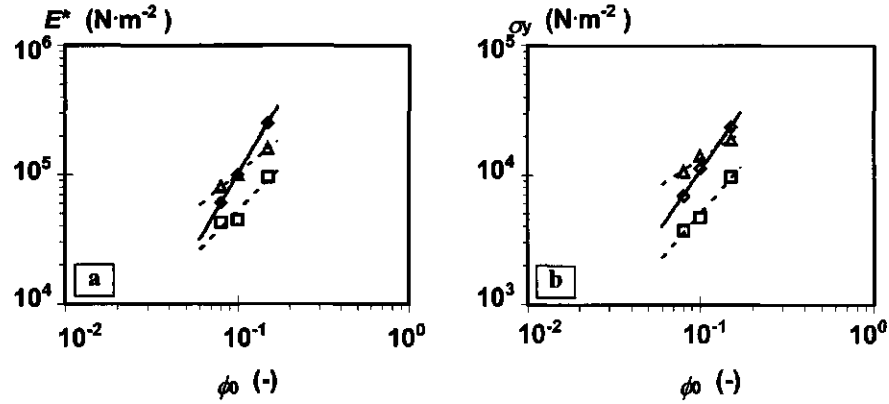

Figure 8-10. *Apparent Young modulus (a) and the yield stress (b) (compression tests) as a function of fraction HP of HP/SF dispersions crystallized in a votator line.* (◊) *after 1 day, rate 50* kg·h^{-1}; (□) *after 1 day, rate 20* kg·h^{-1}; (Δ) *after 16 days, rate 20* kg·h^{-1}.

Table 8-3. *Regression results of the power law plot of Young modulus E* and yield stress σ_y as function of the fraction solids of HP/SF dispersions crystallized in a votator at various rates. μ = slope; r^2 = correlation coefficient*

parameter:	E^*				σ_y			
rate:	20 kg·h^{-1}		50 kg·h^{-1}		20 kg·h^{-1}		50 kg·h^{-1}	
time (days)	μ	r^2	μ	r^2	μ	r^2	μ	r^2
1	1.35	0.90	2.27	1.000	1.55	0.985	1.94	0.997
2	1.10	0.88	2.12	0.980	1.39	0.950	1.83	0.989
4	1.60	0.98	2.65	0.999	0.97	0.857	1.96	0.997
8	1.05	0.83	2.48	0.989	0.90	0.979	1.92	0.977
16	1.10	0.99	2.73	0.999	0.88	0.978	1.75	0.988

From all experiments it was clear that the volume fraction of solid fat has a marked influence on the mechanical properties. Penetration depths decreased and apparent Young moduli, yield stress and viscosity increased on increasing fraction HP. Figure 8-10 shows the relation between E^* and σ_y obtained from compression and the fraction solids plotted for storing times of 1 and 16 days.

The relation between E^* or σ_y as function of the volume fraction solids is described well by a power law for a rate of 50 kg·h^{-1} and less satisfactorily for a rate of 20 kg·h^{-1}. The scaling exponents for the various conditions are compiled in Table 8-3.

The scaling exponents can be discussed in terms of networks that are built from fractal aggregates (Kloek (1998), chapters 5 and 6). A useful scaling relation to describe the elastic moduli as function of the fraction particles is (Bremer (1990, 1992)):

$$E \propto \phi_0^{\mu} \quad \text{with} \quad \mu = \frac{x}{3-D} \tag{8-4}$$

where x is a factor that depends on the way fractal aggregates are connected.

For low volume fraction HP/SF dispersions ($\phi_0 < 0.01$), we determined D to be about 1.7 - 1.8. Due to simultaneous crystallization and aggregation on isothermal crystallization of high volume fraction HP/SF dispersions, higher apparent dimensionalities are expected. For fat dispersions containing about 10 % solids crystallized at high supersaturations at rest we found μ to be about 4 (Kloek (1998), chapter 6). For dispersions crystallized in a votator line we found much lower scaling exponents relating the apparent Young modulus to ϕ_0 (Table 8-3). Dispersions that crystallized completely in shear, yielded μ values ranging from 1.1 - 1.6. Dispersions that partially crystallized at rest and that underwent much less shear, yielded μ values ranging from 2.1 - 2.7. The correlation coefficients show that the fit is worse for dispersions crystallizing completely in shear. The much lower scaling exponents compared to crystallization partially at rest can be explained in two ways. Assuming that the arrangement of the aggregates does not change (*i.e.* x is constant), a lower scaling exponent can only be explained by less compact aggregates *i.e.* lower D values. This seems very unlikely since we showed before that shear causes compaction of aggregates (chapter 5). Polarized light microscopic observations (results not shown) also indicated that the dispersions that completely crystallized in shear, consisted of more compact aggregates. This is also consistent with the whiter colour of the dispersion. The second reason for the lower scaling exponent, if crystallized in shear, may be a change in arrangement of the aggregates *i.e.* a change in x. Up to now, the lowest possible value discussed for x is 2. In this case the stress carrying strands are linear. Scaling exponents of 2.4 (part of the crystallization at rest) and 1.5 (crystallization in shear) would for this case correspond to dimensionalities of 2.17 and 1.67, respectively. The dimensionality for the dispersion that has completely crystallized in shear is unrealistic low. A possible explanation for this can be that due to the high shear the aggregates become very compact and non-deformable due to the sintering of crystals in the compact aggregate. The interaggregate links then are much weaker than the bonds inside the aggregates and the elasticity of the system is determined by the weak inter

aggregate links only. Shih *et al.* (1990) showed that for such a model $x = 1$ and therefore the elastic moduli scale with $\phi_0^{1/(3-D)}$. Applying this model to the observed scaling exponent of 1.5 for complete crystallization in shear would yield $D = 2.33$, which is a realistic value.

One should keep in mind that we are dealing with an apparent Young modulus, determined outside the linear region. Owing to this, already some structure breakdown (fracture of sintered bonds between aggregates) will have occurred. The aggregates will still be almost undeformable while the aggregates can be moved from each other relatively easy. This can explain why the model proposed by Shih *et al.* (1990) can account for the scaling exponents found for the apparent Young moduli. It is likely that within the region of linear deformation a higher x-value is necessary to explain the scaling exponent since in this region both inter-aggregate links and the links in the aggregates are rigid. So on compression outside the linear region, it is likely that the mechanical properties are determined by a system of hardly deformable aggregates that can be separated from each other relatively easy while on compression inside the region of linear deformation, the mechanical properties are determined by the whole system.

The scaling exponents relating the yield stress and the volume fraction solids show the same trends as the scaling exponent for the apparent Young modulus: dispersions completely crystallized in shear yielded μ values ranging from 0.9 - 1.6 and dispersions that had partially crystallized at rest yielded μ values ranging from 1.8 - 2.0. These exponents do not greatly differ from the exponents obtained for the apparent Young moduli. This indicates that the stress carrying strands are already straight or that the bonds are very brittle. The latter seems to be the most realistic in sintered crystal dispersions.

8.4 Conclusions

HP/SF dispersions that had partially crystallized under shear in a votator and partly at rest in a tub, obtained their final consistency within a few hours. HP/SF dispersions that had crystallized completely under shear in a votator obtained their final consistency after about 16 days. This was shown by both penetrometer tests and compression tests. Due to ongoing crystallization at rest, fat crystal aggregates sinter, thereby giving the product its final consistency. Dispersions that have completely crystallized under shear, leave the votator as a dispersion consisting of aggregates that attracted each other by van der Waals forces. Slow recrystallization processes, cause the aggregates to sinter which leads to a slow increase in firmness.

Applying shear to dispersions containing fat crystal aggregates, leads to compaction of aggregates. Apparent Young moduli and yield stresses are related to the fraction HP by a power law. The scaling exponent can be explained by assuming that the system contains very rigid aggregates that are connected to each other by relatively weak links.

8.5 References

Bremer, L.G.B. (1992) *Fractal aggregation in relation to formation and properties of particle gels*, Ph.D. Thesis, Wageningen Agricultural University, the Netherlands

Bremer, L.G.B., Bijsterbosch, B.H., Schrijvers, R., Vliet, T van and Walstra, P. (1990) On the fractal nature of the structure of acid casein gels, *Colloids and Surfaces* **15**, 159

Haighton A.J. (1976) Blending, chilling, and tempering of margarines and shortenings, *J. Am. Oil Chem. Soc.* **53**, 397-399

Haighton, A.J. (1965) Worksoftening of margarine and shortening, *J. Am. Oil Chem. Soc.* **42**, 27

Haigthon, A.J. (1959) The measurement of the hardness of margarine and fats with cone penetrometers, *J. Am. Oil Chem. Soc.* **36**, 345

Heertje, I., Eendenburg, , J van, Cornelissen, J.M. and Juriaanse, A.C. (1988) The effect of processing on some microstructural charateristics of fat spreads, *Food Microstructure* **7**, 189

Kloek, W. (1998) *Mechanical properties of fats in relation to their crystallization*, PhD thesis, Wageningen Agricultural University, the Netherlands

Papenhuijzen, J.M.P. (1971) Superimposed steady and oscillatory shear in dispersed systems II. Influence of the inhomogeneity of the large deformation, *Rheol. Acta* **10**, 503

Persello, J., Magnin, A., Chang, J., Piau, J.M. and Cabane, B. (1984) Flow of colloidal aqueous silica dispersions, *J. of Rheology* **38**, 1845

Putte, K. van and Enden, J.J. van (1974) Fully automated determination of solid fat content by pulsed NMR, *J.Am.Oil Chem.Soc.* **51**, 179

Sassen, C. (1996) personal communication

Shih, W., Shih, W. Y., Kim, S., Liu, J. and Aksay, I.A. (1990) Scaling behaviour of the elastic properties of colloidal gels, *Phys. Rev. A* **42**, 4772

Vliet, T van (1991) Inventory of test methods, *IDF Bulletin- Rheological and fracture properties of cheese* **N° 268**

Wesdorp, L.H. (1990) *Liquid - multiple solid phase equilibria in fat - theory and experiments-*, PhD Thesis Technical University Delft, the Netherlands

Young, F.V.K, Poot, C., Biernoth, E., Krog, N., O'Neill, L.A. and Davidson, N.G.J. (1986) Processing of fats and oils, In *The Lipid Handbook*, Eds: F.D. Gunstone, J.L. Hardwood and F.B. Padley, Chapman and Hall, London

Chapter 9

General Discussion and Conclusions

9.1. General discussion

9.1.1 Introduction

In the previous chapters it is shown that the formation of a structured fat crystal network from a liquid fat blend is a complicated process in which several steps can be distinguished. A simplified scheme is given in Figure 9-1.

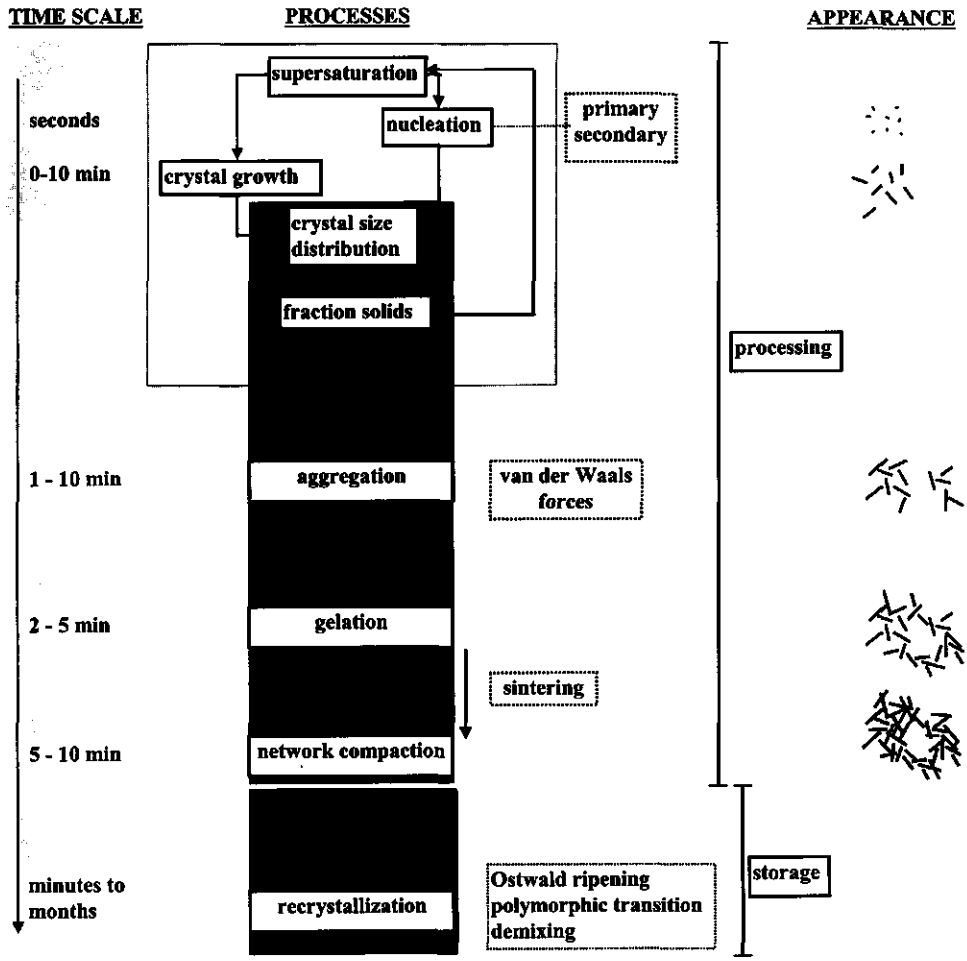

Figure 9-1. *Schematic representation of processes and their time scales during and after crystallization of 10 % HP/SF dispersions (in rest) at moderate supersaturations in the β' polymorph. Some factors are indicated that are important for the mechanical properties of the final fat crystal network.*

The scheme in Figure 9-1 shows that the various processes overlap. This will greatly hamper description of the crystallization process, since aggregation of crystals will cause a lower total crystal surface than in non-aggregating dispersions. Moreover, the simultaneous occurrence of both processes also hampers the description of the aggregation and network formation processes.

In this chapter, I will briefly discuss each of the separated processes that lead to a fat crystal network.

9.1.2 Crystallization of HP/SF dispersions

9.1.2.1 Thermal behaviour

Starting from a liquid fat blend, the solution is cooled to supersaturate a group of triglycerides. This supersaturation is the driving force for crystallization. The supersaturation $\ln\beta$ is hard to define in a multi-component system like a fat blend. In this study the supersaturation was calculated from the crystallization or melting temperature and the fusion or melting enthalpy of the pure HP in either the α polymorph (crystallization) or the β' polymorph (melting) by assuming ideal solution behaviour. By using the peak temperatures from DSC-thermograms, a kind of average temperatures and enthalpies were calculated.

Crystallization in the α polymorph was achieved by rapidly cooling HP/SF solutions in a DSC cup. The peak temperatures, as determined by DSC, were fitted to the mole fraction of HP using Hildebrand's equation, yielding a molar enthalpy of fusion and the crystallization temperature of the α polymorph of pure HP. The results of this procedure will slightly depend on the cooling rate. For higher cooling rates, the onset crystallization temperature will shift to somewhat lower temperatures, leading to a somewhat lower fitted crystallization temperature of the α polymorph of HP. On the other hand it is known that in bulk fats the α polymorph can not be greatly supersaturated, so the errors will not be too large. The enthalpy of fusion and crystallization temperature of the α polymorph of HP obtained by DSC cooling experiments of pure HP yielded about the same values as those obtained from fitting the peak temperatures estimated in DSC cooling experiments on HP/SF dispersions. This may indicate that the mixing behaviour in the α polymorph is virtually ideal. Since we were mainly interested in the supersaturation of the β' polymorph, it was sufficient to know whether a dispersion was supersaturated in the α polymorph or not. Determination of the melting properties of HP/SF mixtures in the α polymorph was not possible since this polymorph rapidly transforms into a more stable polymorph. From the solution properties, we obtained for the α polymorph of HP an enthalpy of fusion of 98 $kJ \cdot mol^{-1}$ and a crystallization temperature of 41.8 °C. Comparison of these numbers with the literature values for the pure triglycerides as compiled in Table 2-2, shows good agreement for the enthalpy of fusion, but the crystallization temperature of the pure components is about 7 K higher than these values.

The enthalpy of fusion and the crystallization temperature of the β' polymorph could not be determined by simple cooling DSC-experiments similar to those carried out for the α polymorph, because also in this way the α polymorph was obtained. The β' polymorph could only be obtained by isothermal crystallization just above the onset crystallization temperature of the α polymorph of a dispersion containing the same fraction of HP. After isothermal crystallization in the β' polymorph, the dispersions were heated and the peak temperatures were fitted to Hildebrand's equation. This yielded reasonable fits but especially the calculated melting enthalpy differed considerably from the melting enthalpy obtained from the pure HP. This may indicate that the mixing behaviour of the various triglycerides in the β' polymorph is markedly non-ideal. The melting enthalpy and the melting temperature obtained from the heating scans after isothermal crystallization in the β' polymorph will depend on crystallization conditions like temperature and time. A higher crystallization temperature will probably lead to fewer crystal defects and therefore to higher melting enthalpies and higher peak temperatures. If crystallization is allowed to proceed for a longer time before a heating scan is carried out, recrystallization (demixing, fewer crystal defects) would also lead to higher melting enthalpies and higher peak temperatures. Isothermal crystallization in the β' polymorph was carried at 4 K above the onset temperature for crystallization of the α polymorph in dispersions with the same fraction of HP. This would mean that, despite the same supercooling, the supersaturation at this crystallization temperature varies with the fraction of HP: dispersions containing larger fractions of HP therefore crystallize at a higher supersaturation in the β' polymorph than dispersions containing smaller fractions of HP. Due to these higher supersaturations this can yield somewhat lower melting enthalpies and melting temperatures for dispersions containing higher fractions HP. The melting enthalpy and melting temperature as determined by fitting DSC peak temperatures to Hildebrand's equation will correspond to properties of the triglycerides in the HP that crystallize when the crystallization rate is highest. Using these numbers for calculation of the supersaturation at the onset of crystallization will therefore be not fully correct.

Since in this study most experiments were carried out on dispersions of which the fraction of HP did not vary too much, the errors made due to the points described above, would not be large. The estimated magnitude of the supersaturation may not be exact but it still allows to compare dispersions that crystallize at the same initial supersaturation.

9.1.2.2 Nucleation

Primary nucleation in bulk fats is always of an heterogeneous nature: impurities catalyze the nucleation process. By dividing the fat in such small volumes that most volume elements contain no impurities, homogeneous nucleation can be studied. Heterogeneous nucleation can best be studied in systems where the fat is dispersed in such droplets that these contain on average only a few catalytic impurities.

Studying nucleation kinetics in dispersed fats by means of ultrasound velocity measurements appeared to be very promising for fat blends with very simple polymorphic behaviour like that of HP/SF mixtures. Nucleation in emulsified fats at temperatures below the α clear point is believed to occur in the α polymorph, although there is no clear evidence that this was also the case in the emulsified HP/SF dispersions. The ultrasound velocity profiles as function of temperature showed that in the case of nucleation in the α polymorph, a transition to a more stable polymorph had occurred, since the fat melted at temperatures corresponding to the β' or β polymorph. The polymorphic transition is supported by the sudden increases of the ultrasound velocity in emulsified HP at a temperature that is a few K above the melting temperature of the α polymorph of HP. This increase in velocity can be explained by a decrease of the adiabatic compressibility due to β' and β crystals, being more compact.

Crystallization of emulsified HP was initiated at a supercooling in the α polymorph of about 7 K. This suggests a heterogeneous type of nucleation since for homogeneous nucleation supercooling up to 20 - 30 K is reported (for pure triglycerides). Furthermore, the crystallization kinetics of emulsified HP could only be modelled using a two-parameter heterogeneous nucleation model. On the other hand, dispersions with a bigger average droplet size crystallized at the same supercooling. This would suggest homogeneous nucleation since the number of impurities per droplet is changed, but no change in supercooling was observed. One way to explain this result is that heterogeneous nucleation takes place at much smaller time scales than the cooling of the dispersions. Another way to explain these results is the broad triglyceride distribution present in the HP. We calculated that triglycerides containing relative long aliphatic fatty acid chains can become more supersaturated than triglycerides containing shorter fatty acids, despite of their low concentrations. Therefore it is likely that triglycerides containing long fatty acids act as nucleating molecules. But due to their presence at low concentrations (small number of crystallizing molecules N in Equation 3-6) and the aliphatic fatty acid chains being long (large decrease of entropy ΔS on crystallization, Equation 3-6 and Equation 9-1), the nucleation rate can be rather small. The nucleation rates caused by the triglycerides present at small amounts may be so small that the kinetics are modelled best using a heterogeneous nucleation model, even though the nucleation in reality would be homogeneous.

The supercooling of 7 K needed to induce crystallization of emulsified HP in the α polymorph is calculated by taking the bulk crystallization temperature of the α polymorph of HP. This is an average property of the HP and therefore probably related to the triglycerides that are present at relative high concentrations (PPS, PSS). However, the triglycerides with long fatty acid chains that induce nucleation in emulsified HP are supersaturated more strongly than the triglycerides present at high concentrations. The supercooling needed to induce crystallization of emulsified HP in the α polymorph would therefore be larger than 7 K. The difference between the bulk melting temperature of long fatty acids containing AAA (trieiconate) and less long fatty acids containing SSS is about 8 K, which may be an indication for the additional supercooling.

Since crystallization kinetics studies and studies on the mechanical properties of crystallized fat dispersions were carried out with dispersions containing 10 % HP/SF, this system was also used

to study the crystallization kinetics in the emulsified state. The crystallization kinetics could be modelled by a homogeneous nucleation model (constant nucleation rate in time) and also the supercooling needed to initiate crystallization suggested homogeneous nucleation. From the temperature dependency of the fitted nucleation rate, a surface free energy for formation of a cubic nucleus in the α polymorph of 4.1 $mJ \cdot m^{-2}$ was calculated. From the same temperature dependency it was calculated that roughly the whole molecule should be in the right conformation to be incorporated in a nucleus. The number of molecules in a nucleus of critical size can be calculated using Equation 3-5. Substituting $\gamma = 4.1$ $mJ \cdot m^{-2}$, a molecular crystal volume v_c of $1.4 \cdot 10^{-27}$ m^3, a temperature T of 283 K and $\ln\beta = 1.90$ ($\Delta H_f = 98$ $kJ \cdot mol^{-1}$, $T_{m,\alpha} = 315$ K), yields about 21 molecules per nucleus. This number is quite small: in a 3 dimensional lattice it would correspond to about 3·3·2 or 2·5·2 molecules.

If such a small number of molecules does suffice, occurrence of secondary nucleation would be likely. Molecules close to a growing crystal surface will be ordered to some extent. It seems likely that there is a kind of transition layer from very ordered near the surface to much more disordered at larger distances from this surface. Only small energy fluctuations will be necessary to order a group of only a few molecules, so it would facilitate the formation of nuclei near a crystal surface. Walstra (submitted) gave a hypothetical explanation for secondary nucleation in fats which implies that clusters of partially oriented triglyceride molecules diffuse away from a crystal face that grows via kinetic roughening. These clusters may give rise to nuclei if the crystal growth rate is small enough to enable considerable diffusion of such clusters.

As mentioned, nucleation in emulsified HP/SF is initiated in the α polymorph although the β' polymorph is greatly supersaturated. At the conditions for homogeneous nucleation of 10 % HP/SF, the supersaturation in the β' polymorph is about 7.5. Can it be explained that nucleation takes place in the α polymorph even if the β' is supersaturated that much? This can be examined by calculating the nucleation rates assuming nucleation to occur in either the α or the β' polymorph. Nucleation in the α polymorph will dominate if the nucleation rate in the α polymorph is about 10 to 100 times higher than that in the β' polymorph. According to the classical nucleation theory as used in chapter 3, the nucleation rate J_i in polymorph i is proportional to:

$$J_i \propto \exp\left[\frac{-\alpha \cdot \Delta S_i}{R_g}\right] \cdot \exp\left[\frac{-32 \cdot \gamma_i^3 \cdot v^2}{(k_b T)^3 \cdot (\ln \beta_i)^2}\right] \qquad \textbf{(9-1)}$$

Table 9-1 shows that if the surface free energy, the fraction α and the molecular crystal volume are the same for both the α- and the β' polymorph, the nucleation rate in the α polymorph is already 11 times higher than the nucleation rate in the β' polymorph. Correcting for the higher density of the β' polymorph would result in somewhat lower relative nucleation rates. So the occurrence of nucleation in emulsified fats in the α polymorph rather then the β' polymorph can be

explained by the higher entropy loss on crystallization in the β' polymorph assuming $\alpha_{\beta'}$ and $\gamma_{\beta'}$ to remain constant. The ratio of the nucleation rates is extremely sensitive to fraction $\alpha_{\beta'}$. It is expected that $\gamma_{\beta'}$ is somewhat higher than γ_{α} as the β' polymorph is packed more densely. This will lead to an even higher value of $J_{\alpha}/J_{\beta'}$, so that in emulsified fats nucleation in the α polymorph must be dominant to nucleation in the β' polymorph

Table 9-1. *The ratio between nucleation rates in the α and the β' polymorph calculated using Equation 9-1 for various combinations of* $\alpha_{\beta'}$, $\gamma_{\beta'}$ *and* $v_{\beta'}$. *The following parameters are assumed:* $\Delta S_{\alpha} = 311.2$ J·mol^{-1}, $\Delta S_{\beta'} = 487.2$ J·mol^{-1}, $\gamma_{\alpha} = 4.1$ mJ·m^{-2}, $v_{\alpha} = 1.4 \cdot 10^{-27}$ m^3 *and* $T = 283.15$ K *(so that* $\ln\beta_{\alpha} = 1.90$ *and* $\ln\beta_{\beta'} = 7.50$*).* ΔS_i *is given by* $\Delta H_{f,i}/T_{m,i}$.

$J_{\alpha}/J_{\beta'}$ (-)	$\gamma_{\beta'} = 4.1$ mJ·m^{-2} $v_{\beta'} = 1.4 \cdot 10^{-27}$ m^3 $\alpha_{\beta'}/\alpha_{\alpha}$ (-)	$\alpha_{\beta'} = 1$ $v_{\beta'} = 1.4 \cdot 10^{-27}$ m^3 $\gamma_{\beta'}$ (mJ·m^{-2})	$\alpha_{\beta'} = 1$ $\gamma_{\beta'} = 4.1$ mJ·m^{-2} $v_{\beta'}$ (10^{-27} m^3)
1	0.959	-3.89	no solution
10	0.998	4.00	1.35
10.94	1.00	4.10	1.40
20	1.010	4.66	1.70
50	1.026	5.32	2.07
100	1.028	5.72	2.31

9.1.2.3 Crystallization kinetics

The crystallization kinetics of HP in the β' polymorph in HP/SF dispersions was modelled using a classical nucleation function that contains (i) a surface free energy γ for nucleus formation; (ii) the fraction of the molecule $\alpha_{\beta'}$ that should be in the right conformation for incorporation in a nucleus; and (iii) an empirical growth rate equation of the form $\log G_c = \log A_g + b_g \cdot \ln\beta$, where G_c is the crystal growth rate. The determined crystallization curves were numerically fitted to the theory. After every time step, the new $\ln\beta$ was calculated which allowed calculation of a new J and G_c. As indicated above, supersaturation $\ln\beta$ is, in the case of crystallization of fat containing numerous different triglycerides, an ill-defined parameter. This will certainly be true if already some HP has crystallized. This is one of the reasons why the observed empirical growth rate equation was not equivalent to a theoretical growth rate equation.

From the induction time for crystallization of HP/SF dispersions with various fractions HP at various initial supersaturations, the surface free energy for nucleus formation in the β' polymorph was calculated at 3.4 - 3.9 mJ·m^{-2}, for heterogeneous nucleation. The real surface free energy for nucleus formation in the β' polymorph will therefore be higher. Above, it was already discussed that

$\gamma_{\beta'}$ is expected to be higher than γ_{α}. This expectation is supported by the $\gamma_{\beta'}$ calculated from the induction times for crystallization (chapter 4).

The determined crystallization curves fitted best for $\gamma_{\beta'} = 3.8$ mJ·m^{-2} an $\alpha_{\beta'} = 0.8$. For these values the G_c - $\ln\beta$ curves coincided for all experiments. This value for $\gamma_{\beta'}$ is comparable to that obtained from the induction times for crystallization. The fraction $\alpha_{\beta'}$ of 0.8 seems to be comparable to the fraction of about 1 found for homogeneous nucleation in the α polymorph, but would give a difference in nucleation rate by a factor 10^5.

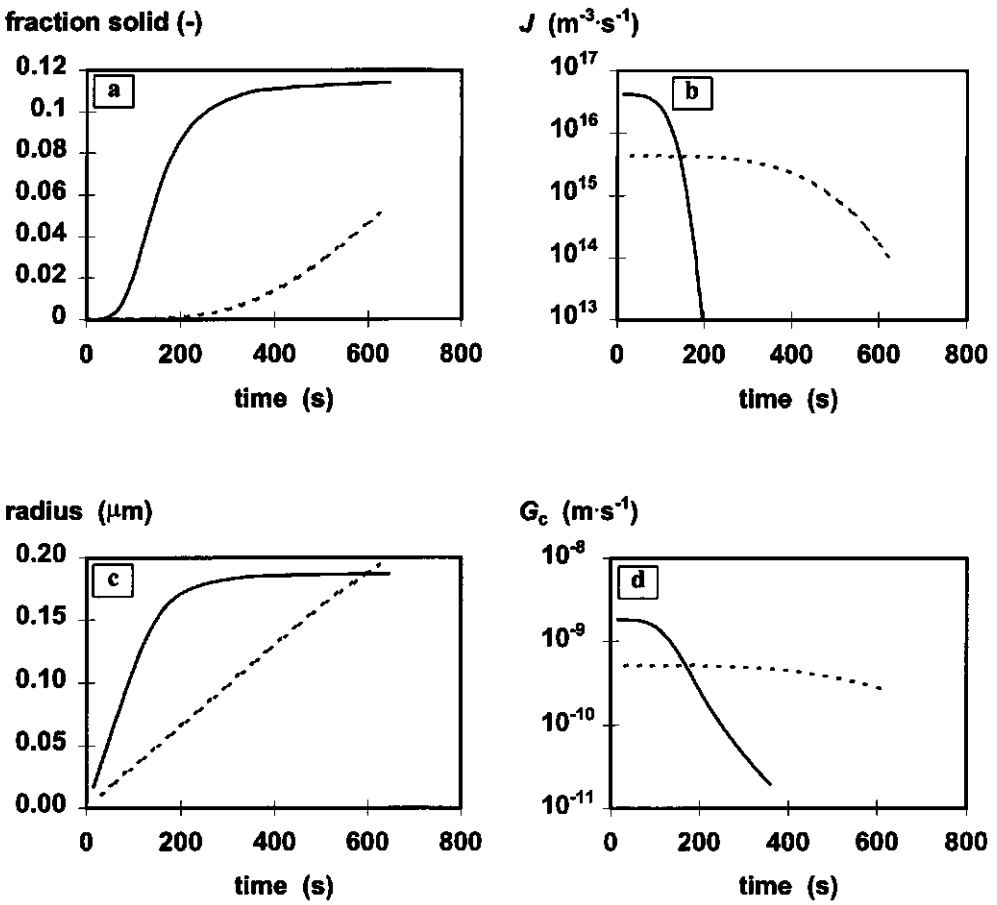

Figure 9-2. *The fraction of solid HP (a), the nucleation rate (b), the volume-number average crystal radius (c), and the crystal growth rate (d), as a function of time for isothermal crystallization of 12 % HP/SF at an initial supersaturation of 3.50 (continuous line) and 2.75 (dotted line).*

Figure 9-2 shows the fitted crystallization curve and the resulting nucleation rate, crystal growth rate and average crystal radius as a function of time for a 12 % HP/SF dispersion crystallized at an initial supersaturation of 3.50. Most particles are produced during the first, say, 80 s. After this time the nucleation rate decreased steeply. The crystal growth rate appears roughly constant for about 100 s and then decreased but not as strong as the nucleation rate. The volume-number average crystal size increased linearly with time until the nucleation rate decreased steeply. Base on these fits, an average crystal radius of about 0.2 μm is expected after crystallization is complete. Supposing the length-width-thickness ratios of the anisometric fat crystals to be 50:10:1 and assuming that an equivalent average volume can be used, a radius of 0.2 μm would correspond to a length of 2.6 μm. This length dimension can be compared with the dimensions obtained from electron microscopic observations of a 10 % HP/SF dispersion that had crystallized at a supersaturation of approximately 4 in the β' polymorph. The observations were made on samples that were de-oiled for 10 days and fractured using a special device designed for this purpose (Heertje *et al.* (1987, 1988)). Figure 9-3 shows that the obtained longest dimension agrees well with the calculated longest dimension. This SEM photograph shows also that considerable clustering of crystals occurs. This will lead to a lower effective crystal surface and therefore will hamper the description of the crystallization kinetics in the way it is described in chapter 4.

Figure 9-3. *SEM photograph of the fat crystal network of a de-oiled 10 % HP/SF dispersion that had crystallized at a supersaturation of about 4 in the β' polymorph.*

9.1.3 Structure of fat crystal aggregates in HP/SF dispersions

9.1.3.1 Aggregation of crystals in dispersions of low volume fraction

An important observation of the aggregation behaviour of HP/SF dispersions of low volume fraction ($\phi \leq 0.01$) was that crystallization in rest yielded a gel-like dispersion, which on shearing showed a very irregular stress-time profile. This is an indication that the bonds in aggregates were sintered and that on shearing probably a part of these bonds, situated in irregularly shaped shear planes, is fractured. If these dispersions were crystallized while applying a high shear rate, and afterwards were allowed to aggregate at a lower shear rate, aggregation of the fat crystals was shown by a gradual increase of the viscosity in time. The occurrence of sintering during crystallization in rest could be explained by the simultaneous occurrence of aggregation and crystallization. Aggregated crystals are in very close contact so that ongoing crystallization can easily glue the crystals together. If the dispersions are crystallized at high shear rates, the contact time between crystals is very short and the viscous stresses in the system would be high enough to keep the crystals separated from each other. This would prevent sintering of crystals.

The observation that on crystallization in rest of an HP/SF dispersion of low volume fraction a gel can be formed, indicates that the aggregates that form the gel must have a very open structure. The time needed to form a gel was shorter than 30 min. These gel times could be explained well using a fractal aggregation model with a fractal dimensionality of 1.7 (Equation 9-3). This value was also derived from light scattering experiments where aggregation occurred at low shear rates (chapter 5) (Vreeker *et al.* (1992)). This value of the dimensionality may be explained by rapid diffusion limited aggregation. The latter is expected, since the only interaction between fat crystals would be due to van der Waals forces. Long range repulsive forces that can result in higher dimensionalities, are absent. At higher shear rates, light scattering yielded higher fractal dimensionalities, which is indicative for more compact aggregates. These high shear rates can lead to more rearrangement of crystals in the aggregate. To minimize the van der Waals attractive energy, the crystals tend to maximize the possible number of crystal-crystal contacts, resulting in more compact aggregates.

The shear rate dependency of the apparent viscosity of low volume fraction HP/SF dispersions could be modelled well by assuming fractal aggregation. However, it was not possible to directly derive the fractal dimensionality from these measurements since a fitting parameter that is indicative for the geometry of the stress-carrying strands was directly related to the fractal dimensionality. Using the dimensionalities obtained from light scattering experiments, the results point to a structure in which the stress-carrying strands are hinged or somewhat more curved. This does not seem irrealistic, since fat crystals have a anisometric shape and the continuous crystal chains are not very thick due to the low volume fraction of crystals. Deformation of the strands can occur between the contact points, but the crystals can also bend, which would imply rather deformable, tortuous stress-carrying strands.

The interparticle bond strength that was derived from viscometry could be explained well by van der Waals interaction and therefore supports the low fractal dimensionalities that are indicative for rapid diffusion limited aggregation. The interparticle bond strength increased with increasing initial supersaturation during crystallization. This was explained by a smaller crystal size at higher supersaturation. It was also derived from crystallization kinetics that the average crystal size decreased with increasing supersaturation.

In fat crystal dispersions in which the aggregation process is separated from the crystallization process, the structure of the aggregates thus can be explained by fractal aggregate models. At low shear rates during aggregation, a low dimensionality (~ 1.7) was obtained while at higher shear rates more compact crystal aggregates were formed.

9.1.3.2 Aggregation of crystals in dispersions of high volume fraction

On crystallization of HP/SF dispersions of high volume fraction ($0.06 \leq \phi \leq 0.14$), the crystallization and aggregation processes can not be separated in time, so they occur simultaneously. The time scale of aggregation can be expressed in the "flocculation time", which is the time needed to reduce the number of particles to half its initial value. Assuming rapid diffusion-limited aggregation in which every collision is effective in creating a permanent bond between particles, the flocculation time $t_{1/2}$ for a dispersion of particles with a radius a present at a volume fraction ϕ_0 is given by (chapter 5) (Smoluchowski (1917)):

$$t_{1/2} = \frac{\pi \cdot \eta_0 \cdot a^3}{k_b T \cdot \phi_0} \tag{9-2}$$

where η_0 is the viscosity of the continuous phase, k_b the Boltzmann constant and T the temperature.

This equation assumes that at $t = 0$ all the particles are present, although during crystallization both the fraction solid and the particle size increase. Therefore, this equation can only give a rough indication of the flocculation time for the number of crystals formed during the preceding crystallization. Furthermore, the anisometry of the fat crystals would not allow any precise calculation. The flocculation time is also a very rough measure for the gel time. An estimate of the gel time in the case of fractal aggregation is given by an equation derived by Bremer (1992):

$$t_g = z^{D-1} \cdot \left(1 - \frac{6D}{2D+3} + \frac{3D}{D+6}\right) \cdot \frac{\pi \cdot \eta_0 \cdot a^3}{k_b T} \cdot \phi_0^{3/(D-3)} \tag{9-3}$$

Figure 9-4 shows the calculated flocculation time and gel time for the crystallization of a 12 % HP/SF dispersion at an initial supersaturation of 3.50 and 2.75. At initial supersaturations of 3.50, already after about 20 seconds the time scale of aggregation is shorter than the time scale of crystallization and after 80 seconds the estimation for the gel time is smaller than the time scale of

crystallization. After 80 seconds only about 1.0 % fat has crystallized. At an initial supersaturation of 2.75, after about 160 seconds the time scale of aggregation is smaller than the time scale of crystallization and after 340 seconds the estimation for the gel time is smaller than the time scale of crystallization. At this time only 0.7 % solid fat has crystallized. One should keep in mind that these numbers are very rough estimates since fat crystals are highly anisometric: nevertheless, the results show that a continuous primary network is already formed at a very low fraction of solid fat and that at the gel point less solid fat would be crystallized for a lower initial supersaturation.

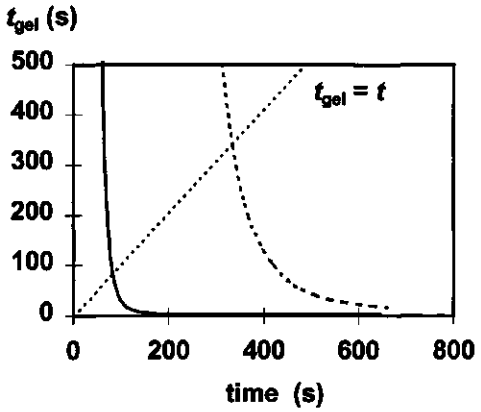

Figure 9-4. *Gel time t_{gel} calculated by Equation 9-3, as a function of crystallization time for a 12 % HP/SF dispersion crystallizing at an initial supersaturation of 3.5 (continuous line) or 2.75 (dotted line) (see also Figure 9-2). D = 1.7.*

From the viscometric- and light scattering studies it was concluded that the dimensionality of fat crystal aggregates at low volume fractions of fat is about 1.7. It is likely that the primary network is built of aggregates of the same dimensionality. After formation of the primary network, the major part of the fat still has to crystallize. This additional crystallization will lead to compaction of the aggregates that form the primary network and therefore will lead to higher dimensionalities. Since the final network is not built of real fractal aggregates, it is better to use the term apparent fractal dimensionality. Determination of elastic moduli G' within the linear region as a function of the fraction crystallized fat yielded a linear relation between $\log G'$ and $\log \phi$. For crystallization in the β' polymorph, scaling exponents varying from 4 at high supersaturation to about 6 for low supersaturations were observed. For crystallization in the α polymorph, a scaling exponent of about 4 was obtained. These linear relations suggest that the elastic properties could be described by a network built of fractal aggregates. The stress-carrying strands of the primary network will becomes less flexible due to ongoing crystallization. Assuming a hinged geometry of these strands, the calculated apparent dimensionalities range from 2.25 for a scaling exponent of 4 to 2.5 for a scaling exponent of 6. These high apparent dimensionalities indeed indicate a compaction of the aggregates

forming the primary network due to ongoing crystallization. The higher dimensionality obtained at a low initial supersaturation can possibly be explained by the amount of solid fat at the gel point. It was shown before that the fraction solid at the gel point was smaller for lower initial supersaturations. Assuming fractal aggregation up to the gel point, would imply that the dimensionless aggregate radius at the gel point is larger for lower initial supersaturation. If it is assumed that the aggregates can not grow anymore after the gel point, and that the primary networks formed at both supersaturations have the same dimensionality, the aggregates that form a network at the lowest fraction of solid fat can compact to the greatest extent.

Can something be said about the crystallization of the fat after formation of the primary network? According to Figure 9-2, there is still considerable nucleation directly after formation of the primary network until about 5 % fat has crystallized. So up to a fraction of solids of 0.05, nuclei are produced that grow out to crystals; these would then aggregate onto the strands of the primary network or aggregate with each other in the pores of the primary network. After 5 % of the fat has crystallized, the nucleation rate has decreased so much that, according to Figure 9-2, further crystallization can only occur by growth of the present crystals. In this case further compaction of the aggregates is hardly expected. Another possibility is that, due to the presence of crystal surfaces, secondary nucleation occurs. In that case during the whole crystallization process, nuclei would be produced that grow out to crystals that aggregate with existing crystals.

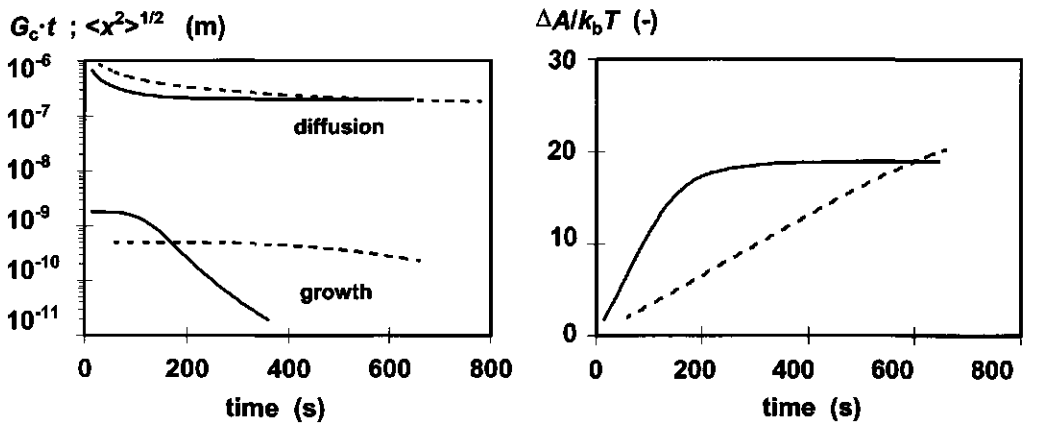

Figure 9-5. *Crystal growth distance, diffusion distance in one second (t = 1) (Equation 9-4) and attractional energy (Equation 6-20) as function of crystallization time for a 12 % HP/SF dispersion crystallizing at an initial supersaturation of 3.5 (continuous line) or 2.75 (dotted line) (see also Figure 9-2).*

Whether a diffusing crystal directly aggregates onto the crystal network, or can diffuse away into the pores of existing aggregates, would depend on the diffusion distance in a relevant time in comparison with the crystal growth distance in the same time and on the attraction energy between

the diffusing particle and the crystal network. The diffusion distance in time period t is calculated by:

$$\langle x^2 \rangle = \frac{k_b T \cdot t}{3\pi \cdot \eta \cdot a} \qquad (9\text{-}4)$$

Figure 9-5 shows that during isothermal crystallization, the diffusion distance in one second is much larger than the crystal growth distance in the same time, indicating that a crystal can easily diffuse away from a crystal surface.
In times scales of 10 seconds, the crystal can diffuse over a distance comparable to the aggregate radius and therefore will probably be captured by the crystal network within this time scale. Comparison of Figure 9-5 and Figure 9-2 shows that the attraction energy becomes sufficient ($\Delta A > 5\ k_b T$) to capture a crystal at time scales at which the average crystal size is about 50 nm

9.1.3.3 Interactions between fat crystals

Another consequence of simultaneous crystallization and aggregation is the formation of sintered bonds. Initially, the crystals aggregate due to van der Waals forces and come in close contact with each other. Sintering of two crystals will occur if some triglyceride molecules are incorporated in the lattices of both crystals. This is more likely to occur at crystal surfaces that have defects due to lattice mismatches and may be related to the occurrence of compound crystal formation. Therefore it is most likely that sintering occurs in fats that contain many different triglycerides. Johansson (1994) showed that also the polymorphic modification is important for the occurrence of sintering. She showed that β' crystals of tristearate were easily sintered by β' bridges of palm kernel fat and that β crystals of tristearate were easily sintered by β bridges of partially hydrogenated rapeseed oil. β' crystals of tristearate could be sintered by β stable partially hydrogenated rapeseed only by rapid cooling so that an supercooled β' form was obtained. This shows that sintering only occurs when the outer part of the crystals and the bridging molecules are in the same polymorph.

If a crystal network, in which the crystals are attracted due to van der Waals attraction, is deformed the separation distance between the crystals is enlarged. If the bending modulus of the crystals is small or the length-to-thickness ratio of the crystal is high, we showed that the maximum van der Waals attractional force can be large enough to allow bending of the crystals. Since the crystals are not connected to each other, they are free to make sliding movements over the crystal surfaces. This would mean that part of the deformation energy can dissipate over relatively short time scales. In the case of non-sintered crystal bonds, the stress needed to break a bond between two crystals depends on the van der Waals force and their geometric arrangement. If the crystals are sintered, deformation of the crystal network will always lead to bending of the crystals or crystal

chains; since the crystals are connected by solid bonds, dissipation of deformation energy over short time scales is probably of minor importance. In the case of sintered crystal bonds, the force needed to break a crystal bond would greatly depend on the deformability of the "crystal": the further it can be deformed before it breaks, the more energy is stored until breaking. In general, a fat having only van der Waals bonds between the crystals will have a lower elastic modulus than a fat of the same structure, but having sintered bonds.

To study the effect of sintering on the elastic properties of fat dispersions, a comparison was made between a rather pure triglyceride, PPP, and HP, a fat containing a fairly wide spectrum of triglycerides. Elastic moduli of 10 % PPP/SF dispersions were much lower than the elastic moduli of a 10 % HP/SF dispersion crystallized under the same conditions and the loss angle of the 10 % HP/SF dispersion was much lower. This was explained by the occurrence of far more sintered crystal bonds in the 10 % HP/SF dispersions, compared to the 10 % PPP/SF dispersion. Since solid bridges are much stronger than van der Waals bonds, sintered dispersions show much more worksoftening after spreading. On storing after working, the elastic modulus of the HP/SF dispersion increased much more than that of the PPP/SF dispersions. The strong increase of the modulus was accompanied by a strong decrease of the loss angle. Both effects can be explained by sintering of the broken crystal bonds. Among the processes that can lead to dissolution and subsequent recrystallization after primary crystallization is more or less complete, are Ostwald ripening, demixing of compound crystals and concomitant polymorphic transitions. Recrystallization will mainly occur at locations with a negative curvature *i.e.* where crystals are in close contact.

The likelihood that crystals of HP/SF dispersions crystallized in rest are sintered was also shown by the determination of the specific fracture energy from wire cutting experiments. The specific fracture energy of a 10 % HP/SF dispersion was about 4 $J \cdot m^{-2}$, which is far too large to be explained by van der Waals forces only. Fracture of crystal bonds could explain the observed specific fracture energy.

9.1.3.4 Large deformation properties of fat crystal dispersions crystallized in shear

low shear conditions

To obtain crystallized HP/SF dispersions that could be used for large deformation experiments, it was necessary to crystallize large volumes. To obtain temperature homogeneity during crystallization, the crystallizing dispersions had to be stirred. To this end, the dispersions were crystallized in a double walled cylinder in which a stirrer was placed that was able the scrape the cooled wall of the cylinder to disperse the crystallized material in the bulk. Stirring could be applied until about 2-3 % fat had crystallized. This means that about 2-3 % of the fat had crystallized and aggregated under shearing conditions. The strain rates in the crystallizing dispersions will strongly depend on the place in the cylinder, but they were not high enough for the aggregates to be completely broken up. By light scattering experiments it was shown that the fat

crystal aggregates became more compact under shearing conditions. Therefore, it is likely that the aggregates formed during crystallization of the first 2-3 % were compacted compared to those formed by crystallization at rest. The first 2-3 % solid fat would be sufficient to form a primary crystal network. The remainder of the HP, which crystallizes at rest, will aggregate onto the existing crystal strands or in the pores of the primary network.

The apparent Young modulus, obtained from compressing experiments, scaled with the fraction of solid fat with an exponent of 3.82. This value is slightly lower than the scaling exponent of 4.1 observed for the storage modulus of dispersions that were crystallized completely at rest. The lower value of the exponent may be explained in two ways: (i) The geometry of the stress-carrying strands remains the same and the aggregates become more open, or (ii) the dimensionality of the aggregates remains the same, or becomes even higher and the stress-carrying strands become more straight / less flexible. Taking into account the expected compaction of aggregates due to shear, it is likely that the stress-carrying strands become less flexible and that the dimensionality of the aggregates increases during the first part of the crystallization. If the stress-carrying strands are straight rather than hinged, a scaling exponent of 3.82 would correspond to an apparent dimensionality of 2.48.

It can be questioned whether comparing results obtained from storage moduli and apparent Young moduli is allowed. The storage moduli are determined at deformations that are within the linear region, so no (irreversible) structure breakdown occurs. The storage modulus of fat crystal networks of a given geometry is determined by the type of interaction between the crystals. The crystals in unworked HP/SF dispersions are sintered. The storage modulus of the HP/SF dispersion is therefore determined by the bending modulus of the fat crystals. The apparent Young modulus could only be determined at deformations far outside the linear region. This means that in this deformation region already irreversible structure break down has occurred due to fracture of part of the sintered bonds. The Young modulus is therefore determined by both the sintered bonds that are left and the van der Waals bonds that are formed after fracture of part of the crystal bonds. This will result in a much lower value of the apparent Young modulus as compared to the storage modulus. Besides the change in interaction between the crystals, the geometrical distribution of the crystals and aggregates can also change due to the large deformations. This would change the geometry of the stress-carrying strands.

Furthermore, the geometry of the stress-carrying strands can also change due to a change in type of interaction. In a completely sintered dispersion all the crystal chains deform on deformation of the gel as long as fracture is absent. If part of the sintered bonds are broken, the resulting van der Waals bonds will determine the deformational behaviour. As shown in Figure 9-6, it is possible that a tortuous strand mechanically behaves like a straight chain

The yield stress as determined from compression experiments scaled with the fraction of solid fat with the same exponent as the Young modulus. This would also agree with the bonds being

partially sintered bonds and partially due to van der Waals forces, whereby the stress-carrying strands would mechanically behave as if being straight (Figure 9-6b).

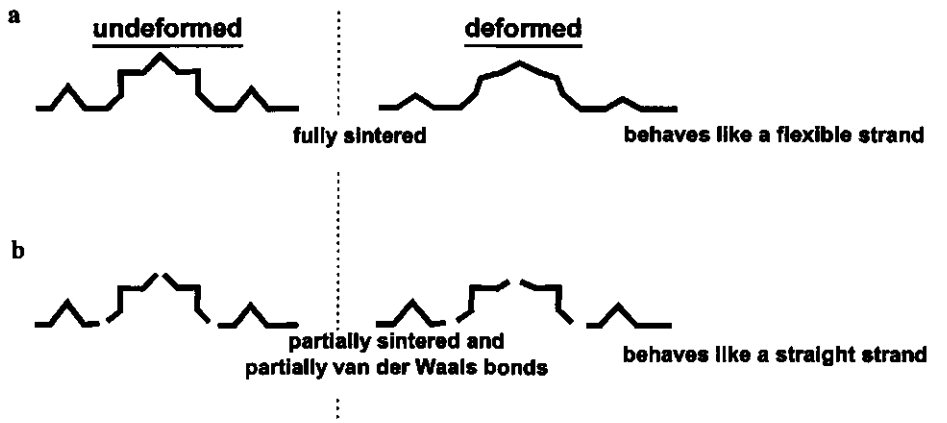

Figure 9-6. *Schematic representation of the stretching behaviour of crystal strands that are (a) completely sintered and crystal strands that are (b) partially sintered and partially aggregated due to van der Waals forces.*

high shear conditions

The HP/SF dispersions that were crystallized in a scraped surface heat exchanger (SSHE), were subjected to high shearing conditions, and considerable compaction of the aggregates is expected. The local strain rates in a SSHE can be very high due to the high angular velocity of the scraper and the small annular gap. The average strain rates in the SSHE varied from 400 to 800 s^{-1}. Scaling exponents that relate the apparent Young modulus to the volume fraction of solid fat were about 1.5 for dispersions that were completely crystallized in shear and about 2.4 for dispersions that were partially crystallized in shear. These scaling exponents are much smaller than the ones for dispersions crystallized at rest (storage modulus) or for dispersions that were crystallized partially in shear at mild shearing conditions. In the latter case, the angular velocity was a factor 2.5 lower and the relevant gap size was about a factor 10 larger. For dispersions containing less than 1 % solid fat, shear rates of about 400 s^{-1} were high enough to break up aggregates to primary crystals or very small dense primary aggregates. However, for dispersions containing much more solid fat, broken up aggregates will directly aggregate again with other aggregates and so become more compacted due to further rearrangements. If the total shearing time is longer, or if the dispersion is completely crystallized in the SSHE, the aggregates will become more compact. The very low scaling exponents of dispersions crystallized completely in shear, actually ranging from 1.1 to 1.6, can almost be explained by the first network model proposed by van den Tempel (1961). This model

assumed linear chains of particles in which the chains are arranged parallel to the axes of an orthogonal co-ordinate system. In the approach of van den Tempel, the particles were equivalent to the crystals. According to our approach the particles are the compacted aggregates, in the case of crystallization in the SSHE under shearing conditions. This is true if the bonds in the interior of the aggregate are very strong compared to the inter-aggregate bonds. Deformation of the network will almost exclusively be due to deformation of the bonds between the aggregates This is incorporated in the fractal network model proposed by Shih *et al.* (1990). This model predicts that the elastic modulus scales with the volume fraction of solids with an exponent of $1/(3-D)$. The apparent Young modulus is determined at deformations at which already some structure breakdown has occurred. It is likely that the interaggregate bonds are broken but that the interior of the aggregates is more or less intact. So the apparent Young modulus corresponds to a dispersion of rigid aggregates that are aggregated by weaker van der Waals bonds. The observed scaling exponent of 1.5 corresponds, according to this model, to an apparent dimensionality of 2.33. The higher scaling exponent that was found in case that the dispersions were partially crystallized under high shear, can be explained by less rigid aggregates compared to the case of complete crystallization in shear. This would cause the numerator in $x/(3-D)$ to be larger, yielding higher scaling exponents for the same dimensionality. A value for x of 2 (straight strands) yields a dimensionality of 2.17 for a scaling exponent of 2.4.

Table 9-2. *Scaling exponent μ and calculated apparent fractal dimensionalities D of HP/SF dispersion crystallized at various shear intensities by assuming various geometries of the stress-carrying strands. The shear intensity increases when going downwards in the table. Grey coloured boxes indicate the most likely geometries of the stress-carrying strands.*

Experiment (in increasing order of shear intensity)		D		
	μ	$x=1$	$x=2$	$x=3$
at rest; rheometer	4.1	-	2.51	2.27
mild shear, compression	3.8	-	2.48	2.21
50 kg·hr^{-1}, SSHE	2.0	2.50	2.00	1.50
20 kg·hr^{-1}, SSHE	1.1	1.90	1.18	0.27

Dispersions that were partially crystallized in shear in the SSHE, and therefore exhibited some post crystallization at rest, obtained their final consistency already within one day and probably already within 5 minutes. The fat that has crystallized in shear is aggregated to compact crystal clusters and these aggregates are sintered due to post crystallization in rest. This was observed for crystallization in the β' polymorph, as well as in the α polymorph. In the case of crystallization in the α polymorph, post crystallization would be largely due to a polymorphic transition from the α to the β'/β polymorph; it is accompanied by an increase in the fraction of solid fat.

Dispersions that had completely crystallized in shear, leave the SSHE as a dispersion of (probably) sintered aggregates that are attracted to each other by van der Waals forces and which may be sintered only to some extent. Slow recrystallization would result in extra sintering between the aggregates and thereby to an increase in consistency on storage. These dispersions obtained their final consistency after storage for about 16 days.

Figure 9-7 shows some examples of cryo-SEM images of deoiled HP/SF dispersions that were crystallized in an SSHE under various conditions. Since there were some problems with the deoiling procedure, the images are of samples that were stored for about one year. Storage over a period of a year can induce changes in the dispersion. It is likely that coarsening of the crystal structure due to recrystallization has occurred. The samples were very inhomogeneous. Fracturing of the deoiled samples in the cryo-stage of the SEM, yielded several different fracture surfaces. By comparing the images in Figure 9-7 with the image in Figure 9-3 of a sample that was deoiled directly after crystallization at rest, it is clear that crystallization under shearing conditions leads to a strong clustering of aggregates.

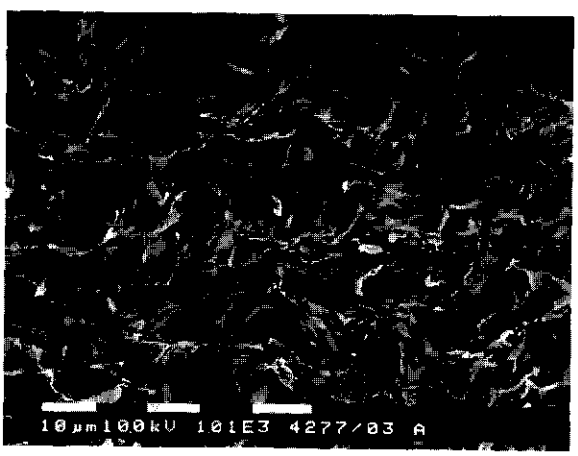

completely crystallized in the SSHE (β' polymorph)

Figure 9-7. *Cryo-SEM micrographs of deoiled 10 % HP/SF dispersions crystallized in an SSHE under various conditions. Dispersions were stored for about one year and were deoiled for 72 hours at 15 °C. The reference bar corresponds to 10 µm.* *Continued on following page.*

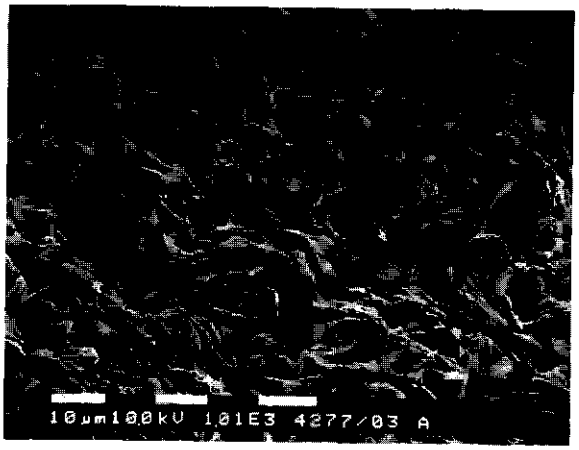

partially crystallized in the SSHE (β' polymorph)

completely crystallized in the SSHE (α polymorph)

Figure 9-7. – *continued from previous page- Cryo-SEM micrographs of deoiled 10 % HP/SF dispersions crystallized in an SSHE under various conditions. Dispersions were stored for about one year and were deoiled for 72 hours at 15 °C. The reference bar corresponds to 10 µm.*

9.1.4 Comparison between butter, margarine and the model system

The elastic deformability of butter is often said to be greater than that of margarine. To test this and to see how the elastic properties of the model system compare with those of butter and margarine, the elasticity of the products was measured in so called strain sweeps. In 10 subsequent strain sweeps, apparent dynamic moduli and loss tangents were determined at increasing strains. Every sweep was started at a strain of about 10^{-4} and the maximum strain was increased so that the effect of high strains on the linear region of deformation could be studied. The results are given in Figure 9-8.

The linear region of deformation increased in the order HP/SF; margarine; butter. It is expected that crystals are sintered in all products, so that the difference in linear region would have to be explained either by differences in geometric arrangement of the crystals, or by different crystal dimensions and therefore different deformabilities of the crystals, as was shown in chapter 6. The initial loss tangents are approximate the same (about 0.2) for all dispersions.

The subsequent strain sweeps for butter shows coinciding G' and $\tan\delta$-curves which indicates that hardly any irreversible structure breakdown occurs up to strains of 0.03. Some reversible changes occur as can be seen from the lower G' and higher $\tan\delta$ with increasing strain. The apparent modulus decreases by a factor of 4 between strains of 10^{-4} and 0.03. Even at high strains, the $\tan\delta$ values are indicative for an elastic structure. Margarine shows a much stronger breakdown of which a considerable part is irreversible. The modulus decreases by almost 2 decades between strains of 10^{-4} and 0.03. At high strains, $\tan\delta$ is much higher than for butter, although at subsequent application of a small strain, $\tan\delta$ is low again. This shows that still much of the structure breakdown is reversible. HP/SF shows a decrease of the modulus of 2 decades between strains of 10^{-4} and 0.03. The structure breakdown is to a large extent irreversible.

These results are consistent with butter having more elastic properties than margarine. The margarine, in turn, has more elastic properties than the HP/SF dispersions. The differences between butter and margarine may possibly be explained by the crystal sizes or the geometric arrangement of the crystals. Boode (1992) showed that the permeability coefficient for milk fat blends was much smaller than for margarine fat blends with a comparable fraction of solid fat. This indicates that either the crystals in crystallized milk fat blends are much smaller or that the crystal network in milk fat blends is much more homogeneous. Smaller crystals are probably also thinner and may give a different deformation behaviour for butter in comparison with margarine.

In butter, fat crystals are present in the outer layer of intact or partially disrupted fat globules and throughout the oil phase. Oortwijn showed that the deformation behaviour of butter and from this butter prepared recombined butter was almost identical which indicates that the presence of crystallized fat in (partially disrupted) globules does not affect the deformation behaviour.

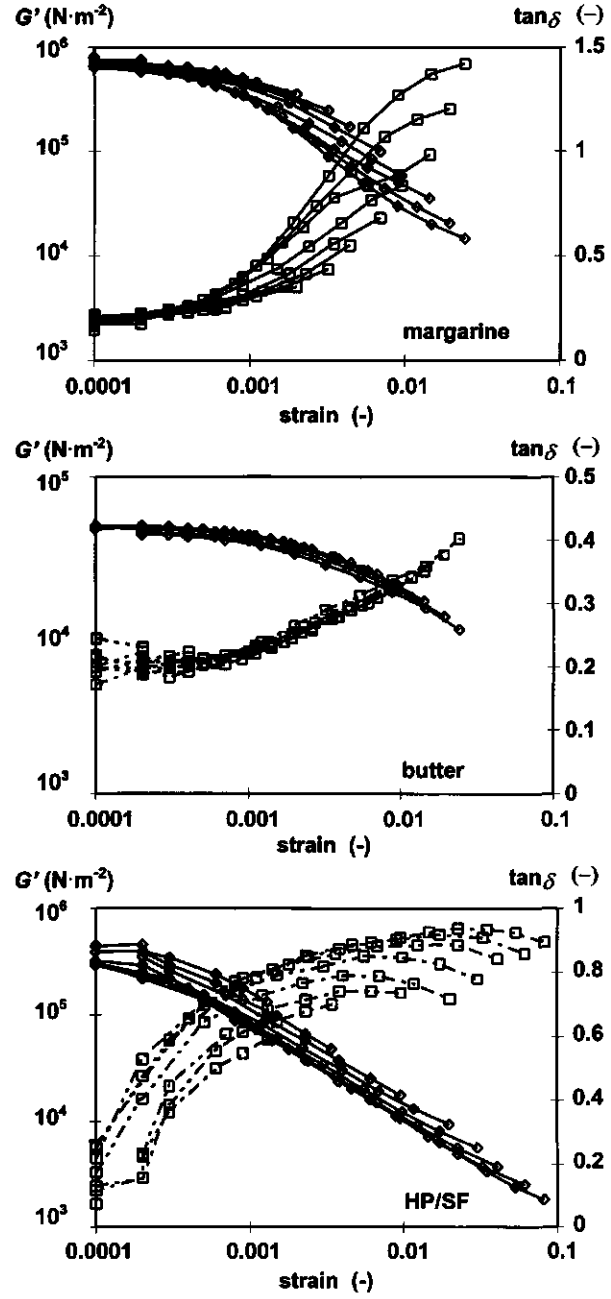

Figure 9-8. *Apparent storage moduli (◊ G') and loss tangents (□ tanδ) determined in successive strains sweeps of increasing maximum strain, starting at a strain of 10^{-4}, of margarine, butter and HP/SF dispersions.*

9.1.5 Applicability to margarine production

Can the conclusions from the work described in this thesis be applied in margarine production? Nowadays, there is a trend to decrease the total fat intake and it is also desirable to change the nature of the fat intake. There are guidelines to lower the consumption of fats containing long-chain saturated fatty acids (especially C12-C16) and *trans* fatty acids. An important consequence of this trend is that less solid fat would be available to structure fat continuous products like margarine. The solid phase should therefore be optimized. In the search for low fat margarines, products are manufactured that even contain "0 % fat". In this product the water phase is structured by monoglycerides that form a gel phase (Zeelenberg-Miltenburg (1995)). A disadvantage of these products is that they can not be used for baking, can not be frozen and lack fat soluble flavouring substances and vitamins. Therefore there is still a need for fat containing margarines.

There are some major differences between the materials and the methods applied in this study and those used for margarine production. In our study we used a simple model system which consisted of an oil phase (sunflower oil) and a solid phase (fully hydrogenated palm oil), which had crystallized in the β' polymorph. The ingredients used for margarine production are much more divers. The solid fat phase of margarine consists of a number of different of fats that are blended in such a way that the final melting point of the dispersion is just below mouth temperature, and that solid fat content does not markedly vary over the temperature range of storage and use. In our study, the solid phase consisted of triglycerides that are built of saturated fatty acids. Fat blends used for margarine production consist of mixed triglycerides that contain high amounts of unsaturated fatty acids. Especially *cis*-unsaturated fatty acids are difficult to incorporate into a crystal lattice due to a kink in the fatty acid chain. This will influence the crystal growth rate and the overall crystallization kinetics. Furthermore, margarine contains water droplets stabilized by emulsifiers. These molecules can adsorb onto or even be incorporated in the crystal surface, and thereby influence the crystallization kinetics. Also stabilizers like diglycerides are added to delay polymorphic transitions from the β' polymorph to the β polymorph (Hernqvist (1984)). Incorporation of these diglycerides will influence the state of the crystal surface and thereby the crystallization kinetics. Moreover, the crystallization kinetics of a fat blend is strongly dependent on fat composition and is therefore difficult to compare with the kinetics of our model system.

However, some results of this work, like the simultaneousness of aggregation and crystallization and the low fraction of solids needed to form an initial fat crystal network also holds for margarine production.

If the fat crystals are aggregated under conditions of no or low shear, very open aggregates structures are formed, so that already at low fractions of solid fat, a continuous crystal network can be formed. Furthermore, the elastic modulus scales with a rather high exponent with the fraction solid. If high shearing conditions are applied during the aggregation, compact crystal aggregates are formed. Much more solid fat is needed to create a continuous network of compact aggregates. The

scaling exponent that relates the elastic modulus to the fraction of solids is much lower than in the case of aggregation at rest.

Because of the trend to lower the intake of the fatty acids that form the triglycerides that readily crystallize, it would be desirable to aggregate the fat crystals under low shearing conditions. During margarine production this can be achieved by cooling the fat blend in the first SSHE in such a way that at the outlet of the first SSHE, hardly any fat has crystallized. Parameters that can be adjusted are the cooling temperature of the SSHE and the flow rate of the fat blend. The main purpose of the first SSHE is then to cool the fat blend to below the crystallization temperature. If this supercooled blend is collected in tubs, it can crystallize and aggregate at rest. This will lead to open aggregates so only little solid fat is needed to form a fat crystal network with a certain strength. Furthermore, both the crystals bonds in the aggregates and the interaggregate bonds will become sintered since aggregation and crystallization occur simultaneously. A disadvantage is that such a product will show much worksoftening by treatments like cutting or spreading. This may give the product an undesirable inhomogeneous appearance. This may be overcome by mechanical treatment of the crystallized product. To this end, the supercooled fat blend that leaves the first SSHE should enter a crystallizer that is equipped with a rotor fitted with pins where the fat can crystallize. The strain rates applied in such a crystallizer should be small enough to prevent considerable compaction of the aggregates, but some shear would be necessary to break sintered bonds between aggregates. Shear should also be applied to keep the material pumpable. Crystallization can be completed in a resting tube. This may cause some extra sintering but a sieve can be placed in the exit of the resting tube so that the product is worked again before it is packed. After packing the product, not too much crystallization should occur, since this would lead to extra sintering. However, recrystallization can never be stopped, and some setting will always occur.

9.2. Conclusions

Conditions for homogenous nucleation in the α polymorph of 10 % HP/SF dispersions could be reached by dispersion of the fat phase using sodium caseinate as an emulsifier. The temperature dependency of the nucleation rate of these dispersions yielded a surface free energy for nucleus formation of about 4 $mJ \cdot m^{-2}$ The found pre-exponential term suggested that almost the whole triglyceride molecule should be in the right conformation to become incorporated in a nucleus.

The polymorphic behaviour of HP/SF dispersions showed that on crystallization in the β' polymorph, the crystals were stable. Initial crystallization in the α polymorph was followed by a transformation to a mixture of mainly β and some β' crystals. The transformation rate was strongly dependent on temperature and the presence of oil.

The crystallization kinetics of HP/SF dispersions in the β' polymorph could be described well using a classical nucleation function and a power-law growth rate equation of the form $G_c = A \cdot \beta^b$ where G_c is the crystal growth rate and β the supersaturation ratio. Heterogeneous nucleation rates

could be described by a 'heterogeneous' surface free energy for nucleus formation of 3.8 $mJ \cdot m^{-2}$ and about 0.8 part of the triglyceride molecule being in the right conformation for incorporation in a nucleus. The crystallization kinetics predicts that the average crystal size decreases with increasing initial supersaturation.

Comparing the time scale for aggregation, as determined from the crystallization kinetics assuming rapid aggregation, and that for crystallization, shows that already at low fractions crystallized fat, considerable aggregation occurs and that a primary crystal network will already be formed at a low fraction of solid fat.

The structure of fat crystals aggregates in low volume fraction solid fat dispersions in which the crystallization and aggregation steps are separated, is described well using fractal aggregate models. Light scattering yielded fractal dimensionalities of about 1.7 at no or low shear; this agrees with rapid diffusion-limited aggregation. High shear rates during the aggregation process lead to compaction of the aggregates. Viscometric data yielded bond strengths between aggregated crystals that could be explained well by van der Waals attraction. Due to their anisometric shapes, fat crystals can easily bend due to external stresses and van der Waals forces between the crystals.

Crystallization and aggregation of higher volume fraction HP/SF dispersions at rest initially leads to formation of a network of crystal aggregates, which structure can described by low fractal dimensionalities. Ongoing crystallization after formation of the primary network, leads to compaction of the primary network. The resulting network is not built of truly fractal aggregates, though its rheological properties can be described well by using a fractal approach; the resulting apparent dimensionalities may not be quite correct.

Applying shear during the crystallization and aggregation processes leads to more compact aggregates, but also to less flexible stress-carrying strands; this results in a weaker dependency of the elastic moduli on the solid fat content.

Due to simultaneous crystallization and aggregation of HP/SF dispersions, crystals and aggregates become easily sintered. Sintering in fat dispersions can also occur due to recrystallization processes like polymorphic transitions, demixing of crystals and Ostwald ripening. Sintering occurs more extensively in solid phases with a wide triglyceride distribution.

Specific fracture energies of HP/SF dispersions could be explained by assuming extensive sintering of crystals. The scale of the inhomogeneities in HP/SF dispersions that cause yielding of the network appears to correspond to the aggregate radius at the gel point.

9.3. References

Boode, K (1992) *Partial coalescence in oil-in-water emulsions*, Ph.D. Thesis, Wageningen Agricultural University, the Netherlands

Bremer, L.G.B. (1992) *Fractal aggregation in relation to formation and properties of particle gels*, Ph.D. Thesis, Wageningen Agricultural University, the Netherlands

Heertje, I., Eendenburg van, J., Cornelissen, J.M. and Jurriaanse, A.C. (1988) The effect of processing on some microstructural charateristics of fat spreads, *Food Microstructure* **7**, 189

Heertje, I., Leunis, M., Zeyl, W.J.M. van and Berends, E. (1987) Product morphology of fatty products, *Food Microstructure* **6**, 1

Hernqvist, L (1984) *Polymorphism of fats*, Ph.D. Thesis, University of Lund, Sweden

Johansson, D. (1994) *Colloids in fats: the fat crystal as a functional particle*, Ph.D. Thesis, Lund University, Sweden.

Kloek, W. (1998) *Mechanical properties of fats in relation to their crystallization*, PhD thesis, Wageningen Agricultural University, the Netherlands

Oortwijn, H., unpublished results

Shih, W., Shih, W. Y., Kim, S., Liu, J. and Aksay, I.A. (1990) Scaling behaviour of the elastic properties of colloidal gels, *Phys. Rev. A* **42**, 4772

Smoluchowski von, M. (1917) Versuch einer mathematischen Theorie der Kogulationskinetik kolloider Lösungen, *Z. Physik. Chem.* **92**, 129

Tempel, van den M. (1961) Mechanical properties of plastic-disperse systems at very small deformations, *J. Colloid. Sci* **16**, 284

Vreeker, R., Hoekstra, L.L., Boer, den D.C. and Agterof, W.G.M. (1992) The fractal nature of fat crystal networks, *Colloids Surf.* **65**, 185

Walstra, P. (1998) Secondary nucleation in triglyceride crystallization, *Progr. Colloid Polym. Sci.* **108**, 4

List of symbols and abbreviations

List of symbols

Roman symbols

symbol	description	unit	chapter
#	number	-	1,3
a	radius of a primary particle	m	1,4,5,6,7,9
a	surface area	m^2	3
a_{32}	volume-surface averaged droplet radius	m	4
a_a	constant in equation for Pe depending on the axis size ratio	m	5
a_d	average droplet surface area	m^2	3
a_g	scaling exponent in the relation $G \propto \Delta c^{a_g}$	-	4
a_i	surface area of plane i	m^2	3
A	empirical constant in relation $\log N_{imp} = A - B \cdot T$	-	3
A	constant in Eq. 6-2	-	6
A	Gibbs energy	J	6
A	proportionality constant in power scaling between G' and ϕ	$N \cdot m^{-2}$	6
A	surface area of test piece	m^2	7,8
A_0	fit parameter in Eq. 6-33	$N \cdot m^{-2}$	6
A_1 , A_2	constants in theoretical growth rate equations	$m \cdot s^{-1}$, -	4
A_g, b_g	constants in empirical growth rate equation (Eq. 4-16)	$m \cdot s^{-1}$, -	4
A_h	Hamaker constant	J	5,6
B	empirical constant in relation $\log N = A - B \cdot T$	K^{-1}	3
B	permeability coefficient	m^2	4,6
c	number concentration of primary particles	m^{-3}	6
Δc	mole fraction difference between saturated and supersaturated conditions = $c_{0,HP} - x_{HP}$	-	4
c_0	initial number concentration of primary particles	m^{-3}	1,5
$c_{0,HP}$	initial mole fraction of dissolved material	-	4
c_i	number concentration of aggregates containing i particles	m^{-3}	5,6
c_p	heat capacity	$J \cdot kg^{-1} \cdot K^{-1}$	4
c_{HP}	mole fraction of dissolved solute	-	all
c_s	number concentration of aggregates in the steady state	m^{-3}	5
C	constant related to aggregate break-up = $(5/2)^m$	-	5
C	constant relating macroscopic strain γ to displacement Δx	m	6
C_2	relative standard deviation of the droplet size distribution	m	3
d	diameter	m	3,6

d	crack width	m	7
d_{32}	volume-surface average diameter	m	3
d_w	cutting wire diameter	m	7
D	fractal dimensionality	-	1,5,6,7,8,9
D	diffusion coefficient	$m^2 \cdot s^{-1}$	4
D^*	heat diffusion coefficient	$m^2 \cdot s^{-1}$	4
D^*	apparent fractal dimensionality	-	6
D_{gel}	fractal dimensionality at the gel point	-	6
D_i	diffusion coefficient of an aggregate containing i particles	$m^2 \cdot s^{-1}$	5
D_r	rotational diffusion coefficient	s^{-1}	5
E	Young's modulus	$N \cdot m^{-2}$	7
E^*	apparent Young's modulus	$N \cdot m^{-2}$	7,8
ΔE^*_a	activation free energy	J	4
E_b	bending modulus	$N \cdot m^{-2}$	6
f	frequency	s^{-1}	6
$f(\theta)$	constant relating activation free energies for homogeneous and heterogeneous nucleation ($0 \le f(\theta) \le 1$)	-	3,4
F	force	N	3,6,7,8
F_c	cutting force	N	7
F_w	van der Waals force	N	5,6
g	acceleration due to gravity	$m \cdot s^{-2}$	6
G	shear modulus	$N \cdot m^{-2}$	1,6,7
G	dimensionless shear rate	-	5
G'	storage modulus	$N \cdot m^{-2}$	6,8,9
G''	loss modulus	$N \cdot m^{-2}$	6,8
ΔG^*	activation free energy for nucleus formation	J	1
ΔG^*_{3D}	activation free energy for nucleus formation	J	1,3,4
$\Delta G^*_{3D,hom}$	activation free energy for homogeneous nucleus formation	J	1,3,4
ΔG_{3D}	change in Gibbs energy for formation of embryo	J	3
G_c	linear crystal growth rate	$m \cdot s^{-1}$	1,4,5,6,9
G_e	contribution of permanent bonds to G'	$N \cdot m^{-2}$	6
ΔG_S	change in Gibbs energy due to surface enlargement	J	3
ΔG_v	change in Gibbs energy per unit volume due to volume enlargement	$J.m^{-3}$	3
ΔG_V	change in Gibbs energy due to volume enlargement	J	3
h	Planck constant ($6.63 \cdot 10^{-34}$)	J·s	1,3,4
h_0	initial height of test piece	m	7,8
h_t	height of test piece at time t	m	7,8
H	separation distance between two particles	m	5,6
$H(\ln\tau)$	relaxation strength of bonds with relaxation time τ	$N \cdot m^{-2}$	6

H_0	interparticle distance at which the net van der Waals force equals zero	m	6
$\Delta H_{f,i}$	molar enthalpy of fusion of polymorph *i*	$J \cdot mol^{-1}$	all
i^*	number of molecules in a nucleus of critical size	-	3
I	moment of inertia	m^4	6
$I(q)$	scattered intensity as a function of the wave vector q	$W \cdot m^{-2}$	5
J	nucleation rate	$m^{-3} \cdot s^{-1}$	1,3,5,6,9
J_0	maximum nucleation rate in emulsified dispersions	$m^{-3} \cdot s^{-1}$	3
J_{coll}	collision frequency due to Brownian motion	$m^{-3} \cdot s^{-1}$	4,6
J_{max}	maximum nucleation rate (zero activation free energy for nucleus formation)	$m^{-3} \cdot s^{-1}$	1
k	reaction rate constant (first order)	s^{-1}	3
k	constant in Eq. 6-8	-	6
k_b	Boltzmann constant ($1.38 \cdot 10^{-23}$)	$J \cdot K^{-1}$	all
k_s	reaction rate constant proportional to droplet surface	s^{-1}	3
k_v	reaction rate constant proportional to droplet volume	s^{-1}	3
K	compression modulus	$N \cdot m^{-2}$	3
K	reaction rate constant for collisions due to Brownian motion	$m^3 \cdot s^{-1}$	4
K	constant depending on angle of penetrometer cone	-	8
$K_{i,j}$	reaction kernel for the aggregation of clusters containing *i* and *j* primary particles	$m^3 \cdot s^{-1}$	5
l	gel length of specimen	m	6
l	crack length	m	7
l_c	length of crystal	m	6
l_c	critical defect length	m	7
l_w	cutting wire length	m	7
m	shear rate thinning exponent	-	5
M	molar mass	$kg \cdot mol^{-1}$	4
n	constant in calculation of yield value; (equals about 0.6 for margarine)	-	8
n_0	refractive index of continuous phase	-	5
N	number density of crystallizing molecules	m^{-3}	3,4,9
N	number of effective strands per unit cross section	m^{-2}	6
N_{av}	Avagadro's number ($6.0 \cdot 10^{23}$)	mol^{-1}	3
N_{imp}	number density of catalytic impurities	m^{-3}	3
N_p	number of particles in an aggregate	-	1,5,6,7
N_{tot}	total number of volume elements in an aggregate	-	5,6
p	penetration of penetrometer cone in units of 0.1 mm	-	8
P	particle shape factor	-	5
ΔP	pressure difference	Pa	6
Pe	Peclet number	-	5

q	wave vector	m^{-1}	5
Q	flow rate	$m^3 \cdot s^{-1}$	6
r	radius of an embryo	m	3
r^*	critical radius of a nucleus	m	1,3,4
R	radius of an aggregate	m	1,5,6
R_g	gas constant (8.314)	$J \cdot K^{-1} \cdot mol^{-1}$	all
R_i	radius of an aggregate containing i particles	m	5
R_s	specific fracture energy	$J \cdot m^{-2}$	7
s_{max}	maximum mass fraction of solid fat	-	4
$s(t)$	mass fraction of solid fat at time t	-	4
S	structure factor	-	5
ΔS	change in entropy on crystallization	$J \cdot mol^{-1} \cdot K^{-1}$	3,4,9
S_{em}	p-NMR liquid signal of emulsion with crystallizing droplets	-	3
S_{liq}	p-NMR liquid signal of emulsion with completely liquid droplets	-	3
S_{sol}	p-NMR liquid signal of emulsion with completely solidified droplets	-	3
S_X	x^{th} -moment of a distribution	m^x	3
t	time	s	all
$t_{0.5}$	time needed to reduce the number of particles to half its initial value	s	1,6,9
$t_{½c}$	time to reach half c_{ss} in a nucleating system	s	6
t_c	thickness of crystal	m	6
t_g	time in which gelation occurs	s	5,9
T	temperature	K	all
ΔT	supercooling (index α refers to α polymorph)	K	3
$T_{m,i}$	melting temperature of crystallizing compound in polymorph i	K	all
v	velocity of sound in emulsion with crystallizing droplets	$m \cdot s^{-1}$	3
v	compression speed	$m \cdot s^{-1}$	7,8
v_c	molecular volume of a crystal	m^3	1,3,4,9
v_d	average droplet volume	m^3	3
v_l	velocity of sound in emulsion with completely liquid droplets	$m \cdot s^{-1}$	3
v_s	velocity of sound in emulsion with completely solidified droplets	$m \cdot s^{-1}$	3
V	volume of a nucleus of critical size	m^3	3
$\bar{V}$	molar volume of a crystal	$m^3 \cdot mol^{-1}$	1
w_c	width of crystal	m	6
W	falling weight of penetrometer cone	g	8
W'	amount of stored energy	$J \cdot m^{-3}$	7
W''	amount of dissipated energy	$J \cdot m^{-3}$	7

x	constant related to geometry of the stress carrying strands	-	1,5,6,7,8
Δx	characteristic distance in compressed material	m	3
x_c	displacement of crystal	m	6
x_x	solubility of compound x in mole fraction	-	all
z	time at which a particle is nucleated	s	4
z	a constant depending on D	-	5,6,9
Δz	characteristic distance in unstrained material	m	3

Greek symbols

α	fraction of a molecule that should be in the right conformation for incorporation in a nucleus	-	3,4,9
α	fraction of solid fat that is incorporated in stress carrying strands	-	6
α	proportionality constant in Eq. 7-4	-	7
α_s	surface entropy factor	-	
β	supersaturation ratio	-	all
$\ln\beta$	supersaturation	-	all
β_0	initial supersaturation ratio	-	4
$\ln\beta_c$	critical supersaturation	-	4
δ	phase angle	deg	6,7,9
$\Delta\mu$	difference in chemical potential	$J \cdot mol^{-1}$	all
ε	relative deformation (strain)	-	6,7
ε	energy gain on formation of a liquid - solid bond	J	4
ε_h	Hencky strain	-	7,8
ε_y	yield strain	-	7
$\dot{\varepsilon}_h$	Hencky strain rate	s^{-1}	7,8
ϕ	volume fraction primary particles	-	1,4,6,7,9
ϕ	volume fraction of crystallized droplets	-	3
ϕ_0	final volume fraction of primary particles	-	4,5,6,8
ϕ^0_d	differential volume fraction of droplet with sizes between d and $d + dd$	-	3
ϕ_a	total volume fraction of aggregates	-	5
ϕ_d	volume fraction of crystallizing component in the dispersed phase	-	3
ϕ^{ff}	bond formation energy of a liquid - liquid bond	J	4
ϕ_{gel}	volume fraction particles at which gelation occurs	-	5,6
ϕ_{int}	volume fraction of primary particles in an aggregate	-	1,5,6
ϕ_m	maximum volume fraction of solidified droplets	-	3
ϕ_m	volume fraction at random close packing (0.63)	-	5
ϕ^{sf}	bond formation energy of a solid - liquid bond	J	4

ϕ^{ss}	bond formation energy of a solid - solid bond	J	4
γ	shear strain	-	6
γ	surface free energy between nucleus and mother phase	$J \cdot m^{-2}$	1,3,4,9
$\gamma(r)$	radial distribution function of particles in an aggregate	-	5
γ_i	surface free energy between nucleus and mother phase of plane i	$J \cdot m^{-2}$	3
$\dot{\gamma}$	shear rate	s^{-1}	5,7
η	viscosity of dispersion	$N \cdot m^{-2} \cdot s$	5,8
η_0	viscosity of the continuous phase	$N \cdot m^{-2} \cdot s$	1,4,5,6,9
η_e	extensional Bingham viscosity	$N \cdot m^{-2} \cdot s$	7,8
κ	adiabatic compressibility	$N^{-1} \cdot m^2$	3
λ	wavelength	m	5,8
λ	induction time for crystallization	s	4
μ	coefficient relating the elastic modulus to the volume fraction of particles	-	5,6,7,8
μ	maximum increase rate in weight fraction of solid fat	s^{-1}	4
μ_p	Poisson ratio	-	7
θ	contact angle	deg	3,4
θ	scattering angle	rad	5
ρ	density	$kg \cdot m^{-3}$	3
σ	stress	$N \cdot m^{-2}$	7,8
$\sigma_{\ln\tau}$	fit parameter in equation 6-33, distribution width	-	6
σ_m	interparticle bond strength	$N \cdot m^{-2}$	5
σ_y	yield stress	$N \cdot m^{-2}$	7,8
τ	relaxation time	s	6
ω	angular velocity	$rad \cdot s^{-1}$	6

Abbreviations

abbreviation	description
DSC	differential scanning calorimetry
EPFM	elastic plastic fracture mechanics
GMS	glycerol monostearate
HP	fully hydrogenated palm oil
LEFM	linear elastic fracture mechanics
p-NMR	pulsed nuclear magnetic resonance
PPP	tripalmitate
SEM	scanning electron microscope
SF	sunflower oil
SSHE	surface scraping heat exchanger
SSS	tristearate

Summary

The study that is described in thesis is focused on the crystallization of fats and the mechanical properties of partially crystallized fat dispersions ("plastic fats"). Nowadays, there is a trend to lower fat consumption. Furthermore, there is an advise of the Dutch Nutrition Council to limit the consumption of saturated and *trans* unsaturated fatty acids, because of supposed positive effects on the prevention of coronary heart disease. However, the fats containing saturated and *trans* unsaturated fatty acids are the ones that crystallize and give fat continuous products their desired mechanical properties, which implies that adherence to the advice of the Dutch Nutrition Council would lead to products with a lower solid fat content. To manufacture products with the same mechanical properties, more knowledge is needed about factors that determine the mechanical properties of partially crystalline fat dispersions, and how these properties are related to the crystallization conditions of fats. Description of relevant processes is extremely complicated by simultaneous occurrence of processes that lead to the formation of a fat crystal network, *i.e.* nucleation, crystal growth, aggregation of crystals, gelation and recrystallization. Other complicating factors are the anisometric shape of fat crystals which it makes it difficult to use aggregation and network models and the non-existence of thermodynamic equilibrium in fat blends.

The model system used in this study consisted of mixtures of fully hydrogenated palm oil (HP) and sunflower oil (SF), the HP being the solid phase and the SF being the liquid phase. HP mainly consists of triglycerides containing saturated fatty acids. The thermal properties and the phase behaviour of the model system were characterized by means of differential scanning calorimetry (DSC) and X-ray diffraction. From the melting enthalpy and the melting temperature of HP it was possible to calculate the supersaturation at a given temperature for every composition of the model system. Supersaturation of the model system for the β' but not in the α polymorph yielded the β' polymorph while supersaturation for the α polymorph yielded a mixture of mainly β polymorph and some β' polymorph.

Prior to growth of a crystal, first a nucleus has to be formed. This is a molecular aggregate of crystalline structure that is large enough for further growth to lead to a decrease of the Gibbs energy. In bulk fats, nucleation is heterogeneous. This means that impurities that are present act as a catalyst for nucleation. To study homogeneous nucleation, *i.e.* nucleation in the absence of catalytic impurities, it was necessary to divide the fat phase over such small droplets that by far most of the droplets would not contain an impurity. Nucleation in such a droplet then occurs at a high supersaturation and directly leads to complete crystallization of the fat in this droplet. The crystallization kinetics then is determined by the nucleation kinetics and it could be studied well by determining the ultrasound velocity in crystallizing emulsions. The low supercooling of 7 K needed for crystallization in the α polymorph suggested heterogeneous nucleation and the kinetics could also be modelled by a heterogeneous nucleation model. On the other hand, the supercooling was independent on the average droplet size which is indicative for homogeneous nucleation. The

determined supercooling may have been underestimated, since it was calculated from the bulk properties of HP. The triglycerides that will become supersaturated first during cooling are the ones that contain long chain fatty acids and therefore have melting enthalpies and melting temperatures that are higher than average values for HP. As these triglycerides were only present in low amounts, the kinetics fitted heterogeneous nucleation models. The supercooling needed to initiate crystallization in emulsified 10 % HP/SF was about 14 K. The crystallization kinetics of these emulsions could be well described by homogeneous nucleation. The temperature dependency of the homogeneous nucleation rate yielded a surface free energy for nucleation in the α polymorph of 4 $mJ \cdot m^{-2}$. From the same dependency, it appeared that almost the whole triglyceride should be in the right conformation for incorporation in a nucleus. If Tween 20 was used as an emulsifier rather than caseinate, the crystallization kinetics of emulsified 10 % HP/SF were described best with a heterogeneous nucleation model and the needed supercooling was 11 K instead of 14 K. It is likely that the lauryl chain of Tween 20 induces some ordering of the aliphatic fatty acid chains at the oil-water interface and therefore lowers the energy needed for surface nucleation.

The crystallization kinetics of HP/SF mixtures at various initial supersaturations in the β' polymorph was determined by pulsed wide-line proton NMR. The determined curves were modelled by a classical nucleation model and an empirical crystal growth function that are both a function of supersaturation. After every time step, the supersaturation was calculated from the fraction of remaining dissolved material using the bulk properties of HP. This supersaturation was then used for calculation of the new nucleation rate and crystal growth rate. Heterogeneous nucleation rates in the β' polymorph yielded a surface free energy for heterogeneous nucleus formation of 3.8 $mJ \cdot m^{-2}$ and a fraction of the triglyceride that should be in a suitable conformation for incorporation of 0.8. The real surface free energy for formation of a homogenous nucleus will be higher than 3.8 $mJ \cdot m^{-2}$ since nucleation is heterogeneous for bulk crystallization and because of the occurrence of secondary nucleation. Induction times for isothermal crystallization in the β' polymorph yielded a surface free energy for heterogenous nucleus formation of 3.4 to 3.9 $mJ \cdot m^{-2}$.

Fat crystals, once formed, aggregate due to van der Waals forces. As no long-range repulsive forces are present, the aggregation is diffusion-limited. Description of the aggregation of crystals in a crystallizing dispersion is complicated by simultaneous nucleation, crystal growth and aggregation. Flocculation times, calculated from the fitted crystallization curves, showed that already at low volume fractions of crystallized fat, the time scale for aggregation is much shorter than the time scale for crystallization. Aggregation of fat crystals was studied by crystallizing low volume fraction HP/SF dispersions at high shear rates so that single crystals or compact crystal aggregates were formed. These primary particles aggregated when the shear rate was decreased. The resulting aggregates occupy a higher volume than the separate single crystals and therefore yield a dispersion with an increased viscosity. The viscosity was modelled as function of shear rate by taking only into account the hydrodynamic interactions. This yielded a bond force between the primary particles in the aggregates *i.e* the crystals, that could be well explained by assuming the bonds to be due to van der Waals forces. Light scattering experiments carried out under shear,

showed that the aggregate structure could be described well by fractal models. In these models, the number of particles in an aggregate scales with the aggregate radius to a power D, the fractal dimensionality. If this dimensionality is smaller than the Eucledian dimensionality, the internal volume fraction of an aggregate decreases on aggregate growth. At low shear rates, the fractal dimensionality was about 1.7 - 1.8 which can be explained by diffusion-limited aggregation. At higher shear rates, the dimensionality was higher. Combination of these results and the shear rate dependency on viscosity, showed that the stress-carrying strands of crystals are very flexible.

Due to the low fractal dimensionality en the rapid aggregation, a solid fat network is already formed at low volume fractions. At the gel point, the volume fraction of particles in an aggregate equals the volume fraction of particles in the dispersion. For a crystallizing HP/SF mixture, this occurs at a volume fraction of about 0.01. The primary network is formed by aggregates with a fractal dimensionality of about 1.7 - 1.8. Ongoing crystallization leads to compaction (decrease of porosity, no shrinkage) of the "aggregates" and therefore to higher apparent dimensionalities. Furthermore, the flexibility of the stress-carrying strands will decrease, because the chains of the primary network sinter due to ongoing crystallization and become thicker due to aggregation

Networks that are built of fractal aggregates have elastic moduli that scale with the volume fraction particles to a power of $x/(3-D)$ where x is a factor that is related to the geometry of the stress-carrying strands and would equal 4 for completely flexible strands, 3 for hinged strands, 2 for straight strands and 1 for aggregates whose internal stiffness is much greater than the inter-aggregate stiffness. On crystallization in the β' polymorph at rest at low supersaturation, scaling exponents between the storage modulus in the region of linear deformation and the fraction crystallized fat of about 6 were obtained. At high supersaturations in the β' polymorph or at crystallization in the α polymorph, scaling exponents of about 4 were obtained. If it assumed that the stress-carrying strands are completely flexible ($x = 4$), scaling exponents of 6 and 4 correspond to fractal dimensionalities of 2.33 and 2.0, respectively. For hinged strands, this is 2.50 and 2.25, respectively. As it is expected that due to simultaneous aggregation and crystallization x becomes smaller, dimensionalities of 2.25 to 2.50 are more likely. This also in line with compaction of primary aggregates due to ongoing crystallization and aggregation after primary network formation. Since the aggregates are not fractal anymore after additional crystallization, it is more correct to speak about apparent fractal dimensionalities. The differences between dimensionalities obtained at high and low initial supersaturations may possibly be explained by differences in time scales for crystallization and aggregation.

To prepare dispersions for compression experiments, it was necessary to crystallize them at mild shearing conditions. The apparent Young modulus of these dispersions scaled with the fraction of solid fat by an exponent of 3.8. This value is about equal for dispersions crystallized in rest. This is remarkable since the Young modulus was determined at deformations that were about 50 times as high as for determination of storage moduli. These large deformations will cause structure break down before the Young modulus can be determined. This was also clear from the Young moduli being much smaller than the storage moduli. The yield stress determined in compression tests,

scaled with the fraction of solid fat by the same exponent as the Young modulus did. In the framework of fractal network models, this means that the geometry of the stress-carrying strands is not strongly changed over the deformation range in which the Young modulus and the yield stress are determined. At these deformations, part of the sintered bonds between aggregates will be broken and these aggregates attract each other by the much weaker van der Waals forces only. The van der Waals bonds will then mainly determine the deformational behaviour. Even if the stress-carrying strands are tortuous, they may mechanically behave like straight strands.

HP/SF dispersions were also crystallized in a scraped-surface heat exchanger (SSHE), where local strain rates are high, to apply more realistic conditions. The dispersions crystallized completely or partially under shear, possibly followed by crystallization at rest. The Young moduli scaled with the fraction of solid fat by an exponent of 2.5 for dispersions that had partially crystallized under shear and 1.5 for dispersions that had completely crystallized under shear. Due to the high shear rates and high fractions of solid fat, compact crystal aggregates were formed in which the crystals are strongly sintered. Dispersions that had completely crystallized under shear thus leave the SSHE as a dispersion of compact aggregates that attract each other by relatively weak van der Waals forces. Recrystallization would result in more sintering between the aggregates, but the inter-aggregate bonds would remain much weaker than the intra-aggregate bonds. For such systems, it is known that the elastic moduli scale with the fraction of solids by an exponent of $1/(3-D)$, which could explain the low scaling exponent. Dispersions that had partly crystallized under shear and partly at rest will have much stronger inter-aggregate bonds. This may give a higher value for x in $x/(3-D)$, hence a higher scaling exponent.

Dispersions that had partly crystallized under shear and partly at rest, obtained their final consistency within 1 day as determined from penetrometer and compression tests. This is explained by the crystallization at rest, which causes sintering between aggregates and thereby formation of strong bonds. Additional recrystallization did not result in an increased consistency. Dispersions that had completely crystallized under shear obtained their "final" consistency only after about 16 days. Recrystallization leads to sintering of the non-sintered aggregates and would therefore cause a slow increase in consistency. The final consistency of these dispersions was comparable to that of dispersions that had partly crystallized under shear.

The degree of sintering was higher in dispersions in which the solid phase consists of triglycerides with a wide range of fatty acids than in dispersions in which the solid phase consists of only one triglyceride. This indicates that sintering of crystals occurs due to presence of compound crystals. HP/SF dispersions appeared to be much more solid-like (lower loss angle) than tripalmitate (PPP)/SF dispersions that had crystallized under comparable conditions. Sintered bonds, like those in HP/SF dispersions, will show far less stress relaxation than the van der Waals bonds that are more predominant in PPP/SF dispersions. Working of HP/SF dispersions that had crystallized at rest showed a much stronger decrease in modulus than working of PPP/SF dispersions, which indicates that on working of HP/SF dispersions far more sintered bonds were broken. The modulus of a worked HP/SF dispersion increased during 20 hours after spreading, much more than a worked

PPP/SF dispersion. Recrystallization in HP/SF dispersions would cause sintering between aggregates that are broken due to working. In PPP/SF dispersions, recrystallization hardly occurs; the biggest increase of the modulus took place in the first hour after working.

An attempt was made to determine the size of the inhomogeneities from which fracture or yielding is initiated. From the elastically stored energy and the specific fracture energy as determined from compression tests and wire cutting tests, a defect length of about 80 μm was calculated. This is the same order of magnitude as the size of a fat crystal aggregate at the moment a gel is formed. Due to the large inaccuracy of the determined parameters, the calculated defect length may be subject to fairly large errors.

Samenvatting

Het onderzoek dat in dit proefschrift wordt beschreven, richt zich op de kristallisatie van vetten en de mechanische eigenschappen van gedeeltelijke gekristalliseerde vetdispersies. Tegenwoordig is er een trend om minder vet te eten. Daarnaast is er het advies van de Voedingsraad om de consumptie van verzadigde vetzuren en *trans*-onverzadigde vetzuren te beperken, wegens vermeende gunstige effecten op het voorkomen hart- en vaatziekten. Het zijn juist de vetten die verzadigde en *trans*-onverzadigde vetzuren bevatten, die kristalliseren en aan vet-continue produkten, zoals margarines, gewenste mechanische eigenschappen geven. Opvolgen van het advies van de Voedingsraad leidt dan tot produkten met minder gekristalliseerd vet. Om deze toch dezelfde mechanische eigenschappen te geven als voorheen, is er meer kennis nodig over de factoren die de mechanische eigenschappen van gekristalliseerde vetdispersies bepalen, hoe die kunnen worden beïnvloed en hoe deze samenhangen met de kristallisatieomstandigheden. Beschrijving van de relevante processen wordt ernstig bemoeilijkt door het gelijktijdig plaats vinden van processen die leiden tot de vorming van een vetkristalnetwerk: kiemvorming, kristalgroei, aggregatie van kristallen, gelering en herkristallisatie. Andere factoren die de beschrijving bemoeilijken zijn de anisotrope vorm van de vetkristallen en het niet-voorkomen van thermodynamisch evenwicht in vetmengsels.

Als modelsysteem werden mengsels van volledig gehydrogeneerde palmolie (HP) en zonnebloemolie (SF) gebruikt, waarbij de HP de gekristalliseerde fase en SF de vloeibare fase moet geven. HP bestaat voornamelijk uit triglyceriden die verzadigde vetzuren bevatten De thermische eigenschappen en het fasengedrag van dit modelsysteem werden gekarakteriseerd met behulp van differentiële-scanningcalorimetrie (DSC) en met Röntgendiffractie. Uit de smeltenthalpie en de smelttemperatuur van HP voor de verschillende polymorfe vormen, was het mogelijk voor elke fractie HP in SF een temperatuur te berekenen waarbij een bepaalde oververzadiging heerst. Wanneer dit modelsysteem kristalliseerde in de β'-polymorf bleef het stabiel in dezelfde polymorf. Kristallisatie in de α polymorf werd gevolgd door een polymorfe overgang naar een mengsel dat vooral de β-polymorf bevatte, maar waarin ook de β'-polymorf aantoonbaar was.

Voordat een kristal kan groeien, moet er eerst een kiem worden gevormd. Dit is een aggregaat van moleculen met een kristalstructuur dat groot genoeg is om bij verdere groei een verlaging van de vrije Gibbs energie te geven. In bulkvetten is kiemvorming altijd heterogeen. Dit wil zeggen dat er onzuiverheden aanwezig zijn die de kiemvorming katalyseren. Om homogene kiemvorming te bestuderen, dat is kiemvorming zonder aanwezigheid van katalytische onzuiverheden, werd de vetfase gedispergeerd in zulke kleine druppels dat verreweg de meeste druppels geen katalytische onzuiverheid bevatten. Kiemvorming in een druppel gebeurt dan bij grote oververzadiging en leidt onmiddelijk tot kristallisatie van het vet in deze druppel. De kristallisatiekinetiek in het geëmulgeerde modelsysteem wordt dan bepaald door de kiemvormingskinetiek en bleek goed te bepalen door meting van de geluidssnelheid. De onderkoeling (7 K) waarbij kristallisatie van

geëmulgeerd HP in de α polymorf optrad, suggereert heterogene kiemvorming en ook de kinetiek kon gemodelleerd worden met heterogene kiemvorming. De onderkoeling was echter niet afhankelijk van de gemiddelde druppelgrootte, wat weer duidt op homogene kiemvorming. De bepaalde onderkoeling is mogelijk een onderschatting, omdat deze werd berekend ten opzichte van de bulkeigenschappen van HP. De triglyceriden die bij afkoeling als eerste oververzadigd zullen zijn, zijn mogelijk degene die lange vetzuren bevatten en daardoor een hogere smeltenthalpie en smelttemperatuur hebben dan overeenkomen met de gemiddelde waarden voor HP. Omdat deze triglyceriden maar in kleine hoeveelheden aanwezig waren, kon de kinetiek gemodelleerd worden als die van heterogene kiemvorming. De onderkoeling die nodig was om geëmulgeerd 10% HP/SF te kristalliseren was ongeveer 14 K. De kristallisatiekinetiek kon beschreven worden als homogene kiemvorming. Uit de temperatuursafhankelijkheid van de homogene kiemvormingssnelheid kon een grensvlakenergie voor kiemvorming in de α–polymorf van 4 $mJ \cdot m^{-2}$ worden berekend. Bovendien kon uit deze afhankelijkheid worden berekend dat vrijwel het gehele triglyceridemolecuul in de juist conformatie moet zijn voor inbouw in een kiem. Wanneer in plaats van caseïnaat, Tween 20 werd gebruikt als emulgator, bleek de kristallisatiekinetiek van geëmulgeerd 10% HP/SF het best gemodelleerd te kunnen worden als heterogene kiemvorming, waarbij de benodigde onderkoeling 3 K minder was. Katalysator in dit kiemvormingsproces was waarschijnlijk de laurylketen van Tween 20 die ordening van de triglyceridemoleculen induceert door een soortgelijke alifatische ketenstructuur.

De kristallisatiekinetiek van HP/SF mengsels bij verschillende initiële oververzadigingen in de β' polymorf werd bepaald met behulp van p-NMR metingen. De gemeten curven werden gemodelleerd met klassieke kiemvorming en een empirische kristalgroeisnelheidsvergelijking. Hierbij werd na elke tijdstap de nieuwe oververzadiging berekend, uitgaande van de bulkeigenschappen van HP. Hieruit werden vervolgens de nieuwe kiemvormingsnelheid en de kristalgroeisnelheid berekend. De heterogene kiemvormingssnelheid in de β'-polymorf kon goed worden beschreven met een grensvlakenergie voor vorming van een 'heterogene' kiem van 3,8 $mJ \cdot m^{-2}$ en een fractie van 0,8 van het triglyceride dat in een gunstige conformatie moest zijn voor inbouw in een kiem. De werkelijke grensvlakenergie voor vorming van een homogene kiem in de β'-polymorf zal groter zijn dan 3,8 $mJ \cdot m^{-2}$ doordat de bestudeerde kiemvorming heterogeen was en mogelijk ook door het optreden van secundaire kiemvorming, d.w.z. kiemvorming door de aanwezigheid van kristaloppervlak. Uit de inductietijden voor kristallisatie in de β'-polymorf kon een grensvlakenergie voor vorming van een 'heterogene' kiem van 3,4 - 3,9 $mJ \cdot m^{-2}$ worden berekend.

De vetkristallen die tijdens de kristallisatie gevormd worden, aggregeren door van der Waals-krachten. Doordat er geen repulsieve krachten met lange dracht aanwezig zijn, is het een snelle, door diffusie bepaalde aggregatie. Beschrijving van de aggregatie van vetkristallen wordt bemoeilijkt doordat er gelijktijdig ook vorming van kristallen plaatsvindt. Uit de berekening van de vloktijden op basis van gegevens uit de beschrijving van de kristallisatiekinetiek, bleek dat al bij lage volumefracties aan gekristalliseerd vet de tijdschaal voor aggregatie korter is dan de tijdschaal

voor kristallisatie. De aggregatie van vetkristallen werd bestudeerd door dispersies met een lage volumefractie HP (≤ 0,01) eerst te kristalliseren in de β'-polymorf onder hoge afschuifsnelheden, zodat losse kristallen of zeer kleine compacte kristalaggregaten werden gevormd. Deze primaire deeltjes aggregeren onder invloed van van der Waals krachten als de afschuifsnelheid wordt verlaagd. De resulterende aggregaten nemen meer volume in dan de afzonderlijke primaire deeltjes waardoor de viscositeit toeneemt tijdens aggregatie. De viscositeit werd gemodelleerd als functie van de afschuifsnelheid, waarbij alleen rekening werd gehouden met hydrodynamische interactie. Hieruit volgt o.a. een maat voor de sterkte van de interactiekrachten tussen de primaire deeltjes, die verklaard kon worden door uit te gaan van van der Waals-krachten tussen de deeltjes. Uit proeven met lichtverstrooiing onder afschuiving bleek dat de aggregaatstructuur beschreven kon worden met fractale modellen. Dit zijn modellen waarbij het aantal deeltjes in een aggregaat schaalt met de aggregaatstraal tot een bepaalde macht, welke macht de fractale dimensionaliteit wordt genoemd. Als deze kleiner is dan de Euclidiaanse dimensionaliteit (in dit geval 3), neemt de interne volumefractie aan deeltjes in zo'n aggregaat af met toenemende aggregaatdiameter. Bij lage afschuifsnelheden was de fractale dimensionaliteit ongeveer 1,7 - 1,8, wat verklaard kan worden met snelle, door diffusie bepaalde aggregatie. Bij hogere afschuifsnelheden was de dimensionaliteit groter. Combinatie van deze resultaten met de afschuifsnelheidsafhankelijkheid van de viscositeit, laat zien dat de spanningsdragende kristalketens buigbaar zijn

Door de lage dimensionaliteit en de snelle aggregatie kan al bij een lage volumefractie aan gekristalliseerd vet een netwerk worden gevormd. Tijdens simultane kristallisatie en aggregatie van HP/SF mengsels was dit bij een volumefractie van ongeveer 0,01. Dit primaire netwerk is opgebouwd uit aggregaten met een dimensionaliteit van ongeveer 1,7 - 1,8. Verdergaande kristallisatie leidt tot een verdichting van de aggregaten wat leidt tot hogere dimensionaliteiten. Verder zal de flexibililteit van de spanningsdragende ketens afnemen doordat de ketens van het primaire netwerk dikker worden door aggregatie maar ook doordat de kristallen gaan sinteren waardoor de onderlinge bindingen steviger en brosser worden.

Indien een netwerk is opgebouwd uit fractale aggregaten, schaalt de elasticiteitsmodulus van dit netwerk met de fractie gekristalliseerd vet tot de macht $x/(3-D)$, waarin de D de fractale dimensionaliteit is en x een faktor die gerelateerd is aan de geometrie van de spanningsdragende ketens. Deze laatste is voor buigbare ketens 4, voor scharnierende ketens 3, voor rechte ketens 2 en voor aggregaten waarbij de stevigheid van de aggregaten zeer groot is ten opzichte van de bindingen tussen de aggregaten 1. Bij kristallisatie in de β'-polymorf in rust werden bij lage oververzadigingen schalingsexponenten tussen de opslagmodulus in het lineaire gebied en de fractie gekristalliseerd vet gevonden van ongeveer 6 en bij hoge oververzadigingen schalingsexponenten van ongeveer 4. Bij kristallisatie in de α–polymorf in rust werd ook een exponent van ongeveer 4 gevonden. Als wordt aangenomen dat de spanningsdragende ketens volledig kunnen buigen, corresponderen exponenten van 6 en 4 met dimensionaliteiten van respectievelijk 2,33 en 2,00. Voor scharnierende ketens is dit respectievelijk 2,50 en 2,25. Omdat verwacht wordt dat de waarde van x kleiner wordt ten gevolge van gelijktijdige aggregatie en kristallisatie, zijn scharnierende

ketens waarschijnlijker. Doordat na vorming van het primaire netwerk nog verdergaande kristallisatie optreedt, zijn de aggregaten niet meer echt fractaal en is het beter om te spreken van schijnbare fractale dimensionaliteiten. Het verschil tussen de dimensionaliteiten bij lage en hoge overzadigingen kan mogelijk verklaard worden door het verschil in de tijdschalen voor kristallisatie en aggregatie.

Om dispersies te bereiden voor compressieproeven was het nodig om de dispersies gedeeltelijk te kristalliseren onder milde afschuiving. De schijnbare Young-modulus schaalde met de fractie gekristalliseerd vet in de β'-polymorf bij hoge oververzadigingen met een exponent van 3,8. Dit is ongeveer gelijk aan die voor kristallisatie in rust. Dit is opmerkelijk omdat de schijnbare Young-modulus werd bepaald bij vervormingen die al snel een factor 50 groter zijn dan die bij de bepaling van de opslagmoduli. Door deze grote vervormingen zal er al aanzienlijke structuurafbraak zijn opgetreden voordat de Young-modulus kan worden bepaald. Dit bleek ook uit de veel lagere waarde van de Young-modulus vergeleken met de opslagmodulus. De zwichtspanning, die werd bepaald uit de compressiemetingen, schaalde met dezelfde exponent met de fractie gekristalliseerd vet als de Young-modulus. Vertaald in fractale netwerkmodellen, betekent dit dat de geometrie van de spanningsdragende ketens niet sterk verandert door vervormingen nodig ter bepaling van de Young-modulus en de zwichtspanning. Doordat de gesinterde bindingen al gedeeltelijk verbroken zijn, bestaan de spanningsdragende ketens uit zeer stevige, gesinterde bindingen en veel zwakkere van der Waals-bindingen. Ten gevolge van uitwendige krachten zal vervorming dan ook vooral optreden tussen structuurelementen die door van der Waals-krachten bij elkaar worden gehouden. Ook al is de spanningsdragende keten sterk gekronkeld, dan zal die zich reologisch ongeveer gedragen als een rechte keten.

Ook werden dispersies gekristalliseerd in een schrapende warmtewisselaar (SSHE) onder lokaal hoge afschuifsnelheden. De dispersies kristalliseerden geheel of gedeeltijk in de SSHE, gevolgd door eventuele nakristallisatie in rust. De Young-modulus schaalde met de fractie gekristalliseerd vet met een exponent van ongeveer 2,4 wanneer de dispersie gedeeltelijk onder afschuiving kristalliseerde, en met een exponent van 1,5 in het geval van volledige kristallisatie onder afschuiving. Door de hoge afschuifsnelheden en de hoge fracties gekristalliseerd vet zullen compacte kristalaggregaten worden gevormd die intern sterk gesinterd zijn. Als de dispersie volledig kristalliseert onder afschuiving, bestaat het produkt dat de SSHE verlaat uit een dispersie van intern rigide aggregaten, die elkaar onderling aantrekken door de vrij zwakke van der Waals-krachten. Herkristallisatie zal leiden tot meer sintering tussen de aggregaten maar de interne bindingen blijven sterker. Elasticiteitsmoduli voor dit soort systemen schalen met de fractie aan deeltjes met een exponent van $1/(3-D)$, wat de lage exponent kan verklaren. In dispersies die gedeeltelijk onder hoge afschuiving kristalliseerden en daarna gedeeltelijk in rust, zal minder compactie van aggregaten zijn opgetreden en zal het verschil tussen bindingssterkte in de aggregaten en tussen de aggregaten minder groot zijn. Dit levert een hogere waarde voor x in $x/(3-D)$.

Dispersies die gedeeltelijk onder afschuiving in de SSHE en gedeeltelijk in rust kristalliseerden, bereikten binnen 1 dag hun eindstevigheid, zoals werd bepaald met een penetrometer en met compressie, en waarschijnlijk nog veel sneller. Dit komt doordat bij kristallisatie in rust de aggregaten onderling sinteren, zodat direct de stevigste binding wordt gevormd. Eventuele herkristallisatie verandert daardoor de stevigheid niet. Dispersies die volledig onder afschuiving kristalliseerden bereikten hun eindstevigheid pas na ongeveer 16 dagen. Deze dispersies verlaten de SSHE als compacte kristalaggregaten, die onderling weinig gesinterd zijn. Herkristallisatie leidt tot verdergaande sintering tussen de aggregaten en daardoor tot een duidelijke toename in de stevigheid. De eindstevigheid van deze dispersies was vergelijkbaar met die van de gedeeltelijk onder afschuiving gekristalliseerde dispersies.

De mate van sintering is sterker in dispersies waarin de gekristalliseerde vetfase bestaat een breed spectrum van triglyceriden dan in dispersies waarin de gekristalliseerde vetfase bestaat uit een enkel triglyceride. Dit duidt er op dat kristallen sinteren door het optreden van mengkristallisatie. HP/SF dispersies bleken veel meer een vaste-stof karakter te hebben (lagere verlieshoek) dan tripalmitaat (PPP)/SF dispersies die kristalliseerden onder dezelfde omstandigheden. Gesinterde bindingen, zoals in HP/SF dispersies zullen veel minder spanningsrelaxatie vertonen dan van der Waals-bindingen, welke meer voorkomen in PPP/SF dispersies. Spatelen van in rust gekristalliseerde dispersies liet zien dat de modulus van HP/SF dispersies veel sterker daalde dan van PPP/SF dispersies, wat er op duidt dat in de HP/SF dispersies meer gesinterde verbindingen werden verbroken. De modulus van een gespatelde HP/SF dispersie was 20 uur na het spatelen weer veel meer toegenomen dan die van de gespatelde PPP/SF dispersie. Herkristallisatie in HP/SF dispersies veroorzaakte weer sintering van de door spatelen verbroken inter-aggregaat-bindingen over lange tijdschalen (>20 uur) terwijl in PPP/SF dispersies vrijwel geen herkristallisatie plaats vond en de grootste verandering binnen korte tijd (binnen 1 uur).

Tenslotte werd geprobeerd met behulp van compressie- en snijproeven de grootte te bepalen van de inhomogeniteiten van waaruit breuk van het kristalnetwerk wordt geïnitieerd. Uit de elastisch opgeslagen energie en de specifieke breukenergie werd een defectlengte van ongeveer 80 μm berekend. Dit is van dezelfde orde van grootte als de afmeting van een aggregaat op het moment dat een gel wordt gevormd. Door de grote onnauwkeurigheden in de gemeten parameters is de waarde voor de defectlengte echter een grove schatting.

Een woord van dank.....

Het hele proces dat zich afspeelt tussen het moment dat je het projectvoorstel leest en het moment dat je een punt plaatst achter de laatste zin van het dankwoord in het proefschrift, doe je niet alleen. Een heleboel mensen hebben een bijdrage geleverd aan het gereed komen van dit proefschrift en verdienen het om genoemd te worden.

Allereerst wil ik mijn promotor, Pieter Walstra, en copromotor, Ton van Vliet, bedanken voor het vertrouwen dat ze in me hebben gesteld door me de mogelijkheid te geven dit onderzoek onder handen te nemen. Pieter, jouw stokpaardjes zoals sintering en het belang van secundaire kiemvorming bleken in dit onderzoek van wezenlijk belang. Bij Ton kon ik altijd langskomen om al dan niet bevestiging van mijn ideeën te krijgen. Naast Pieter en Ton, wil ik ook Albert Jurgens en Marleen Fontyn bedanken voor het mede-initiëren van dit onderzoek en het opstellen van het projectvoorstel.

De leden van de begeleidingscommissie wil ik bedanken voor de ideeën en kritiek die zij hebben geuit naar aanleiding van mijn verslagen. Ik wil me excuseren aan degenen die vonden dat er af en toe misschien iets te veel rekenwerk in stond. Zonder iemand te kort te doen, wil ik speciaal Wouter Meeussen bedanken voor de vele goede ideeën en zetjes in de goede richting. De faxen en E-mailtjes uit pajottenland heb ik altijd erg gewaardeerd.

Barbara Bosch, Marc Evans, Martine van den Berg, Jan van Iersel, Wouter Zijlstra en Michel Veneman hebben in het kader van een afstudeeropdracht of Erasmus-stage bijgedragen aan deelprojecten van dit onderzoek. Katja Grolle heeft een serie permeabiliteitsmetingen voor haar rekening genomen en geassisteerd bij de analyses voortgekomen uit pilot-plant experimenten. Henny Haman zorgde ervoor dat er überhaupt gekristalliseerd vet uit de votator kwam. Jerry van Maanen heeft talloze DSC metingen uitgevoerd om de modelsystemen te karakteriseren. Adrie de Jager heeft ervoor gezorgd dat de p-NMR nog net zijn werk heeft kunnen doen. Henk Verduin en Jan d'Hondt wil ik bedanken voor de mogelijkheid om lichtverstrooiingsexperimenten onder afschuiving uit te voeren en voor de hierbij geboden hulp. Marcel Paqûes en Peter Zandbelt hebben er voor gezorgd dat de vet dispersies gevisualiseerd werden middels electronenmicroscopische opnames. I would like to thank Malcolm Povey for the nice time in Leeds and his help on using the ultrasound velocity equipment. I share your enthusiasm about the ultrasound technique.

Al die 8 jaren dat ik bij de sectie heb gewerkt, heb ik een gezellige tijd gehad. s'Ochtends koffie drinken, zwemmen, klaverjassen, fitness (ja, ja), op vrijdag naar de kroeg en de verschillende eetclubjes waarbij je toch vaak weer dezelfde mensen zag (André, Anita, Frans en Iekje). En dan is er natuurlijk nog kamer 208, garant voor ludieke projecten. Eerst met z'n drieen en later met z'n vieren zijn we zowel letterlijk als figuurlijk dichter bij elkaar gekomen. Margrethe, Vesna en Ine, bedankt voor de gezelligheid. Mijn 208 project is nu afgerond!

Jeanine wil ik bedanken voor het feit dat ze er altijd is geweest, ook op de momenten dat ik weer eens achter de computer zat terwijl jij liever een stukje met mij ging wandelen. Jij hebt me geleerd

dat er wel degelijk een verschil is tussen een "poster" en een echt kunstwerk. Door de omslag die dit proefschrift siert, is het ook een beetje jouw proefschrift geworden. Het resultaat mag gezien worden. Bedankt!

Curriculum Vitae

William Kloek werd geboren op 24 maart 1965 in Kamperveen (gemeente IJsselmuiden). In 1982 haalde hij het HAVO diploma aan het Johannes Calcijn Lyceum te Kampen. Daarna volgde hij de propadeuse aan de Christelijke Hogere Agrarische School te Dronten. In 1983 begon hij aan de Rijks Hogere Agrarische School, afdeling laboratoriumtechniek te Wageningen (voorheen STOVA, tegenwoordig IAH-Larenstein) een opleiding tot chemisch analist welke in 1987 met een diploma werd afgerond. Tijdens de studie werden stage- en afstudeeropdracht afgerond aan respektievelijk de toenmalige Landbouwhogeschool te Wageningen en de Stichting voor Plantenverdeling eveneens te Wageningen.

Vervolgens werkte hij gedurende een aantal maanden bij het Instituut voor Onderzoek naar Bestrijdingsmiddelen (IOB-Wageningen), onderbroken voor vervulling van de militaire dienstplicht. In 1989 werd hij aangesteld als onderzoeksassistent bij de toenmalige sectie Zuivel en Levensmiddelennatuurkunde van de Landbouwuniversiteit te Wageningen op een onderzoek naar de reologische eigenschappen van sterke en zwakke polysaccharidegelen. Van 1 januari 1993 tot 1 januari 1997 was hij bij dezelfde sectie werkzaam als assistent in opleiding op het onderzoek dat in dit proefschrift is beschreven.

Vanaf februari 1997 is hij werkzaam als onderzoeker bij het Instituut voor Agrotechnologisch onderzoek (ATO-DLO) te Wageningen waar hij werkte binnen de afdeling Grensvlak- en Scheidingstechnologie. Vanaf maart 1998 is hij vanuit het ATO-DLO gedetacheerd bij het Wageningen Centre for Food Sciences (Technologisch Top Instituut - Voeding) waar hij binnen het thema Structuur en Functionaliteit onderzoek doet op het gebied van emulsies en schuimen.